# A STUDY OF OPHTHALMO ACROMELIC SYNDROMES IN HUMAN AND MOUSE

Joe Rainger

A thesis submitted for the degree of Doctor of Philosophy
University of Edinburgh

2009

*For Otto*

I declare that this thesis is composed of original research and analysis undertaken by myself, and where the work of others is included, their contributions have been duly acknowledged.

Joe Rainger

September 2008

# 1. Abstract

The combination of severe ocular and distal limb malformations is rare. Ophthalmo-acromelic syndrome (OAS; MIM 206920) is characterised by anophthalmia with lower limb oligodactyly. To date <40 cases of this autosomal recessive disorder have been reported. Genome-wide analysis of ~10,000 SNPs typed on two apparently unrelated families - comprising a total of three affected individuals, four unaffected siblings and their consanguineous parents - identified a large region of overlapping autozygosity on chromosome 14q. Adding data from a third consanguineous family gave a combined LOD score of >5 with no evidence of locus heterogeneity. Collaborative data from a further 6 individuals refined the critical interval to a 3.4 Mb region on chromosome14:69,652,605-73,059,612 Mb. To sequence all 19 known protein-coding genes in the region, the 238 exons were ranked by evolutionary sequence conservation and divided equally between the Edinburgh and Nijmegen groups. Complete sequence coverage has been obtained for 61% of the "Edinburgh" exons but no potentially causative mutations have been identified. Further mutation analysis of the OAS locus is on-going.

Mice homozygous for the X-ray induced *Mp* mutation were reportedly anophthalmic with hind limb oligodactyly and thus represented a potential model for human OAS. This line was rederived in Edinburgh and phenotypic analysis of *Mp*/*Mp* homozygotes showed runting, malformed pinnae with microphthalmia but not anophthalmia. The apparent hind-limb oligodactyly was due to osseous syndactyly. *Mp*

heterozygotes had milder microphthalmia and pinnae deformities, but lacked the syndactyly. In both heterozygotes and homozygotes the eye malformations were fully penetrant, pan-ocular and characterised by failure of both the ciliary apparatus and vitreous body to form and abnormal retinal lamination.

Genome-wide microsatellite marker analysis showed linkage of the *Mp* phenotype to chromosome 18. *Fbn2* mapped within the linkage interval and was a good candidate for *Mp* based on the finding of hind limb osseous syndactyly in *Fbn2*-null mice. However, *Fbn2*-null mice have no eye phenotype. 3'-RACE identified that *Mp* was as a 660 kb inversion affecting the 3'-regions of *Fbn2* and the adjacent gene *Isoc1*. This created two aberrant reciprocal fusion transcripts: *Fbn2* exons 1-63 are fused to *Isoc1* exon 5; and *Isoc1* exons 1-4 are fused to *Fbn2* exons 64-65. This predicts nonsense-mediated decay of the *Isoc1*$^{Mp}$ transcript and production of a truncated Fbn2$^{Mp}$ protein.

Ocular development was analysed in homozygote and wild type embryos to define the basis of the "worse than null phenotype" seen in *Mp* mice. RNA *in situ* hybridisations (ISH) failed to detect expression of *Isoc1* in the embryonic eye. In contrast, normal expression of *Fbn2* in the ciliary body and retina was consistent with the *Mp* phenotype. A combination of EM and immunocytochemistry showed that truncated Fbn2 (Fbn2$^{Mp}$) was retained within the ER. Fbn2$^{Mp}$ co-localised with markers of *ER stress*: *Grp78* expression and UPR-specific *Xbp1* splicing. Signalling by Wnt2b is

thought to be critical for ciliary development and *Lef1,* a Wnt-responsive transcription factor, showed increased and ectopic ocular expression in the region affected by ER stress. Sox2 is a direct transcriptional target of Lef1 and we observed apparent ectopic expression of *Sox2* in the ciliary body. Throughout the developing retina in mutant embryos we also observed individual cells that were ectopically expressing the transcription factor *Chx10* and other cells expressing the apoptotic marker *Activated-Caspase-3*. The apoptotic marker did not specifically co-localise with $Fbn2^{Mp}$.

Taken together, these findings suggest that the ocular malformations in *Mp* are a direct result of the ER stress induced by $Fbn2^{Mp}$ in a specific group of cells in the early ciliary body. The ER stress presumably halts post-translational modification of a developmentally critical signaling molecule, possibly Wnt2b, which happens to be expressed in the same cells. We have termed the resulting pathological mechanism a synodiporic effect (synodiporia = the ones walking the street together or fellow travellers). Such effects may have significant implications for human genetic disease analysis, and may provide an explanation for other "worse than null" mutations.

**Contents** **Page**

## List of Figures

## List of tables

| Abbreviation | Abbreviated Term |
|---|---|
| aCGH | array comparative genomic hybridisation |
| AER | apical ectodermal ridge |
| AP | alkaline phosphatase |
| A-P | anterior-posterior |
| bHLH | basic helix-loop-helix |
| BLAT | basic local alignment tool |
| BMP | bone morphogenic protein |
| bp | base pairs |
| BSA | bovine serum albumen |
| bZIP | beta-Zipper |
| CB | ciliary body |
| cDNA | single stranded complimentary deoxyribonucleic acid |
| cGy | Centigrays |
| CN | Cornea |
| CNS | central nervous system |
| CS | carnegie stage |
| Ct | critical threshold |
| CT | computed tomography |
| DAPI | 6-diamidino-2-phenylindole dihydrochloride |
| DEPC | diethyl dicarbonate |

| | |
|---|---|
| $dH_2O$ | deionised $H_2O$ |
| DIG | Digoxigenin |
| DMEM | Dulbecco's modified Eagles medium |
| DMSO | di-methyl sulfoxide |
| DNA | deoxyribonucleic acid |
| dNTP | deoxynucleotide triphosphate |
| E | embryonic day |
| ECM | extracellular matrix |
| EDTA | ethylenediaminetetraacetic acid |
| EF | eye field |
| EM | electron microscopy |
| ER | endoplasmic reticulum |
| ERAD | endoplasmic reticulum associated protein degradation |
| EtOH | Ethanol |
| FAM | Carboxyfluorescein |
| FCS | foetal calf serum |
| FGF | fibroblast growth factor |
| GCL | ganglion cell layer |
| h | Hour |
| H&E | haematoxylin & Eosin |
| HEX | hexachloro-6-carboxyfluorescein |
| HMG | high mobility group |

| | |
|---|---|
| HSP | heat shock protein |
| ICSI | intracytoplasmic sperm injection |
| IgG | immunoglobulin G |
| ILM | inner limiting membrane |
| INL | inner nuclear layer |
| IPL | inner plexiform layer |
| IVF | *in vitro* fertilisation |
| kb | Kilobases |
| kDa | kilo Daltons |
| LMS | Lenz microphthalmia syndrome |
| LOD | logarithm (to the base 10) of odds ratio |
| LP | lens placode |
| LPS | lipopolysaccharide |
| LTBP | latent transforming growth factor binding protein |
| LV | lens vesicle |
| MAb | monoclonal antibody |
| Mb | mega base pairs |
| mg | Milligrams |
| MGI | mouse genome informatics |
| MIM | mendelian inheritance in man |
| min | minutes |
| ml | millilitres |

| | |
|---|---|
| MOPS | morpholinepropanesulfonic acid |
| mRNA | messenger ribonucleic acid |
| MRI | magnetic resonance imaging |
| *n* | number |
| NCBI | national resource for molecular biology information |
| ng | nanograms |
| NMD | nonsense mediated decay |
| NR | neural retina |
| nt | nucleotide |
| O/N | overnight |
| OAS | Ophthalmo acromelic syndrome |
| ºC | degrees centigrade |
| ODDD | oculodentodigital dysplasia |
| ONL | outer nuclear layer |
| OPL | outer plexiform layer |
| OPT | optical projection tomography |
| OS | outer segment |
| OV | optic vesicle |
| P | post-natal day |
| PAb | polyclonal antibody |
| PBS | phosphate buffered saline |
| PBT | PBS Tween-20 |

| | |
|---|---|
| PCD | programmed cell death |
| PCR | polymerase chain reaction |
| PFA | para-formaldehyde |
| pH | activity of dissolved hydrogen ions (Measurement) |
| PHA | Phytohaemagglutinin |
| PZ | proximal zone |
| RACE | Rapid Amplification of cDNA Ends |
| RGC | retinal ganglion cells |
| RNA | ribonucleic acid |
| RNAi | RNA interference |
| RPE | retinal pigment epithelium |
| rpm | revolutions per minute |
| RPMI | Roswell Park Memorial Institute |
| RT | room temperature |
| RT-PCR | reverse transcription-PCR |
| s | seconds |
| SE | surface epithelium |
| SNP | single nucleotide polymorphism |
| SRY | sex-determining region Y |
| $sdH_2O$ | sterile deionised $H_2O$ |
| TBE | Tris/borate/EDTA |
| TBS | Tris buffered saline |

| | |
|---|---|
| TBST | Tris buffered saline Tween-20 |
| TEA | Triethanolamine |
| TEM | transmission electron microscopy |
| TET | Tetracycline |
| TGF | transforming growth factor beta |
| Tm | melting temperature |
| Tn | Tunicamycin |
| $\mu$l | microlitre |
| $\mu$M | micromolar |
| U | units of specific enzyme activity |
| UMS | Ulnar-mammary syndrome |
| UPR | unfolded protein response |
| USP | United States pharmacopeia |
| VB | vitreous body |
| wt | wild type |
| x g | x gravity |
| ZPA | zone of polarizing activity |

# 2. Introduction

## 2.1. Anophthalmia and microphthalmia

Anophthalmia (absence of the eye) and microphthalmia (small eye) are congenital structural abnormalities that are typically associated with significant loss of vision that have a prevalence rate of 0.2 and 1.7, respectively, per 10,000 live births (Stoll et al., 1997). Clinically, anophthalmia is heterogeneous and refers to a complete absence of the globe in the presence of normal ocular adnexa (eyelids, conjunctiva and lacrimal apparatus). Classification can be separated into true or primary anophthalmia, secondary anophthalmia, or apparent or clinical anophthalmia. In true primary anophthalmia, there is no evidence of tissues derived from the optic vesicle; in secondary anophthalmia the orbits of the eyes may contain some remnants derived from the optic vesicles. For the criteria for these classifications to be met, scanning by CT or MRI, or post-mortem is required. Therefore, the generally accepted classification is the clinical one, which refers to the apparent absence of an eyeball from examination at birth. Microphthalmia is classified as a small ocular globe that is less than two standard deviations below the mean for that age (Bardakjian, 2007). This is typically <21mm in adult eyes, and generally requires scanning for diagnosis.

However, the classification of severe ocular malformations can also be based on the developmental programme that is interrupted and is more clinically robust than categorisation solely on the basis of eye size. Under this schema, anophthalmia results

from a disruption to events surrounding formation of the optic vesicle and the lens placode, whereas microphthalmia is more likely to result from aberrant processes that occur after these early events, and which coincide with a failure in correct retinal differentiation, lens-surface ectoderm separation, and closure of the optic fissure (Fitzpatrick and van Heyningen, 2005).

Thorough knowledge of the major morphological processes determining early stages of normal eye development, complimented with identification and understanding of the genetic pathways and factors that are critical for these events, is required to further our understanding of anophthalmia/microphthalmia pathogenesis. One useful method of identifying critical genetic factors involved in human development is to study rare mendelian syndromes. For example, understanding of the diverse functions of cell cilia during development has been enhanced through identification of the multiple gene loci mapped by studies of the genetically heterogeneous Bardet Biedl syndrome (MIM #209900), which in turn have lead to an increased understanding of the developmental pathways involved (Badano et al., 2006). This thesis describes genetic and molecular studies of a unique human anophthalmia syndrome, and a complementary mouse model, to advance our understanding of severe ocular disease.

## 2.2. Introduction to Ophthalmo acromelic syndrome

Ophthalmo–acromelic syndrome (OAS) (MIM 206920) is a rare inherited disorder characterised by the association of severe ocular malformations, most commonly bilateral anophthalmia, with symmetrical and distinct distal limb abnormalities in the 4th and 5$^{th}$ rays of the hands and, more severely, the 5$^{th}$ ray of the feet (Figure 2.2.1 and Tables 1.1 & 1.2).

**Figure 2.2.1**

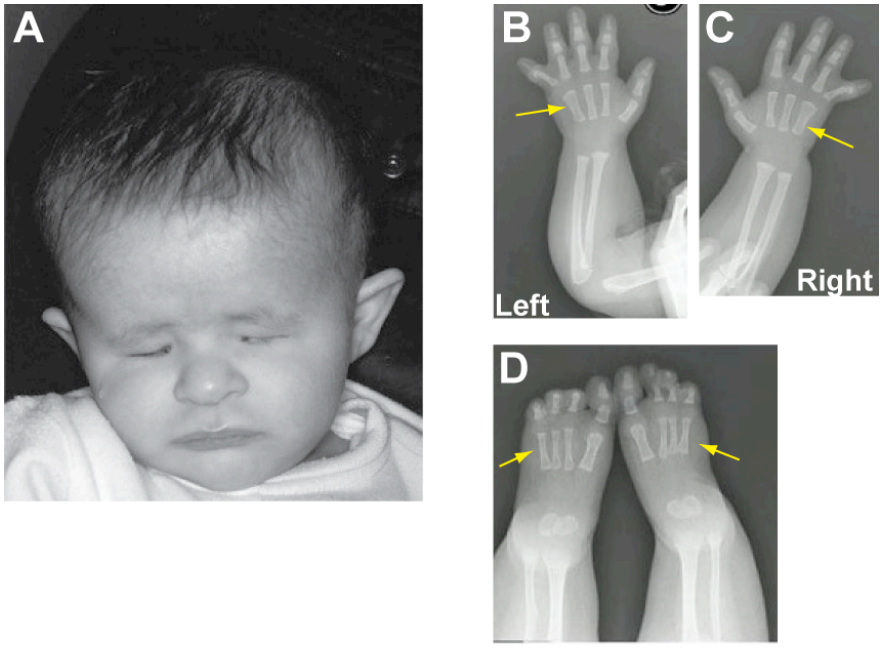


**Figure 2.2.1 Clinical features of OAS.** OAS patients characteristically present with anophthalmia but normal external ocular features (A). Forelimbs (B & C) display fused metacarpals [arrows], while hindlimbs (D) are lacking the entire fifth rays (arrows). Images used and adapted with permission from Garavelli et al., 2006.

The inheritance pattern is clearly autosomal recessive (see below) but the genetic basis of the condition is unknown. Waardenburg (Waardenburg, 1961) first described the condition as the "association of anophthalmia with anomalies of hands and feet" in two families. Subsequent reports of individuals with very similar phenotypic features led Traboulsi (Traboulsi et al., 1984) to suggest the name "Waardenburg Anophthalmia Syndrome" to describe the entity. Le Merrer (and later Al Gazali) (al Gazali et al., 1994; Le Merrer et al., 1988) argued that the title "ophthalmo-acromelia" is more appropriate as the pattern of limb malformations is very specific and, with the anophthalmia, is a defining feature of this condition. Both terms are used in the literature but in this thesis the term Ophthalmo-acromelic syndrome (OAS) is the term of choice. The total number of cases known to us is 37.

**Table 2.1. Summary of the characteristic features of OAS.**

| | | |
|---|---|---|
| **Index cases** | | **26** |
| **Sex (Ratio)** | | **11F/15M (1:1.36)** |
| **Family** | | **19** |
| **Consanguinity** | | **17 (89%)** |
| **Ocular defect** | | **26 (100%)** |
| | **Anophthalmia** | **23** |
| | Bilateral | **20** |
| | Unilateral | **3** |
| | **Microphthalmia** | **3** |
| | Bilateral | **1** |
| | Unilateral | **2** |
| **Lower limb** | | **26 (100%)** |
| | Oligodactyly | **21** |
| | Metatarsal synostosis | **10** |
| | Syndactyly | **13** |
| **Upper limb** | | **23 (85%)** |
| | Synostosis/ syndactyly | **15** |
| | Brachydactyly | **11** |
| | Camptodactyly | **9** |
| **Craniofacial** | | **7 (27%)** |
| | Retro/ micrognathia | **2** |
| | Cleft palate | **1** |
| **Other defects** | | |
| | Mental retardation | **10 (38%)** |
| | Death | **3 (12%)** |
| | *Low birth height/weight (<p25) | **13 (50%)** |
| | **Growth delay (<p25) | **9 (35%)** |
| **OAS Sibs** | | **11** |
| Family | Abortions/ miscarriages/ stillbriths | **15** |
| **OAS Total cases** | | **37** |

## 2.3. Detailed OAS phenotype description

A table of the phenotypes for all OAS cases published is presented (Table 1.2). In the first family described by Waardenburg (Waardenburg, 1961), there were two sisters with unilateral anophthalmia, one with a retinal coloboma in her cognate eye. Both had bilateral absence of the 5th ray of the foot with soft tissue syndactyly, and synostosis of the 4th and 5th metacarpals. 6/7 of their other siblings were normal, one brother had the same limb involvement but with no ocular phenotype and was thus considered as having mild OAS. The second family Waardenburg described consisted of a girl with bilateral anophthalmia, lower limb oligdactyly missing the 5th ray in both of her feet, short fingers bilaterally, and mental handicap. A younger sister was reportedly normal. These first described cases of OAS illustrated the specificity of the limb anomalies, affecting the distal-most rays of both hands and feet, while also demonstrating the severity and range of the ocular malformations.

The penetrance of ocular defects in all subsequent OAS cases published is particularly striking: 100% of 26 index cases reported (i.e. probands described in original publications) had a severe ocular phenotype, of which 20 (77%) were bilaterally anophthalmic. Anophthalmia is the most common ocular presentation in cases (88%), however some cases have been reported with a microphthalmia phenotype, and also in some multiplex families, affected sibs with limb malformations but no eye involvement have been reported. This represents a wide range in the penetrance of the ocular phenotype and suggests that although the eyes may be affected throughout the

developmental process, in the majority of cases there is a failure in formation of the optic vesicle. However, identification of optic nerve structures on scanning in some cases suggests an arrest in development after optic vesicle formation possibly coinciding with or immediately prior to lens induction. The cases with microphthalmia suggest a later defect; possibly due to aberrant proliferation of retinal progenitor cells. Coloboma has been reported in only one OAS case so far (Waardenburg, 1961). In this individual it unilateral and was associated with contralateral anophthalmia. There have been no further reports of colobomas in OAS patients since.1

The limb phenotype is variable in severity but shows a consistent pattern with significant pathology most commonly restricted to the 4$^{th}$ and 5$^{th}$ rays of the hands and feet. Of the 26 index cases all had lower limb involvement, with the majority of these being 5$^{th}$-ray oligodactyly (81%). Oligodactyly was generally reported as associated with cutaneous syndactyly of the 2-3$^{rd}$ toes, and with a "sandal" gap present between the 1$^{st}$ and 2$^{nd}$ toes. Talipes equinovarus was reported in two OAS cases from separate families (Kara et al., 2002; Richieri-Costa et al., 1983), and 4 cases had tibial bowing (Kara et al., 2002; Le Merrer et al., 1988; Richieri-Costa et al., 1983; Suyugul et al., 1996). Involvement of the upper limb was reported in 23 (85%) cases, mostly with osseous synostoses between the proximal metacarpals of the 4$^{th}$ and 5$^{th}$ rays. This was often associated with cutaneous syndactyly, brachydactyly, clinodactyly, bifid thumb and camptodatyly.

All of the cases studied in this thesis (Table 1.2), and the reported cases that are included in the review of clinical features, have been reviewed by Dr David FitzPatrick, a consultant in clinical genetics with an interest in dysmorphology. Anophthalmia and involvement of the 4$^{th}$ and 5$^{th}$ digital rays are considered cardinal features and both should be present in an affected sibship. Two cases with severe eye malformations that were reported as OAS were excluded from further consideration as they are probably misdiagnoses; one case reported with ectrodactyly and polydactyly (Quarrell, 1997) and another with polydactyly of both the hands and feet (Megarbane et al., 1998).

## Table 2.2. Key features of Published OAS cases.

| | Published Reference | | | | | | | | | | | | | | |
|---|---|---|---|---|---|---|---|---|---|---|---|---|---|---|---|
| | Waardenburg, 1961 | | | Richeria costa, 1983 | | Pallotta, 1984 | | | Traboulsi, 1984 | Le Merrer, 1988 | | | | | |
| **Index cases** | 2 | | 1 | 1 | 1 | 1 | 2 | | 1 | 3 | | | | 2 | |
| **Age at examination** | 5+Yrs | 5+Yrs | 2 Mo | 3 Mo | 6 Yrs | 9 Yrs | 9 Yrs | 9 Yrs | NEONATE | DECEASED | DECEASED | 1 Yrs | 10 Yrs | NEONATE | |
| **Sex (Ratio)** | F | F | F | M | F | M | M | M | M | F | M | F | F | M | |
| **Family** | A | | B | A | B | A | B | | A | A | | | A | | |
| **National origin** | Netherlands | | Netherlands | Brazil | Brazil | S. Italy | S. Italy | | Lebanese | Iraqi | | | Algerian | | |
| **Consanguinity** | + | | + | + | + | - | + | | + | + | | | + | | |
| **Ocular defect** | + | + | + | + | + | + | + | + | + | + | + | + | + | + | |
| Anophthal | + | + | + | + | + | + | + | + | + | + | + | | + | + | |
| Bilateral | | | + | + | | + | + | + | + | + | + | | + | + | |
| Unilateral | + | + | | | + | | | | | | | | | | |
| Microphthalmia | | | | | | | | | | | | + | | | |
| Bilateral | | | | | | | | | | | | + | | | |
| Unilateral | | | | | | | | | | | | | | | |
| **Lower limb** | + | + | + | + | + | + | + | + | + | + | + | + | + | + | |
| Oligodactyly | + | + | + | + | + | + | | | + | + | + | + | + | + | |
| Metatarsal synostosis | + | + | + | + | + | | | | + | | | | | | |
| Syndactyly | | | + | + | + | | + | + | + | | | | | | |
| **Upper limb** | + | + | + | + | + | + | + | + | | + | + | + | + | + | |
| Synostosis/ Syndactyly | | | | + | + | + | | | | + | + | + | + | + | |
| Brachydactyly | | | + | | + | + | | | | | + | | | | |
| Camptodactyly | | | | + | + | + | | | | | | | | | |
| **Craniofacial** | | | | + | | + | + | + | | + | | | | | |
| Retro/ micrognathia | | | | + | | | | | | | | | | | |
| Cleft palate | | | | | | | | | | + | | | | | |
| **Other defects** | | | | | | large incisors | Mute | Mute | Absent prepuce | Deafness | hypertrophic external genital organs | | | | |
| Mental retardation | | | + | | | + | + | + | | | | | + | | |
| Death | | | | | | | | | | 3 Mo | 3.5 Mo | | | | |
| *Low birth height/weight (<p25) | | | | + | | | + | + | + | + | + | | | | |
| **Growth delay (<p25) | | | | + | + | + | + | + | | | | | | | |
| **OAS Sibs** | 1 | | | | 3 | | | | 2 (Stillborn) | | | | | | |
| Abortions/miscarriages & stillbriths | | | | - | – | | | | 4 | | | | | | |
| **Karyotyped** | | | | | | | | | | | | + | + | + | |

## Table 2.2. Key features of Published OAS cases, continued.

| | Publsihed References | | | | | | | | | | | |
|---|---|---|---|---|---|---|---|---|---|---|---|---|
| | Al Gazali, 1994 | Sayli, 1995 | | Suyugul, 1996 | | | Tekin, 2000 | Cogulu, 2000 | Kara, 2002 | Casken, 2002 | Garavelli, 2007 | Teiber, 2007 |
| **Index cases** | 1 | 2 | | 2 | | 1 | 1 | 1 | 1 | 1 | 1 | 1 |
| **Age at examination** | 8 Mo | 14 Yrs | 7 Yrs | 6 Yrs | 2 Yrs | 11 Yrs | NEONATE | 8 Yrs | NEONATE | NEONATE | NEONATE | 1 yr |
| **Sex (Ratio)** | M | M | M | F | F | M | M | F | M | M | M | F |
| **Family** | A | A | | A | | B | 1 | A | A | A | A | A |
| **National origin** | Syrian | Turkish | | Turkish | | Turkish | Turkish | Turkish | Turkish | Turkish | Italian | Argentinian |
| **Consanguinity** | + | + | | + | | + | + | + | + | + | + | - |
| **Ocular defect** | + | + | + | + | + | + | + | + | + | + | + | + |
| Anophthal | | + | + | + | + | + | + | + | + | + | + | |
| Bilateral | | + | + | + | + | + | + | + | + | + | + | |
| Unilateral | | | | | | | | | | | | |
| Microphthalmia | + | | | | | | | | | | | + |
| Bilateral | | | | | | | | | | | | |
| Unilateral | + | | | | | | | | | | | + |
| **Lower limb** | + | + | + | + | + | + | + | + | + | + | + | + |
| Oligodactyly | + | | | + | + | + | + | + | + | + | + | |
| Metatarsal synostosis | | + | | + | + | + | | | | | | |
| Syndactyly | | + | + | + | + | + | | | | | + | + |
| **Upper limb** | + | + | + | + | + | + | + | + | | | + | + |
| Synostosis/ Syndactyly | + | | | + | + | + | + | + | | | | + |
| Brachydactyly | + | + | + | + | + | + | + | | | | | |
| Camptodactyly | | | | + | + | + | + | | | | + | + |
| **Craniofacial** | | | | | | | + | | | | | + |
| Retro/ micrognathia | | | | | | | + | | | | | |
| Cleft palate | | | | | | | | | | | | |
| **Other defects** | | | | Mute | | | Absence of inferior vena cava (liver level) | | one umbilical artery | | Horseshoe Kidney | Cervical fusion & spinal hemivertebrae |
| Mental retardation | + | | | + | + | + | | | | | | + |
| Death | | | | | | | | | + | | | |
| *Low birth height/weight (<p25) | | | | + | + | + | + | + | | | + | + |
| **Growth delay (<p25) | | + | | + | | + | | + | | | | |
| **OAS Sibs** | | 1 | | | | | | | 1 | 3 | | |
| Abortions/miscarriages & stillbriths | | | | 2 | | | 4 | | | 1 | | |
| **Karyotyped** | + | + | | + | + | + | + | + | + | | + | + |

Neurological developmental abnormalities have been described in 10 OAS cases (38%), ranging from severe psychomotor retardation and very poor communication skills to slightly delayed motor development in comparison to an unaffected sib. The data on neurocognitive impairment in OAS should be considered preliminary as many cases have been only examined during infancy, when accurate assessment of cognition is difficult. Another feature of this condition is early post-natal death, which has been reported to occur in 12% of index cases and 8 siblings retrospectively diagnosed with OAS, together totalling 29 % of all OAS cases. Most OAS deaths occurred as infants (less than 1 year old) with the causes of deaths largely unspecified further than as: "sudden" (e.g. after feeding time) (Le Merrer et al., 1988) or from a "failure to thrive"(Richieri-Costa et al., 1983), while others died as a result of apparently treatable infections. There is also a report of stillbirths occurring in 2 OAS siblings (Richieri-Costa et al., 1983), and further reports of multiple early-miscarried pregnancies in families with OAS cases. Low birth weight (<p25) was reported in 50% and growth delay (<p25) was observed in 35% of OAS cases.

A characteristic facial appearance has been suggested with a prominent forehead; short or slanting palpebral fissures, flat maxillary regions, long and wide philtrum, flat nasal bridge, thick-lobed and angulated ears, and flared nostrils. Some of these are secondary to the anophthalmia and are not specific. Isolated cleft palate has been described in a single patient.

Moderate deafness and two cases of mutism have been reported. Large incisors have been noted as has an absent prepuce. Recently diagnosed patients have had additional features, including: horseshoe kidney, absence of interior vena cava, a single umbilical artery, cervical fusion and spinal deformities.

## 2.4. Inheritance of OAS

An autosomal recessive pattern of inheritance for OAS has been suggested on the basis of definite or probable consanguinity in 17/19 families (89%). Many individuals had affected sibs within the same generation and no vertical transmission has been observed. This pattern of inheritance is also supported by the lack of any reported cytogenetic abnormalities where karyotypes have been analysed ($n$=13) and also by the observation that both males ($n$=15) and females ($n$=11) were similarly affected. There have been no reports of maternal illness, substance abuse, or exposure to teratogens, pathogens or radiation during pregnancy, and pregnancies have been generally described as ‘uneventful’.

The reported cases are from a limited number of ethnic backgrounds, with the majority being either Turkish ($n$=9, 7 families) or from Arabic countries ($n$=7, 4 families). There have also been three families from Italy ($n$=4), two from the Netherlands ($n$=3), two from Brazil ($n$=2), and one from Argentina ($n$=1).

## 2.5. Differential Diagnosis of OAS

Anophthalmia and microphthalmia have a combined birth incidence of ~1 per 10,000 (Morrison et al., 2002). Associate malformations are relatively common in severe eye abnormalities; however, distal limb anomalies and specifically post-axial oligodactyly are very rare. Thus OAS is a relatively easy condition to diagnose and there are few conditions that can be considered in a differential diagnosis.

Oculodentodigital dysplasia syndrome (ODDD) (MIM#164200) is characterized by microphthalmia or microcornea with upper limb cutaneous postaxial syndactyly. A common feature of ODDD is hypoplasia or aplasia of the middle phalanx of those toes that normally have three phalanges (digits 2-5). Nasal and dental dysmorphisms are characteristic in this condition.

Lenz microphthalmia syndrome (LMS) (MIM 309800) is an X-linked recessive disorder presenting anophthalmia and microphthalmia, but also involving mental handicap, urogenital abnormalities, microcephaly, external ear, cardiac, dental and skeletal anomalies. However, there are currently no reports of syndactyly or oligodactyly in LMS.

Isolated postaxial tetramelic oligodactyly (MIM 176240) is a yet unmapped autosomal dominant, non-syndromic congenital abnormality where the 5$^{th}$ metatarsals and metacarpals are absent.

In Ulnar-Mammary Syndrome (MIM #181450), postaxial limb defects range from hypoplasia of the terminal phalanx of the 5$^{th}$ digit to total absence of forearm and

hand. UMS can be caused by mutations in the *TBX3* gene (Bamshad et al., 1999), but no ocular deformities have so far been reported.

Miller syndrome cases (MIM %263750) present with post-axial oligodactyly of both hands and feet, together with cleft palate, retrognathia and renal anomalies, features which overlap with the clinical spectrum of OAS. Nevertheless, there are no ocular phenotypes associated so far with this autosomal recessive syndrome.

Another syndrome affecting the post-axial rays is Pallister-Hall syndrome, caused by loss of function mutations in the *GLI3* gene (Kang et al., 1997). Postaxial polydactyly is a defining feature of this condition and ocular anomalies are not generally reported.

In Tukel syndrome (MIM %609428), mapping to chromosome 21q22, patients have postaxial oligodactyly highly similar to the oligodactyly seen in the feet of OAS patients, namely the complete absence of postaxial rays. However, they do not present with a hind limb phenotype and furthermore the ocular findings are mild, with ophthalmoplegia and blepharoptosis (ocular muscle failure and droopy eyelids, respectively) the main features.

Therefore, the association of severe ocular malformations with postaxial oligodactyly is extremely rare and it is the association anophthalmia with such a consistent and distinctive distal limb abnormality, bilateral postaxial foot oligodactyly, which is particularly intriguing in OAS, suggesting there are common pathways or genetic mechanisms in the development of the two distinct fields and that the genetic

lesion(s) in OAS patients contributes significantly to both developmental programmes. This condition therefore warranted genetic and molecular investigation.

## 2.6. Utility of mouse models for human developmental diseases

Although the human genome project is now complete, the developmental function of many genes remains largely unknown. Additionally, many human developmental abnormalities have not been ascribed to mutated genes or genomic lesions. These situations are mainly associated with the general rarity of many interesting developmental diseases, a paucity of tissue samples and problems gaining sufficient DNA quantities for effective mapping strategies. In addition, there is a lack of *in situ* molecular information as a result of appropriate ethical constraints of working with human samples and subjects. Nevertheless, human genetic analysis of individuals and families segregating severe eye and limb malformations has identified mutations in several developmentally regulated genes that have furthered our understanding of their underlying developmental processes. Inevitably however, much of our knowledge of the mechanisms involved in embryonic development has come from animal models, with the laboratory mouse contributing vast amounts of data and often the model of choice for understanding the molecular mechanisms in vertebrate eye and limb development. Human and mouse eyes are very similar, and share many structural and functional similarities in their ocular systems throughout both development and adulthood.

In both species, genes share common interacting partners at the protein level and are located in homologous chromosomal segments, with most genes being highly conserved at the sequence level due to similar selection pressures. In addition, the mouse provides other benefits to research of genetic diseases: inbred strains of the laboratory mouse are available to facilitate genetic mapping strategies using identical genetic backgrounds behind the disease locus; animals can be kept under uniform conditions to reduce the effects of environment of gene expression; tissue samples can be easily collected, stored, processed and manipulated; large pedigrees can be generated over short periods of time; and of huge importance, a wealth of genetic and molecular information is already available to researchers, while genes can also be specifically inactivated or can be non-specifically targeted by various different types of mutation screens.

## 2.7. The *Mp* mouse as a model for human OAS

The *Mp* mouse line (MGI 97070; Micropinna Microphthalmia) was generated in a screen for radiation-induced mutations at Oak Ridge National Laboratory by X-ray irradiation. It was described (Phipps, 1964) as:

*"Dominant mutation affecting eyes, external ears and feet. This mutation appeared in the offspring of an irradiated male. Heterozygotes invariably have Microphthalmia and often, in addition, reduced pinnae. Homozygotes appear to be eyeless and have oligodactyly of the hind feet (usually 3 toes, occasionally 4). They are of very small size and most die around 12 days of age; none has survived to weaning. The pinnae is pesent and probably reduced in size, but, because of the early death, no accurate comparisons to heterozygotes can be made in this respect."*

The phenotypic features of this line overlap with human OAS, namely apparent anophthalmia or microphthalmia associated with hindlimb oligodactyly. This line was not being managed as active colonies and samples of sperm had been stored from affected heterozygote males. Therefore, the *Mp* mouse line was rederived for mutation and phenotype analysis in Edinburgh for the present study for genetic mapping and molecular analysis.

## 2.8. Vertebrate eye development

### 2.8.1. Key morphogenetic events during eye development

Mammalian ocular development can be divided into five distinct morphological events: (i) formation and outgrowth of the optic vesicle, (ii) lens induction and optic cup invagination, (iii) lens and retinal differentiation, (iv) anterior chamber formation and (v) formation of the periocular structures.

Around the end of the third gestational week in human development and ~E8.0-9.0 in the mouse, bilateral and symmetrical evaginations of neuroepithelium appear on the lateral aspects of the anterior prosencephalon and grow towards the overlying surface ectoderm of the primitive head. These structures, the optic vesicles, make contact with the surface ectoderm in regions that are visible externally as the optic eminences at around Carnegie Stage 12 (CS12 & ~E9.5 in mouse). Contact between the neural ectoderm and surface ectoderm results in a local thickening of the surface ectoderm to form the lens placode. The placode begins to invaginate forming the lens pit, which is visible at the surface ectoderm, and then finally separates from the surface ectoderm to form the lens vesicle at CS15, or E11.5. A simultaneous conformational change in the underlying optic vesicle forms the optic cup. This is the result of invagination of the optic vesicle occurring primarily in medial and ventral regions, with these tissues destined to become neural retina and optic nerve, respectively. The dorsal optic vesicle will become the outer layer of the optic cup, which develops into the

retinal-pigmented epithelium (RPE) distally and proximally will envelop the optic nerve after closure of the optic fissure along the proximal-distal axis of the developing eye. Lens and retinal differentiation occur concomitant with closure of this fissure. The primitive lens buds off from the surface epithelium to form an independent hollow vesicle structure. The cells within the vesicle undergo differentiation into lens-specific cells and the vesicle is then filled-in by the elongation and maturation of lens cells. Cellular organelles are then cleared from the lens cells to create the clear and functional lens. The highly organised multilayered mature retina containing the photoreceptors and their auxiliary cells develops from the region of neural retina that was in intimate contact with the placodal surface ectoderm at CS12-14. Dividing mitotic cells are maintained in their progenitor state in the morphologically developing optic cup to create sufficient cell numbers to supply all of the layers required in the mature retina. Periodically, the environment of intrinsic and extrinsic factors is mutually convivial for subsets of these cells to undergo specific differentiation, a process that ultimately provides the retina with the full complement of cell types.

Further development of ocular structures such as cornea, anterior chamber, iris, and the ciliary processes occurs at later stages and is dependent on contributions from cell types of various origins and requires normal development of the lens.

### 2.8.2. Genes involved in early optic development and implicated in major ocular malformations

Mutations in various genes have been identified as causative for anophthalmia and microphthalmia (Table 2.3). All of these genes encode transcription factors and the successful activation or repression of their transcriptional targets requires the cooperation of multiple binding partners to facilitate either an inductive or repressive response. They are expressed in many ocular tissues throughout the various stages of eye development, often within overlapping domains. Additionally, they probably operate as critical components of a complex network involving multiple feedback loops to ensure exquisite control of their own and each-others expression in a spatially and temporal specific manner.

| Gene | Locus | Inheritance | Human phenotype | Expression |
|---|---|---|---|---|
| *PAX6* | 11p13 | Haploinsufficient | Aniridia/ Peter's anomaly | EF; OV; LP; LV; NR; CN |
| *SOX2* | 3q26 | Haploinsufficient | Anophthalmia/ Microphthalmia | LP; LV; NR; CN |
| *RX* | 18q21 | Recessive | Anophthalmia/ Microphthalmia | EF; OV; NR |
| *OTX2* | 14q21 | Haploinsufficient | Anophthalmia/ Microphthalmia/ Retinal defects | OV; RPE; NR |
| *CHX10* | 14q24 | Recessive | Microphthalmia/ cataracts/ Iris abnormalities | OV; NR |
| *MAF* | 16q23 | Dominant | Microphthalmia/ Lens, Iris & Anterior Segment abnormalities | LV; LP |
| *BCOR* | Xp11 | X-linked/ Dominant | Lenz Microphthalmia Syndrome / Oculofaciocardiodigital Syndrome | Retina; Lens |

**Table 2.3. Genes involved in severe ocular malformations**. CN, cornea; EF, eye field; LP, lens placode; LV, lens vesicle; NR, neural retina; OV, optic vesicle; RPE, retinal pigmented epithelium.

Therefore the exact embryopathological mechanisms for severe ocular pathologies involving these genes are obscured. Superficially, it could be assumed that disruption to the function of those genes expressed at early stages, such as in the eye field or in the optic vesicle or lens placode, results in the most severe disorders of anophthalmia or microphthalmia. However, expression of mutant genes within the proliferating or differentiating retina, or in the RPE or developing lens vesicle, may also lead to equally severe malformations. The genes so far implicated in anophthalmia or microphthalmia are discussed below.

*OTX2* is a homeodomain containing transcription factor of the bicoid class, whose expression precedes expression of other eye transcription factors (Chow and Lang, 2001). Although *OTX2* expression disappears from the eye field, expression in the anterior neural plate prior to gastrulation suggests a role in neural induction. *OTX2* expression is subsequently activated in the dorsal region of the optic vesicle, then becoming refined to the developing RPE. Heterozygous loss-of-function mutations result in a range of severe ocular malformations, ranging from anophthalmia and microphthalmia to retinal defects, often associated with learning disability and brain defects (Ragge et al., 2005). Impaired retinal function is a universal phenotype in *OTX2* mutations, and suggests a major role in retinal differentiation, which may be the cause of anophthalmia if ablated during early stages (Fitzpatrick and van Heyningen, 2005).

The paired box gene 6, *PAX6*, has multiple roles in the development of the vertebrate eye and was the first gene to be identified as disrupted in human anophthalmia (Glaser et al., 1994). Subsequently, *Pax6* has been described as the *master regulator* for eye development, with *Pax6* expression and transcriptional targets identified in a wide range of tissues and processes; in the establishment and outgrowth of the eye field, patterning the optic vesicle and the presumptive neural retina, in RPE development, neural retina layer specification and differentiation, and in the formation of the lens pit, placode, vesicle and mature lens. Biallelic mutations in humans are rarely found in *PAX6* as they are anophthalmic but lethal, however haploinsufficiency results in the highly penetrant Aniridia and Peter's Anomaly, both significant ocular defects (van Heyningen and Williamson, 2002). Loss of *Pax6* in the mouse causes the *small eye* (*Sey*) phenotype in heterozygotes (Hill et al., 1991) and anophthalmia with lethality in *Sey*/*Sey* homozygotes (Grindley et al., 1995).

*RX* (or *RAX*) is another homeodomain-containing transcription factor and is the first retinal patterning gene to be expressed during eye development where it specifically marks the eye field in the anterior neural plate. Continual expression is observed in the optic vesicles and the neural retina throughout ocular development. Human haploinsufficiency for *Rx* has results in anophthalmia or microphthalmia (Voronina et al., 2004) and recessive loss of function in the mouse results in bilateral anophthalmia, as a result of failure to form optic vesicles (Mathers et al., 1997). Loss of *Rx* in the

mouse eye field results in a failure of *Pax6* expression, indicating *Pax6* is downstream of *Rx* and is dependent of *Rx* expression (Chow and Lang, 2001).

Heterozygous loss of function mutations in *SOX2*, a HMG domain-containing transcription factor, have been reported as the cause of between 10-20% of human anophthalmia and severe microphthalmia cases, with most cases presenting with bilateral anophthalmia (Fantes et al., 2003; Ragge et al., 2005). These are commonly deletions, translocations and point mutations, consistent with haploinsufficiency for the SOX2 protein during ocular development, where either loss of function mutations or the presence of a single allele result in the same phenotype.

In mice, a gene-dosage allelic series of *Sox2* mutations has confirmed the requirement for *Sox2* during eye development (Taranova et al., 2006). SOX2 synergistically activates the expression of other eye-development genes in different regions of the eye anlagen, depending on the binding partner. In the developing chick lens, Sox2-Pax6 binding activates developmental expression of crystallin genes (Kamachi et al., 2001), while the cooperative binding of Sox2 to Otx2 at a conserved non-coding sequence upstream of the *Rx* promoter can synergistically activate *Rx* gene expression (Danno et al., 2008).

*CHX10* is expressed in the neural retina in development and in the inner nuclear layer in adult eyes. Specific expression in the presumptive neural retina during contact of the optic vesicle with the lens placode contributes to the proliferation of retinal

progenitor cells. Recessive loss of function resulting from missense changes in the homeodomain of this transcription factor cause human microphthalmia, cataracts and abnormal iris development (Ferda Percin et al., 2000). In the mouse, mutations in *Chx10* cause the *ocular retardation* phenotype (*or*), characterised by blindness, microphthalmia, cataracts and an absence of the optic nerve (Burmeister et al., 1996). The poorly differentiated retina in the *or* mouse is explained by a reduction in the proliferation of retinal precursor cells. Mutations in mouse and human *CHX10* therefore reflect the potential for retinal dysgenesis after the optic vesicle stage to cause microphthalmia.

The *BCOR* gene is a key transcriptional regulator during early embryogenesis and mutations result in Lenz microphthalmia and Oculofaciocardiodental syndromes, both X-linked pattern of inheritance and characterised by severe ocular malformations (Ng et al., 2004). Knock-down of the *Bcor* orthologue in zebrafish caused developmental anomalies consistent with these syndromes. In the developing mouse eye, *Bcor* expression is not obvious until after E11.5, where it is identified in the retina and lens tissues (Wamstad and Bardwell, 2007), temporally coinciding with the differentiation of these tissues.

Mammalian *MAF* genes are involved in lens induction and differentiation and loss of function by a point mutation in a DNA binding domain in the mouse results in defective lens formation and microphthalmia (Lyon et al., 2003). *MAF* genes are

expressed in lens placode, lens vesicle and within the differentiating lens. Distant translocations affecting genomic control regions of the *MAF* locus in humans are associated with microphthalmia, together with other ocular deformities affecting the lens, anterior segment and iris, which can also arise from dominant intragenic missense mutations (Jamieson et al., 2002).

Most of these transcription factors continue to be expressed within the neuroectoderm as the optic vesicles grow and come into contact with the overlying surface ectoderm and then differentiate into optic stalk, RPE and neural retina structures.

### 2.8.3. Patterning within the optic vesicle

The highly organised laminar structure of the mature retina is closely dependent on the correct position and organisation, and therefore the subsequent differentiation and migration of different cell types during neural retina development. Additionally, the RPE and optic stalk must be specified in the dorsal and ventral regions of the optic vesicle, respectively. Formation of a correctly oriented and patterned optic vesicle is therefore fundamental to normal ocular development. This process requires permissive gradients of morphogens to pattern the optic vesicle along opposing axes and the localised expression domains and boundaries of specific transcription factors to specify the neuroectoderm to differentiate into distinct regions of RPE, optic stalk and neural retina. Understandably, failure in this process can result in severe ocular malformations.

Ventral morphogenic signals, such as Sonic hedgehog (Shh), retinoic acid and noggin act to pattern the optic stalk through transcription factors *Vax2* (*ventral anterior homeobox 2*), *Pax2* (*paired box like transcription factor 2*), whereas *Pax6* expression in the presumptive RPE and neural retina is a consequence of dorsally expressed *Bmp4* (Chow and Lang, 2001).

*Vax2* is almost exclusively expressed in the ventral part of the optic vesicle during early mouse and human ocular development and is vital for dorsal-ventral axis determination in the optic vesicle (Barbieri et al., 1999; Kim and Lemke, 2006). *Vax2* overexpression in *Xenopus* optic vesicle leads to a ventralisation of the eye, including an expanded optic stalk, and a dorsalisation of *Pax2* expression with a reduction in dorsal markers (Barbieri et al., 1999). No human ocular malformations have yet been described linked to mutations in *Vax2*. Human loss of function mutations in *Pax2* cause optic nerve colobomata, a failure of correct optic fissure closure, while in mice, a range of mutations cause various optic nerve abnormalities (Barbieri et al., 1999; Favor et al., 1996; Torres et al., 1996). Additionally, the optic nerve closure defect colobomata occurs in *SHH* mutations, indicating an upstream role in *Pax2* expression regulation (Schimmenti et al., 2003)

An opposing gradient of Bmp4, a member of the transforming growth factor beta family of signaling molecules, emanating from the dorsal-distal optic vesicle, determines a Pax6-positive region encompassing future RPE (dorsal) and neural retina (central).

Overexpression of *Bmp4* in the optic vesicle expands the *Pax6* expression domain at the expense of repressed *Pax2*. Phenotypically, this results in the extension of RPE into the presumptive forebrain regions and an absence of the optic stalk (Sasagawa et al., 2002). Additionally, expression of the constitutively active nuclear form of *Vax2* in optic vesicles repressed *Pax6* expression and resulted in eyeless chick embryos (Mui et al., 2005).

### 2.8.4. Lens induction and development

The vertebrate lens develops from surface ectoderm in a process triggered by its intimate contact with optic vesicle. Initially, all head surface ectoderm is thought to be competent for lens development, but with a subsequent reduction to the areas over the outgrown optic vesicles. The surface ectoderm and optic vesicle both thicken at their respective regions of contact, with the presumptive lens region becoming a "placode" of tissue specific for lens fate. This represents the first morphologically identifiable stage of lens development and is visible by the end of the fourth week (CS12; ~ E9.0-9.5 in mouse).

The presumptive lens begins to invaginate and initiates the process of lens-specific cell differentiation. It buds off from the surface ectoderm, leaving a discrete hollow lens vesicle beneath the now intact surface ectoderm (the future cornea). Cells at the proximal pole of the lens, closest to the neural retina, differentiate into primary lens fibre cells and elongate to fill the entire lens lumen, while epithelial cells at the

equatorial region, or lens bow, simultaneously differentiate and elongate into the secondary lens fibres, migrating inwardly and increasing the size of the lens. The anterior cells in the lens vesicle persist as a single layer of undifferentiated stem cells that 'feed' the secondary lens cell population throughout this lens growth and throughout adult life.

### 2.8.5. Molecular aspects of early lens development

*Pax6* is essential to lens induction and functions throughout lens development and its expression in the SE is necessary for lens development in vertebrates (Chow and Lang, 2001). Initially *Pax6* is expressed throughout the head ectoderm during the period of lens forming bias, but then becomes spatially restricted to the region overlying the OV during the period of initial contact between the two tissues (Grindley et al., 1995). This initial pre-placodal *Pax6* expression is followed by a second wave of expression, apparently via autoregulation. *Pax6* expression, together with expression of the *Meis* family of transcription factors, *Bmp7*, and *Fgf* signaling, define the pre-placodal stage of lens induction (Lang, 2004). *Sox2* is expressed in the pre-placodal ectoderm, but at very low levels. Up-regulation of Sox2 expression is achieved through action of Bmp4 (Furuta and Hogan, 1998). Its activation is required for the expression of crystallin genes later in the lens anlage by forming a complex with its DNA-binding partner, Pax6 (Kondoh et al., 2004).

The presence of Sox2 and Pax6 proteins together in the nuclei of surface epithelial cells defines the placodal stage of lens development. Their combined presence is necessary for the expression of *crystallin* genes, which is a characteristic feature of this stage of lens development. Crystallin genes are vital for lens development and function, with mutations often the cause of lens opacities (Graw, 2003).

Placodal *Pax6* up-regulation enhances the already increased expression of *Sox2* in the lens placode (Chow and Lang, 2001). The cooperative binding of Pax6 to its binding partners regulates the expression of lens-specific differentiation genes. Such binding is both sufficient and necessary to produce lens differentiation in the placode (Kondoh et al., 2004). Although the delta crystallin gene is not present in mouse, the alphaA-crystallin promoter is composed of multiple Pax6 and Maf binding sites and its activation is regulated by recruitment of these factors, while disruption of these sites results in reduction of promoter activity in lens cells (Yang and Cvekl, 2005).

Other transcription factors vital for lens development are expressed in the developing lens; *Six3* is expressed in the presumptive lens in mouse and chick and persists in epithelial cells during differentiation stages. Mice that do not express *Pax6* are deficient in *Six3* expression. *MAF* transcription factors are also expressed in the lens placode, the lens vesicle and, later, in the primary lens fibres, and are important for the expression of *Crystallins*. Mutations in *MAF1* have been associated with opacities in the lenses of both humans and mice (Graw, 2003; Lyon et al., 2003). The forkhead family

gene *FoxE3* is expressed in the presumptive lens SE throughout lens induction. *FOXE3* mutations in humans cause anterior chamber malformations. Analysis of the enhancer element in the chick delta-crystallin gene identified that, in addition to Sox2, Sox1 can also form a complex with Pax6 and bind to the control region of DNA, resulting in the initiation of crystallin expression. *Sox1* is expressed in the developing lens in both mouse and chick. It is active in the developing lens pit and its deletion in mouse causes microphthalmia, consistent with an important role in lens development, perhaps through vesicle closure (Nishiguchi et al., 1998).

### 2.8.6. Differentiation of the neural retina

The fully differentiated adult retina is a highly organised and laminated structure of photoreceptors, auxiliary neurons and glial cells. The molecular mechanisms and temporal sequence of events involved in retinal differentiation appear to be well conserved among vertebrates, beginning in the mouse at around E13.5-14.5 and continuing until approximately postnatal day 21 (Chow and Lang, 2001; Hatakeyama and Kageyama, 2004). In humans, the differentiation process in the neural retina begins to occur at around week 6 and continues until the first month after birth.

For correct retinal development, neuroectoderm of the primitive neural retina in the optic vesicle becomes directly apposed to the lens placode and neuroblastic cells begin to proliferate. This region of multipotent cell proliferation is highly positive for *Sox2* and *Chx10* expression. The contact between lens placode and optic vesicle triggers

invagination of the optic cup and the development of the neural retina distinct from the optic stalk and the RPE (Chow and Lang, 2001).

Correct differentiation of the multipotent retinal progenitors involves the interaction of specific homeodomain transcription factors with basic helix-loop-helix (bHLH) transcriptional regulators to establish temporal and spatial microenvironments of permissive factors for specific cell-type differentiation (Hatakeyama and Kageyama, 2004). Repressive bHLH inhibit bHLH activators to maintain retinal progenitors, while bHLH activators interact with homeodomain factors to promote differentiation into the required cell type. Each retinal cell type therefore has a unique bHLH and transcription factor combinatorial code.

Initially, *SOX2* expression maintains proliferation in the ventricular zone of the neural retina and is widely expressed in neural progenitors. Closely related *SOX* transcription factors are markers for neural progenitors throughout the vertebrate CNS where they prevent the differentiation of neural progenitors by counteracting the effects of the proneural bHLH factors (Bylund et al., 2003; Graham et al., 2003). Hypomorphic mutations in mouse *Sox2* result in the loss of RGCs and cause disrupted cell lamination within the neural retina. The decreased levels of Sox2 are associated with reduced expression of anti-proneural genes, while bHLH activators are up regulated, concomitantly with *Pax6* expression (Taranova et al., 2006). As retinal progenitors begin to differentiate, *Sox2* is down regulated, with the only cells that retain *Sox2*

expression in the fully differentiated retina being displaced amacrine cells within the GCL (Taranova et al., 2006).

Within the differentiating INL, multiple transcription factors define the layer specification, while the expression of specific combinations of bHLH genes defines the neuronal cell type within that layer. *Chx10* is required for bipolar cell fate, while horizontal cells require *Pax6* and the forkhead-family transcription factor, *Foxn4* (Li et al., 2004), and the combined expression of *Pax6* and *Six3* is required for amacrine cell differentiation (Inoue et al., 2002). Muller glial cells are the last to differentiate and are characterised by the continued expression of bHLH repressors until ~P10 in the mouse (Hatakeyama and Kageyama, 2004). In the outer nuclear layer (ONL), rod and cone photoreceptors require the combined expression of *Crx* and *Otx2*. *Crx* is necessary for normal cone and rod function and is implicated in human photoreceptor degeneration and Leber's Congenital Amaurosis (LCA; MIM#602225). It binds to the promoter sequences of several additional photoreceptor-specific genes. In mice, *Crx* expression is observed in both developing and mature photoreceptor cells and in *Crx*-null mice, abnormal photoreceptors are formed (Morrow et al., 2005). *Otx2* can also promote photoreceptor development (Hatakeyama and Kageyama, 2004) and is essential for photoreceptor cell fate determination. Deficiency of *Otx2* leads to a conversion of differentiating photoreceptors to amacrine-like neurons (Nishida et al., 2003). Additionally, binding sites for *Otx2* are found in the mouse *Crx* promoter, and *Otx2*

transactivates *Crx* (Nishida et al., 2003), providing evidence that *Otx2* is a direct upstream regulator of *Crx* and thus a key regulator of photoreceptor development.

### 2.8.7. Development & developmental function of the RPE

The developing RPE is essential for the correct morphogenesis of the neural retina and is important in maintaining the organization of neural cell layers during later stages of development. Disruption of the RPE in early developmental stages results in disorganization of the neural retina and an arrest of eye development causing anophthalmia or severe microphthalmia (Raymond and Jackson, 1995). Microphthalmia associated transcription factor, *Mitf*, a basic helix-loop-helix leucine zipper family gene, is expressed in the future RPE in both mouse and chick. Missexpresion studies in both species result in aberrant RPE phenotypes (Martinez-Morales et al., 2004), while mutations in *Mitf* cause microphthalmia in the mouse *mi* mutant, resulting from defects associated with the RPE layer of the optic cup (Graw, 2003).

### 2.8.8. The importance of ciliary body development

The ciliary body has become of great recent interest in the field of eye development. Not only is it vital as a foundation for the correct formation of iris, trabecular meshwork and the zonules connecting the ciliary muscles to the lens, but also it is thought to synthesise the major constituents of the vitreous body (Bishop et al., 2002; Ihanamaki et al., 2004). Additionally, further focus has been warranted due to the identification of retinal stem cell population within the non-pigmented ciliary body in

various organisms (Kubo and Nakagawa, 2008). Finally, an additional role as a signaling centre to promote and maintain correct lamination of the neural retina during development and growth has also been identified (Cho and Cepko, 2006; Nakagawa et al., 2003).

### 2.8.9. Development of the ciliary body

At the distal most edge of the adult retina, and directly apposed to the lens, is the ciliary body. It has three main functions during development and adult life: (i) secretion of aqueous humour; (ii) maintenance of intraocular pressure; and (iii) accommodation of the lens. The ciliary body is composed at its interior of ciliary muscles and stroma, while at the exterior are the pigmented and unpigmented layers of the ciliary epithelium. The pigmented layer lies between the RPE and the outer iris. The non-pigmented ciliary epithelium is continuous with the neural retina and the iris stroma, and secretes the aqueous humour constituent molecules. The aqueous humour then exits the eye through the trabecular meshwork, which is positioned in the 'angle' of the eye at the junction between cornea and iris. This process is vital for the maintenance of intraocular pressure. At the region adjacent to the lens, the ciliary epithelium is extensively folded in to create the ciliary processes. At the tips of these processes are the zonular fibres, suspensory ligaments connected to the lens, which facilitate the process of lens accommodation in conjunction with the action of the ciliary muscles.

The ciliary epithelium differentiates from the two layers of neuroepithelial cells at the distal rim of the optic cup (Beebe, 1986). The optic cup 'rim' is created by the inward folding of the neural retina that forms the inner and outer layers of neuroectoderm destined to become neural retina and RPE, respectively. The differentiation of the ciliary body is a relatively late event in eye development, with morphologically identifiable structures not developing until E18.5 and continuing until postnatal stages in the mouse. However, specification and patterning occur much earlier in development. Failure in correct development of the ciliary body may result in ocular malformations, possibly resulting in microphthalmia if dysgenesis occurs early during its development (Beebe, 1986).

Molecular aspects of ciliary body development are now beginning to be understood. While the rest of the neural retina undergoes separate differentiation programmes, repression of neuronal differentiation in the presumptive ciliary epithelium is maintained by elements of the Wnt/beta-catenin pathway (Cho and Cepko, 2006; de Iongh et al., 2006; Kubo et al., 2005). Canonical Wnt activity was identified in the peripheral retina in mice, and Wnt2b was identified as the likely ligand (Liu et al., 2003). Specifically, in chick embryos, *Wn2b* is identified in the distal optic cup and determines peripheral fates (ciliary body and iris) in the eye. *Wnt2b* and *Lef1* expression are not typically identified in the central neural retina, however activation of canonical Wnt signaling by a constitutively active beta-catenin induced expression of ciliary markers *collagen* IX and *Bmp7* and inhibited neuronal differentiation (Cho and Cepko,

2006). Ectopic expression of mouse *Wnt2b* in central chick retina resulted in folding reminiscent of ciliary epithelium, associated with the inhibition of retinal markers *Notch1* and *NF-M*, and the expression of the ciliary markers *collagen type IX* and *Pax6* (Cho and Cepko, 2006; Kubo et al., 2003). Additionally, inhibition of Wnt signaling in the peripheral retina resulted in precocious differentiation into retinal ganglion cells, whereas in wild types, cells in the presumptive ciliary region proliferate over longer periods than cells in the central retina (Cho and Cepko, 2006; Kubo et al., 2003).

Expression of the signaling molecules *Bmp4*; *Bmp7*, together with the transcription factors *Msx1* and *Otx1* are also specifically identified in the normal developing ciliary epithelium. *Otx1* null mice fail to develop ciliary body (Acampora et al., 1996), and the expression of these transcription factors are responsive to changes in *Bmp* signaling (Zhao et al., 2002). However, evolutionary conserved signals emanating from the lens are also thought to be vital for differentiation within the ciliary epithelium and induced removal of lens signals results in inhibition of iris and ciliary body formation (Beebe, 1986). It has been shown that the lens produces currently unknown instructive signals that induce the development of iris and ciliary body (Thut et al., 2001). Fgfs are good candidates for this effect (Dias da Silva et al., 2007). Inhibition of *Bmp* signaling in the ciliary epithelium, from transgenic *noggin* expressed in the lens, prevents normal ciliary formation and promotes differentiation of retinal ganglion cells. This phenotype can be reversed by over-expression of ciliary *Bmp7* (Zhao et al., 2002).

Together, this data suggests that canonical Wnt and *Bmp* signaling, combined with specific combinations of transcription factor expression and function, demarcates the presumptive ciliary cells of the peripheral retina, supports ciliary specific differentiation and prevents neuronal cell fates.

## 2.9. Limb Development relevant to OAS

In tetrapods such as humans and mice, primordia for two pairs of limbs originate in four specific areas of the flanks of the early embryo. Increased rates of cell division in comparison to those outwith the limb fields, generate outgrowth of the limb primordia, or 'limb-buds' from the ventrolateral body wall. These limb buds are therefore composed of proliferating mesenchymal cells pocketed by an ectodermal sheath. Limb buds appear at around CS13 in the human embryo, and at around E9.5 in the mouse. In both cases, the appearance of the forelimb slightly precedes that of the hindlimb and this staggered developmental pattern continues throughout embryogenesis.

### 2.9.1. Organising centres control development along different limb axes

As the limb bud becomes visible, an organising centre is created at distal-most region of the SE, the apical ectodermal ridge (AER). The AER is a collective of cells at the midline of the limb bud running along the anterior to posterior (A-P) axis and is essential for limb outgrowth and patterning via reciprocal interactions with cells of the underlying mesenchyme and expression of FGFs, and the continued outgrowth of the limb bud requires this FGF signaling to be maintained. The fate of cells in the growing limb bud depends on the time spent in the progress zone (PZ), a region of highly proliferating mesenchymal cells immediately proximal to the AER, and thus exposure to AER signals, with those residing longest becoming more distal elements of the limb. Thus, the AER controls development in the proximodistal axis.

The autopod skeletal elements are formed in a posterior-first order, where the metatarsals and metacarpals of the feet and hands, respectively, are formed before the phalanges. This fits the PZ model of limb bud development and differentiation.

A separate organising centre in the developing limb is the zone of polarizing activity (ZPA), positioned in the posterior mesenchyme of the developing limb bud and crucial for defining patterning across the anterior-posterior (A-P) axis. Signals coming from the ZPA help delineate the formation of separate digits with distinct morphologies organised across the autopod (Capdevila and Izpisua Belmonte, 2001; Tickle, 2006). Patterning along the A-P axis is principally achieved through the action of the highly conserved signaling molecule Sonic Hedgehog (Shh)(Riddle et al., 1993), emanating from the ZPA (Riddle et al., 1993).

### 2.9.2. Determining digit identity

*Shh* is thought to be vital for determining both digit number and identity. This process involves modification of Shh-responsive Gli proteins, which positively and negatively mediate the patterning effects of Shh. For example, high amounts of Gli3R (repressor) are present in anterior regions of the limb bud where Shh is unable to diffuse, while the activator form, Gli3A, is predominant in posterior regions in close proximity to the ZPA. This mediates the response to the Shh morphogen gradient across the A-P axis of the limb bud, which contributes to the creation of permissive and inhibitory

domains for the expression of target genes, and ultimately leads to the correct specification of digit number and identity required for distal limb development. In the absence of Shh (e.g. in *Shh*-/- mutant mice), Gli3R prevails throughout the limb bud resulting in the loss of digits (Tickle, 2006).

In addition to the morphogen gradient model of anterior-posterior patterning of digits whereby concentration of SHH determines digit identity, the length of exposure to SHH may also be important (Tickle, 2006). In this model, the posterior-most digit 5 is exposed to SHH for the greatest length of time and concentration, whereas digits 4, 3, and 2 have reducing lengths and intensities of exposure, respectively. In accordance with this model, in the posterior-most digits it is the temporal element that is most critical (Scherz et al., 2007). However, whether or not Shh *itself* determines digit identity is not clear.

Individual digit morphologies are controlled by endogenous signals from the interdigital mesenchyme, possibly mediated through Bmp signaling (Dahn and Fallon, 2000), although this is currently controversial (Bandyopadhyay et al., 2006). However, *Bmp2* is expressed posteriorally in limb buds and can be induced in response to ectopic Shh doses, where it can posterioralize duplicated digits (Drossopoulou et al., 2000).

The targets of such signals (Bmps and Shh) remain unknown (Tickle, 2006), however Bmps act in part through the T-box transcriptional repressors, expressed in the

posterior region of the limb and likely to be important for posterior digit morphology and identity. One target is the T-box gene transcription factor *Tbx3*. *Tbx3* mutations have been identified in the human condition Ulnar Mammary Syndrome (UMS; MIM #181450), which has phenotypes of posterior (ulnar or postaxial) upper limb defects ranging from hypoplasia of the terminal phalanx of the fifth finger to complete loss of forearm and hand. Additionally, the 5'Hoxd-genes are expressed across the anterior-posterior axis in the developing limb bud and are likely to be important in determining digit identity. *Hoxd13* has the most posterior expression domain, and mutations in humans can result in Synopolydactyly (MIM #186000), a condition of soft-tissue syndactyly and rudimentary extra digits affecting the posterior rays of the hands and feet (Muragaki et al., 1996).

### 2.9.3. Chondrogenesis & apoptosis for formation of digits & interdigital regions

Within the developing autopod, mesenchymal cells are specified to undergo two opposite fates: forming skeletal elements of the digits, or becoming interdigital tissue that will be removed by programmed cell death (PCD). To form the digits, mesenchymal cells aggregate to form precartilagenous condensations. These are subsequently replaced by bone through the process of endochondral ossification, where mesenchymal cells differentiate into osteoblasts. In the interdigital regions, tissue is removed to free the individual digits by apoptosis. The exact mechanisms for the contrasting fates of these mesenchymal cells remains obscure, however the specific location and levels of growth factors and their receptors appears crucial (Capdevila and Izpisua Belmonte, 2001).

*Bmps* are expressed throughout the developing autopod and therefore have roles as inducers of PCD and cartilage fate. In the prechondrogenic digit regions, the combined expression of *TGF-β2* and *BmpR-1b* determines digital development, together with the expression of the Bmp antagonist *noggin*. In the interdigital regions, however, expression of *BmpR-1a* and the absence of *TGF-β2*expression induces PCD. An additional role is played by Fgf signals emanating from the AER, whose function appears to be to protect cells in the PZ from PCD (Capdevila and Izpisua Belmonte, 2001). Once a chondrogenic fate has been determined, expression of the HMG-domain containing transcription factor *Sox9* is up-regulated. This occurs throughout the embryo in regions of endochondral ossification during mesenchymal cell condensation and cartilage formation (Wright et al., 1995).

## 2.10. Genetic mapping

The aim of genetic mapping is to identify disease genes that segregate with affected individuals. The principle of genetic mapping for any trait is therefore straightforward and is centred on identifying chromosomal regions that have shared features among affected individuals, usually family relatives, but differ from unaffected individuals. Once a genetic localisation is identified, genes within the region are considered as potential candidates to effectuate disease by virtue of their position. Occasionally, genes within identified regions may offer themselves as candidates based on previously known function alone, or by being the sole gene within that region.

### 2.10.1. Methods available for mapping

Often the first step taken in disease gene identification is cytogenetic analysis to identify chromosomal rearrangements, duplications or deletions. However such methods are useful only for low-resolution identification of genetic lesions and are thus not always successful in mapping genetic diseases. Typically, for smaller mutations, use is made of genetic markers: loci that have more than one allele and thus display polymorphism within populations. Microsatellite markers such as simple-tandem repeats, e.g. $(CA)_n$ generally have multiple alleles and are highly informative between individuals. Such markers can be analysed rapidly by PCR, using the unique flanking sequences for specific primer annealing, and can be tagged with fluorescent probes to enable multiplex reactions and accurate, high throughput computational analysis.

However, the use of microsatellite markers is limited in that many markers are required for whole genome mapping, and $(CA)_n$ repeats are predicted to occur only once every 30 kb (Stallings et al., 1991) and hence can only be used in mapping to restricted resolutions.

### 2.10.2. SNPs and autozygosity mapping

Single nucleotide polymorphisms (SNPs) occur at least once every 250 base pairs (NCBI assembly 36). Due to this high density and their known locations, together with their diallelic nature being amenable to full automation, they have been utilised in microarray chips to analyse many thousands of SNPs simultaneously in a single experiment. Sufficiently high numbers of informative markers results in large genetic power for screening whole genomes for linkage.

Autozygosity mapping is a powerful tool for the discovery of autosomal recessive gene loci in consanguineous families (Lander and Botstein, 1987).
In such families, there is a high probability that an affected individual has inherited both copies of a disease gene, one from each parent, which originated from a recent common ancestor. These alleles are generally inherited with regions of flanking genomic DNA sequence and together, these whole regions are referred to as being *identical by descent* or *autozygous*. Thus, autozygosity mapping seeks regions of homozygosity in affected individuals from consanguineous families. Recent strategies for autozygosity mapping incorporate SNP-chip data for thousands of SNPs.

### 2.10.3. Genetic mapping in mice

Mouse genetics has the advantage over human studies of being able to plan and select matings to facilitate linkage analysis. If a mutation has arisen on a particular strain background, and the heterozygous phenotype of interest is fully penetrant, multiple crosses to a separate inbred, or *tester* strain, (back- or outcrosses) can be set up, segregating phenotypic animals. The choice of tester strain depends on the availability of different alleles from the mutant strain that can be readily genotyped at multiple loci. The carrier parent is thus heterozygous for the mutant, or *target* loci and the mating partner is fully homozygous for all the tester strain loci. F1 progeny from the first outcross will therefore have one homologous chromosome from either parent. Meiotic recombination events in subsequent crosses will increase the amount of tester strain background, but by segregating heterozygotes for further outcrosses the original strain background close to the target loci will be retained. Hence, further crosses of phenotypic progeny with the tester strain will refine the target loci and facilitate whole genome mapping with markers informative between tester and target strains.

### 2.10.4. Genetic linkage in mapping

Linkage mapping has been essential for mapping the locations of genes that cause genetic disease. Loci on the same chromosome are connected physically and therefore usually segregate together during meiosis. However, the greater the distance between two loci on the same chromosome, the greater the chance of non-sister

chromatids crossing over during meiosis between loci, the process of meiotic recombination. Conversely, recombination occurs less frequently between two loci close together on the same chromosome. Linkage occurs when recombination events between two markers is identified as occurring less than 50% of the time, thus indicating the markers are close to each other on the same chromosome. Linkage analysis tests whether the recombination fraction (θ, the ratio of recombinant progeny to the total progeny) observed between markers differs from 0.5 and can be used to test the null hypothesis of no linkage when 5 out of 10 ($\theta$= 0.5) meioses are recombinant.

In most families or pedigrees however, it is impossible to assign recombination fractions unambiguously. The overall likelihood of a pedigree can be calculated by using the alternative assumptions that loci are linked (θ= 0 <θ <0.5) or not linked (θ= 0.5), where a range of values for θ within a given data set of loci for defined pedigrees (Strachan & Read). The ratio of these two likelihoods is the odds ratio, and the $\log_{10}$ of the odds ratio is the LOD score, *Z*. LOD scores are therefore statistical likelihood tests used to determine linkage between a two loci, or a particular trait and a marker (Morton, 1955). In reality, computational analyses of pedigrees, gene frequencies and genotypes are now routinely used to calculate LOD scores for individuals and can also be used to calculate linkage across multiple families, where cumulative LOD scores can be added up. The currently used critical values for accepting and rejecting linkage in simple mendelian traits in humans are $Z \geq 3.3$ and $Z \leq -2$, respectively, for significance levels of 0.05 (Lander and Kruglyak, 1995; Morton, 1955).

# 3. Materials and Methods

## 3.1. Materials and methods for the OAS project

### 3.1.1. Mapping OAS using Affymetrix 10K array

DNA was collected from families with OAS by collaborative clinicians and sent to Dr. David FitzPatrick at the MRC Human Genetics Unit (Edinburgh, UK). Samples were quantitated and checked for quality using a NanoDrop™ 1000 (Thermo Scientific) and agarose gel electrophoresis, respectively. DNA samples were sent to RZPD (Berlin, Germany) for analysis using the Affymetrix GeneChip® Human Mapping 10K Array Xba 131 platform. Primary chromosomal SNP raw data was produced in Excel spreadsheets from the output Affymetrix GeneChip® DNA Analysis Software (GDAS). For each affected individual, the data was sorted by chromosome and genetic distance and was then analysed for genome wide linkage using ExludeAR spreadsheets (http://leedsdna.info/science/Autozygozity/spreadsheets.htm). Linkage was tested using ALOHOMORA, a data conversion software tool to facilitate genome-wide linkage studies. The linkage analysis programme Allegro (v1.2c) was used to undertake a genome-wide multipoint linkage analysis of linked regions. Gene data within the candidate region was retrieved using the Biomart application in Ensembl human genome browser (http://www.ensembl.org/Homo_sapiens/index.html).

### 3.1.2. Whole genome amplification of sample genomic DNA

OAS patient and family genomic DNA samples were limiting and therefore whole genome amplification reactions were required to facilitate a PCR-based sequencing strategy. The GenomiPhi™ DNA Amplification Kit (Amersham) was used to generate large volumes of DNA for template in PCR-sequencing reactions from patient DNA according to the manufacturers instructions. Amplified DNA samples were diluted to 100 ng/$\mu$l in RNAse and DNAse free Ultrapure water.

### 3.1.3. Development of oligonucleotide primers for an OAS sequencing strategy

The physical coordinates for the critical interval linked to OAS were used to extract all coding exons from the Ensembl database using the Biomart tool (http://www.ensembl.org/biomart/martview//def0f0e79955dcf569528e09fd74245f) on ensembl v38 (April 2006). In order to evaluate a general level of evolutionary conservation in the coding regions, a table available from the UCSC table browser website (http://genome.ucsc.edu/cgi-bin/hgTables) was downloaded that displayed the critical region with a measure of evolutionary sequence conservation across 17 vertebrates including mammalian, amphibian, avian, and teleost species. This data was generated using PhastCons17way, based on a hidden Markov model, PhastCons (Siepel et al., 2005). The table contained a single score per base pair reflecting the level of conservation in all the species: 1 being the maximum score and 0 denoted a non-conserved element. In house scripts were then used to parse the information from the

conservation table and to generate oligonucleotide primers for each exon using the EMBOSS eprimer3 script. For the primer design, all of the exons in the region were downloaded with the flanking 100 bp of genomic sequence on both sides, with the positions of the coding regions defined. Changes to standard parameters for eprimer3 primer design were as follows: GC clamp = 1 nt; Optimum Tm= 60ºC; Minimum Tm = 57ºC; Maximum Tm = 63ºC; and optimum primer size = 19 nts. Exon details, together with sequence conservation and the generated primers sequences were shared between the Edinburgh (Dr. D. FitzPatrick & Joe Rainger, MRC Human Genetics Unit, Edinburgh, UK) and Nijmegen (Drs. H. Brunner & H. van Bokhoven, Radbound University Nijmegen Medical Genetics, Department of Human Genetics, Nijmegen, The Netherlands) collaborating groups for this project and are in Appendix 6.1. These primers were purchased from various suppliers throughout the project and were synthesised with no modifications and were desalt-purified.

### 3.1.4. PCR based sequencing of exons for OAS patients

Oligonucleotides were rehydrated to stock solutions and 10 $\mu$M working solutions were set up, containing both forward and reverse primers in each primer-pair. PCR reactions were set up with reagents as described below, with the exception that 2 $\mu$l of WGA DNA (20 ng/$\mu$l) was added to 25 $\mu$l reactions at a final concentration of 1.6 ng/$\mu$l and the final dilution of primers was 0.4 $\mu$M. PCR reactions were run on DNA Engine Tetrad™2 (BioRad, CA, USA). Agarose gel electrophoresis was used to analyse success of PCR reactions. Sequencing reactions were performed by the Technical

Service Department at the MRC Human Genetics Unit. Sequence analysis was performed with Mutation Surveyor™ Software (SoftGenetics® LLC, PA, USA) or Sequencher™4.8 (GeneCodes Corp. MI, USA).

## 3.2. Materials and methods for the *Mp* project

### 3.2.1. Genetic background and breeding schedule of the *Mp* mouse line

The *Mp* (micropinna microphthalmia) line was produced by exposing spermatogonia of an F1 male (101/R1 x C3H/R1) to a total of 7 x 200 cGy doses of X-ray irradiation over 7-day intervals at a dose rate of ~ 90 cGy/min at Oak Ridge Nuclear Laboratory (Phipps, 1964). The irradiated male was bred to a multiple-recessive tester (T-stock) female and offspring were crossed once to mice of Bl10 background. Further crosses were made to inbred background strains 101 and C3H a total of 37 times. Sperm was isolated and cryogenically stored from *Mp* affected males. Mutant sperm was used to perform intra-cytoplasmic sperm injection (ICSI) using oocytes from a donor female F1 (CBA x C57Bl/6). Generation-0 (G0) affected offspring from this dam were intercrossed for gross mutant phenotype analysis of progeny and also outcrossed to a genetically distinguishable inbred strain (C57Bl/6) to facilitate genetic mapping. A total of four backcrosses (to C57Bl/6) followed this initial outcross, selecting for heterozygous phenotype, to generate informative recombinants within chromosomal regions from the original mutagenised background (C3H/101) co-segregating with the *Mp* phenotype.

### 3.2.2. Gross phenotyping and penetrance analysis of *Mp* Mouse line

The *Mp* mutation phenotype has been described (Phipps, 1964). Phenotypes were classified grossly at, or as close to, post-natal day 21. Heterozygote animals were identified by small eyes with/ or without reduced pinnae size. In contrast, ocular absence (demonstrated by failure in opening of the palpebral fissures) in combination with distal limb oligodactyly or syndactyly was used to identify homozygote animals. For penetrance analysis, records of each perceived genotype were accumulated for each backcross generation in out-crosses to both C57Bl6/j and CD1 strains, and calculated as each phenotype percentages and ratios for comparison to expected numbers.

### 3.2.3. Skeletal analysis

Animals at various ages were culled with lethal intravenous doses of Euthatal (Merial Animal Health Ltd. Essex, UK) and were washed in 70% Ethanol. Animals were weighed for weight comparisons between genotypes and then completely eviscerated with abdominal tissues and organs removed. Carcasses were then placed in 95% ethanol for 24 hours, followed by 72 hours in 100% acetone, at least 3 days in stain solution (1 part 0.3% alcian blue in 70% ethanol; 1 part 0.1% alazarin red in 95% ethanol; and 1 part acetic acid, in 17 parts 70% ethanol); followed by 3 days clearing in 1% potassium hydroxide (KOH); 3 days in 1% KOH/30% glycerol; and two 24 hour periods in 1% KOH/50% glycerol; in 1% KOH/70% glycerol and finally were stored in 100% glycerol.

### 3.2.4. Mouse Eye processing for histology and immunohistochemistry

Eye tissue was dissected from culled animals at recorded stages and periocular tissues removed to reveal globes and optic stalks, taking care to remove as much extraocular tissue as possible. Eyes were rinsed in cold PBS and then fixed in 4% PFA overnight at 4ºC; rinsed again in PBS, and dehydrated in serial dilutions of 30%; 50%; 70% ethanol for 1 hour each at room temperature. They were then either stored at 4ºC in 70% ethanol, or paraffin embedded. Paraffin embedding was performed by sequential 15 min rinses in each of 85%; 95% and 100% ethanol, followed by 2x 30 min in xylene, the second of which was at 50 ºC. Xylene was then replaced by 1x 30 min wash in 50ºC paraffin and then manually embedded in fresh paraffin at 50ºC for cutting in either sagittal, coronal or transverse planes. Sectioning was done on a manual microtome set to cut at either 4 $\mu$m or 6 $\mu$m. Dewaxing of slides was performed by serial washes of 5 min in xylene (3x washes) and 100% ethanol (3x washes), followed by 2 min washes each in 90%; 70%; 50% and 30% ethanol and finally rinsed in $dH_2O$.

### 3.2.5. Karyotype analysis of *Mp* pro-metaphase chromosomes

(Adapted from protocol at jax.org/cyto/blood_preps.html) Para-cardiac blood samples (0.05–0.1 ml) were collected from 11-week old phenotypically heterozygous male *Mp* animals, and supplemented with heparin to 500 USP units/ml. Samples were added directly to 0.95 ml RPMI media (Gibco) with 1% penicillin/streptomycin; 1% L-glutamine; and 0.5% MOPS (1.25 M); supplemented with 0.15 ml PHA (0.01% v/v); 0.1

ml LPS (750 $\mu$g/ml); and 0.15 FCS. Samples were cultured in 15 ml falcon tubes at 37ºC with regular, light agitation. At 43 hours incubation, 7.2 $\mu$l Colcemid (Gibco; 10 $\mu$g/ml) was added to cultures and incubated for 15-20 min. Cultures were centrifuged at 400 x g for 10 min and supernatants removed. Cultures were gently resuspended in 2-3 ml of pre-warmed (37ºC) KCl (0.56%; 0.075 M) and further incubated for 15 min at 37ºC. Cells were harvested by centrifugation at 500 x g for 10 min and supernatants removed without removal of Buffy layer. Cell pellets were resuspended in 3:1methanol:glacial acetic acid fixative and left overnight at 4ºC. Cells were centrifuged at 400 x g and resuspended in fixative a total of three times with final resuspension in 0.25-0.5 ml fixative. Cell suspensions were dropped on slides pre-cleaned with fixative and rapidly dried to facilitate spreading of chromosomes. Chromosome preparations were mounted in Vectashield (Vector Laboratories) containing DAPI fluorescent stain at 0.1 $\mu$l/ml and visualised by fluorescence microscopy as described below. Karyotype analysis was performed using SpectraVysion software (Vysis, Illinois USA).

### 3.2.6. Brightfield and fluorescent microscopy

For fluorescence imaging, the imaging system comprised a Coolsnap HQ CCD camera (Photometrics Ltd, Tucson, AZ) Zeiss Axioplan II fluorescence microscope with Plan-neofluar objectives, a 100W Hg source (Carl Zeiss, Welwyn Garden City, UK) and Chroma #83000 triple band pass filter set (Chroma Technology Corp., Rockingham, VT) with the excitation filters installed in a motorised filter wheel (Ludl Electronic Products, Hawthorne, NY). For brightfield colour imaging, colour additive filters

(Andover Corporation, Salem, NH) installed in a motorised filter wheel (Ludl Electronic Products, Hawthorne, NY) were used sequentially to collect red, green and blue images, that were then superimposed to form a colour image. Image capture and analysis were performed using in-house scripts written for IPLab Spectrum (Scanalytics Corp, Fairfax, VA).

### 3.2.7. Morphometric eye measurements

Embryos were dissected at E15.5 and the heads removed. They were then rinsed in cold PBS and then fixed in 4% PFA overnight at 4ºC; rinsed again in PBS, and placed in 30% Sucrose/PBT O/N at 4ºC. Heads were then dehydrated in serial dilutions of 30%; 50%; 70% ethanol each for 3 h at room temperature, or O/N at 4ºC. They were then processed for *Optical Projection Tomography* (OPT) as follows: heads were mounted in 1% agarose, dehydrated in methanol and then cleared overnight in BABB solution (1 part Benzyl Alcohol: 2 parts Benzyl Benzoate). The sample was then imaged using a Bioptonics OPT Scanner 3001 (Bioptonics, UK) using brightfield to detect the LacZ staining and for tissue autofluorescence (with wavelengths for excitation set to 425nm, and emission set to 475nm) to capture the anatomy (Sharpe et al., 2002). The resulting images were reconstructed using Bioptonics propriatory software (Bioptonics, MRC Technology, Edinburgh, UK), automatically thresholded and merged to a single 3D image output using Bioptonics Viewer software. Scans were analysed with Amira 4.1.2 (Visage Imaging, CA, USA) with measurements taken for head lengths and widths, eye depth and width, and lens depth and width, all in Voxels. Measurement data was then processed in Excel worksheets.

### 3.2.8. DNA extraction from mouse tissues

Tail tips were taken and incubated in 500 $\mu$l tail lysis buffer (100 mM Tris-HCl, pH8.5; 5 mM EDTA; 0.2% SDS; 200 mM NaCl) with 10 $\mu$l Proteinase K (10 mg/ml) and incubated overnight at 50ºC. Samples were centrifuged at 13,000 rpm for 30 min at 4ºC. Supernatants were transferred to fresh tubes and 1/8$^{th}$ volume Sodium Acetate (3 M; pH8) and 2x volume of (-20ºC) 100% ethanol were added and mixed. Samples were stored at -20ºC overnight and centrifuged at 13,000 rpm for 30 min at 4ºC. Pellets were washed twice with 70% ethanol and air-dried. DNA was resuspended in sd$H_2O$.

### 3.2.9. RNA extraction from mouse tissues and cell cultures

RNA was isolated from tissues collected from animals culled as described above, or from cultured mouse embryonic fibroblast (MEF) cells. For cells, media was removed and cells were washed once in sterile PBS. Accutase (Innovative Cell Technologies, Inc., CA) was used, according to the manufacturers instructions, to remove monolayers from tissue-culture flasks. Cells were then centrifuged at 1200 rpm for 5 min, the supernatants were removed and cells were resuspended in TRIzol® Reagent (Invitrogen, 15596-026). For RNA isolation from tissue, fresh tissues were dissected and frozen on dry ice, and then stored at -80ºC prior to, or homogenised immediately in TRIzol Reagent. RNA was extracted by following the manufacturers instructions, with the slight modification of mixing a fifth volume of Phenol:chloroform:isoamyl (25:24:01) alcohol (Sigma, P3803) to the

TRIzol/homogenised tissue, instead of chloroform. The aqueous phase was collected and RNA was precipitated, washed and resuspended in sterile ultrapure $H_2O$ and stored at -80$^{o}$C. RNAs were run on agarose gels (1% in TBE) to check for quality, degradation and genomic contamination, and yield was calculated with a NanoDrop$^{TM}$ 1000 (Thermo Scientific).

### 3.2.10. Single-stranded cDNA synthesis & RT-PCR

RNA was used for single-stranded cDNA synthesis by reverse transcription. The 1$^{st}$ Strand cDNA Synthesis Kit for RT-PCR (AMV) (Roche, Cat. No. 1 483 188) was used according to the manufacturers instructions using oligo-dT primers and with various RNA input quantities. Controls were set up for each sample without enzyme to identify genomic contamination. Reverse transcriptase (RT)-PCR with primers specific for the 18s ribosomal subunit (*18sRNA_Fwd* & *18sRNA_Rev*) was used to check cDNA for genomic contamination. These primers produced a single amplicon of ~500 bp in the presence of cDNA alone, but also produced an additional amplicon of ~1 kb if genomic contamination is present.

### 3.2.11. Polymerase chain reaction (PCR)

All PCR reactions (including non-quantitative RT-PCRs) were carried out using Faststart Amplitaq Gold enzyme (Roche Applied Science) at a final reaction concentration of 0.06 U/$\mu$l in reaction mixes with PCR buffer containing $MgCl_2$ (Roche

Applied Science, Product no. 12 032 945 001) and 0.4 mM dNTPs (Abgene, diluted 1/10 in sd$H_2O$). Oligonucleotide primers were diluted to working solutions containing 10 $\mu$M of both forward and reverse primers in sterile d$H_2O$, and were diluted to a final reaction concentration of 0.2 $\mu$M. Total DNA input for PCR reactions varied within the range 40-200 ng, with the reaction volumes being 10-50 $\mu$l, respectively, giving a general DNA reaction concentration of 4 ng/$\mu$l. Mastermixes were made up where multiple reactions were performed, with all reaction mixed prepared on ice, with DNA and primers generally added last to avoid contamination. Filter tipped pipettes were used where possible in dedicated, clean, PCR set-up areas. Specific reaction cycle conditions are listed in Appendix, however a general programme was used for all oligonucleotide primer pairs as a first-pass attempt: 95ºC x 3 min, followed by 30x cycles of 95ºC x 30 s; 58ºC x 45 s; 72ºC x 45 s, followed by a single extension of 10 min at 72ºC and final holding at 4ºC, with the thermal cycler lid tracking at 5ºC each stage temperature. Details of primers and cycles used are in Appendix. All products were run on agarose gels (1% in TBE with 0.5 % TBE running buffer) with either 100 bp or 1 kb molecular DNA size markers (Invitrogen, Product Nos. 15628-050 and 15615-016, respectively).

### 3.2.12. DNA preparation for Whole Genome 768 SNP Panel Array for *Mp* mapping

Genomic DNA was extracted from tails of 8x phenotypically heterozygous animals as described above from the 2$^{nd}$ outcross to C57Bl6/j, together with parental G0 and F1 genomic DNAs. DNAs were quantitated and checked for quality by recording

their 260/280 nm absorbances using a NanoDrop 1000 spectrophotometer (NanoDrop Technologies, DE, USA) and by running samples on 1% agarose gel to check for degradation. All had 260/280 ratios >1.80 and were undegraded and therefore were considered of good enough quality for the array analysis. 4 $\mu$g total DNA was sent for each sample to be analysed on the 768 SNP genotyping panel (Moran et al., 2006).

### 3.2.13. Genome-wide mapping of *Mp* using fluorescently tagged microsatellite markers

PCR amplifiable microsatellite markers were used for mapping using tail-tip DNA samples from heterozygous *Mp* animals from the 3$^{rd}$ generation of outcrosses to C57Bl6/j. DNAs were quantitated, and checked for quality by recording their 260/280 nm absorbances, using a NanoDrop 1000 spectrophotometer (NanoDrop Technologies, DE, USA). Markers were selected according to whether their oligonucleotide primers were held in the laboratory of Professor Ian Jackson (MRC Human Genetics Unit) and if so, whether they were informative between the background strains C3H and 101 and C57Bl6/j, according to details publicly available on an annotated electronic database: http://www.ncbi.nlm.nih.gov/sites/entrez?db=unists. Primers specific for those markers selected were used in PCR reactions with positive control DNAs collected from C3H and C57Bl6/j mice. The PCR-products were run on agarose gels (1% TBE with 0.5% TBE running buffer) to check for presence and the specificity of product(s) and were then run on an ABI PRISM® 310 Genetic Analyzer. This single-capillary genetic analyser ran 3 different coloured markers concomitantly, together with a size marker in

each single lane. Hence, microsatellite-specific oligonucleotide primers were conjugated with FAM, TET, or HEX dyes and used for amplicon fragment analysis. In total 73x markers were selected that were informative between C3H and C57Bl6/j alleles. The markers used, their fluorescent tag and chromosomal location, and peak sizes for each allele are listed below. Genomic DNA was collected from 30x wild type and 38x heterozygote animals from the 3rd outcross. Samples were quantitated and checked for DNA quality as described above and then diluted to 50 ng/$\mu$l. Equal amounts (20 $\mu$l) of these equilibrated samples were then pooled together and used to create two samples containing DNA from either wild type or heterozygote samples only. The heterozygous and wild type pooled DNAs were then used separately as templates for PCR reactions, using the reagents and quantities described above, for each of the selected markers (Table 3.1) and run on the ABI PRISM® 310 Genetic Analyzer. The PCR cycle conditions for all markers was: 94ºC x 3 min; 30x cycles of (i) 94ºC x 30 s; (ii) 55ºC x 45 s; (iii) 72ºC x 1 min, followed by a single step of 72ºC x 2 min and holding at 4ºC. Oligonucleotides were used at a final concentration of 0.5 $\mu$M. PCR reactions were removed from the thermal cycler and run on agarose gels to check for PCR success. 2 $\mu$l of each PCR product was mixed with 4 $\mu$l sd$H_2O$ and mixed well. Samples were then diluted with 14 $\mu$l Genescan-350 TAMRA® (ABI PRISM) molecular markers/formamide mix (1:28) and denatured at 95ºC for 5 min and cooled on ice prior to loading onto the ABI PRISM® 310 Genetic Analyzer. When completed, data was removed from the Genetic Analyzer and organised in Excel worksheets. Peak heights for

each allele were recorded and the ratios of C57Bl6/j:C3H peak heights were calculated and presented graphically.

**Table 3.1. Informative markers per chromosome used for whole genome mapping panel.**

| Chromosome | Size (Mb) | Number of markers | Average Density (Mb/marker) |
|---|---|---|---|
| 1 | 195.1 | 4 | 48.8 |
| 2 | 181.8 | 5 | 36.4 |
| 3 | 158.9 | 4 | 39.7 |
| 4 | 154.7 | 4 | 38.7 |
| 5 | 150.3 | 4 | 37.6 |
| 6 | 150.2 | 5 | 30.0 |
| 7 | 139.7 | 5 | 27.9 |
| 8 | 127.9 | 4 | 32.0 |
| 9 | 124.1 | 3 | 41.4 |
| 10 | 130.3 | 4 | 32.6 |
| 11 | 121.8 | 4 | 30.5 |
| 12 | 115.8 | 4 | 28.9 |
| 13 | 114.7 | 4 | 28.7 |
| 14 | 118.9 | 3 | 39.6 |
| 15 | 103.6 | 4 | 25.9 |
| 16 | 97.4 | 2 | 48.7 |
| 17 | 92.9 | 4 | 23.2 |
| 18 | 90.3 | 4 | 22.6 |
| 19 | 60.6 | 2 | 30.3 |

### 3.2.14. Fine mapping of *Mp* using non-fluorescent microsatellite markers

Using the same principle as for the whole genome mapping of *Mp* written above, fine mapping was performed around the chromosome 18 and 11 regions identified as candidate loci for *Mp*. In these case, in addition to some markers being tested using the ABI PRISM® 310 Genetic Analyzer, other marker alleles were PCR amplified and products were run on resolving 4% agarose gels (4% agarose in 0.5% TBE with 0.5% TBE running buffer) to discriminate between background alleles. The microsatellite markers used for fine mapping the chromosome 18 locus are listed in table 3.1.The primer pairs used, and the nucleotide sequences, are listed in the primer list in Appendix 6.4.1.

**Table 3.2. Microsatellite markers on chromosome 18 and their amplicon sizes used for haplotype analysis of heterozygotes from 3rd outcross to C57Bl6/j.**

| Marker | Physical position (Mb) | C3H size (bp) | C57Bl6/j size (bp) | Gel or Fluorescence analysis |
|---|---|---|---|---|
| D18 MIT 94 | 38 | 124 | 141 | Gel |
| D18 MIT 149 | 45 | 116 | 136 | Fluorescence |
| D18 MIT 74 | 53 | 184 | 220 | Gel |
| D18 MIT 184 | 67 | 127 | 172 | Gel |

### 3.2.15. 3'-End cDNA amplification using RACE

Rapid Amplification of cDNA Ends (RACE) was used for the identification of the 3'-end of the *Fbn2* transcript in the *Mp* mouse. An adaptor oligonucleotide primer (*3'-RACE_d$_{(T)}$*: see table in appendix for primer sequences) with 17x 3'-thymine residues was used as the only primer in separate reverse transcription reactions with RNA extracted from phenotypically mutant and wild-type animals as described above, using 1$^{st}$ Strand cDNA Synthesis Kit for RT-PCR (Roche) with standard conditions. The single-stranded cDNA species (cDNA) were then used in gene-specific PCR reactions with an adaptor-only primer (*3'-RACE_adaptor*) and the *Fbn2*-specific primer (*FBN2cDNA10_Fwd*). Products from these separate reactions were then gel electrophoresed and analysed for the presence of different bands between the wild-type and mutant samples. Candidate bands were excised and purified from the gel and TA-cloned into the pGEM-Easy vector system (Promega), according to the manufacturers instructions, for sequence analysis using T7 and SP6 vector-specific primers (*T7_Fwd* & *SP6_Rev*). The sequences obtained were analysed using Sequencher Version 4.8 (Gene Codes Corp. MI, USA) and then used as query sequences in BLAT search alignments against the mouse genome (http://genome.ucsc.edu/cgi-bin/hgBlat).

### 3.2.16. Long-range PCR for Fbn2 breakpoint mapping

The regions between the last 3'-exons of the *Fbn2* gene were amplified with primers listed as *Fbn2 3'-exon primers* in Appendix 6.4.2 & 6.4.3. The Roche Expand Long Template PCR kit (Roche, IN, USA) with buffer 1 was used as per the manufacturers guidelines with genomic DNA from heterozygote, homozygote and wild type animals.

### 3.2.17. PCR-based genotyping assay

Based on the genomic rearrangement identified at the *Mp* locus, it was possible to devise a PCR-based genotyping assay to genetically distinguish heterozygous, homozygous and wild type embryos and neonates. Primers *Fbn2_FineMap_Fwd*, *Fbn2_FineMap_Rev* and *Isoc1Ex5_4_Fwd2* were used in multiplex PCR reactions using DNA isolated from mouse tail-tip samples. The *Fbn2*-specific primers produced an amplicon of 956 bp, indicative of the wild-type allele, whereas the *Fbn2_FineMap_Rev* and *Isoc1Ex5_4_Fwd2* specific primers will produce an amplicon of 500 bp, signifying the presence of an *Mp* allele. The presence of both amplicons indicated heterozygote animals, whereas a single upper band or a single lower band signified wild types or homozygotes, respectively. Thus separation of these amplicons with 1% agarose gel electrophoresis (1% in TBE with 0.5% TBE running buffer) was used to identify genotypes (figure 3.2.1.).

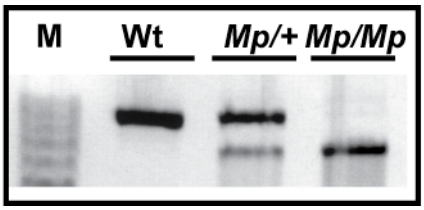


**Figure 3.2.1. PCR-based genotyping assay for *Mp*.** Agarose gel electrophoresis indicating the different amplicons produced using wild type (Wt), heterozygote (*Mp*/+) and homozygote (*Mp*/*Mp*) input genomic DNA as templates for the genotyping-PCR reaction described with the Fbn2 and Isoc1-specific primers described above (M = 100 bp molecular weight marker).

### 3.2.18. Strong fix protocol for Transmission-Electron Microscopy (TEM)

For sample preparation, tissues (epidermis, perichondrium and tendon from hind limbs, ears and eyes) from culled neonates was collected and placed into sterile serum-free Dulbecco's modified eagles media (DMEM) for immuno-EM and into strong-fix for regular EM. For Strong-fix (1.5 % Glutaraldehyde/ 1.5 % Paraformaldehyde in 0.1 M Sodium Cacodylate/ 0.05 % Calcium Chloride/ 0.05 % Tannic Acid), tissue samples were fixed for 3 h at RT, followed by 3x rinses in Cacodylate buffer (0.1 M Sodium Cacodylate/ 0.05 % Calcium Chloride). Tissues were shipped on ice in serum-free DMEM or Cacodylate buffer for immuno-EM and regular-EM, respectively. EM analysis was performed by Doug Keene and Sara Tufa (Shriners Hospitals for Children, Oregon Health and Sciences University, Portland, Oregon). Briefly, for immuno-EM, tissues were rinsed briefly in DMEM and then immunolabeled en bloc by immersing in

primary antibody diluted 1:5 in DMEM overnight at 4°C. They were then rinsed extensively in DMEM and immersed in 5-nm secondary gold conjugate (Amersham) diluted 1:3 in DMEM, rinsed again in DMEM. The immuno-labelled tissues were fixed in 1.5% glutaraldehyde/1.5% paraformaldehyde containing 0.05% tannic acid in DMEM followed by 1% buffered $OsO_4$ and then rinsed, dehydrated, and embedded in Spurrs epoxy. Tissues were examined in a Philips EM410 transmission electron microscope. For regular EM, tissues were examined on a Philips EM410 transmission electron microscope following fixation in 1.5% paraformaldehyde/1.5% glutaraldehyde with 0.05% tannic acid and osmium tetroxide, dehydration in ethanol and embedding in Spurrs epoxy.

### 3.2.19. Primary MEF cultures

Primary Mouse Embryonic Fibroblast (MEF) cultures were established for RNA and immunocytochemistry analysis. Embryos were collected at E13.5 and separated into individual wells of a tissue culture plate and held in culture media: DMEM with 20% foetal calf serum; 1% penicillin/streptomycin. Tail-tips were removed for genotyping (as described above) and the abdominal cavity, and head, of each embryo was removed and discarded, or processed for sectioning, respectively. The limbs and skin from each embryo were then finely chopped with a sterile scalpel in 1 ml of culture media, passed several times through a pastette and then carefully injected into a 25 ml tissue culture flask (T25) and gently spread to cover the greatest amount of area possible. Flasks were then inverted and incubated upside-down at 37ºC/ 5% $CO_2$ for 3 h,

then returned to right-side-up and cultured overnight. Flasks had media removed and replaced after 48 h and were checked for growth of fibroblast colonies. Large pieces of tissue debris were removed after cultures were established with large areas of fibroblast cells. When cultures were 80% confluent, they were passaged at a ratio of 1:2 by washing cultures once with PBS, incubating with Accutase (Innovative Cell Technologies, Inc., CA) at 37ºC/ 5% $CO_2$ for 5-10 min, and then centrifugation at 1200 rpm for 5 min. Cell pellets were resuspended in culture media and separated evenly into two T25 flasks. These cells were then cultured as described above, and allowed to reach 80% confluence. They were passaged in the same way, or alternatively the entire contents of a single T25 flask was used to seed a 75 ml culture flask. In addition, some cells were used to seed 16 mm glass coverslips placed into 6-Well tissue culture plates for immunocytochemistry analysis, using the same culture conditions described above.

### 3.2.20. Tunicamycin assay

2x separate MEF cultures for each genotype were grown in 6-well tissue culture plates for 72 h with normal media and conditions. Culture media was removed and replaced with normal media containing the carrier substance DMSO (Sigma) at 0.05 % with Tunicamycin (Manufacturer) at either 0 $\mu$g/ml; 0.5 $\mu$g/ml or 5.0 $\mu$g/ml doses for 30 min. The experimental media was removed and replaced with normal culture media. Plates were then cultured under normal conditions and RNA was extracted after 24 h as described above.

### 3.2.21. *Xbp1* splicing assay

The alternatively spliced *Xbp1*transcripts were differentially identified using RT-PCR and the ABI PRISM® 310 Genetic Analyzer. A FAM-labelled forward (Xbp-1_Fwd_FAM: 5'-[6FAM]-TTACGGGAGAAAACTCACGGCC-3') and an unlabelled reverse ( *Xbp1*_Rev: 5'-GGGTCCAACTTGTCCAGAAT-3') oligonucleotide primer specific for generating amplicons that covered the splicing region of the *Xbp1* transcript were used in PCR reactions with single stranded cDNA produced as described previously from RNA isolated from MEF cultures and dissected E16.5 eyes. In this assay, an unspliced *Xbp1* transcript will amplify a 289 bp product, while a spliced transcript will produce a 263 bp amplicon, and if both transcripts were present then both amplicons should be amplified. The ABI PRISM was used to identify peak heights for each splice-form of the *Xbp1* transcript from samples of different genotypes, and the ratios of peak heights were then calculated and displayed graphically. Relative quantitation of *Fbn2* and *Xbp1* transcripts was analysed using QuantiTect SYBR Green RT-PCR (QIAGEN, CA, USA) according to manufacturers instructions, with the same RNA samples as were used for the 1$^{st}$-strand synthesis in the *Xbp-1* splicing assay. Primer pairs for specifically amplifying *Fbn2*, *Xbp1* and *Hprt* cDNA were used to generate ct values for each sample in triplicate. The averages ct values were used to generate Δct values for *Fbn2* and *Xbp1* normalised to *Hprt* expression, and then ΔΔct values were subsequently calculated for each of the samples for *Xbp1* expression relative to *Fbn2* expression.

### 3.2.22. Immunocytochemistry

Cells were cultured on 16 mm glass coverslips in 6-well culture plates as described above and analysed for Fbn2 protein localisation with the rabbit polyclonal anti-Fbn2 antibody PAb-868. Cultures were grown for 72 hours and media was removed and cells were fixed with 3.7% formaldehyde at RT for 5 min. Cells were then washed 3x in PBS and were either stored or processed immediately. Cells were permeabilised in PBS + 0.5% Triton-X-100 (Sigma) for 5 min. Coverslips were then blocked in PBS + 10% foetal calf serum for at least 30 min at room temp, or overnight at 4ºC. Fbn2 antibody was diluted 1:150 in blocking solution and coverslips were incubated for 1 h at RT, then washed 3x in PBS + 0.1% Tween-20 (Promega). Secondary antibody (goat anti-rabbit Fab' Alexa Fluor® 488, Invitrogen) in blocking buffer for 1 h at RT. Coverslips were then washed 3x in PBS followed by PBS + 0.1% Tween-20 and then mounted in Vectashield (Vector Laboratories) containing DAPI fluorescent stain at 0.1 $\mu$l/ml to visualize cell nuclei and inverted onto glass microscope slides, sealed and stored at 4ºC in dark conditions. A list of antibodies used is presented in table 3.3.

### 3.2.23. Immunohistochemistry

Slides with paraffin sections (cut at 4-7 $\mu$m) were de-waxed as described above. Antigen retrieval was carried out to reveal epitope sites by boiling in 0.1 M Citrate buffer (pH 6.0), boiled prior to application, and then brought back to the boil and left to cool for 20 min at RT. Slides were then rinsed twice in PBS and once in PBT. Slides were blocked for 1 hr at RT in buffer containing 10% sheep serum (heat inactivated at 60ºC for 1 hr); 1% BSA; 0.1% Tween-20; 0.05% Triton-X-100, all in PBS. Slides were then rinsed 2x PBS. Primary antibodies were applied diluted in blocking buffer (for dilutions and antibody details, see table below), and incubated overnight at 4ºC. The sections were then washed as above and then incubated in the relevant fluorescent conjugated secondary antibody, either Alexa Fluor® 488 Fab' fragment or Alexa Fluor® 594 Fab' fragment (Invitrogen) in blocking buffer for 1 h at RT (for reactive species used, see table below). Sections were washed extensively in PBS followed by PBT and then mounted in Vectashield (Vector Laboratories) containing DAPI fluorescent stain at 0.1 $\mu$l/ml to visualize cell nuclei. For Lef1 primary antibody, the manufacturer's immunohistochemistry protocol (paraffin) was followed up to the point of incubation in blocking solution. Instead, blocking solution was made up according to the vectastain® ABC-AP kit protocol (Rabbit IgG; Vector Labs, Switzerland, product ID: AK-5001), which was followed from the blocking stage to completion. The substrate used was BM-Purple AP Substrate Solution (NBT/BCIP) (Roche) and slides were mounted in Vectashield (Vector Laboratories). A list of antibodies used is presented in table 3.3.

| Antigen | Dilution | Species | Manufacturer/ Reference | Secondary Antibody |
|---|---|---|---|---|
| Fbn2 | 1:150 | Rabbit anti-mouse (PAb) | L. Sakai, Portland, OR | Goat anti-rabbit |
| Sox2 | 1:1000 | Rabbit anti-mouse (PAb) | Chemicon AB5603 | Goat anti-rabbit |
| Pax6 | 1:20 | Mouse (MAb) | V. v Heyningen, MRC HGU | Goat anti-mouse |
| Lef1 | 1:1000 | Rabbit MAb | Cell Signaling #2230 | Goat anti-rabbit* |
| A-Caspase-3 | 1/500 | Rabbit MAb | BD Pharminogen #559565 | Goat anti-rabbit |
| Rhodopsin | 1/2000 | Mouse (MAb) | Abcam ab5417 | Goat anti-mouse |
| GFAP | 1/500 | Mouse (MAb) | Sigma G3893 | Goat anti-mouse |
| Calbindin | 1/1000 | Rabbit anti-mouse (PAb) | Millipore AB1778 | Goat anti-rabbit |
| PKCα | 1/2000 | Rabbit anti-mouse (PAb) | Sigma P4334 | Goat anti-rabbit |
| Chx10 | 1/100 | Sheep anti – human (PAb) | Millipore AB9014 | Rabbit anti goat |

**Table 3.3. Details of antibodies used.** * Colourmetric reaction used for Lef1 antibody (see above).

### 3.2.24. RNA In Situ Probe Synthesis

Probe synthesis was performed with cDNA prepared as described above. 2-4 $\mu$L cDNA template was mixed with 10x PCR buffer (Roche, Faststart Amplitaq); 1.0 $\mu$l dNTP mix (10 mM each dNTP); 0.6 $\mu$l Amplitaq polymerase enzyme; 1.0 $\mu$l Oligonucleotide mix (see appendix 6.4 for the sequences of individual primers); with the total reaction mix made up to 50 $\mu$l. Reaction conditions were as follows: 94ºC x 3 min;

35 cycles of: 94ºC x 30s; 57ºC x 40s; and 72ºC x 1 min 25 s; followed by a single step of 72ºC x 10 min. PCR products (5 $\mu$l) were run on 1% agarose gel containing ethidium bromide to visualise the presence of specific amplicons of correct size and were then purified (QiaGen PCR Purification Kit) according to the manufacturers instructions. Purified PCR product (~150 ng) was incubated for 37ºC for 2 h in a 20 $\mu$l reaction containing: 2 $\mu$l transcription buffer; 1 $\mu$l RNase inhibitor (Roche); 2 $\mu$l DIG RNA labelling mix; T7 RNA polymerase; and ultra-pure $H_2O$. An additional 1 $\mu$l T7 RNA polymerase enzyme was added after 1 hr incubation to increase yield. Transcription of probes was confirmed by running 1 $\mu$l product on an agarose gel (1% TBE with 0.5% TBE running buffer) containing ethidium bromide. 10 Units of DNaseI were added to 80 $\mu$l ultra-pure $H_2O$, which was subsequently added to the probe reaction to remove template DNA, and together the mix was incubated for 10 min at 37ºC. RNA probe was then precipitated with 10 $\mu$l sodium acetate (3 M; pH5.4) and 250 $\mu$l ethanol (pre-cooled to -20ºC) on dry ice for 1 h and centrifuged at 13,000 x rpm for 30 min at 4ºC. RNA pellets were washed once in 500 $\mu$l 70% EtOH (DEPC-treated $H_2O$) and air-dried before rehydrating in 50 $\mu$l ultrapure $H_2O$, quantifying on a NanoDrop, and then stored at –40ºC.

### 3.2.25. Section In Situ Hybridisation

For section *in situs*, tissues were dissected and processed as described for immunohistochemistry, with the exception that PBS or graded dilutions of ethanol were prepared in 0.1% DEPC-treated water. For section *in situs*, all solutions were made

using 0.1% DEPC-treated sterile water or PBS for all pre-hybridisation stages. Washes and incubations were carried out at RT, unless otherwise stated, in 4h baked glassware free of RNases, and paraffin sections were cut at 6 $\mu$m. Solutions were generally made up to 50 ml in Falcon tubes and numbered accordingly for convenience. Coplin jars were used as vessels for each wash or incubation stage, unless stated otherwise. The steps for this procedure are listed in tables 3.4 and 3.5.

**Table 3.4. Slide preparation and hybridisation for section *In Situ* hybridisation**
(Note: *TEA treatment requires vigorous agitation for the first min of each stage)

| Step | Solution | Temperature | Incubation time |
|---|---|---|---|
| 1 | Xylene | RT | 1 h |
| 2 | Xylene | RT | 15 min |
| 3 | 100% EtOH | RT | 15 min |
| 4 | 100% EtOH | RT | 5 min |
| 5 | 100% EtOH | RT | 5 min |
| 6 | 90% EtOH | RT | 5 min |
| 7 | 70% EtOH | RT | 5 min |
| 8 | 50% EtOH | RT | 5 min |
| 9 | 30% EtOH | RT | 5 min |
| 10 | PBS | RT | 5 min |
| 11 | PBS | RT | 5 min |
| 12 | 4% PFA | RT | 20 min |
| 13 | PBS | RT | 5 min |
| 14 | PBS | RT | 5 min |
| 15 | PBS + Proteinase K | RT (pre-warmed to 37ºC) | 28 min |
| 16 | 4% PFA | RT | 10 min |
| 17 | PBS | RT | 5 min |
| 18 | PBS | RT | 5 min |

| | | | |
|---|---|---|---|
| 19 | 0.2 M HCl | RT | 10 min |
| 20 | PBS | RT | 5 min |
| 21 | PBS | RT | 5 min |
| 22 | 0.1 M TEA | RT | 1 min* |
| 23 | 0.1 M TEA + acetic anhydride | RT | 5 min* |
| 24 | 0.1 M TEA + acetic anhydride | RT | 10 min* |
| 25 | PBS | RT | 5 min |
| 26 | PBS | RT | 5 min |
| 27 | 30% EtOH | RT | 2 min |
| 28 | 50% EtOH | RT | 2 min |
| 29 | 70% EtOH | RT | 2 min |
| 30 | 90% EtOH | RT | 2 min |
| 31 | 100% EtOH | RT | 2 min |
| 32 | 100% EtOH | RT | 2 min |

Slides were then air-dried in the Coplin jar for 10 min while the hybridisation chamber was prepared by soaking Whatmann paper with humidity solution (5x SSC pH 4.5/50% Formamide) and laying cut pastette shafts adjacently to raise slides and keep them horizontal). Aliquots of hybridization buffer were preheated to 85ºC for 15 min and then probe was added at concentration of ~500 ng/$\mu$l, allowing for 200 $\mu$l total hybridisation mix per slide, and incubated for a further 10 min 85ºC and then placed on ice. Hybridisation mix was added to each slide and then covered neatly with cut parafilm to prevent evaporation. Slides were placed in hybridisation chamber and incubated at 55ºC for 16-20 h. Proteinase K (10 mg/ml) was added to PBS for a final concentration of 20 $\mu$g/ml (100$\mu$l to 50 ml PBS). For 0.2 M HCl: a 1:5 dilution of 1 N HCl was prepared (9 ml concentrated HCl; 241 ml $H_2O$). For TEA (0.1 M), 6.7 ml of 98% Triethanolamine

(Sigma) was added to 500 ml sterile ultrapure $H_2O$ and filtered. 125 $\mu$l acetic anhydride (Sigma) was then added to 50 ml TEA (0.1 M) for washes 23 & 24. Hybridisation buffer (50 ml) was made using 25 ml distilled formamide; 12.5 ml 20x SSC (DEPC) pH 4.5; 2.5 ml 20% SDS; 250 $\mu$l yeast tRNA (50 mg/ml); 125 $\mu$l Heparin (20 mg/ml); and 10 ml ultrapure $H_2O$.

**Table 3.5. Post-hybridisation steps for section *In Situ* hybridisation.** (Note: *Blocking and antibody incubation steps were carried in post-RNase humidity chambers prepared as before but by substituting 5xSSC/50% formamide with dd$H_2O$. ** TBST-Levamisole treatment required agitation)

| Step | Solution | Temperature | Incubation time |
|---|---|---|---|
| 1 | 5x SSC (to remove parafilm) | 60ºC | 5 min |
| 2 | 2x SSC/50% formamide | 60ºC | 20 min |
| 3 | TNE | RT | 10 min |
| 4 | TNE | 37ºC | 10 min |
| 5 | TNE + RNase A | 37ºC | 35 min |
| 6 | TNE | RT | 10 min |
| 7 | TNE | RT | 10 min |
| 8 | 2x SSC | 60ºC | 15 min |
| 9 | 2x SSC | 60ºC | 15 min |
| 10 | 0.2x SSC | 60ºC | 15 min |
| 11 | 0.2x SSC | 60ºC | 15 min |
| 12 | 1x TBST | RT | 15 min |
| 13 | Dry slides | - | - |
| 14 | 1x Blocking Reagent | RT | 1 h* |
| 15 | Anti-DIG-AP (1:2000) | RT | 1 h* |
| 16 | 1x TBST + Levamisole | RT | 15 min** |
| 17 | 1x TBST + Levamisole | RT | 15 min** |
| 18 | APB Buffer | RT | 15 min** |
| 19 | BM Purple substrate | RT/4ºC | **User defined** |

Reactions were stopped by 3x 5 min washes in dd$H_2O$, followed by dehydration in 3x 2 min washes in 100% EtOH and 4x 2 min washes in Xylene. Slides were then mounted in Permount and covered with a coverslip and air-dried in a fume-hood. Dilutions of SSC were made from 20x stock SSC. TNE buffer was made using 100 ml of 5 M NaCl; 5 ml of 1 M Tris HCl (pH 8.0); and 1 ml of 0.5 M EDTA, adding deionised $H_2O$ to 500 ml. 120 $\mu$l RNase A (10 mg/ml) was added to 50 ml TNE buffer. A stock solution of 10x Blocking reagent (Roche) was made in 1 M Maelic acid and stored in aliquots at –20ºC and working solutions (1x) were made by adding 5 ml to 45 ml TBST. Anti-DIG-AP (Roche) was diluted 1:2000 in 1x blocking reagent, allowing ~ 500 $\mu$l per slide. Levamisole (800$\mu$l of 125 mM) was added to 50 ml TBST to a final concentration of 2mM. APB buffer (50 ml) was made from 0.5 ml Tween-20; 1 ml 5 M NaCl; 2.5 ml Tris-HCl (pH 9.5); 800$\mu$l of 125 mM Levamisole; 12.5 ml of 200 mM $MgCl_2$ and 32.5 ml deionised $H_2O$. BM-Purple AP Substrate Solution (NBT/BCIP) (Roche) was applied liberally until colour development and rinsed off with sd$H_2O$. Slides were mounted in Vectashield (Vector Laboratories).

### 3.2.26. Whole mount In Situ hybridisation

Embryos were dissected as described for immunohistochemistry. All solutions were made from RNase-free, DNase-free sterile Ultrapure d$H_2O$. Dissected embryos were washed 2x in PBS and fixed in 4% PFA in PBS overnight at 4ºC. The steps for this procedure are listed in tables 3.6 and 3.7.

**Table 3.6. Pre-hybridisation steps for whole mount *In Situ* hybridisation.**

| Step | Solution | Temperature | Incubation time |
|---|---|---|---|
| 1 | PBT | RT | 2x 5 min |
| 2 | 25% Methanol:PBT | RT | 5 min |
| 3 | 50% Methanol:PBT | RT | 5 min |
| 4 | 75% Methanol:PBT | RT | 5 min |
| 5 | 100% Methanol | RT | 5 min |
| 6 | 100% Methanol | RT | 10 min |
| Optional | 100% Methanol | -20oC | Storage < 2 months |
| 7 | 75% Methanol:PBT | RT | 5 min |
| 8 | 50% Methanol:PBT | RT | 5 min |
| 9 | 25% Methanol:PBT | RT | 5 min |
| 10 | PBT | RT | 10 min |
| 11 | 6% $H_2O_2$ in PBT | RT | 1 h |
| 12 | PBT | RT | 3x 5 min |
| 13 | 10 $\mu$g/ml Proteinase K | RT | E10.5=20 min; E11.5=25 min; E13.5=30 min |
| 14 | 2 mg/ml Glycine in PBT | RT | 5 min |
| 15 | PBT | RT | 2x 5 min |
| 16 | Pre-hybridisation buffer | Pre-warmed 65ºC | Until embryos sink |
| 17 | Pre-hybridisation buffer | Pre-warmed 65ºC | O/N |

Hybridisation buffer for whole mount *In Situs* is the same as for section *In Situs*, and aliquots were preheated to 85ºC for 15 min. Riboprobes were added at concentration of ~500 ng/$\mu$l and cooled immediately on ice. Hybridisation buffer with riboprobe mixes was added to embryos and together were incubated 2x O/N.

**Table 3.7. Post-hybridisation and detection steps for whole mount *In Situ* hybridisation.**

| Step | Solution | Temperature | Time |
|---|---|---|---|
| 1 | Solution A | 65ºC | 5 min |
| 2 | 50:50 solution | 65ºC | 5 min |
| 3 | 2x SSC; 0.1% CHAPS | 65ºC | 2x 30 min |
| 4 | 0.2x SSC; 0.1% CHAPS | 65ºC | 2x 30 min |
| 5 | Cool on bench | RT | 5 min |
| 6 | TBST | RT | 3x 5 min |
| 7 | TBST | 4ºC | 72 hr |
| 8 | 10% Sheep serum in TBST | RT | 6 h (rocking) |
| 9 | 1:2000 Anti-DIG 1°Ab in 1% sheep serum in TBST | RT | 1 min |
| 10 | 1:2000 Anti-DIG 1°Ab in 1% sheep serum in TBST | 4ºC | O/N |
| 11 | TBST | 4ºC | 3x 5 min |
| 12 | TBST | RT | 5x 12 min |
| 13 | TBST | 4ºC | O/N |
| 14 | Repeat steps 11-13 | - | - |
| 15 | NTMT | RT | 1 min |
| 16 | NTMT | RT | 3x 10 min |
| 17 | BM-Purple with Levamisole | RT | Colour development |
| 18 | NTMT | RT | 2x 10 min |
| 19 | PBS (pH 5.5) 1% Triton-X-100 | RT | 10 min |
| 20 | 4% PFA/ 0.1% Glutaraldehyde | RT | 20 min |
| 21 | 1% PFA or PBS | 4ºC | Store |

Solution A contained 5x SSC (pH 8.0), 0.1% Triton-X-100, 0.5% CHAPS, 50% Ultrapure Formamide. Anti-DIG-AP (Roche) antibody was diluted 1:2000 in blocking buffer, which has the same ingredients as for section *in situs* NTMT buffer contained

0.1% Triton-X-100, 100 mM NaCl, 100 mM Tris, 50 mM $MgCl_2$. Levamisole (125 mM) was added to BM-Purple Substrate (Roche) to a final concentration of 0.5 mM.

# 4. Results

## 4.1. Genetic mapping and analysis of the OAS locus

### 4.1.1. DNA was obtained from two separate OAS families

DNA was obtained with consent from affected patients, unaffected sibs and parents from two separate families containing a total of three OAS patients (figure 4.1.1A & B). No further pedigree information was available for these families to illustrate the nature of the consanguineous relationships

Family C was an unpublished multiplex OAS family, of Turkish origin and was a 1$^{st}$-cousin marriage. There were five sons, two of whom were affected with OAS. The first proband (Family_C; severe) had bilateral anophthalmia, oligodactyly of both feet affecting the fifth rays, syndactyly of both feet, severe mental retardation, horseshoe kidney and cleft palate. The other affected brother (Family_C; mild) had syndactyly of toes 3-5 and 4 & 5 on the right and left feet, respectively, and horseshoe kidney. He did not have an eye phenotype. Two of the other brothers had horseshoe kidney but no features of OAS and the other boy was normal. The presence of horseshoe kidney in this family may extend the phenotype range of OAS. Indeed, another case from a separate family (Garavelli et al., 2006) described a male patient with bilateral anophthalmia and hindlimb oligodactyly who also inherited horseshoe kidney. Renal ultrasounds of the parents were normal. There are no other reports of kidney abnormalities in any other reported cases, however this may reflect that only 5 other OAS reported patients

received a renal ultrasound examination. Horseshoe kidneys are the most common type of fused kidneys and can be inherited as isolated, or associated with other syndromic disorders (van Allen, 1993). In the case of the two boys who have horseshoe kidney but no OAS features in the family recruited for this study, this poses the possibility that these boys either have non-penetrant OAS, or that the kidney anomaly is a separately inherited condition. For the purpose of this study these two boys were classified as being unaffected and no further investigation of horseshoe kidney was undertaken.

Family_140 (al Gazali et al., 1994)was from a 1st cousin Syrian marriage with one boy of twins presenting with OAS and the other boy was normal. The OAS case had unilateral microphthalmia, bilateral oligodactyly of the fifth toes, fusion of 4th and 5th metacarpals and a slight delay in motor development.

DNA from patients, parents and affected sibs was used for 10k Array analysis. The autozygosity mapping was performed using data from affected individuals only.

### 4.1.2. 10K SNP arrays identified an OAS candidate interval on chromosome 14

DNA from these individuals was used for SNP genotyping analysis with the Affymetrix GeneChip® Human Mapping 10K Array Xba 131 platform. This array contains approximately 11,500 SNPs tiled on a single array with an average heterozygosity rate of 0.37 and an average distance of 210 kb between SNPs. Primary chromosomal SNP raw data was produced in Excel spreadsheets from the output

Affymetrix GeneChip® DNA Analysis Software. For each affected individual, the data was sorted by chromosome and genetic distance and was then analysed for genome wide linkage using ExludeAR spreadsheets. The output was listed as the 10x largest runs of homozygous SNPs by physical distance, including the genomic coordinates, the number of consecutive homozygous SNPs and the numbers of 'no-calls' contained in the run.

For analysis of a single patient, a run of 46 consecutive homozygous SNPs would appear by chance less than 1 in 1000 times, for two sibs, this would be 23 SNPs, and additionally the same probability is assigned to a run of 10 consecutive, homozygous and concordant SNPs in the analysis of 2 siblings and 1 unrelated individual. For both OAS affected individuals in Family_C, an overlapping run of 72 consecutive homozygous SNPs was identified on chromosome 14. This region was within the proximal and distal boundaries of a larger run of 194 consecutive, homozygous SNPs identified on chromosome 14 in the OAS patient of Family_140. These were the only significant regions of overlapping autozygosity detected. Combined together as data from 2 siblings and 1 unrelated individual, this constitutes a highly significant run of 72 consecutive, homozygous and concordant SNPs. The physical distances of these regions are defined by the genomic locations of the first flanking heterozygous SNPs of each run. For Family_140 these are at 53,193,709-99,862,235 bp, for Family_C (mild) 53,596,965-75,862,258 bp, and for Family_C (severe): 51,074,896-75,862,258 bp (figure 4.1.1C). Thus, chromosome 14: 53,596,965-75,862,258 bp was a 22.3 Mb candidate interval for OAS.

**Figure 4.1.1.**

**A**

**Family_C**

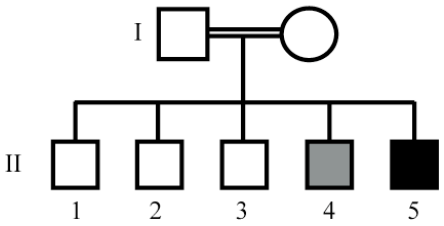


**B**

**Family_140**

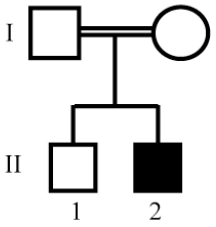


**C**

| Affecteds | Proximal | Distal |
|---|---|---|
| Family_C_Mild | 53596965 | 75862258 |
| Family_C_Severe | 51074896 | 75862258 |
| Family_140 | 53193709 | 99862235 |
| | | |
| Nijmegen_20384 | 62850464 | 81246696 |
| Nijmegen_20386 | 62850464 | 82604311 |
| Nijmegen_15781 | 65980882 | 77920731 |
| Nijmegen_15782 | 65980882 | 80741859 |
| Nijmegen_18176 | 53274830 | 73892603 |
| Nijmegen_15124 | 69652605 | 79553340 |
| | | |
| **Critical interval (1):** | **69652605** | **73892603** |

**Figure 4.1.1. Patients overlap for regions of extended autozygosity on human chromosome 14 to define a 4.2 Mb critical interval for OAS.**
Pedigrees for two families (A & B) recruited for mapping study by this research group (Edinburgh). (A) Family C (unpublished) is the product of a Turkish consanguineous marriage and contains five boys examined during childhood, two of which have the OAS phenotype. One boy is severe for OAS (II5; filled box), while another is mildly affected (II4; grey box). Two boys had isolated horseshoe kidney but do not have OAS phenotype (II1 & II2). The other boy is normal (II3). (B) Family 140 (al Gazali et al., 1994) contains one OAS boy (II2; filled box), examined at both and 8 months old, of twins from a 1st cousin Syrian marriage. The other boy is normal (II1). (C) DNA from OAS families from the Edinburgh cohort was analysed for regions of extended autozygosity in affected individuals using Affymetrix 10K SNP arrays. All three affected individuals overlapped at a region on chromosome 14 between 53,596,965-75,862,258 bp. By including similar analyses of data from a collection of OAS patients gathered by collaborators in Nijmegen, The Netherlands, this interval was reduced to 4.2 Mb, between 69,652,605-73,892,603 bp on chromosome 14. No other regions of overlap were observed and this interval was referred to as critical interval 1.

### 4.1.3. Data from OAS patients analysed by Collaborators reduced the chromosome 14 interval to 4.2 Mb

Similarly analysed data from 6x OAS patients from 4x separate families (2x multiplex families: sibs 20384 & 20386 and sibs 15781 & 15782; 2 simplex families: patients 18176 and 15124. Patient 15124 from non-consanguineous parents, all other patients were from marriages of 1$^{st}$-cousin parents) belonging to collaborators from Radbound University Nijmegen Medical Genetics, Department of Human Genetics, was added to the Edinburgh OAS cohort. These additional OAS cases also mapped to the same region on chromosome 14 and refined this interval to 69,652,605-73,892,603 bp (figure 4.1.1C). This 4.2 Mb region was defined as OAS critical interval 1, and using the Ensembl BioMart application to extract all coding genes, there were a total of 36 genes identified within this region (figure 4.1.2).

## Figure 4.1.2.

| Gene Start (bp) | Gene End (bp) | Associated Gene Name | Ensembl Gene ID |
|---|---|---|---|
| 69580687 | 69725540 | SLC8A3 | ENSG00000100678 |
| 69680762 | 69896147 | C14orf112 | ENSG00000133983 |
| 69907901 | 69953497 | SYNJ2BP | ENSG00000213463 |
| 69993970 | 69996375 | ADAM21P. | ENSG00000139985 |
| 70058832 | 70071485 | ADAM20 | ENSG00000134007 |
| 70120710 | 70137137 | MED6 | ENSG00000133997 |
| 70178257 | 70211830 | TTC9 | ENSG00000133985 |
| 70264605 | 70345641 | MAP3K9 | ENSG00000006432 |
| 70443875 | 70651852 | PCNX | ENSG00000100731 |
| 71065795 | 71275871 | SIPA1L1 | ENSG00000197555 |
| 71501247 | 72102990 | RGS6 | ENSG00000182732 |
| 72145495 | 72430562 | DPF3 | ENSG00000205683 |
| 72462838 | 72496109 | WDR21A | ENSG00000119599 |
| 72505912 | 72563600 | ZFYVE1 | ENSG00000165861 |
| 72595021 | 72657740 | RBM25 | ENSG00000119707 |
| 72672908 | 72756862 | PSEN1 | ENSG00000080815 |
| 72773958 | 72811098 | PAPLN | ENSG00000100767 |
| 72811671 | 72892230 | NUMB | ENSG00000133961 |
| 73014949 | 73095404 | HEATR4 | ENSG00000187105 |
| 73073571 | 73080206 | ACOT1 | ENSG00000184227 |
| 73105698 | 73112110 | ACOT2 | ENSG00000119673 |
| 73128163 | 73132221 | ACOT4 | ENSG00000177465 |
| 73153301 | 73156345 | ACOT6 | ENSG00000205669 |
| 73181455 | 73232937 | DNAL1 | ENSG00000119661 |
| 73249034 | 73250095 | PNMA1 | ENSG00000176903 |
| 73251587 | 73323649 | C14orf43 | ENSG00000156030 |
| 73388381 | 73421915 | ZADH1 | ENSG00000140043 |
| 73423327 | 73468733 | ZNF410 | ENSG00000119725 |
| 73470458 | 73486588 | C14orf44 | ENSG00000156050 |
| 73486396 | 73499564 | COQ6 | ENSG00000119723 |
| 73502946 | 73552387 | ENTPD5 | ENSG00000187097 |
| 73555873 | 73602546 | C14orf45 | ENSG00000119636 |
| 73621419 | 73736870 | LIN52 | ENSG00000205659 |
| 73775928 | 73799187 | VSX2 | ENSG00000119614 |
| 73821733 | 73839512 | ABCD4 | ENSG00000119688 |
| 73884919 | 73896461 | C14orf115 | ENSG00000133980 |

**Figure 4.1.2. The 4.2 Mb critical interval for OAS contains 36 known coding genes.**
Using Ensembl to mine the critical interval, 36 known coding genes were identified in this region and are listed according to their genomic location.

### 4.1.4. SNP data from another OAS family reduced the critical interval to 3.6 Mb

Recruitment of a third family to the collection of OAS families in the Edinburgh cohort enabled further genetic mapping. This family contained an OAS-affected boy and a normal younger sib, the products of an Italian gipsy 2nd-cousin marriage (Figure 4.1.3A). No further pedigree information was available for this family.

The proband had bilateral anophthalmia, fused 4th-5th metacarpals bilaterally, and fifth-toe oligodactyly with 2nd and 3rd toe syndactyly on both feet, and horseshoe kidney. Affymetrix GeneChip® 10k Array analysis using the ExcludeAR software revealed a region of autozygosity in the OAS child on chromosome 14:69,652,605-73,059,612 bp (Figure 4.1.3B). This overlapped with critical interval 1 and refined it distally by 830 kb to 3.6 Mb, creating OAS critical interval 2.

Linkage analysis was performed using SNP data from the four affected OAS patients from the three Edinburgh families. Exported SNP data was converted into conventional linkage format, together with pedigree files that were generated for each family, allele frequencies for the Caucasian ethnic group and the required SNP marker data, to enable the running of ALOHOMORA, a data conversion software tool to facilitate a genome-wide linkage study of the data. Following error removal, the linkage analysis programme Allegro (v1.2c) was then used to undertake a genome-wide multipoint linkage analysis, based on a recessive model of inheritance and using a disease allele frequency of 0.0001. A LOD score of $Z$=5.3 was obtained between

14q22.3-24.2 (Figure 4.1.3C) with the genomic position 53.156-71.254 cM, delimiting an OAS critical interval between 53.60-72.22 Mb. This further reduced the critical interval for OAS. The calculated LOD score for this region exceeded the threshold of *Z*=3.3 set for parametric analysis recommended by Lander and Krugylak (Lander and Kruglyak, 1995) and was therefore considered as statistically significant. Linkage analysis was performed with the help of Dr. Louise Bicknell (MRC Human Genetics Unit).

**Figure 4.1.3.**

**A**

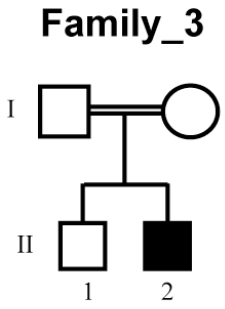


**B**

| Affecteds | Proximal | Distal |
|---|---|---|
| Family_3 | 69425921 | 73059612 |
| **Critical interval (2):** | **69652605** | **73059612** |

**C**

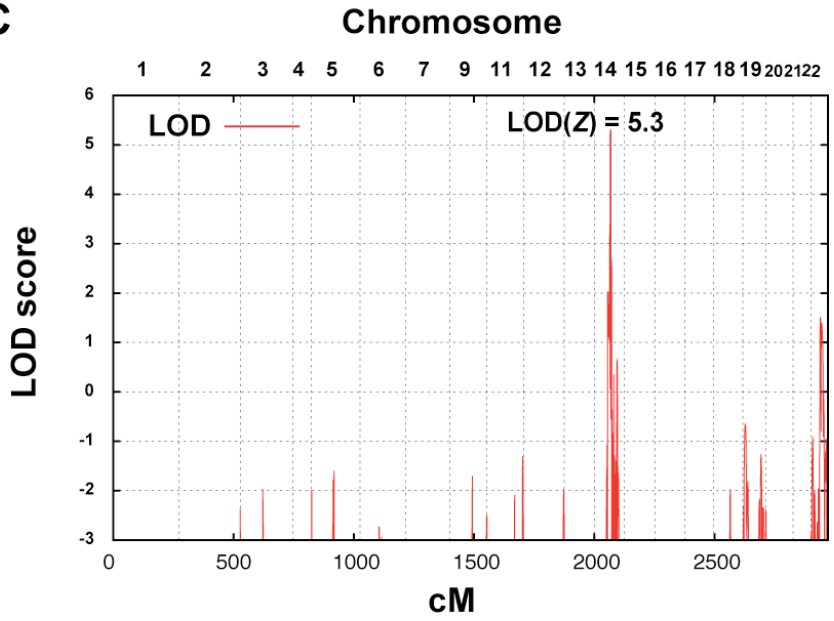

**Figure 4.1.3. The OAS critical interval was refined to 3.4 Mb and linkage was calculated.**

A third family was added to the Edinburgh cohort. (A) This was a 2$^{nd}$-cousin gipsy marriage containing two boys, one of whom had severe OAS. The other was unaffected. (B) Analysis by 10k Xba 131 SNP array identified a region of autozygosity on chromosome 14, between 69,425,921-73,059,612 bp. This mapping region overlapped with the other cases and reduced the critical interval distally by 830 kb to chromosome 14:69,652,605-73,059,612 bp. This refined interval was referred to as Critical Interval 2. (C) The overlapping regions of autozygosity from the four affected individuals from the separate consanguineous families of the Edinburgh cohort achieved a significant LOD score of $Z$=5.3 following parametric multipoint linkage analysis using Allegro (v1.2c) and the ALOHOMORA data conversion software. The significance level for parametric linkage analysis is set to $Z$=3.3.

### 4.1.5. A PCR-based sequencing strategy was employed to identify coding changes in OAS patients

The Ensembl application BioMart identified there were now only 19 known coding genes in critical interval 2 (figure 4.1.4A). A PCR-based sequencing strategy was designed to identify genetic mutations within the critical interval. Genes were divided into individual exons, which were ranked according to degree of evolutionary sequence conservation using PhastCons17. This programme calculated sequence similarity as a measure of evolutionary conservation across 17 vertebrates including mammalian, amphibian, avian, and teleost species (Siepel et al., 2005). Oligonucleotide primers were designed for sequence analysis using a modified script of Primer3 (http://frodo.wi.mit.edu/). This bioinformatics work was carried out by Phillipe Gaultier (MRC Human Genetics Unit)

Exons were divided equally between the two collaborative groups and PCR-based sequencing was performed using unamplified and whole-genome amplified genomic DNA samples from 8x OAS patients (Figure 4.1.4B). Using 8x patients allowed for high-throughput strategy using 96-well PCR plates with primer pairs for 12x exons. The final status of this project was that 61% of all exons in the Edinburgh cohort were successfully sequenced for ≥4 patients and a further 11% of exons were either partially completed (i.e. for large exons), or had full-exon sequence for between 1-3 patients. Only 28% of exons had no sequence data generated (figure 4.1.4C). The status of sequencing for exons on a gene-by-gene basis is illustrated in figures 4.1.5 and 4.1.6.

**Figure 4.1.4.**

**A**

| Gene Start (bp) | Gene End (bp) | Associated Gene Name | Ensembl Gene ID |
|---|---|---|---|
| 69580687 | 69725540 | SLC8A3 | ENSG00000100678 |
| 69680762 | 69896147 | C14orf112 | ENSG00000133983 |
| 69907901 | 69953497 | SYNJ2BP | ENSG00000213463 |
| 69993970 | 69996375 | ADAM21P. | ENSG00000139985 |
| 70058832 | 70071485 | ADAM20 | ENSG00000134007 |
| 70120710 | 70137137 | MED6 | ENSG00000133997 |
| 70178257 | 70211830 | TTC9 | ENSG00000133985 |
| 70264605 | 70345641 | MAP3K9 | ENSG00000006432 |
| 70443875 | 70651852 | PCNX | ENSG00000100731 |
| 71065795 | 71275871 | SIPA1L1 | ENSG00000197555 |
| 71501247 | 72102990 | RGS6 | ENSG00000182732 |
| 72145495 | 72430562 | DPF3 | ENSG00000205683 |
| 72462838 | 72496109 | WDR21A | ENSG00000119599 |
| 72505912 | 72563600 | ZFYVE1 | ENSG00000165861 |
| 72595021 | 72657740 | RBM25 | ENSG00000119707 |
| 72672908 | 72756862 | PSEN1 | ENSG00000080815 |
| 72773958 | 72811098 | PAPLN | ENSG00000100767 |
| 72811671 | 72892230 | NUMB | ENSG00000133961 |
| 73014949 | 73095404 | HEATR4 | ENSG00000187105 |

**B**

| CASE ID | CASE REF. | ORIGIN | CONSANGUINITY | SEX | PUBLISHED REF |
|---|---|---|---|---|---|
| A | FAMILY_3 | ITALIAN | 2nd COUSINS | M | GARAVELLI (2006) |
| B | FAMILY_140 | SYRIAN | 1st COUSINS | M | AL GAZALI (1994) |
| C | FAMILY-C (SEVERE) | TURKISH | 1st COUSINS | M | UNPUBLISHED |
| D | 18176 (NIJMEGEN) | SICILIAN | 1st COUSINS | M | PALLOTTA (1984) |
| E | 15781 (NIJMEGEN) | DUTCH | 1st COUSINS | F | WAARDENBURG (1961) |
| F | 20384 (NIJMEGEN) | TURKISH | 1st COUSINS | M | SAYLI (1995) |
| G | 17715 (NIJMEGEN) | TURKISH | 1st COUSINS | M | UNPUBLISHED |
| H | 15124 (NIJMEGEN) | PUERTO RICAN | NO | F | UNPUBLISHED |

**C**

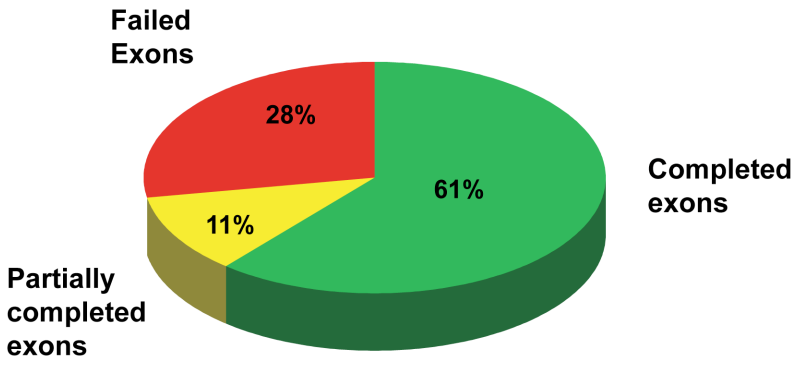

**Figure 4.1.4. Sequencing of all exons within the refined 3.4 Mb critical interval was attempted for a panel of 8 patients.**
**(A)** Using Ensembl to mine the critical interval, 19 known coding genes were identified in this region and were listed according to their genomic location. The exons in these genes were ranked according to their sequence conservation across 17 species (PhasCons17) and were divided up equally between collaborators for DNA sequencing. (**B**) Table with information for patient DNA samples used in the panel for sequencing. (**C**) Progress of sequencing for Edinburgh cohort, where completed exons refers to those where good quality sequence data was produced for the whole exon in four or more patients. Partial coverage was applied for exons either with less than four, but more than one, patients with complete exon coverage, or for larger exons where all patients had incomplete coverage.

## Figure 4.1.5.

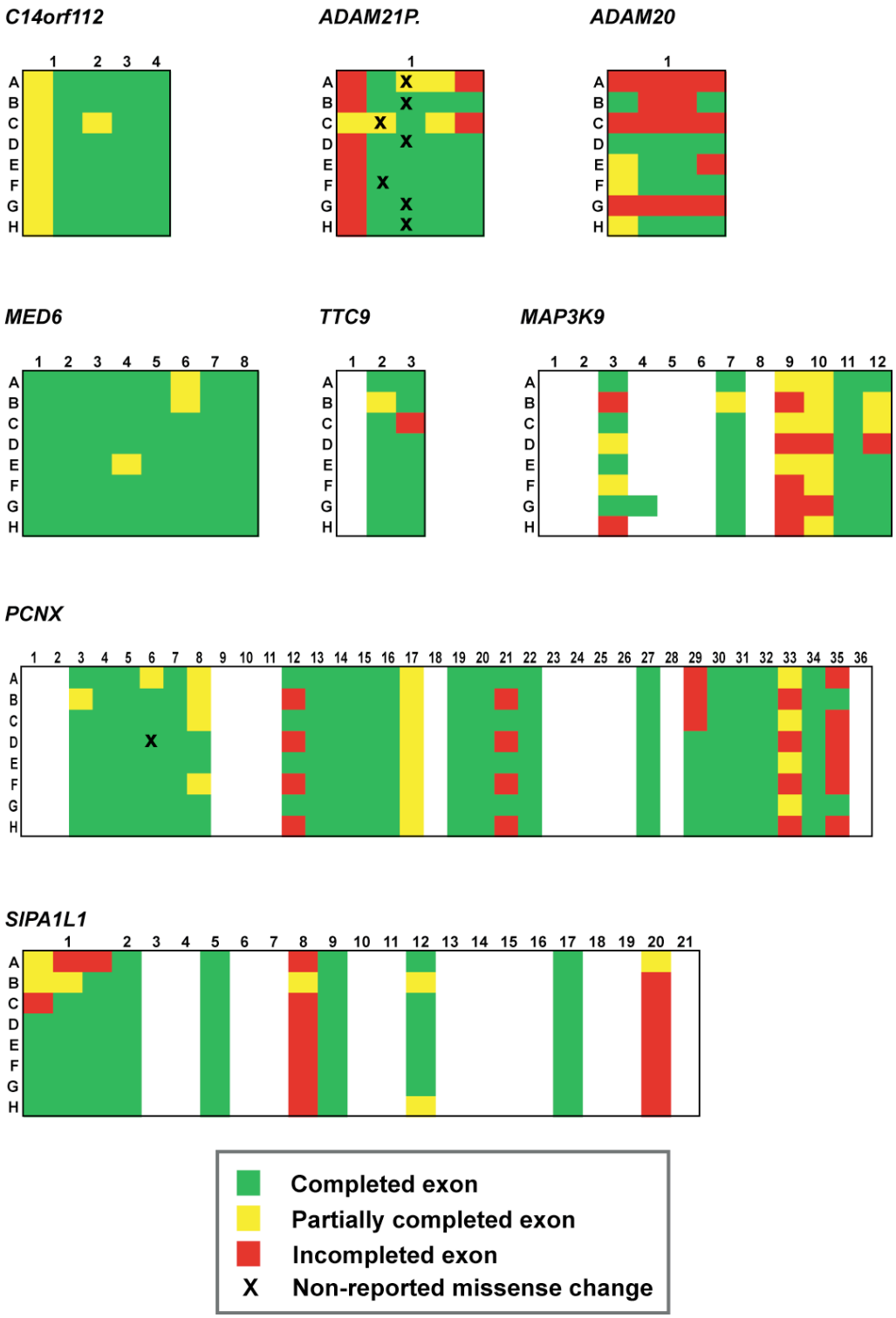
C14orf112
ADAM21P.
ADAM20
MED6
TTC9
MAP3K9
PCNX
SIPA1L1
Completed exon
Partially completed exon
Incompleted exon
X Non-reported missense change

**Figure 4.1.6.**

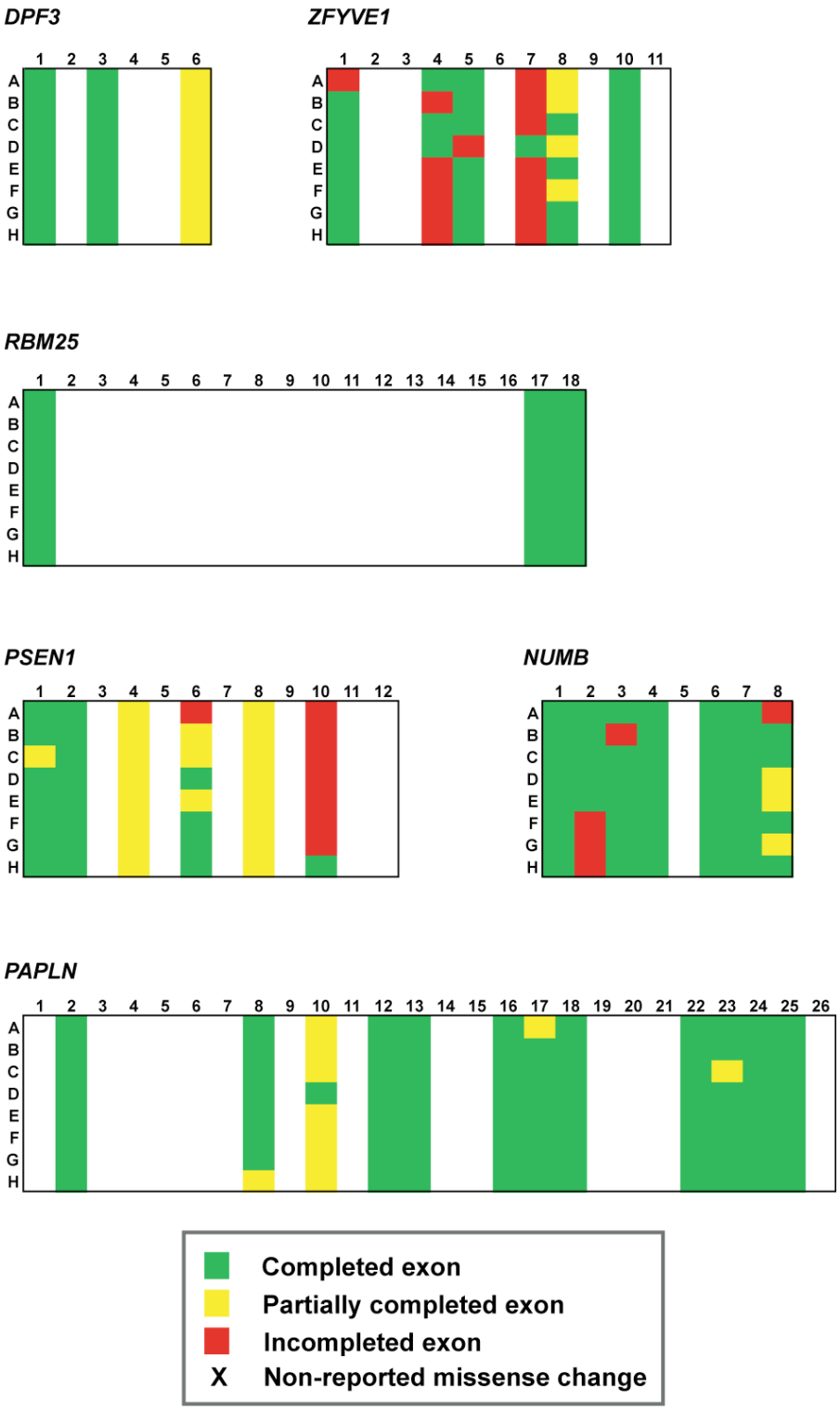
DPF3
1 2 3 4 5 6
A B C D E F G H
ZFYVE1
1 2 3 4 5 6 7 8 9 10 11
A B C D E F G H
RBM25
1 2 3 4 5 6 7 8 9 10 11 12 13 14 15 16 17 18
A B C D E F G H
PSEN1
1 2 3 4 5 6 7 8 9 10 11 12
A B C D E F G H
NUMB
1 2 3 4 5 6 7 8
A B C D E F G H
PAPLN
1 2 3 4 5 6 7 8 9 10 11 12 13 14 15 16 17 18 19 20 21 22 23 24 25 26
A B C D E F G H
Completed exon
Partially completed exon
Incompleted exon
X Non-reported missense change

**Figures 4.1.5 & 4.1.6. Sequencing coverage for the coding regions of each gene.**

Genes that had sequence data generated for the patient panel in the Edinburgh cohort are displayed graphically. Green indicated full coverage for that exon and patient, yellow was partial coverage for an exon for each patient, whereas red indicated there was no sequence data for that exon and patient. Note there is no sequence data for any region of genes SYNJ2BP, RGS6, WDR21A, and HEATR4 due to PCR or sequencing failure and the majority of exons within these genes belonging to the Nijmegen data set. Green indicated complete sequence for that exon, yellow was for incomplete coverage for that exon and red was for no coverage due to sequencing failure. X = Identification of missense changes not previously reported.

### 4.1.6. The sequencing strategy identified numerous coding and non-coding changes in patient DNA

For those exons that have been successfully sequenced in the Edinburgh data set, many nucleotide changes have been identified (figure 4.1.7). Silent changes, defined as not creating a difference in the encoded amino acid at that location, and changes in non-coding regions were identified throughout the critical interval (figure 4.1.7A). There were 14 known polymorphic SNPs identified, of which 8 were within the *ADAM21* gene. Additionally, this gene contained 2x silent changes not previously reported. There were also silent changes noted in *PCNX, MAP3K9, SIPA1L1, ZFYFE1,* and *PSEN*. Previously reported non-synonymous missense changes were identified in the *ADAM21, MED6, DPF3, ZFYFE1,* and *PAPLN* genes (figure 4.1.7B), with *ADAM21* containing 3 missense changes alone. Additionally, there were 4x missense changes identified in the *ADAM21* gene that had not been previously reported (F129C, V158L, I161V, AMD V216M; figure 4.1.7C) and a novel non-synonymous change in *PCNX* (T471A). These were all of the nucleotide changes identified in the Edinburgh sequencing project during this study.

# Figure 4.1.7.

**A**

| Case ID | ADAM21 | | | | | | | | | | MED6 | PCXN | MAP3K9 | SIPA1L1 | | | ZFYVE1 | PSEN1 |
|---|---|---|---|---|---|---|---|---|---|---|---|---|---|---|---|---|---|---|
| | rs3751520 | rs3751521 | rs3751522 | rs3751523 | rs3751524 | 69,994,319 | rs3829453 | 69,994,451 | rs12436346 | rs2022624 | rs2233137 | rs3814871 | Intronic: 70,279,073 | rs34631533 | rs1859643 | rs8017465 | rs12931 | rs165932 |
| A | - | - | C | - | - | - | - | G | G | C | A | - | 8XAs | - | - | C | G | T |
| B | A | G | C | G | A | T | T | G | G | C | A | A | 8XAs | C | - | T | G | T |
| C | - | - | T | G | - | C | - | - | G | C | A | - | 8XAs | - | - | C | G | T |
| D | A | G | C | G | A | C | T | G | G | C | A | G | 8XAs | C | C | C | A | T |
| E | C | A | C | G | A | C | T | A | G | C | A | G | 8XAs | C | C | C | G | G |
| F | C | A | C | G | C | C | A | G | G | T | T | A | 9XAs | A | C | C | G | T |
| G | C | A | C | G | A | T | T | G | G | C | A | G | 8XAs | C | C | C | G | G |
| H | C | A | C | G | A | T | T | G | G | C | A | G | 9XAs | C | T | C | A | G |
| RefSeq | C | A | C | A | A | C | A | G | A | T | A | G | 8XAs | C | C | C | G | T |

**B**

| Case ID | ADAM21 | | | DPF3 | ZFYVE1 | PAPILN | |
|---|---|---|---|---|---|---|---|
| | rs3829456 | rs8010994 | rs3829452 | rs10649920 | rs2286838 | rs2280792 | rs4903104 |
| A | A | - | G | 3xT | C | A | C |
| B | A | G | G | 5xT | C | A | C |
| C | - | G | G | 5xT | C | A | C |
| D | A | G | G | 5xT | C | A | C |
| E | C | C | G | 5xT | C | A | C |
| F | A | G | C | 5xT | C | A | C |
| G | A | C | G | 3xT | C | G | T |
| H | A | C | G | 3xT | T | A | C |
| RefSeq | A | C | C | 3xT | C | A | A |
| AA Change | K247Q | D95E | A117G | TV183 -/AA | S408R | S33G | T1158M |

**C**

| Case ID | ADAM21 | | | | PCNX |
|---|---|---|---|---|---|
| A | T | G | A | A | - |
| B | T | G | A | A | C |
| C | G | - | - | - | - |
| D | T | G | A | A | G |
| E | T | C | G | G | C |
| F | T | G | A | G | C |
| G | T | G | A | A | C |
| H | T | G | A | A | C |
| RefSeq | T | G | A | G | C |
| AA Change | F129C | V158L | I161V | V216M | T471>S |

**Figure 4.1.7. Nucleotide changes identified in the OAS patient panel in the Edinburgh cohort.**

(**A**) Silent changes, including previously identified SNPs, indicating case number, SNP ID or genomic position if not previously recorded, gene ID, nucleotide change and Refseq nucleotide for that position. (**B**) Missense changes identified were all previously published and were presented with gene ID, AA change and Refseq nucleotide for that position. (C) Predicted missense changes identified in the Edinburgh OAS panel that were not already listed as SNPs, presented with gene ID, AA change and Refseq nucleotide for that position. Note the absence of data for patient A and C for some changes due to PCR or sequencing problems.

## 4.2. Establishing *Mp* phenotypes for genetic mapping of the *Mp* locus

### 4.2.1. The first generations of *Mp* displayed eye, limb and ear phenotypes

The first generation born (G0) from ICSI IVF using the *Mp* sperm produced a litter of five pups. Brendan Doe, formerly of MRC Human Genetics Unit, expertly performed the ICSI IVF for this line. Four of these animals, three females and one male, were identified as heterozygous for the *Mp* phenotype, based on the described phenotype of combined inheritance of small, flattened ears and microphthalmia. At six weeks of age, intercrosses were set up between the affected male and affected females from the G0 litter to produce homozygous offspring.

All progeny from the first heterozygote x heterozygote intercrosses were analysed ($n$=21). In contrast to the described phenotype, we noted no mortality in homozygotes. At 35 days old (P35) the homozygous *Mp* phenotype was noted in three animals that displayed apparent anophthalmia with complete failure of palpebral fissure opening, an event that should usually occur between P12-P15 in laboratory strain mice. All of these animals also displayed small, unfolded pinnae and had hind-limb oligodactyly (Figure 4.2.1A-F). Animals born with the heterozygous microphthalmia phenotype did not display distal limb anomalies. We were thus able to categorise heterozygotes and homozygote adults phenotypically.

**Figure 4.2.1**

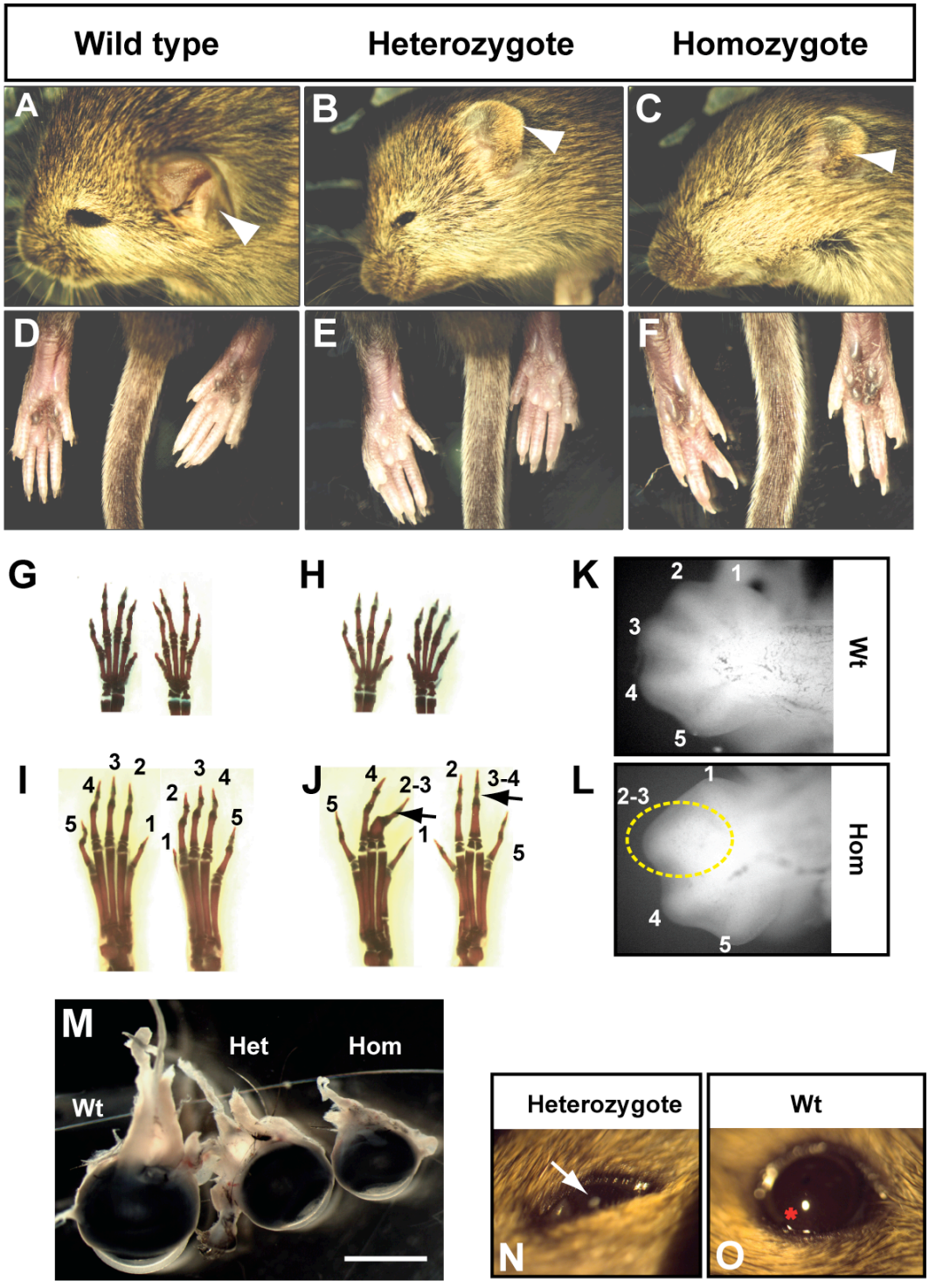
Wild type
Heterozygote
Homozygote
A
B
C
D
E
F
G
H
K
2
1
3
4
5
Wt
I
3
2
4
5
1
2
3
4
1
5
J
4
2-3
5
1
2
3-4
5
L
1
2-3
4
5
Hom
M
Het
Hom
Wt
Heterozygote
Wt
N
O

**Figure 4.2.1 Macroscopic phenotypes of *Mp* homozygote and heterozygote mice**

Gross phenotype analysis illustrated ocular, limb and external ear abnormalities in *Mp* mice (**A-F**). From analysis of external head features, *Mp/Mp* animals were identifiable by a failure of the palpebral fissures to open (**C**). In contrast, the palpebral fissures of both the heterozygote (**B**), and the wild type (**A**) were opened and revealed the presence of eyes. In addition, homozygote and heterozygote animals displayed smaller and less complex folding of the pinnae (arrowheads), in comparison to wild-type animals. Gross analysis of external limbs illustrated hindlimb oligodactyly in homozygote animals (**F**), with digits missing in the axial region of the foot. Heterozygotes (**E**) did not display a hindlimb phenotype and were comparable to the wild type (**D**). Wild-type forelimbs (**G**) and hindlimbs (**I**) displayed five rays. In contrast, homozygote hindlimbs displayed oligodactyly (**J**), with osseous fusions between phalanges 2-3-4 in their axial digits. Homozygote forelimbs were normal (**H**). Analysis of embryonic limbs (**K** & **L**) during development revealed that hindlimb oligodactyly was an embryonic phenotype, and was identifiable in the homozygote (**L**) at E13.5. No obvious ocular defect was noted by morphological analysis during embryogenesis. A graded reduction in the size of dissected ocular globes was noted in *Mp* genotypes at P35 (**M**), with homozygote and heterozygote eyes appearing considerably smaller than wild type, and with the homozygote most severely affected (Scale bar = 3.0 mm). Heterozygotes had lens cataracts, identifiable at P15 (**N**). No cataracts were observed in wild types **(O**). Asterix is artefactual folding of tissue during processing.

### 4.2.2. *Mp*/*Mp* hindlimbs had osseous oligodactyly and were identifiable during embryogenesis

Skeletal analysis of mutant hindlimbs (Figure 4.2.1G-J) indicated that oligodactyly was a result of osseous fusion between mid-axial phalanges, and that metatarsal bones remained unaffected. The fusions affected rays 2 and 3; or 3 and 4; or 2, 3 and 4, but did not ever affect rays 1 or 5.

Macroscopic analysis of embryonic development in mutant litters revealed that the homozygous hindlimb oligodactyly was unequivocally evident from E13.5 (figure 4.2.1L & K), with large and irregular condensations, consistent with the osseous fusion of several digits, present in the central digital regions of the developing footplate, which clearly differed from the discrete, regular digits seen in the wild type at equivalent stages.

### 4.2.3. Dissection revealed mutant eyes were microphthalmic

Dissection of eyes from adult mice showed that *Mp*/*Mp* were not anophthalmic but had markedly reduced eye size, i.e. were microphthalmic. A graded reduction in size was seen from wild type, to heterozygote to homozygote (Figure 4.2.1M), with the mutant eyes appearing considerably smaller than the wild type.

### 4.2.4. *Mp*/*Mp* neonates were runted

Animals were weighed to analyse the runted phenotype of the homozygote mutants described previously. In intercrosses between heterozygotes, homozygous progeny at P21 or younger showed a significant reduction in weight compared to the other phenotypes, with the mean weight of homozygotes less than half that of heterozygote and wild-type animals (Figure 4.2.2A). In contrast, there was no

significant difference observed between the weights of wild-type animals and heterozygotes in this age range. In outcrosses of heterozygotes to wild-type C57Bl6/J animals, where only adult heterozygote and wild-type progeny weights were analysed, there was no significant difference noted between the weights of these phenotypes (figure 4.2.2B). The weighing of animals for these analyses was performed by Margaret Keighren (MRC Human Genetics Unit).

## Figure 4.2.2

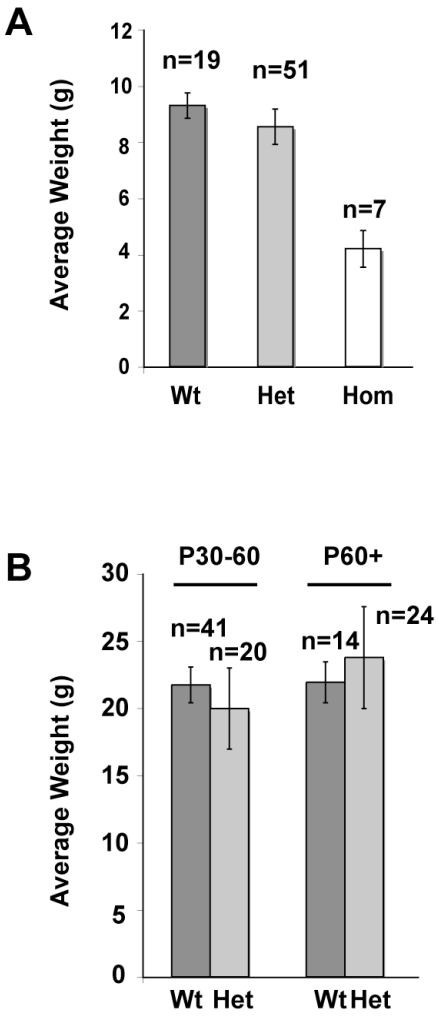


**Figure 4.2.2 Homozygous *Mp* mice were runted.**
Average weights of animals were recorded from both intercrosses (**A**) and outcrosses (**B**) of the *Mp* line. (**A**) Weights from the three genotypes recorded between post-natal days 14-22 shows there to be no significant weight difference between heterozygotes and wild-types, but that homozygotes have significantly lower weighs than both of these classes. (Wt, *n*=19; *Mp/+, n*=51; *Mp/Mp*, *n*=7). (**B**) Weights for heterozygotes and wild-types show no significant difference at age ranges P30-60, and P60 and older (*n* values are: Wt=41; Het=20 and Wt=14; Het=24, for P30-60 and P60+, respectively). For both analyses, confidence intervals of 95% were used.

### *4.2.5.* Sufficient phenotype information was therefore established for genetic mapping *Mp*

Taken together, these phenotypic features were sufficient to differentiate between wild-type mice and those homozygous or heterozygous for Mp. Therefore, to develop a genome mapping strategy to identify the disease locus, these features were used to phenotypically analyse all offspring from post-natal day 21 onwards.

## 4.3. Analysis of the *Mp* ocular phenotype

### 4.3.1. Adult *Mp* eyes displayed pan-ocular malformations

Histological analysis of the *Mp* ocular phenotype was begun with animals at P15 using Haematoxylin & Eosin (H&E) staining (Figures 3.2.3 & 3.2.4). At this stage, the Wt cornea, ciliary body, anterior segment and iris were formed normally. Vitreous body physically separated the central lens from the retina, the lens is mature and all retinal layers are present (Figure 4.2.3A). In contrast, mutant animals at the same stage appeared to lack vitreous body and had disruptions to the laminar structure of the retina (Figure 4.2.3B & C), indicated by the presence of abnormal folding of the cell layers and circular, rosette-like structures composed of cells and their processes interrupting the normal uniform lamination of the retina. In addition, the *Mp*/*Mp* eye displayed a thickened and abnormal cornea, and the lens appeared structurally abnormal and regionally displaced the retina (Figure 4.2.3C). These additional phenotypic features were not seen in *Mp*/+ eyes (Figure 4.2.3B). The extension of RPE in the mutant to between lens and cornea was an artefact due to the plane of sectioning in this specimen and is not thought to be indicative a mutant phenotype.

**Figure 4.2.3**

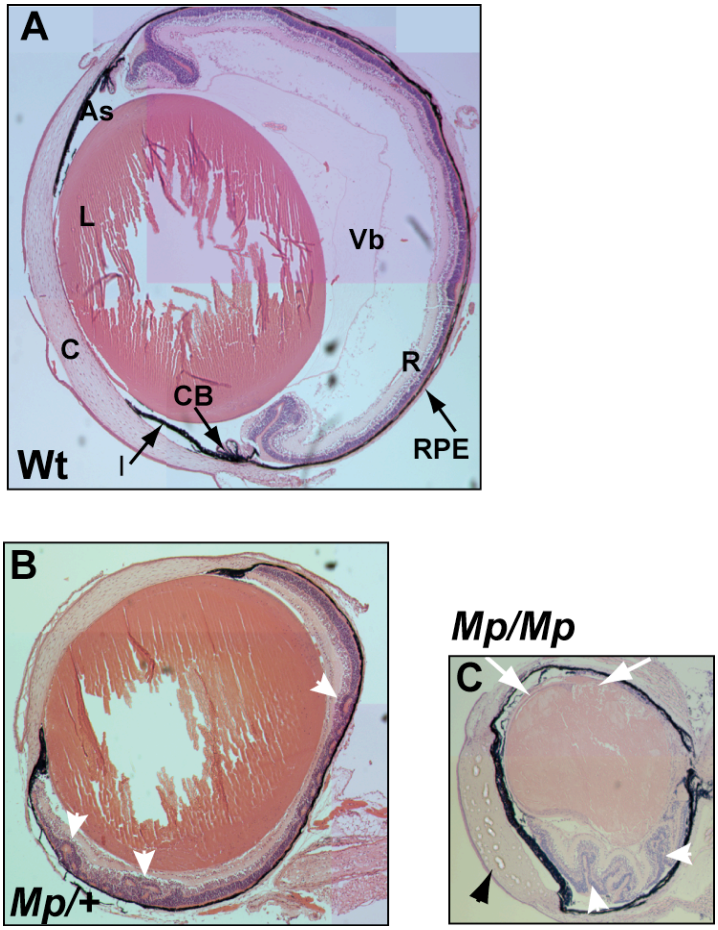

**Figure 4.2.3 Histological analysis revealed *Mp* mice display a severe pan-ocular phenotype.**
Haemotoxylin & Eosin (H&E) analysis of full eye composites from paraffin-embedded coronal sections at post-natal day (P)15 indicated gross structural malformations. In the Wt eye (**A**) the cornea (C), iris (I), anterior-segment (AS), and RPE were fully formed, and the vitreous body (VB) separated the lens (L) and retina (R). In contrast, the space occupied by VB between lens and retina was missing in heterozygotes (**B**) and homozygotes (**C**). In addition, mutant retinas displayed disorganisation in the normal lamination of cell types and were folded, or had rosettes, in discrete regions, as indicated by white arrowheads (**B** & **C**). The retinal phenotype was more severe in the homozygote, with increased folding than heterozygote, and was associated with increased corneal thickness and a structurally malformed lens, which had dorsally displaced the retinal tissue in this sample. These features were not seen in the heterozygote eye. The RPE continuation across the lens in the anterior region of the homozygote was an artefact of planar deviation on sectioning.

### 4.3.2. *Mp* retina layers were abnormally patterned and presented with rosette structures

Higher magnification analysis of retinas revealed major differences between wild type and mutant retinas (figure 4.2.4A-C). The rosettes observed in the heterozygote retina affected cells from both the inner and outer layers and their associated plexiform layers (Figure 4.2.4B). The homozygote retina (Figure 4.2.4C) was more severely disrupted than the heterozygote and individual cell layers were not easily identified, although homozygous rosettes appeared to be composed only of cells from the outer nuclear and plexiform layers. In addition, homozygote retinas appeared to have reduced numbers of ganglion cells.

### 4.3.3. Mp/Mp eyes displayed additional abnormalities in cornea, lens and ciliary body

Macroscopic analysis of lenses, corneas and anterior segments (Figure 4.2.4D-F) revealed that in the homozygote, stromal cells of the cornea were not correctly organised into the linear configuration seen in Wt and heterozygotes. Additionally, the lens of the homozygote did not have the normal stratified appearance of both the wt and heterozygote lenses. Instead the homozygote lens appeared globular in structure and displayed various vacuoles. Furthermore, there were disruptions to the anterior segment of heterozygote and homozygote animals, with the complete loss of ciliary processes in homozygotes and only rudiments of these processes present in the heterozygote. Together, these features constitute major pan-ocular malformations in the *Mp* mouse.

**Figure 4.2.4.**

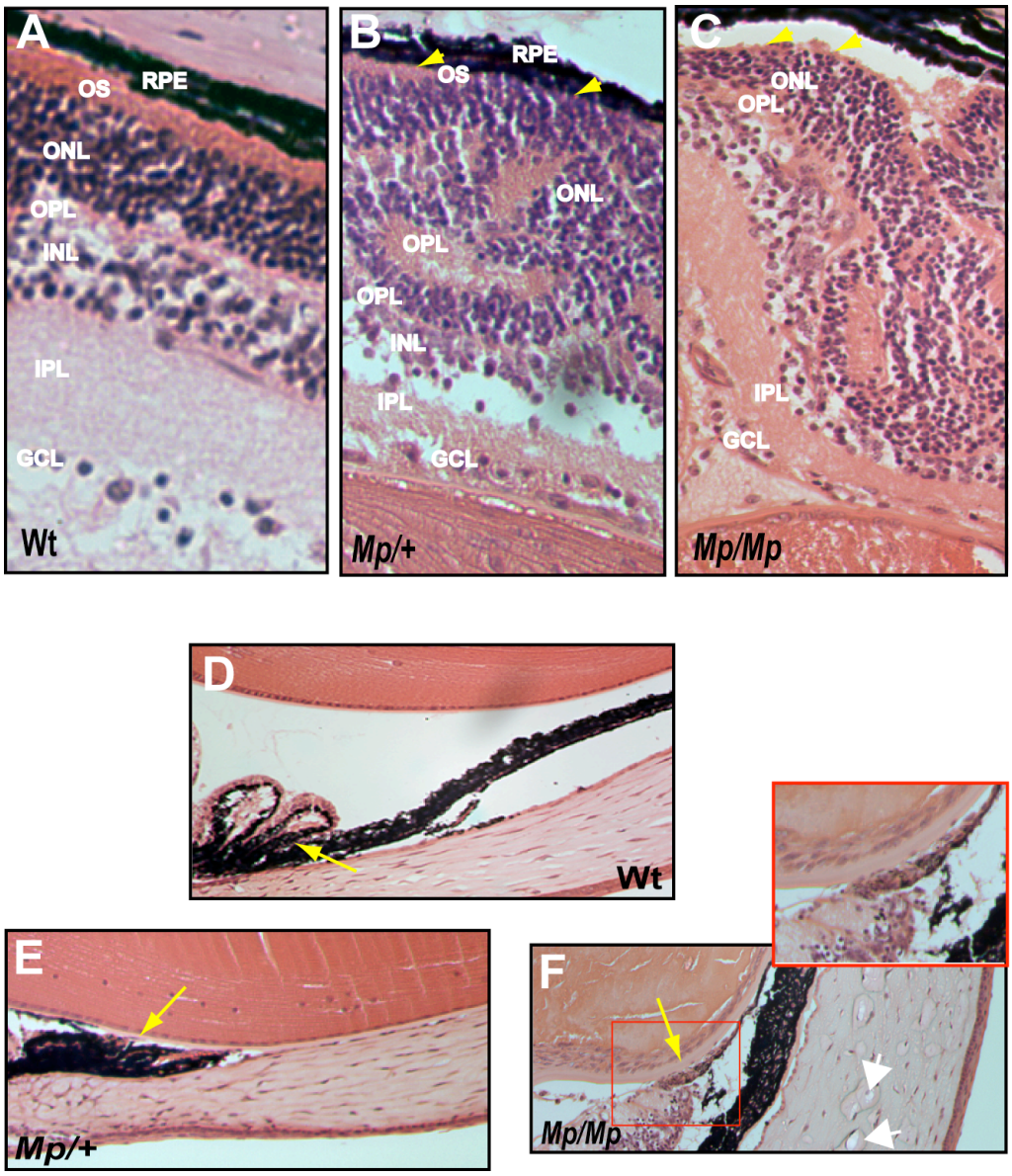
A
OS
RPE
ONL
OPL
INL
IPL
GCL
Wt
B
OS
RPE
ONL
OPL
OPL
INL
IPL
GCL
Mp/+
C
ONL
OPL
IPL
GCL
Mp/Mp
D
Wt
E
Mp/+
F
Mp/Mp

**Figure 4.2.4 Higher magnification analysis of mutant eyes revealed severe retinal and anterior-eye abnormalities.**
Higher magnification analysis revealed the rosettes were possibly composed of cellular projections from the outer nuclear layer in the heterozygote (**B**) but in the homozygote (**C**), the severity of the folding inhibited the identification of particular cell types of the rosettes. Some ganglion cells were identifiable in the inner-most region of the homozygote retina, whereas in both heterozygote and homozygote the outer segment was only present between RPE and outer nuclear layer in certain regions and was not continuous (arrowheads). Enlarged images of the anterior ocular regions (**D-F**) reveal a graded disruption to ciliary processes (arrows), with none identifiable in the homozygote (**F** & **inset**), and a reduced structure in the heterozygote (**E**), compared to the Wt (**D**). In addition, the cornea of the homozygote is disrupted in the stromal layer, with a loss of normal layer organisation and vacuolar spaces between some cells (filled arrowheads), resulting in a thickened corneal structure overall. GCL, ganglion-cell layer; INL, inner nuclear layer; ONL, outer nuclear layer; IPL, inner plexiform layer; OPL, outer plexiform layer; OS, outer segment; RPE, retinal pigmented epithelium.

### 4.3.4. Rosettes in the retinas of mutant eyes were predominantly composed of disorganised rod-photoreceptor cells

Paraffin embedded eye sections from adult (P56) wild type, heterozygote and homozygote mice were analysed by immunofluorescence using primary antibodies as markers for specific retinal cell types. Although I prepared these samples, this immunostaining work was performed by Dr. Sebastien Mella (MRC Human Genetics Unit).

The anti-Rhodopsin primary antibody is a recognised general marker for rod photoreceptors and stains cytoplasmic regions within the outer segment (OS) and outer nuclear layer (ONL) of the wild type retina (figure 4.2.5A), consistent with the distribution of rod cells within the proximal layers of the retina. The distribution of Rhodopsin in the heterozygote (figure 4.2.5B) retina was similar to the wild type in ONL and OS, however it was noted that there was no region of non-staining between the proximal-most nuclei of the ONL and the Rhodopsin-positive OS, a region which was clearly defined in the wild type. The homozygote retina showed severe disruption to the distribution of Rhodopsin staining (figure 4.2.5C). There was no outer segment visible, and there were large foci of intense staining that were spatially and morphologically consistent with the retinal rosettes previously seen with H&E staining. Adjacent to these regions were cell nuclei with perinuclear Rhodopsin staining, similar to those seen in the heterozygote and wild type rods of the ONL, suggesting that rosettes were composed of rod photoreceptor cells that were disorganised in orientation. Regions of inner nuclear

layer (INL) and ONL, as well as outer plexiform layer (OPL) were indistinguishable in the homozygote.

### 4.3.5. Mutants had increased retinal levels of the astrocyte and retinal stress marker, Gfap but showed reduced horizontal cell numbers by Calbindin staining

Antibodies to the astrocyte marker and indicator of retinal stress; Glial fibrillary protein (Gfap), and the horizontal and amacrine marker; Calbindin, were used to examine the spatial distribution of these cells in *Mp* mutants. Wild type Gfap was observed adjacent to the ganglion cell layer (GCL), possibly within the inner limiting membrane of the retina, with some projections penetrating the IPL (figure 4.2.5D). No signal was detected elsewhere in the retina. In both of the mutants (figure 4.2.5E & F), Gfap signal was identified throughout the INL and the number of projections into the IPL was considerably increased compared tot the wild type. Additionally, there was a substantial and graded increase in the levels of Gfap signal adjacent to the GCL in the heterozygote and homozygote.

Calbindin signal was identified within the inner nuclear layer and inner plexiform layer of wild type retinas (figure 4.2.5D), but the strongest signal was observed in the outer plexiform layer (OPL). In heterozygote (figure 4.2.5E) and homozygote (figure 4.2.5F) retinas, this distribution was unchanged, however there was an obvious and graded decrease in the numbers of positive foci within the OPL in heterozygotes and homozygotes. Nevertheless, there were positive cells present in the

homozygote, and these cells provided a possible landmark to spatially differentiate the INL and ONL.

### 4.3.6. Staining for Chx10 and Pkc∝ revealed a reduced INL in homozygote retinas

Bipolar cells located in the INL were identified with co-immunofluorescence using antibodies specific for Chx10 and Pkc∝ (rod-bipolar cells). In wild type (figure 4.2.5G), heterozygote (figure 4.2.5H) and homozygote (figure 4.2.5I) retinas, co-localisation was observed within nuclei of the proximal INL, while there were Chx10-only positive nuclei within central regions of the INL. There was an additional region of ILN that was non-staining for either marker, and that appeared to contain an equal number of cell nuclei to the positive staining INL. A further Pkc∝-positive domain was identified in the distal-most region of the IPL, immediately adjacent to the CGL. In this region the protein localisation was cytoplasmic.

There was a general reduction in positive staining nuclei for both markers within the homozygote INL, and additionally there were fewer non-staining nuclei in the distal INL. Staining of both markers in the heterozygote was equivalent to the wild type. Therefore, there were no clear differences in the distribution of these proteins between the genotypes (figure 4.2.5G-H), and although bipolar cells are not specifically affected, overall the INL is reduced in cell number in *Mp* homozygotes.

**Figure 4.2.5.**

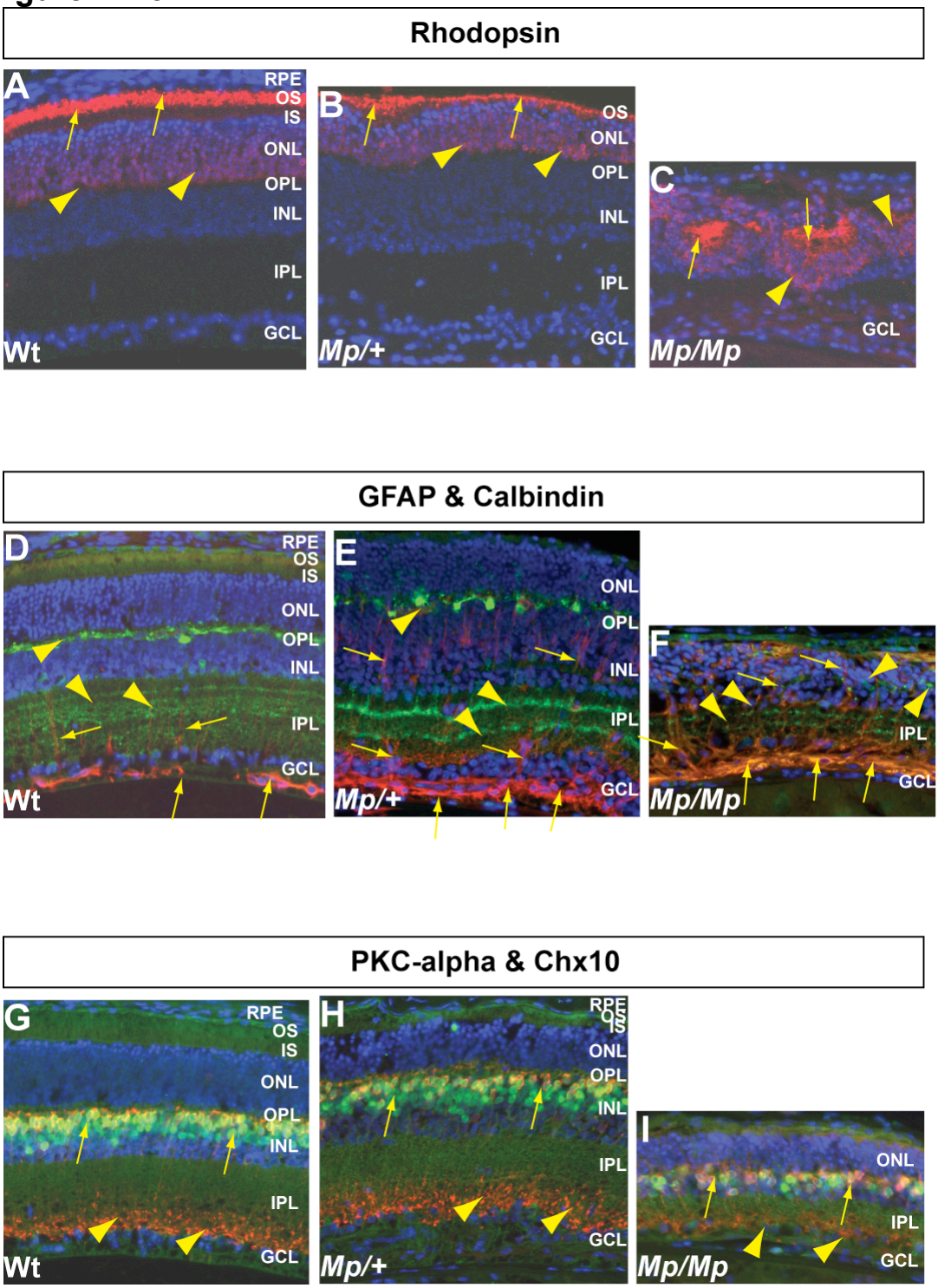
Rhodopsin
A
RPE
OS
IS
ONL
OPL
INL
IPL
GCL
Wt
B
OS
ONL
OPL
INL
IPL
GCL
Mp/+
C
GCL
Mp/Mp
GFAP & Calbindin
D
RPE
OS
IS
ONL
OPL
INL
IPL
GCL
Wt
E
ONL
OPL
INL
IPL
GCL
Mp/+
F
IPL
GCL
Mp/Mp
PKC-alpha & Chx10
G
RPE
OS
IS
ONL
OPL
INL
IPL
GCL
Wt
H
RPE
OS
IS
ONL
OPL
INL
IPL
GCL
Mp/+
I
ONL
IPL
GCL
Mp/Mp

**Figure 4.2.5 Immunofluorescence analysis of adult eyes revealed multiple retinal abnormalities in *Mp*.**

Adult eyes (at P56) were analysed by immunofluorescence with antibodies to Rhodopsin (**A-C**), by co-immunofluorescence for Glial Fibrillary Protein (Gfap) and Calbindin (**D-F**), and by co-immunofluorescence for Protein Kinase C-alpha (Pkc∝) and the homeobox protein Chx10 (**G-I**). DAPI was used to counterstain cell nuclei. Rhodopsin specifically stained rod photoreceptor cells (red) and in the wild type (**A**), signal was seen in cytoplasmic regions of both the outer segment (arrows) and the outer nuclear layer (arrowheads) consistent with projections of rod cells. The heterozygote (**B**) Rhodopsin distribution was comparable to wild type in the ONL (arrowheads) and in the outer segment of rod cells (arrows); however, there was reduced space between outer segment staining and the nuclei of the ONL, indicating loss of the inner segment (white arrowheads). The homozygote (**C**) had no outer segment staining (white arrowheads) and displayed perinuclear cytoplasmic signal (arrowheads); presumably these were cells of the ONL based on the morphological similarity to ONL cells of wild type and heterozygote. In addition, homozygotes displayed large and dense foci of signal (arrows) consistent with central regions of rosettes and which displayed similarity to the staining seen in outer segments of heterozygote and wild type. Regions of INL and ONL, as well as OPL were indistinguishable in the homozygote. In the wild type retina (**D**) Gfap (red) stained astrocytes at the region of the inner limiting membrane (arrows), with some projections into the IPL. Calbindin (green signal) stained horizontal cell and amacrine cell projections in both the OPL and IPL (arrowheads), with strongest staining in the OPL. In both mutants (**E** & **F**), there was a considerable increase in Gfap signal and the spatial distribution was markedly different, with signal found among cells of the internal-most layer of nuclei in homozygote (**F**) and INL of the heterozygote (**E**; arrows). In contrast, Cabindin signal was reduced in the OPL of the heterozygote, while in the homozygote; some signal was visible within the central region of the internal mass of nuclei (arrowheads), indicating a possible boundary between nuclei of INL and ONL. In both mutants, signal in the IPL remained comparable to wild type. Pkc∝ (red signal) and Chx10 (green signal) were mostly distributed in the proximal layers of nuclei (arrows) in the INL in wild type retina (**G**), with some Pkc∝ observed in the IPL adjacent to ganglion cells (arrowheads). There was additionally a layer of Chx10-only positive nuclei in the central region of the INL, which was apposed to a region of non-staining cells of the distal-most region of INL. Although the number of cells in the INL that positively stained for both markers, and Chx10-only were reduced in the homozygote (**I**), they were spatially comparable to both wild type (**G**) and heterozygote (**H**) (arrows). Additionally, there was no clear difference between genotypes for Pkc∝ staining in IPL regions directly adjacent to the GCL (arrowheads). RPE, retinal pigmented epithelium; OS, outer segment; IS, inner segment; ONL, outer nuclear layer; INL, inner nuclear layer; IPL, inner plexiform layer; OPL, outer plexiform layer, GCL, ganglion cell layer.

## 4.4. Histological examination of the developing *Mp* eye

### 4.4.1. Embryonic stages E13.5 to E15.5

Histological staining with Haematoxylin and Eosin was used on sections cut from paraffin-embedded embryos and post-natal eyes. Initial analyses were performed on eyes from E13.5 embryos (figure 4.2.6A). In all genotypes (wt, *Mp*/+ and *Mp*/*Mp*) the major components of the ocular system, the lens; retina; RPE; periocular mesenchyme; optic stalk; and neural crest cells within the vitreous were present and appeared normal, strongly suggesting that early embryonic developmental processes, pathways and events were not perturbed in the *Mp* mouse eye.

As no phenotype was identified in either *Mp*/+ or *Mp*/*Mp* at this stage, further analyses were applied to later embryonic stages, beginning at E15.5 (figure 4.2.6B & C). By this stage there was an apparent difference in total ocular size noted in the mutants compared to the wild type, especially in the homozygote (figure 4.2.6B). Otherwise the eyes of the different genotypes displayed comparably normal histological features. It was noted that there were aggregates of cells within the developing vitreous body of both mutants. These were larger in the homozygote than in the heterozygote and there were none initially seen in the wild type. However, further analysis of other animals

revealed similar collections in wild types (inset) and that in some mutant eyes they were absent. Higher magnification of the developing ciliary body for the different eyes identified an apparent difference in the homozygote, compared to the heterozygote and wild type (figure 4.2.6C): there were fewer nuclei present and the structure did not extend towards the distal lens. This was noted as a possible phenotypic difference but with the caveat that it may have been due to slight differences in angle of section.

**Figure 4.2.6.**

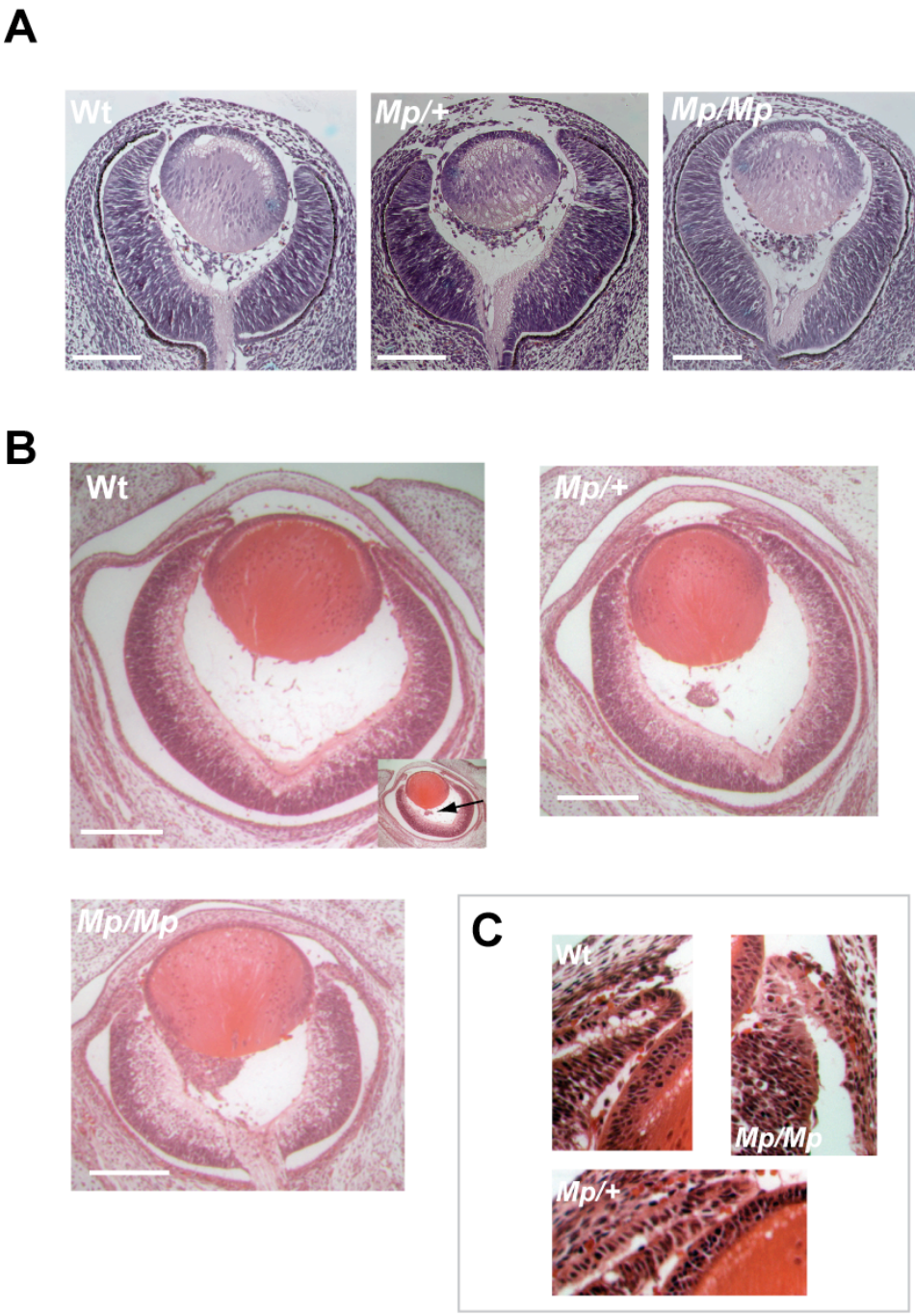

**Figure 4.2.6 Early ocular developmental events appear normal in *Mp* at E13.5 but phenotype presents at E15.5.**
The lens, retina, RPE, peri-ocular mesenchyme, vitreous and optic stalk were present and appeared to have been normally developed in *Mp/+* and *Mp/Mp* eyes at E13.5 by histological examination (**A**) Scale bar = 100 μm. Similarly, by E15.5, the major ocular structures were present and appeared normal (**B**), however the mutant appeared reduced in size in comparison to the wild type. There was a also suggestion of persistent neural crest cells in the vitreous of mutant eyes, however these were not always found in mutants and also were found in some wild type eyes (arrowed in inset) Scale bar = 200 μm. Additionally, higher magnification analysis revealed possible under-development of the ciliary body in the homozygote, with fewer nuclei present and an apparent truncation in growth towards the anterior lens region relative to the heterozygote and wild type (**C**).

### 4.4.2. The *Mp* eye had a growth phenotype identifiable by stage E15.5

Further investigation of the apparent difference in eye size was carried out using OPT (Sharpe et al., 2002) analysis of whole heads from embryos at E15.5. Crosses were set up between heterozygotes on the CD1, non-pigmented strain background. Litters were collected and embryos were genotyped, dehydrated and processed for OPT analysis. Measurements were taken of head length and head width (figure 4.2.7A) using Amira software (Amira 4.1.2, Visage Imaging, Carlsbad CA, USA) on virtual sections in the horizontal plane running through the centre of both eyes (figure 4.2.7B). Measurements were in Voxel units and averages were plotted for each genotype (figure 4.2.7C). No significant difference was observed for either average head length or width (95% confidence limits, wt, $n$=5; *Mp*/+, $n$=17; *Mp*/*Mp*, $n$=8), however it was noted that there was a slight reduction in the average head width sizes from wild

type to heterozygote to homozygote. Similarly, measurements were taken for each eye for the genotypes (figure 4.2.7D). These were: eye width (taken as the distance between lateral edges of retina at the widest point, measurement B), eye length (taken as a sum of the lens depth and vitreous measurements at the widest point, measurements A and D) and lens diameter (the means of measurements A and C). For each genotype, *n* values were double those for the head measurements, on the basis that each embryo had two eyes. The plane of the horizontal virtual section is shown in figure 4.2.7E. All sections were aligned so the optic stalk was simultaneously visible for both eyes in each sample. The homozygote average eye width measurements were significantly different from those of the wild type and heterozygote. Although none of the other measurements showed significant differences, there was a graded reduction in both average eye length and average lens diameter, indicating that the overall eye size in mutant animals is reduced at E15.5, with the homozygotes more severely affected. This result reflects the semi-quantitative histological findings seen in this chapter and defines an ocular phenotype for *Mp* at E15.5.

Although I performed the dissections of embryos and eyes, and initial sample preparation, OPT analysis and morphometrics were performed by Mr Harris Morrison and Dr. Malcolm Fisher, respectively (based at the MRC Human Genetics Unit).

**Figure 4.2.7.**

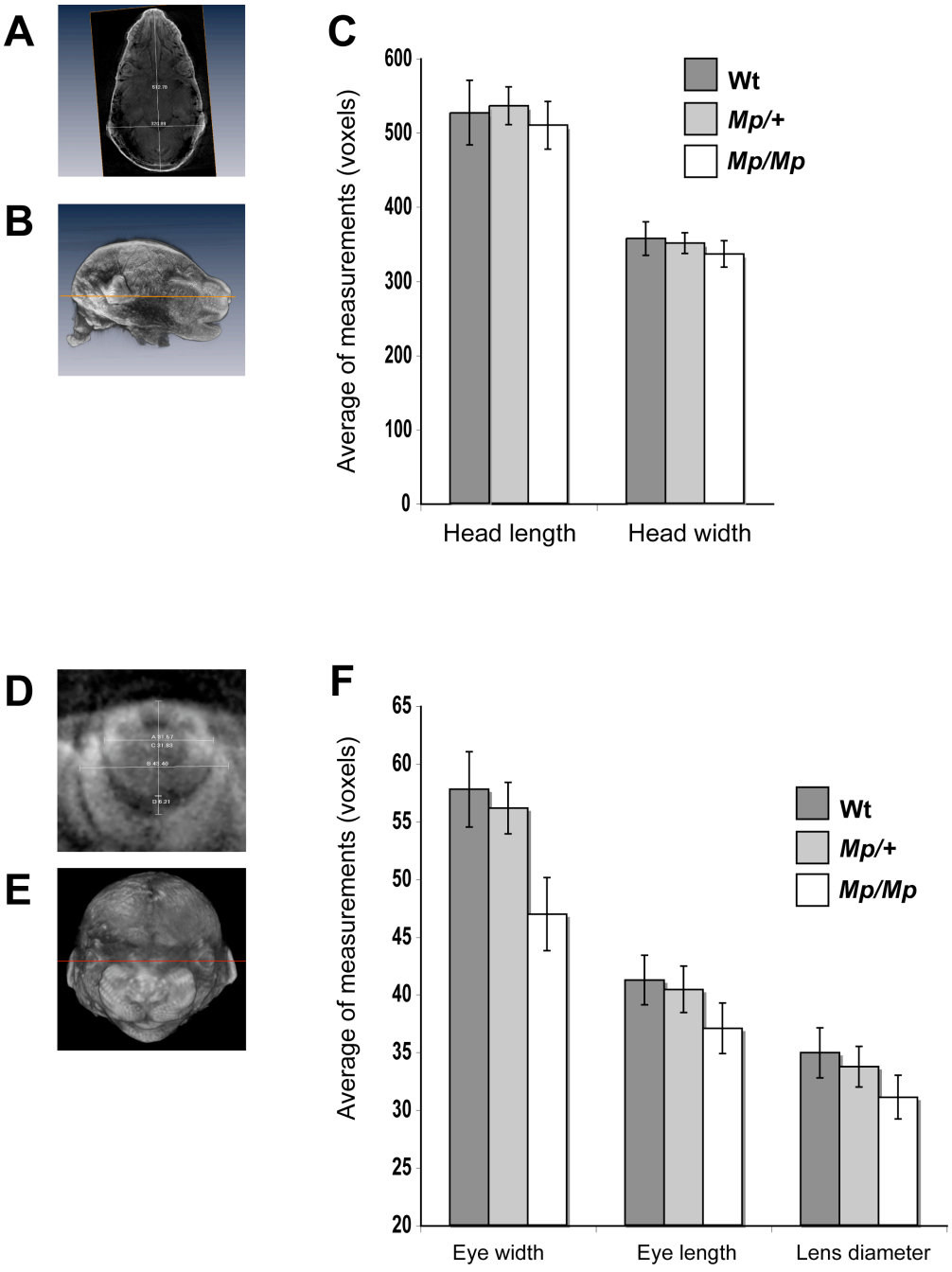
A
B
C
600
500
400
300
200
100
0
Average of measurements (voxels)
Wt
Mp/+
Mp/Mp
Head length
Head width
D
E
F
65
60
55
50
45
40
35
30
25
20
Average of measurements (voxels)
Wt
Mp/+
Mp/Mp
Eye width
Eye length
Lens diameter

**Figure 4.2.7. Morphometric analysis of embryos at E15.5 revealed a graded reduction in ocular size in mutant animals.**
Using length and width measurements (**A**) taken in the plane of section running through the centre of the eye in the horizontal plane (**B**), there was no overall difference seen between genotypes in head lengths (**C**). However, there was a suggestion of a graded reduction in head width sizes, although no level of significance was reached. Measurements of ocular sizes, including total eye width, eye length, and lens diameter (**D**) taken from the horizontal plane through the midline of the eye (**E**). (Note the eye length measurements were the sum of measurements A + D from the distal lens to the distal retinal edge and did not include the thickness of the proximal retina due to lack of clarity of many scans). For all measurements, there was a graded reduction in eye size from wild type to heterozygote to homozygote (**F**). There was significant difference between the eye width of homozygotes to both heterozygotes and wild types, however none of the other measurements reached significance. Nevertheless, the trend of eye size reduction in mutants is consistent for all three measurements analysed. For (**C**): $n$=5 [wt]; $n$=17 [*Mp/+*]; $n$=8 [*Mp/Mp*]; for (**F**): $n$=10 [wt]; $n$=34 [*Mp/+*]; $n$=16 [*Mp/Mp*]. Averages were calculated from measurement readings recorded in Voxel units using Amira software (Amira Release 4.1.2, Visage Imaging, Carlsbad CA, USA). Original images were captured by OPT analysis set at a constant magnification. All error bars set to confidence limits of 95%.

### 4.4.3. Mutant eyes display defects to vitreous, ciliary body and neural retina

Gross histological examination of homozygote versus wild type eyes at E16.5 (figure 4.2.8A & B) corroborated the reduction in eye size observed at E15.5, but did not reveal any major differences other than a reduction in vitreous body size in the mutant. In these samples, the lens, cornea, outer and inner retinal layers and anterior segment all appeared normal. Additionally, the pupillary membrane is clearly visible in the mutant eye in the anterior chamber extending from iris to lens. Although the angles of section were not identical in these sections, a different section through the same eye (inset) reveals the optic stalk (arrow) yet maintained the reduction in vitreous.

Heterozygote eyes were not analysed at E16.5 and later stages as it was thought that the initial ocular phenotype in *Mp* may be too subtle to identify and therefore comparison between homozygote and wild types would be sufficient to identify clues towards the pathogenic mechanisms in this mutant line. Higher magnifications in the region of the ciliary body (figure 4.2.8C & D) showed thinning in the unpigmented region of the mutant ciliary body compared to in the wild type. However, the pigmented region of the ciliary, as well as mesenchymal cells of the future iris and cells of the lens and cornea, all appeared normal in mutants. Analysis of retinas in equivalent regions between mutants and wild types identified the presence of cells with abnormal morphology within the neuroblastic region of mutant retinas. These cells resembled the differentiated ganglion cells of the inner region of the retina and were seen throughout mutant retinas and may therefore be ectopic retinal ganglion cells. Additionally the orientation of the cytoplasmic projections of the normally positioned ganglion cells in the mutant was more disorganised than in the wild type, where they were oriented in a strict apical-basal direction. These observations add to the ocular phenotype of *Mp*.

**Figure 4.2.8.**

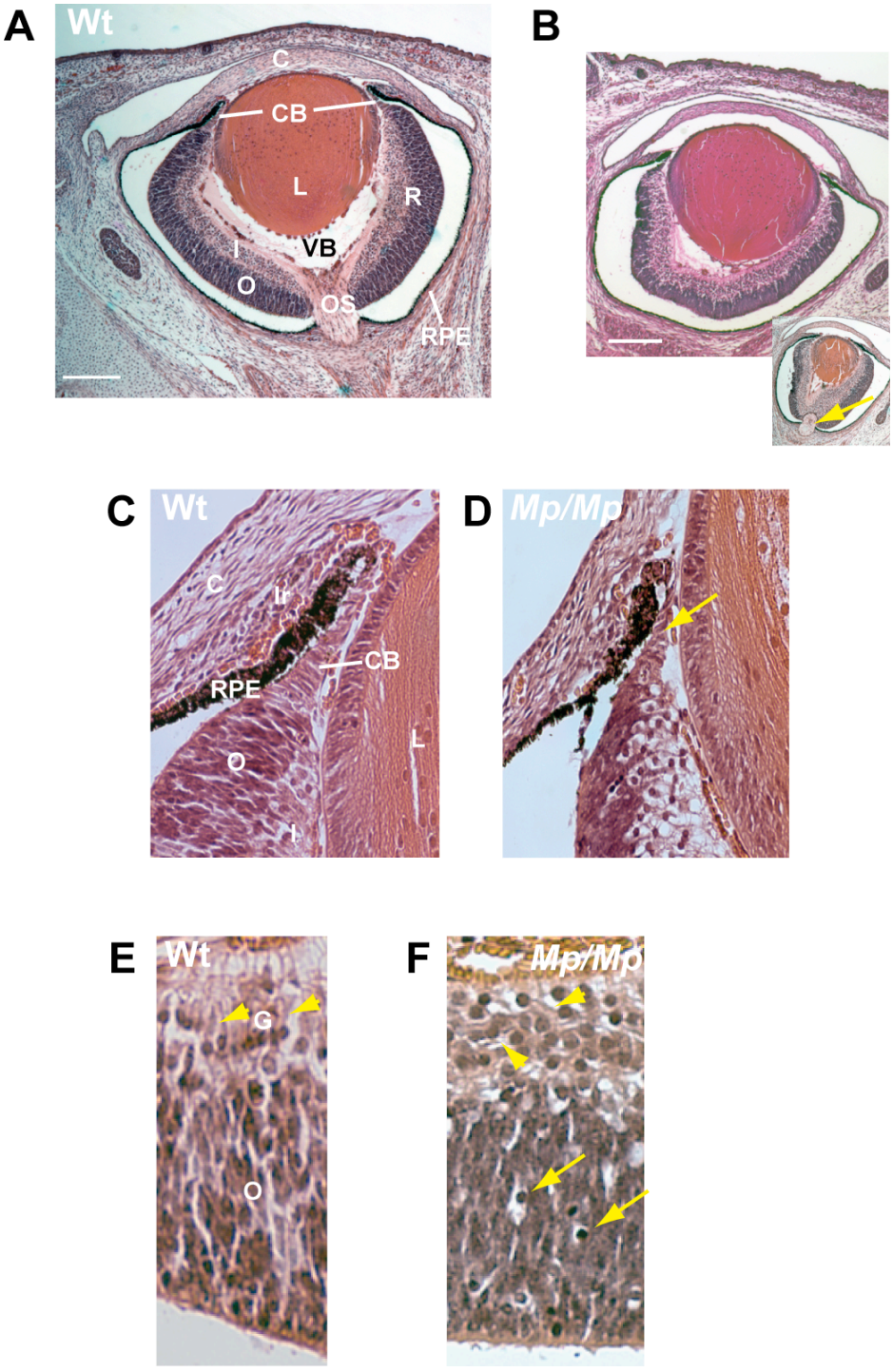

**Figure 4.2.8. E16.5 *Mp/Mp* mice display phenotype in multiple ocular components.**
Gross histological examination of wild type (**A**) and *Mp/Mp* (**B**) eyes at E16.5 revealed a reduction in overall eye size in the mutant with an absence of vitreous body. However, the main structures of the eye (lens, retina, cornea and RPE) were present and appear grossly normal. The planes of section are not equivalent for these, however a different section from the same mutant eye indicates the presence of optic stalk (arrowed in inset). Higher magnification images identified the developing ciliary body as being thinner and less extended in the mutant (**D**) than in the wild type (**C**), consistent with analysis of E15.5 mutant eyes (Figure 4.2.6). It was also noted in these magnifications that the lens and lens-fibre cells, iris stroma and cornea appeared normal. Retinal examination of mutant retina (**E**) identified the presence of ectopic rounded, darker-staining cells (arrows) in the neuroblastic layer, with similar appearance to the inner-layer differentiated ganglion cells. In addition, the pink-stained cytoplasmic projections (arrowheads) from ganglion cell nuclei appeared to lack the linearly arranged, apical to basal orientation of the equivalent cells in the wild type retina (**E**). Scale bar = 150 μm. C, cornea; CB, ciliary body; G, ganglion cell layer; I, retinal inner segment ; Ir, iris stroma; L, lens; O, retinal outer segment; OS, optic stalk; R, retina; RPE, retinal pigmented epithelium; VB, vitreous body. * The detachment of RPE from retina is processing artefact.

### 4.4.4. Late embryonic and newborn developmental stages were perturbed in the *Mp* eye.

In the E18.5 eye the retina is thinner and there is no apparent vitreous in the mutant compared to the wild type (figure 4.2.9A & D). However, the other main features of the developing eye appear normal, e.g. lens, cornea, RPE, and retinal layers. Close up views of the ciliary body (figure 4.2.9B & E) showed a thinner non-pigmented ciliary in the mutant, which was not undergoing the folding seen in the wild type. In this respect, now both pigmented and non-pigmented ciliary body development was affected in *Mp*. Higher magnification views of the retina in both samples identified the ectopic cells in

the neuroblastic outer layer of the neural retina, but that otherwise the development of retinal layers appeared to be normal.

Consistent with at E18.5, mutant eyes analysed at one day after birth (P1) had no vitreous, a thin neural retina, and an obvious disruption to the ciliary body (Figure 4.2.9J). Nevertheless, lens cornea, anterior segment, and retinal layering appeared grossly normal and comparable to wild type (figure 4.2.9G). Although these samples were from non-pigmented animals, it was visible that the wild type had begun the complex folding process of both 'pigmented' and 'unpigmented' ciliary body, and that the iris stroma had extended towards, and reached the lens (figure 4.2.9H). In the mutant (figure 4.2.9K), there were remnants of the 'unpigmented' ciliary apposed to the lens capsule and severely disrupted. There were loose cells visible between the 'pigmented' ciliary, which was also abnormally arranged, while the iris had not extended towards the lens. No ectopic cells were identified in the mutant retina although the ganglion cells maintained their cytoplasmic processes with disturbed orientation compared to wild types (figure 4.2.9I & L).

**Figure 4.2.9.**

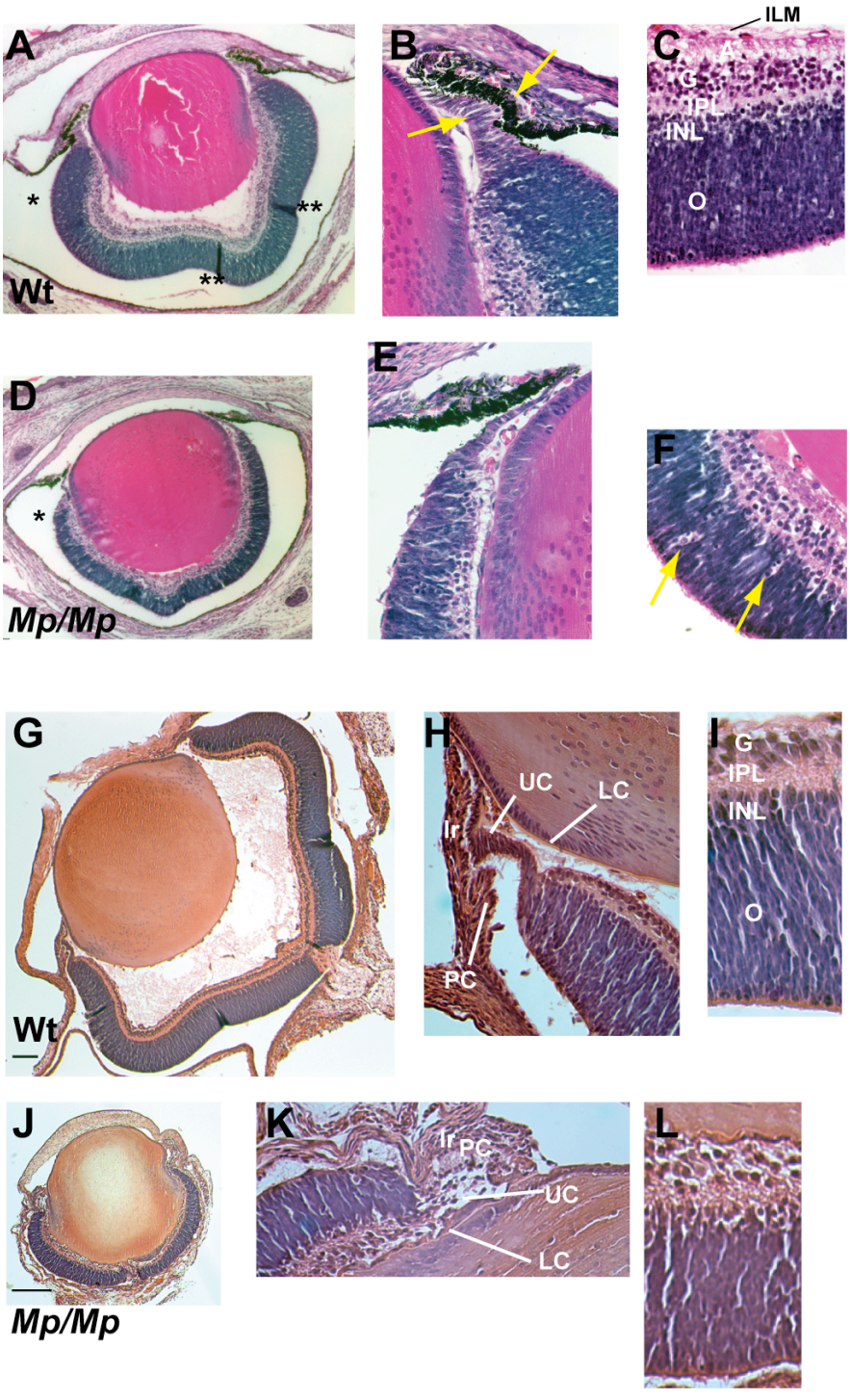
A
*
**
**
Wt
B
C
ILM
A
G
IPL
INL
O
D
*
Mp/Mp
E
F
G
Wt
H
UC
LC
Ir
PC
I
G
IPL
INL
O
J
Mp/Mp
K
Ir
PC
UC
LC
L

**Figure 4.2.9. Severe malformations are present at E18.5 and P1 in *Mp/Mp* eyes.**

At E18.5, the Mp/Mp eye (**D**) was smaller, had a thinner retina and lacked vitreous body in comparison to the wild type eye (**A**). The wild-type ciliary body (**B**) was thicker and more complex than the mutant (**E**) and had begun the process of folding (arrows) at the future ciliary epithelium (pigmented and non-pigmented) to produce the ciliary processes. No such folding was observed in the mutant and the iris stroma also appeared thinner and less well developed than the wild-type. In both the wild-type (**C**) and mutant retina (**F**), internal limiting membranes were present, the ganglion cell nuclear layer was present and around four cells thick, together with axonal projections and inner plexiform layer, and future inner nuclear layer. Ectopic nuclei were again observed in the outer nuclear layer of the mutant retina and not in the wild type (arrows). In the newborn (P1) eyes from unpigmented animals, there was a marked difference in size between the wild-type (**G**) and mutant (**J**). Additionally, there was no vitreous in the mutant, with the lens and retina directly apposed to each other. The retina appeared thinner in the mutant and the ciliary body was grossly abnormal. However, lens, cornea, RPE and retinal layers are present and were comparable to the wild-type. Comparison of the developing wild-type (**H**) and mutant (**K**) ciliary body at higher magnification revealed severe structural disorganisation in the mutant to the pigmented ciliary processes, while the unpigmented region was unidentifiable. In contrast, mutant lens was of normal appearance and lens capsules were identified in both mutant and wild-type. In the mutant retina (**L**), again the projections from ganglion cells appear to be disorganised and were not arranged in the apical to basal orientation typical of the wild-type retina (I). Scale bars = 100 μm. ILM, inner limiting membrane; LC, lens capsule; PC, pigmented ciliary processes; UP, unpigmented ciliary processes. * The detachment of RPE from retina is processing artefact. ** These darker stained regions of wild-type retina are folds caused by processing.

### 4.4.5. Late neonates displayed severe retinal defects

Retinas were examined at P21, by which time full retinal differentiation should have occurred. The wild type retina (figure 4.2.10A) displayed all of the features consistent with a mature, correctly laminated retina, however both heterozygote and homozygote displayed rosetting in the outer nuclear layer (figures 1.10B & C). These rosettes consisted of a central core of non-nuclear cell processes surrounded by multiple nuclei of photoreceptor cells. Additionally, in both mutants there was a complete lack of the inner and outer segments between the RPE and outer nuclear layer (arrows). In the homozygote, it was also noted that the outer plexiform layer was thinner and had various deviations towards the photoreceptor nuclei in regions between rosettes (arrowheads), suggesting that in fact the rosettes were forcing the overlying retinal layers anteriorally and that where there were no rosettes this didn't occur. Indeed, the combination of rosettes and photoreceptor nuclei seemed to result in a thickened outer nuclear layer in both mutants. In contrast, the inner nuclear layers of mutant retinas seemed unaffected but there was a suggestion of thinner inner plexiform layers in both. Additionally, the ganglion cell layer was thinner in the homozygote (filled arrows) and was less well organised than in the wild type and heterozygote, and in both mutants this cell layer was directly apposed to the lens and the inner limiting membrane was unidentifiable.

**Figure 4.2.10.**

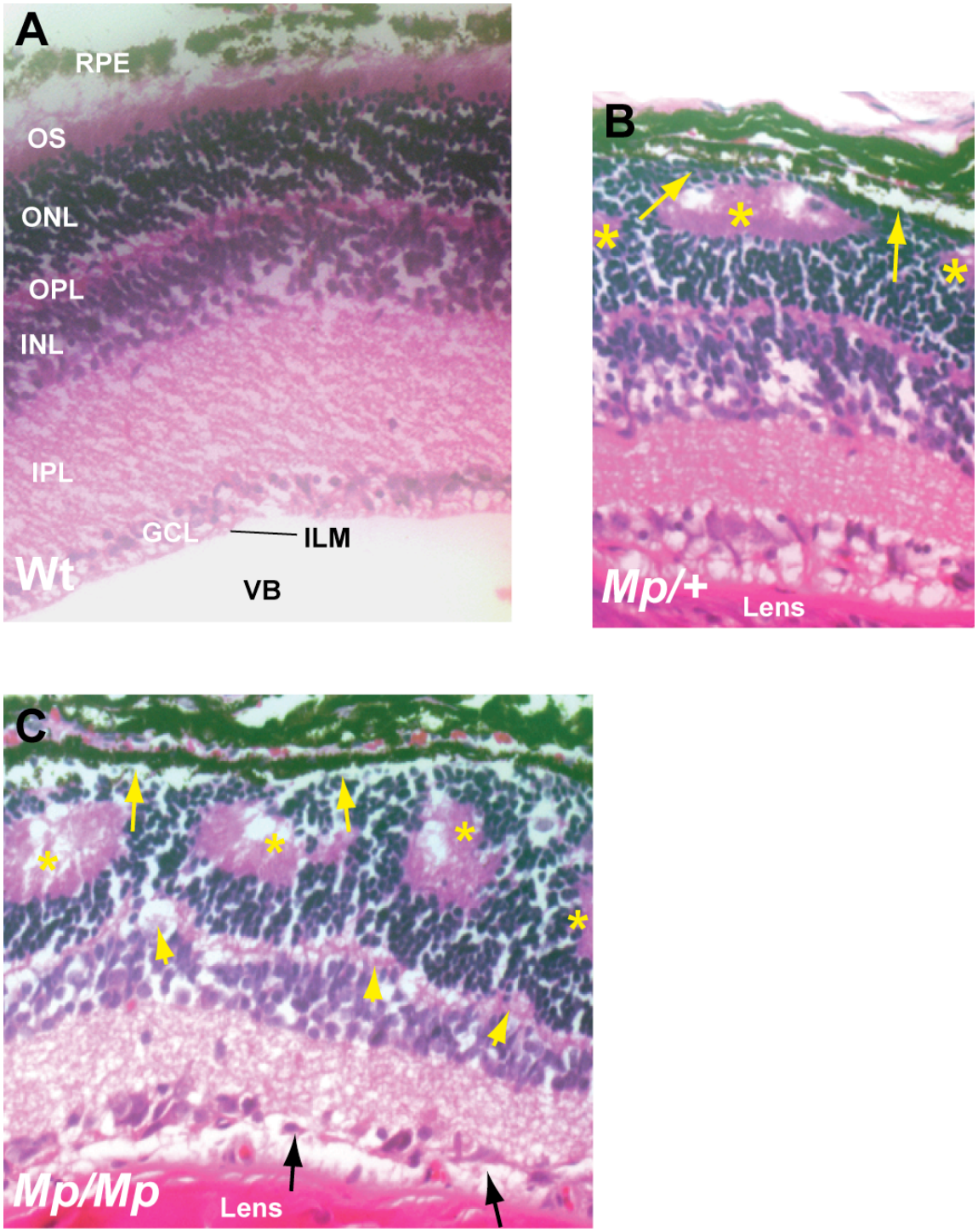

**Figure 4.2.10 Retinal layer organisation abnormalities are present in postnatal mutant eyes.**

Postnatal eyes of wild type (**A**), and both mutant genotypes (**B** & **C**) were analysed at P21 for retinal abnormalities. In both mutants, rosetting (*) was observed in the outer nuclear layer and was characterised by foci of tightly organised non-nuclear cell projections surrounded by multiple nuclei of cells from the outer layer. Lens was directly apposed to the internal retina, and in addition, mutants lacked an outer segment between the RPE and the outer nuclear layer (arrows). In the homozygote, there was also disruption in the inner plexiform layer at regions adjacent to the rosettes, with an apparent deviation towards the gaps between rosettes observed (arrowheads). In contrast to both wild-type and heterozygote, the mutant ganglion cell layer was thinner and appeared to lack an inner limiting membrane (filled arrows).

## 4.5. Genetic mapping of the *Mp* locus

### 4.5.1. Mapping crosses

Crosses were set up to facilitate mapping of the *Mp* locus (figure 4.3.1A). The original background of this line was a mix of inbred strains C3H and 101. To rederive the line ISCI IVF was performed with oocytes from F1 female C57Bl6/j x CBA mice. The G0 progeny were outcrossed to the inbred strain C57Bl6/j. Phenotypically heterozygous F1 animals were then backcrossed to C57Bl6/j. To generate a second independent line, heterozygous F1 animals from the initial cross were crossed to the CD1 outbred strain. These mice have a mutation in the *tyrosinase* gene (Jackson and Bennett, 1990) that results in albinism. These animals lack pigmentation in the RPE and are thus advantageous for OPT analysis of gene expression. Within both backgrounds, mice were also intercrossed to produce litters containing homozygote *Mp* progeny. Spleens or tails were used for genomic DNA extraction.

### 4.5.2. Karyotyping revealed normal chromosomes in Mp

Karyotyping analysis was performed on chromosomes prepared from cardiac blood samples collected from two11-week, phenotypically heterozygous male *Mp* animals from the 3$^{rd}$ backcross to C57Bl6/j. A total of 7 metaphase preparations were analysed, with some incomplete for the full complement of chromosomes. Nevertheless,

chromosomes were arranged according to homologous pairs and size and a composite analysis was performed and indicated there to be no chromosomal abnormality greater than 10 Mb detectable (Figure 4.3.1B). Sample preparation and analysis was done with the guidance of Dr. Judy Fantes (MRC Human Genetics Unit). Analytical software analysis of *Mp* chromosome images was done exclusively by Dr. Judy Fantes (formerly MRC Human Genetics Unit).

**Figure 4.3.1.**

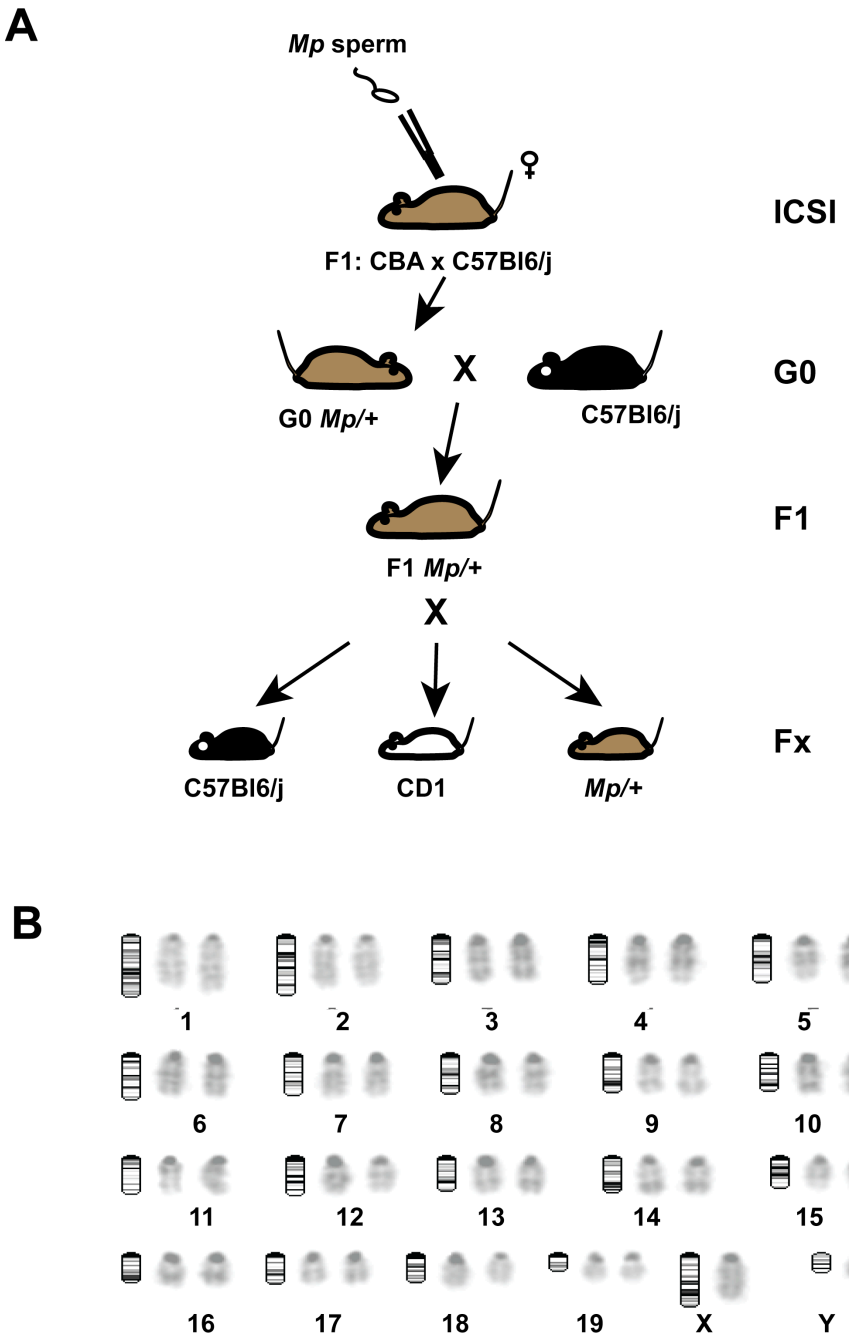
A
Mp sperm
♀
ICSI
F1: CBA x C57Bl6/j
G0
X
G0 Mp/+
C57Bl6/j
F1
F1 Mp/+
X
Fx
C57Bl6/j
CD1
Mp/+
B
1
2
3
4
5
6
7
8
9
10
11
12
13
14
15
16
17
18
19
X
Y

**Figure 4.3.1 Mapping strategy and karyotype analysis of *Mp* mice revealed no detectable large chromosomal abnormality.**
(**A**) *Mp* sperm was injected into oocytes of a F1 (C57Bl6/j x CBA) female. The affected progeny, G0 heterozygotes, were outcrossed to unaffected C57Bl6/j. These F1 progeny were then successively outcrossed to C57Bl6/j for genetic mapping, to CD1 for phenotype analysis, or were intercrossed to produce litters containing homozygotes. (**B**) Karyotype preparations from para-cardiac blood samples of heterozygote males from the 3rd backcross to C57Bl6/j were arranged in homologous pairs according to size. There was no obvious chromosomal abnormality detected ≥10 Mb.

### 4.5.3. The *Mp* phenotype has full penetrance on two different strain backgrounds

Phenotype data was recorded for all backcrosses and intercrosses, on both backgrounds, for penetrance analysis. The expected number of heterozygous progeny from matings between a heterozygote and an unaffected animal is 50% for a monogenic, autosomal trait (or a 1:1 ratio). Similarly, in matings between two heterozygous animals full penetrance is indicated by the presence of 25% wild type, 50% heterozygous, and 25% homozygous progeny (or a 1:2:1 ratio, respectively). Numbers were not analysed for penetrance in the 2$^{nd}$ outcross to C57Bl6/j. However, no evidence of unequal distribution was found by chi-square goodness of fit tests (Appendix 6.3) in the 3$^{rd}$, fourth or 5$^{th}$ outcross to C57Bl6/j and to the first outcross to CD1. In the 3$^{rd}$ outcross to C57Bl6/j (figure 4.3.2A) there were 57% heterozygotes and 43% wild-type animals recorded ($n$=131, $\chi^2$ = 2.76, P<0.1). In the 4$^{th}$ cross these were 45% and 55%, respectively ($n$=95, $\chi^2$ =0.85; p<0.36); and 61% and 39% in the 5$^{th}$ cross ($n$=18, $\chi^2$ =0.89; p<0.35). While intercrosses between affected animals (figure 4.3.2B) of all generations recorded on this background were: 22% wild type; 20% homozygote and 58% heterozygote ($n$=87, $\chi^2$ =2.68; p<0.26). In the F1 outcross to the CD1 background

(figure 4.20C), there were 51% wild type and 49% heterozygotes ($n$=39, $\chi^2$ =0.026; p<0.87), while intercrosses between these affected animals gave 23% wild types; 27% homozygotes and 50% heterozygotes (figure 4.3D) ($n$=23; $\chi^2$ =0.09; p<0.96). Thus the null hypothesis of the phenotype data having an unrelated distribution is rejected, and the alternative hypothesis, that the data are consistent with full penetrance, is accepted. These data are consistent with full penetrance of the *Mp* phenotype on both genetic backgrounds.

## Figure 4.3.2.

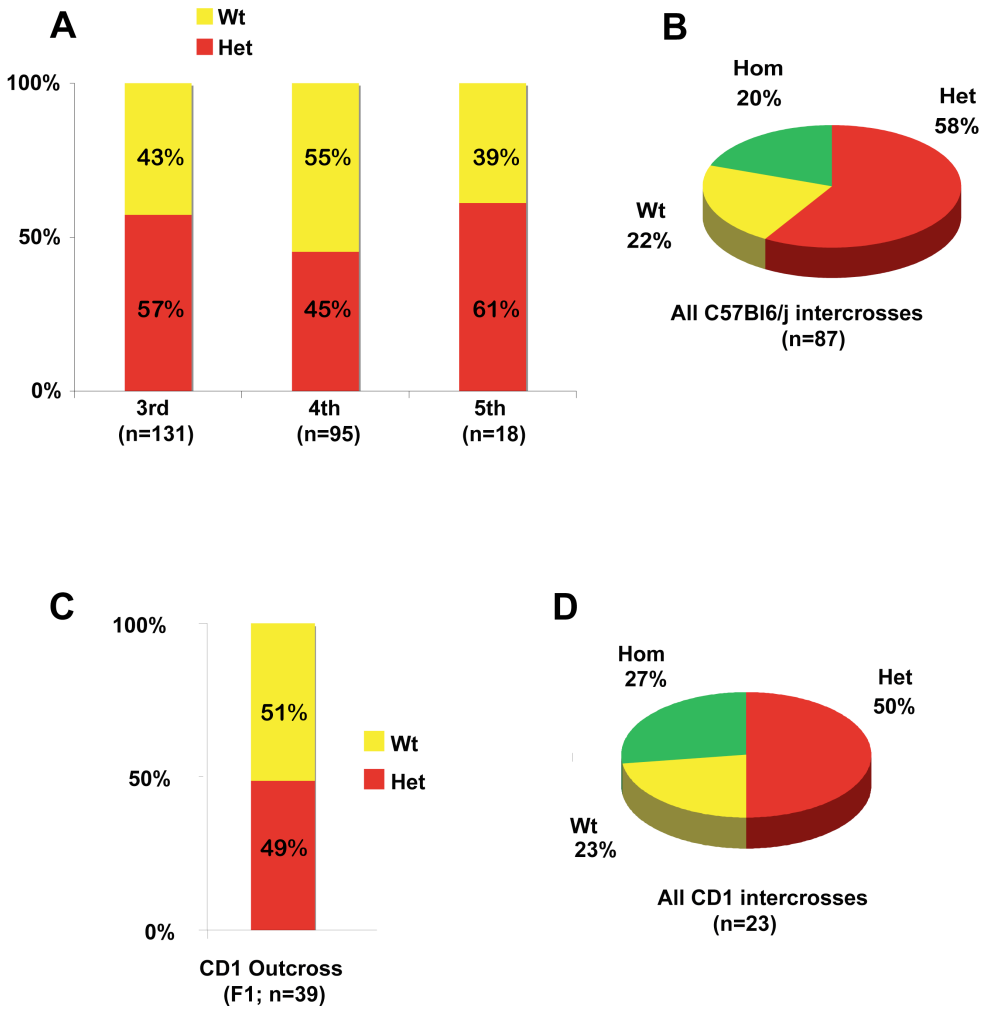


**Figure 4.3.2 Analysis of crosses revealed full penetrance of the *Mp* phenotype.**
Data from 3rd; 4th and 5th outcrosses to C57Bl6/j revealed values consistent with full penetrance of the heterozygous phenotype (**A**) with percentages of heterozygotes recorded as 57%; 45%; and 61%, respectively, with *n* values of 131; 95; and 18, respectively. Intercrosses between affected animals on the same background yielded 58% heterozygotes; 20% homozygotes and 22% wild-types, where *n*=87 (B). On the F1 generation of *Mp* outcrossed to the CD1 outbred background, there were 49% heterozygotes to 51% wild-types (C; *n*=39), while intercrosses between F1 affected animals gave 50% heterozygotes; 27% homozygotes and 23% wild-type progeny (D; *n*=22).

### 4.5.4. Genetic Mapping of *Mp* Using a Whole Genome 768 SNP Panel Array

Initial whole genome analysis was performed on genomic DNA from 8 x F2 generation heterozygous animals using the 768 SNP Genotyping Panel (Moran et al., 2006) together with the F1 and G0 parental DNAs. There were 594 informative SNPs between C3H and C57Bl6/j; 430 between 101 and C57Bl6/j; 288 between 101:CBA; and 111 between C3H:CBA. Candidate regions were identified by loci showing heterozygosity for markers specific for C57Bl6/j and other background strains (C3H/HeJ, CBA/J and 101) indicating no meiotic recombination on the host strain (C3H) had occurred. The largest candidate interval on this basis was on chromosome 11, between markers rs3705751 and 11.114.529 (Figure 4.3.3.A), at 75.432 – 113.477 Mb, respectively with a genetic distance of ~38 Mb. This region contained a total of 10 markers that could discriminate between C57Bl6/j and the C3H/HeJ, CBA/J and 101 backgrounds strains. However, one segment of ~10 Mb between markers rs3697441-rs13481185 (89.4 Mb-99.6 Mb, respectively) which was indistinguishable between C57Bl6/j and 101. Using an additional 3x phenotypically heterozygote animals of the F2 generation, however, this critical interval was discounted on the basis that all were genetically homozygous for C57Bl6/j at 6x fully informative microsatellite PCR markers used, with an average genetic distance of 5.5 Mb (figure 4.3.3B). Chromosome 11 was therefore discounted as a candidate for *Mp* with no other obvious candidate region identified with this analysis.

**Figure 4.3.3.**

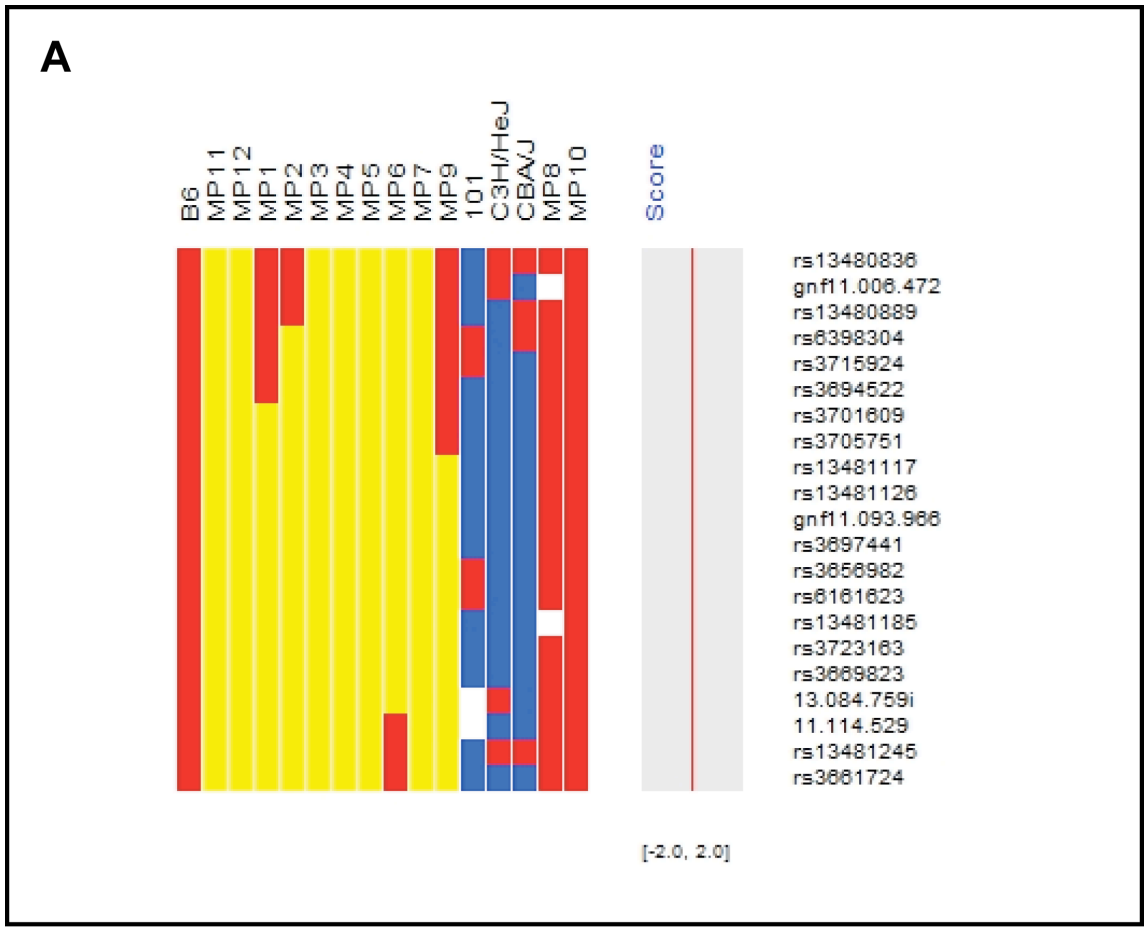
A
B6
MP11
MP12
MP1
MP2
MP3
MP4
MP5
MP6
MP7
MP9
101
C3H/HeJ
CBA/J
MP8
MP10
Score
rs13480836
gnf11.006.472
rs13480889
rs6398304
rs3715924
rs3694522
rs3701609
rs3705751
rs13481117
rs13481126
gnf11.093.966
rs3697441
rs3656982
rs6161623
rs13481185
rs3723163
rs3669823
13.084.759i
11.114.529
rs13481245
rs3661724
[-2.0, 2.0]
B
C57Bl6/j
C3H
CBA
101
Mp4-11
Mp4-12
Mp4-13
D11Mit 40 (79.1 Mb)
D11Mit 35 (83.4 Mb)
D11Mit 286 (90.1 Mb)
D11Mit132 (99.3 Mb)
D11Mit 360 (103.2 Mb)
D11Mit 61 (112.3 Mb)

**Figure 4.3.3 Analysis of a candidate region for *Mp* on chromosome 11.** (**A**) SNP array identified a candidate region on chromosome 11 between markers rs3705751-11.114.529, where DNA was from animals *Mp*1-9 of the 2nd backcross to C57Bl6/j, and *Mp*11 and *Mp*12 were parental DNAs from 1st backcross and initial microinjections, respectively. *Mp*8 and *Mp*10 were wild-type animals miscalled as heterozygotes due to their phenotyping being carried out at P16, prior to full opening of the eyelids. (**B**) Further analysis using 3 x F2 heterozygote animals ruled out this region as a locus for *Mp* as all 6x markers tested were homozygous for C57Bl6/j. For each marker, red indicated homozygosity for C57Bl6/j; yellow was heterozygosity for C57Bl6/j and any other background discriminative from C57Bl6/j where the corresponding marker was blue for that strain. Red colouring for background strains indicated that a marker could not be discriminated from C57Bl6/j. Mp4-11; -12; and –13 were additional 2nd backcross *Mp* heterozygotes added to the mapping assay. C57Bl6/j (B6); 101; C3H/HeJ; and CBA/J were control DNAs.

### 4.5.5. Whole genome mapping was performed using microsatellite markers

An alternative mapping strategy was adopted using PCR-amplifiable microsatellite markers that discriminate between C57Bl6/j and C3H strains. An initial panel was used for analysis of DNA from an F1 affected parent to identify those markers that were fully informative, i.e. displayed heterozygosity for C57Bl6/j and C3H in control DNA samples. In total, 73x autosomal markers were chosen, with an average density of ~33.8 Mb per marker. Genomic DNA extracted from phenotypically heterozygote ($n$=38) and wild-type ($n$=30) animals from the 3$^{rd}$ outcross was pooled by phenotype category, using equal amounts of total DNA per animal. The PCR markers were then analysed for the enrichment of C3H alleles segregating with the heterozygous pool. Peak sizes were recorded and ratios of C57Bl6/j to C3H were calculated for each marker, with these values then used to further calculate the ratios between wild types and heterozygotes (figure 4.4.3).

### 4.5.6. Evidence of *Mp* linkage to chromosome 18 was identified

Of the 73 markers used, 57 (79.1%) gave peaks of a recordable size corresponding to C57Bl6/j alleles only. For the remaining 16 markers, only chromosomes 5; 10; 11 and 18 were identified with >1 marker showing enrichment for C3H peaks versus C57Bl6/j in the heterozygous pool, with chromosome 5 having a single marker with a ≥ 2x fold enrichment for C3H: C57Bl6/j, while there were two on chromosome 18. However, one of these markers on chromosome 18, D18MIT149 at a

genomic position ~45 Mb, was >28 fold enriched for C3H (figure 4.3.4), strongly indicating this region as a candidate for the *Mp* locus.

**Figure 4.3.4.**

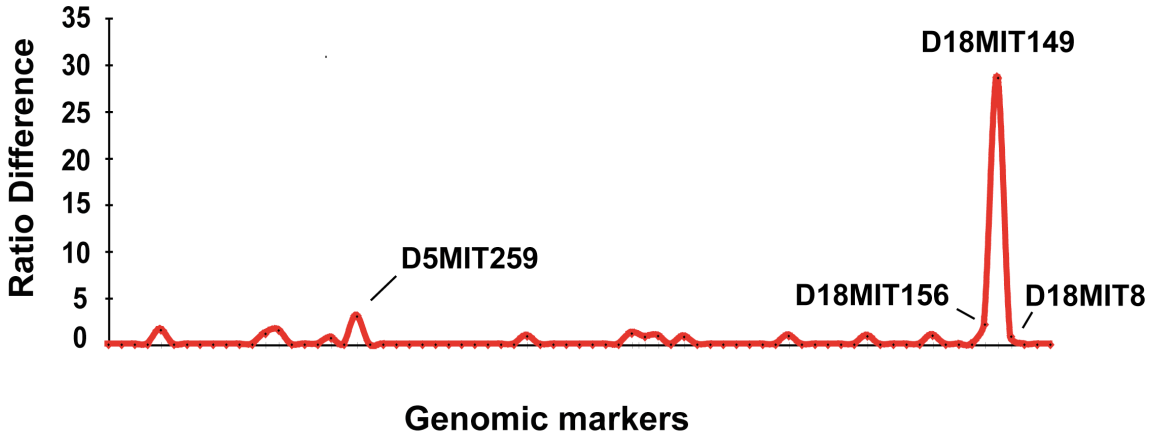


**Figure 4.3.4 Mapping *Mp* using a whole genome microsatellite marker analysis.**
Ratios of peak sizes from C3H:C57Bl6/j for alleles of fully informative autosomal microsatellite markers amplified from pooled wild-type and heterozygote DNA samples were calculated. Enrichment for C3H was seen for 3x consecutive markers (D18MIT146; D18MIT 149; and D18MIT8) on chromosome 18, co-segregating with heterozygosity, and thus implicated chromosome18 as a candidate locus for Mp. There was also enrichment for C3H at a single marker on Chromosome 5 (D56MIT259).

### 4.5.7. Analysis of chromosome 18 as a candidate for *Mp*

The heterozygote DNA samples used for the pooled sample analysis ($n$=38) were then analysed separately for a series of microsatellite markers on chromosome 18 to confirm the linkage and to identify meiotic recombinants. 4 different haplotypes were identified within this group of animals (figure 4.3.5A). Critically, there were two animals with a haplotype displaying a meiotic recombination event between markers D18MIT74 and D18MIT184, positioned at 53 and 67 Mb, respectively (figure 4.3.5A). This indicated a candidate interval for *Mp* between these two markers, however there was also the possibility that the locus lies distal to 67 Mb, as markers were not used in these regions, although this would require a double recombination to have occurred. However, this was unlikely as on review of the SNP marker panel data (figure 4.3.5B), two heterozygotes displayed homozygosity for C57Bl6/j for all SNP markers distal to 66.9 Mb. In contrast the other animals were all consistent with the *Mp* locus being proximal to this marker, except for a single animal who appeared as homozygous for C57Bl6/j across all of chromosome 18. This may have been a result of the non-informativeness of certain SNP markers used proximal to 57.7 Mb between strains 101 and C57Bl6/j in the genetic background, or possibly due to the poor density of coverage, that particular animal may have been incorrectly phenotyped, or may have been a double meiotic recombinant. Therefore, the critical interval for *Mp* was defined as between 53-67 Mb on chromosome 18.

**Figure 4.3.5.**

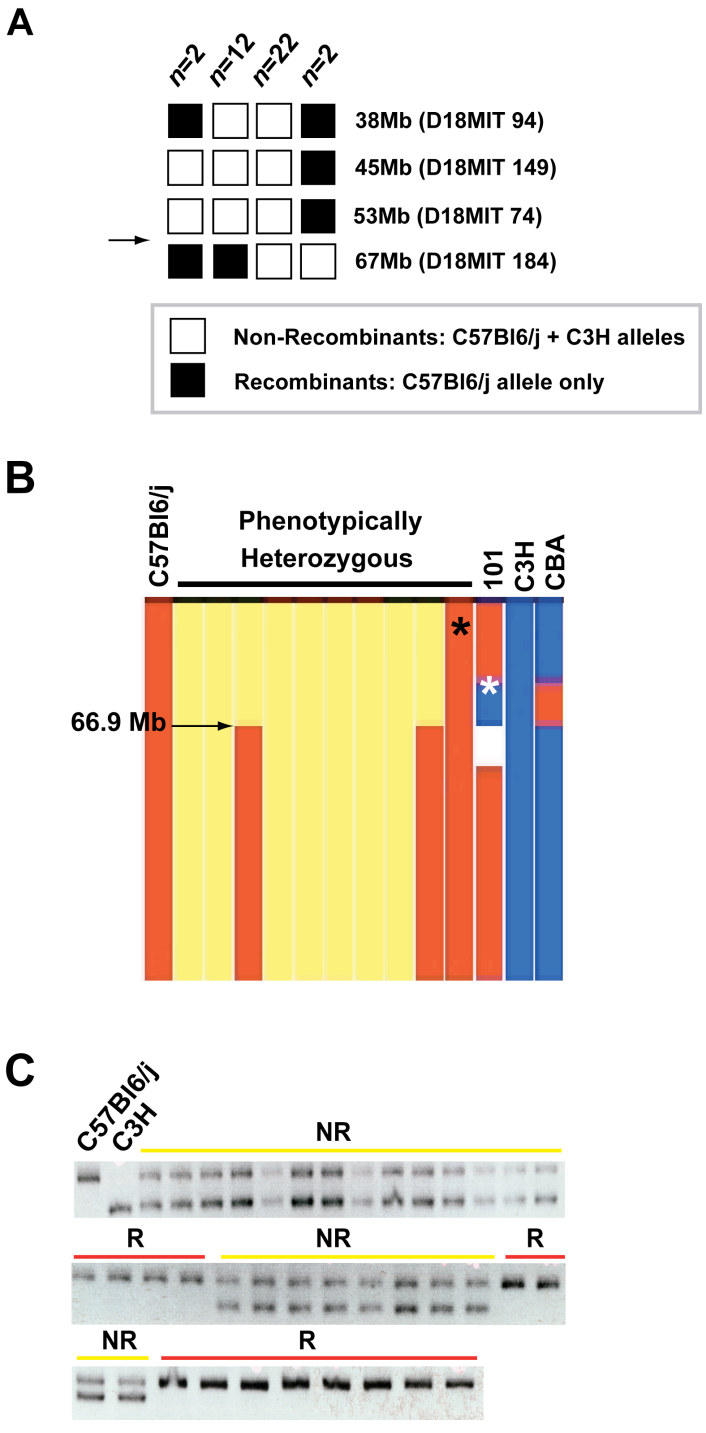
A
n=2
n=12
n=22
n=2
38Mb (D18MIT 94)
45Mb (D18MIT 149)
53Mb (D18MIT 74)
67Mb (D18MIT 184)
Non-Recombinants: C57Bl6/j + C3H alleles
Recombinants: C57Bl6/j allele only
B
C57Bl6/j
Phenotypically Heterozygous
101
C3H
CBA
66.9 Mb
C
C57Bl6/j
C3H
NR
R
NR
R
NR
R

**Figure 4.3.5 Haplotype analysis of strain specific markers on chromosome 18 refined the *Mp* interval to between 53- 67 Mb.**
DNA samples of 38x heterozygotes from 3rd outcross to C57Bl6/j were used in individual PCR reactions for microsatellite markers discriminatory for strain-specific alleles (**A**). Analysis of the 4x haplotypes generated indicated there to be no meiotic recombinants between markers D18MIT74 and D18MIT184, at 53Mb and 67Mb respectively. This data was arranged according to genomic position (right) and for the number of animals displaying each haplotype (top). Filled boxes indicated homozygosity for C57Bl6/j at that locus, whereas empty boxes were assigned for alleles heterozygous for C57Bl6/j and C3H. Arrow indicates region without recombinants. (**B**) SNP marker analysis on chromosome 18 of animals from 2nd outcross to C57Bl6/j, and their parental G0 and F1 heterozygotes, indicated that at least 2 animals were homozygous for C57Bl6/j at loci distal from 66.9 Mb (arrow), indicated by red fill. Background strains with blue fill indicated that markers were discriminatory from the C57Bl6/j background, whereas red indicated markers to be non-informative between that strain and C57Bl6/j. There was a single animal that displayed apparent homozygosity for C57Bl6/j at all markers on chromosome 18 (asterix), however this may have resulted from markers at loci proximal to marker rs3705107 being non-informative for the different strain backgrounds (white asterix). (**C**) Agarose gel electrophoresis of PCR products from D18Mit184 identifying recombinant animals with single amplicon for C57Bl6/j allele, and meiotic non-recombinants with amplicons for both C57Bl6/j and C3H alleles.

### 4.5.8. Identifying *Fibrillin-2* as a candidate for *Mp*

The *Fibrillin-2* (*Fbn2*) gene is located on chromosome 18, positioned at ~58 Mb. Homozygous loss-of-function mutations in *Fbn2* give rise to hindlimb oligodactyly in the mouse but do not exhibit an eye phenotype (Arteaga-Solis et al., 2001; Chaudhry et al., 2001). Thus, *Fbn2* is a reasonable candidate for *Mp*. PCR-based sequencing analysis of the *Fbn2* mRNA was decided as an appropriate strategy for identifying mutations in the gene and to check for transcript integrity, due to the large size of the full gene (20.1 kb). RT-PCR reactions were designed to amplify 10 overlapping portions covering the entire coding sequence from 65 exons of *Fbn2* from

cDNA samples prepared from RNA extracted from excised hearts of phenotypically wild-type, heterozygote and mutant adult animals. Amplicons were generated for all fragments in all representative genotypes, except for fragment 10, specific for exons 61-65, which was not amplified in the homozygote sample (figure 4.3.6A). The bands from the heterozygote and homozygote samples appeared as more intense than those of the wild-type for fragments 1-9, yet the homozygote band was missing completely for this terminal amplicon and the heterozygote was less intense than the wild-type, implying a reduction in dosage of the template in the heterozygote sample and a loss of template in the mutant. This result was replicated in RNA isolated from eye tissue from the same animals. This implied that the failure in amplification of *Fbn2* cDNA fragment 10 was not a result of a mutation affecting the annealing of these primers to the DNA template, but rather that the mutation specifically affects the 3'-end of the *Fbn2* transcript in the proximity of exons 61-65 (figure 4.3.6B).

**Figure 4.3.6.**

**A**

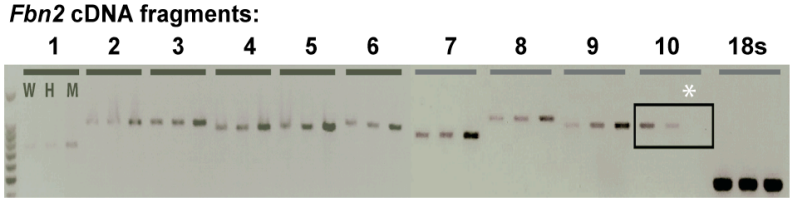


**B**

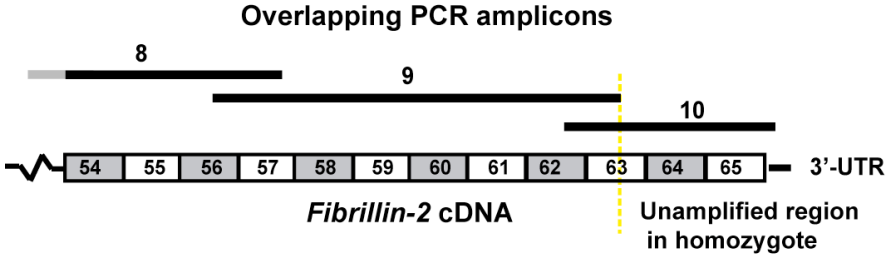

**Figure 4.3.6. RT-PCR analysis failed to amplify several 3'-exons of *Fibrillin-2* in *Mp*.**
(**A**) RT-PCR using overlapping amplicons for the entire coding sequence of *Fbn2* indicated that amplicon 10 (boxed area) at the 3'-most region could not be amplified using cDNA generated from homozygote (M) animals (white asterix) and that there was reduced band intensity in the heterozygote (H) compared to wild type (W). The remaining amplicons were successfully amplified in all samples. (**B**) Figure (not to scale) indicating the positions of the RT-PCR amplicons relative to the 3'-end of the wild-type transcript illustrated the approximate position of the *Mp* genetic lesion. Note that primers 10-forward and 9-reverse overlapped each other and therefore reduce the affected region to beyond the distal end of the 9-reverse primer.

### 4.5.9. The *Mp* candidate interval was refined to within intron 62 of *Fbn2*

The next step was to identify whether the 3'-most exons 61-65 of *Fbn2* were present in mutant animals. As the forward primer for Fbn2 cDNA amplicon 10 overlapped with the reverse primer for fragment 9 (figure 4.3.6B) the candidate region for *Mp* was refined from between exons 62-65, to between exons 63-65, at the positions of the relevant forward and reverse primers. A PCR reaction using primers that annealed to Intronic DNA flanking each of the last four exons showed that these exons were present in genomic DNA of mutant animals (figure 4.3.7A). Subsequent sequence analysis revealed no mutations in these regions. The causative mutation for *Mp* was likely therefore to be within intronic DNA between these exons. PCR reactions were designed to amplify the intronic sequences between these four exons, with the same primers used to amplify the exons but in different combinations. It was possible to

amplify the introns between exons 61-62; 63-64; and 64-65 (referred to as introns 61; 63; and 64, respectively from here on) for all three genotypes (figure 4.3.7B); however amplifying the largest intronic region (4.8 kb) between exons 62-63 was initially not possible for any sample. This region was therefore divided into 7x overlapping fragments (figure 4.3.7C) that covered the entire intron. Fragments E and F did not produce amplicons from the mutant DNA (figure 4.3.7D), thus localising the possible mutation to this region. Using the reverse and forward primer positions of fragments D and G, respectively, the candidate *Mp* locus interval is refined to 451 bp (figure 4.3.7C), between 58,175,797-58,175,345 Mb on chromosome 14.

**Figure 4.3.7.**

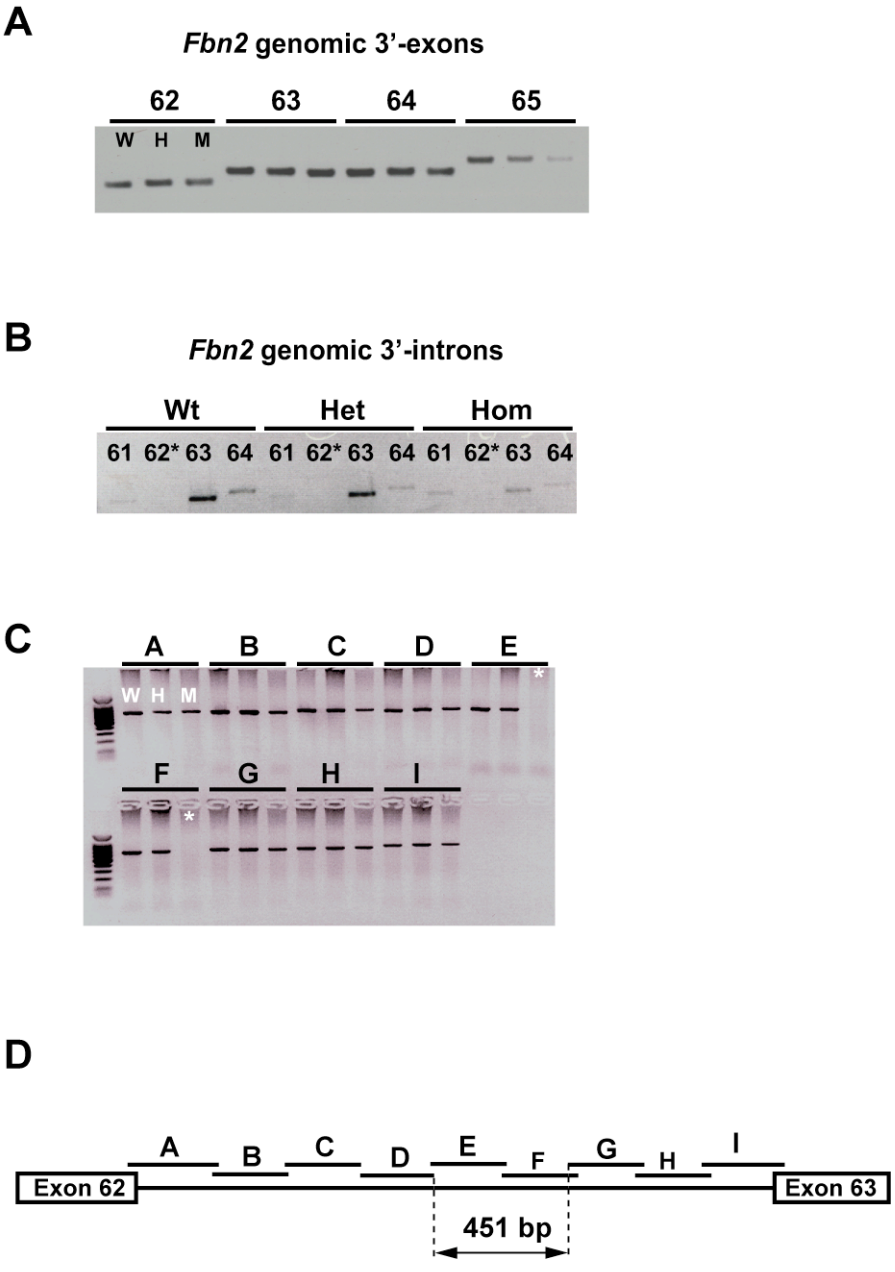
A
Fbn2 genomic 3'-exons
62
63
64
65
W H M
B
Fbn2 genomic 3'-introns
Wt
Het
Hom
61 62* 63 64 61 62* 63 64 61 62* 63 64
C
A
B
C
D
E
W H M
F
G
H
I
*
D
A
B
C
D
E
F
G
H
I
Exon 62
Exon 63
451 bp

**Figure 4.3.7 The *Mp* genetic lesion was refined to within 450 bp of intron 62 in the *Fbn2* gene.**
(**A**) Exons 62-65 of *Fbn2* were all amplified successfully from mutant genomic DNA samples with no apparent deviation in size of amplicons, indicating their presence within the genome of mutant animals. These products were subsequently sequenced and found not to contain any mutations. (**B**) Intronic regions between the last four exons were PCR-amplified as normal-sized fragments compared to the wild type, for all except intron 62, which initially was unable to amplify in all samples (asterix). (**C**) This intron was split into overlapping amplicons for PCR amplification of genomic DNA and analysis revealed that there were two adjacent regions that did not amplify from the mutant sample- amplicons E & F (white asterix). (**D**) Figure (not to scale) indicating the positions of genomic amplicons relative intron 62. This illustrated the approximate location of the *Mp* genetic lesion and implied that the critical region affected in *Mp* was positioned between primers for D-reverse and G-forward, an interval of 451 bp.

### 4.5.10. 3'-RACE identifies two genetic lesions in *Fbn2* and the adjacent *Isoc1* gene

Total RNA isolated from hearts of mutant and wild-type animals was subjected to 3'-RACE PCR (as described in the methods section). The resulting PCR products were run out on an agarose gel and inspected for the presence of any differential bands. The predicted size of the Wt *Fbn2*-fragment using the *Fbn2*-specific and adaptor primers in reactions was ~ 1.1 Kb. Consistent with this there was a strong band present in the Wt that was absent in the mutant (figure 4.3.8A). Conversely, a strong band of approximately 750 bp was seen in the mutant but not in the Wt. These bands were subsequently cloned and sequenced. A BLAT Search of the sequences confirmed the Wt-specific band as *Fbn2,* with 100% sequence identity to the *Fbn2* locus between 58,169,774-58,180,136 bp on chromosome 18 (figure 4.3.8B), corresponding to the 3'-most end of the transcript. For the 750 bp mutant band, two separate hits on

chromosome 18 were identified, each with 100% sequence identity to the query sequence. The genomic coordinates of these were 58,837,418-58,837,929 bp and 58,178,391-58,180,136 bp, and included the coding regions of two separate genes: *Isoc1* (*Isochorismatase domain-containing protein-1*) and *Fbn2*, respectively.

*Isoc1* is a 5-exon gene positioned at 58.8 Mb on chromosome 18, within 1 Mb from *Fbn2* and the two genes are separated by the solute channel gene *Slc27a6*, positioned at 58.7 Mb (figure 4.3.8C). The sequence obtained from the mutant indicates that the transcript is specific for *Fbn2* up to, and including, the final nucleotide of exon 62 (Ensembl ID ENSMUSE00000143682). The sequence then reads directly into the fifth and final exon of *Isoc1* (Ensembl ID ENSMUSE00000659305) without the additional of any non-endogenous nucleotides. The mutant transcript is therefore likely a fusion of these two genes, where exons 63-65 of *Fbn2* have been replaced by the last exon of *Isoc1*. This would be consistent with the localisation of the genomic mutation to intron 62.

## Figure 4.3.8.

**A**

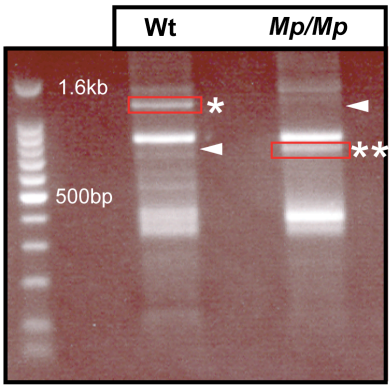


**B**

Mouse BLAT Results

BLAT Search Results

| ACTIONS | QUERY | SCORE | START | END | QSIZE | IDENTITY | CHRO | STRAND | START | END | SPAN |
|---|---|---|---|---|---|---|---|---|---|---|---|
| browser details | YourSeq | 1133 | 1 | 1139 | 1156 | 100.0% | 18 | - | 58169774 | 58180136 | 10363 |

Mouse BLAT Results

BLAT Search Results

| ACTIONS | QUERY | SCORE | START | END | QSIZE | IDENTITY | CHRO | STRAND | START | END | SPAN |
|---|---|---|---|---|---|---|---|---|---|---|---|
| browser details | YourSeq | 485 | 233 | 719 | 752 | 100.0% | 18 | + | 58837418 | 58837929 | 512 |
| browser details | YourSeq | 232 | 1 | 233 | 752 | 100.0% | 18 | - | 58178391 | 58180136 | 1746 |

**C**

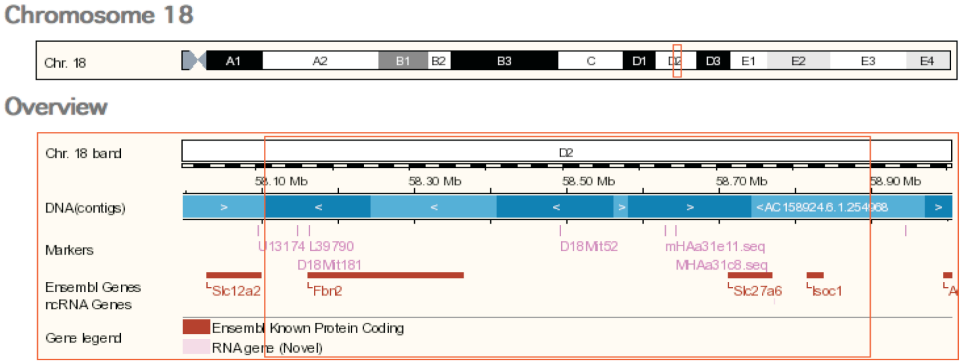

**Figure 4.3.8 3'-RACE identified a fusion of *Fbn2* to the adjacent *Isoc1* gene.**

Analysis of differential PCR bands between wild-type and mutant transcripts generated by 3'-RACE identified a band (single asterix) at ~1.1 kb not present in the mutant (arrowhead) and a 750 bp band present in the mutant (double asterix) that was not present in the wild-type (arrowhead) (**A**). These amplicons were then excised, cloned and sequenced. The wild type band was confirmed as being fully *Fbn2* by its genomic position identified using BLAT against the mouse genome (B; top panel), while similarly the mutant was identified as being *Fbn2* between nucleotides 1-232, then reading into the *Isoc1* gene from nucleotides 233-719 (B; bottom panel). All hits for the query sequences displayed 100% identity to the reference sequence identified. The genomic positions of these two genes on chromosome 18 are within 1 Mb of each other and separated by the solute-channel gene Slc27a6, as depicted using the Ensembl (http://www.ensembl.org/index.html) gene viewer (**C**).

### 4.5.11. Sequence analysis reveals a balanced genomic inversion within non-coding regions of the Isoc1 and Fbn2 genes

Using combinations of primers specific for intron 62 of the *Fbn2* gene, and primers specific for the last intron of *Isoc1*, amplicons were successfully generated by standard PCR using genomic DNA from a homozygote animal. Amplicons from a reaction with an *Isoc1* forward and a *Fbn2* reverse primer were sequenced and identified the location of the fusion to the single-nucleotide level (Figure 4.3.9A). In the *Fbn2* gene, within intron 62, the sequence reads up to nucleotide 58,175,674 and in *Isoc1*, the sequence reads up to base 58,835,147 bp (*Isoc1*, intron-4) on mouse chromosome 18, suggesting a chromosomal rearrangement (figure 4.3.9B).

## Figure 4.3.9.

A

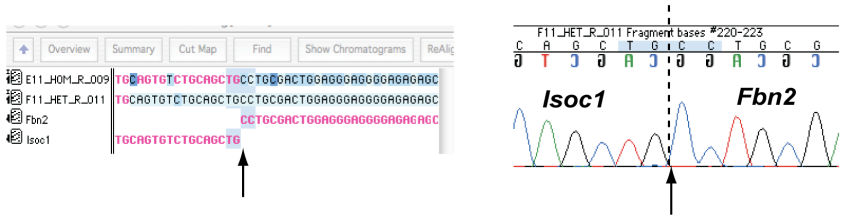


B

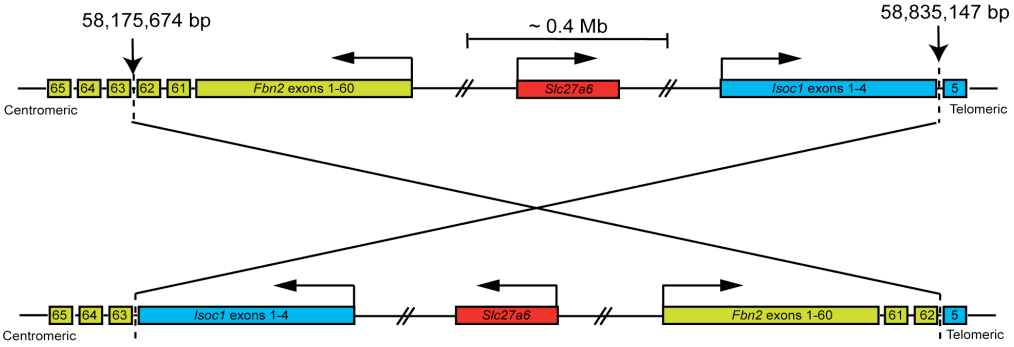


**Figure 4.3.9 Chromosomal breakpoints were identified within 3'-introns of both *Fbn2* and *Isoc1*.**
(**A**) Sequence data from PCR reactions with *Isoc1* forward and *Fbn2* reverse primers of heterozygote and homozygote genomic DNA identified the balanced breakpoint at the nucleotide level (left panel; arrow) from chromatogram data indicating the position of *Fbn2* and *Isoc1* specific sequence (right panel; arrow). (**B**) Figure indicating the positions of the balanced inversion affecting the *Fbn2* and *Isoc1* genes at 58,175,674 and 58,835,147 bp, respectively. Note that transcription of *Fbn2* is considered to be from the minus strand, and *Isoc1* is from the plus strand.

### 4.5.12. The *Mp* genomic inversion results in reciprocal fusions of the Fbn2 and Isoc1 mRNAs

To confirm the *Fbn2-Isoc1* fusion identified by 3'-RACE, and to ascertain whether this was reciprocated by an *Isoc1-Fbn2* fusion, RT-PCR was designed using primers specific to each gene. As mentioned above, it was only possible to amplify *Fbn2* fragment 10 from the wild type and heterozygous cDNA samples. Additionally, using primers specific for the 3'-most region of *Isoc1* cDNA, it was also only possible to generate amplicons from the wild type and heterozygous cDNA samples (Figure 4.3.10A, top two panels). In contrast, the combination of *Fbn2*-forward and *Isoc1*-reverse primers generated amplicons from cDNA of mutant and heterozygote, as did using forward and reverse primers specific for *Isoc1* and *Fbn2,* respectively (Figure 4.3.10A, bottom two panels). This confirmed the fusion of *Fbn2-Isoc1* and also revealed that a complementary fusion had occurred between the two genes, confirming the inverted genomic rearrangement (Figure 4.3.9B). Sequence data generated from these amplicons revealed that the sequence read was continuous from the final nucleotide of exon 62 of *Fbn2* into the first nucleotide of *Isoc1* exon 5, with no extra nucleotides present (figure 4.3.10B).

**Figure 4.3.10.**

**A**

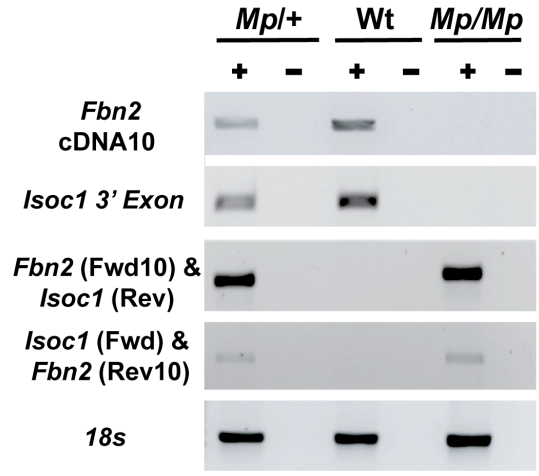


**B**

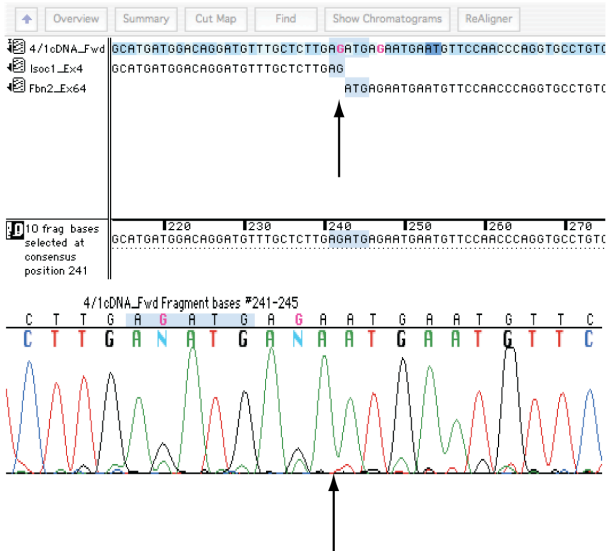

**Figure 4.3.10. The transcripts of *Fbn2* and *Isoc1* in *Mp* were reciprocally fused.**
(A) Top panels: RT-PCR using primers specific for the 3'-ends of each *Fbn2* and *Isoc1* mRNAs failed to amplify products from homozygous cDNA. Central panels: using different combinations of these same primers confirmed the reciprocal fusion event between *Fbn2* and *Isoc1 cDNAs*. Bottom panel: control RT-PCR of 18s ribosomal DNA. (B) Sequence data from *Isoc1* forward and *Fbn2* reverse primer RT-PCR indicated that the fusion read directly from exon 4 of *Isoc1* to exon 63 of *Fbn2* (arrows), with no extra nucleotides incorporated.

### 4.5.13. Predicted consequence for translation of Fbn2$^{Mp}$

Fbn2 is a 2907 amino acid protein of 313.6 kDa (unprocessed-precursor), containing 47x EGF-like domains, of which 42 are calcium binding (cbEGF), and 9x TB (TGFβ-binding) domains (Figure 4.3.11A). The coding-sequence for the fused *Fbn2-Isoc1* transcript of was used to generate a predicted protein for Fbn2$^{Mp}$ using the translate tool on the ExPASy website (http://expasy.org/tools/#translate). The adjoined *Isoc1* sequence was immediately knocked out of frame and resulted in the addition of 7x amino acids, with no known motif or functional domain, followed by a termination codon (Figure 4.3.11B). A polyclonal anti-Fbn2 antibody (PAb0868), specific to the N-terminal region of the Fbn2 protein (Figure 4.3.11C), was kindly provided by Professor Lynn Sakai (Shriners Hospital for Children, Oregon Health and Sciences University, Portland, Oregon).

**Figure 4.3.11.**

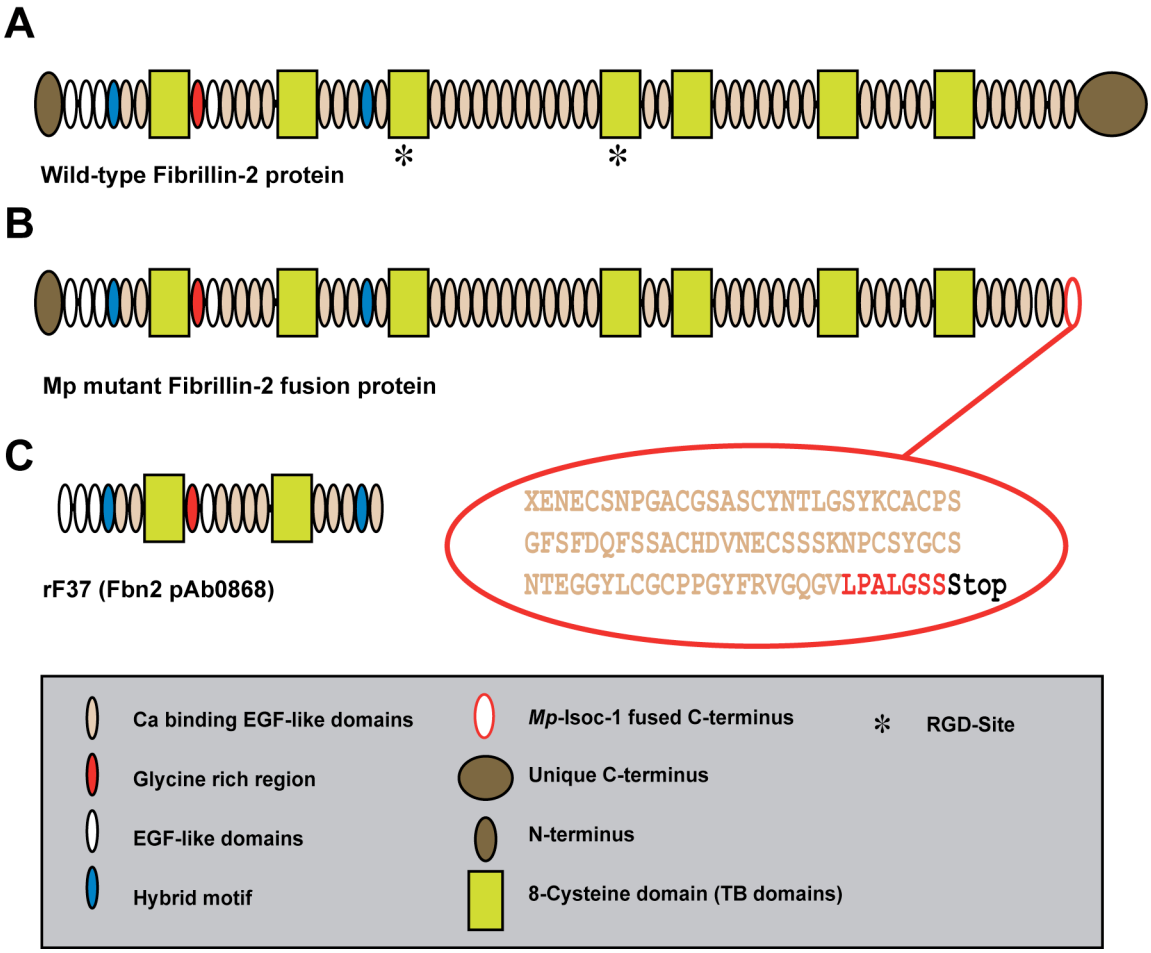


**Figure 4.3.11. Protein structure of Fbn2 and Fbn2$^{Mp}$**. Cartoon indicating functional domains present in the wild type Fbn2 protein (**A**). The *Mp* protein is missing the final cbEGF domain and the unique C-terminus, which have been replaced by 7x amino acids and (red text) a premature stop codon (**B**). The polyclonal antibody (PAb0868) is reactive to a peptide generated from the N-terminal of Fbn2 and therefore is predicted to be reactive to Fbn2$^{Mp}$ (**C**).

## 4.6. Developmental expression analysis of *Fbn2* and *Isoc1* in Mp

### 4.6.1. Developmental expression of *Fbn2* is consistent with phenotype in *Mp*

Although I performed the image capture and analysis, whole mount *In Situs* were done by Dr. David McBride (University of Cambridge, formerly MRC Human Genetics Unit), Expression of *Fbn2* was analysed at embryonic stages E10.5, E11.5 and E12.5 in wild type embryos (figure 4.4.1). Ocular expression was identified at all three stages, beginning in the dorsal-most region at E10.5 and then spreading laterally to surround the entire developing eye by E12.5 (figure 4.4.1A & B). This early expression domain was considered to be within the peri-ocular mesenchyme adjacent to the neural retina and RPE, however as development proceeded, *Fbn2* expression was also noted in the distal-most region of the neural retina as a 'ring' of expression. This area corresponds to the developing ciliary body (CB). Little or no expression was noted in the central neural retina or lens, however there was signal observed in the region of the closing choroid fissure in the ventral eye at E11.5 and E12.5 (figure 4.4.1B).

*Fbn2* expression was also observed in limbs from the same embryos (figure 4.4.1A & C), although signal was not identified at E10.5. At E11.5, Expression was noted mostly in central areas of the proximal fore and hindlimb buds, but not in the distal regions, i.e. the developing hand plates (figure 4.4.1C). By E12.5, the expression pattern had extended to include proximal and distal regions of both fore- and hindlimbs. However, it was noted that expression pattern differed between the distal fore and

hindlimbs. In the forelimbs expression appeared to be located within the developing digit condensations, with digits 2-4 expressing strongest. In the hindlimbs however, there was expression between, but not within, the developing digit condensations and was strongest at these regions between digits 2-4.

Figure 4.4.1.

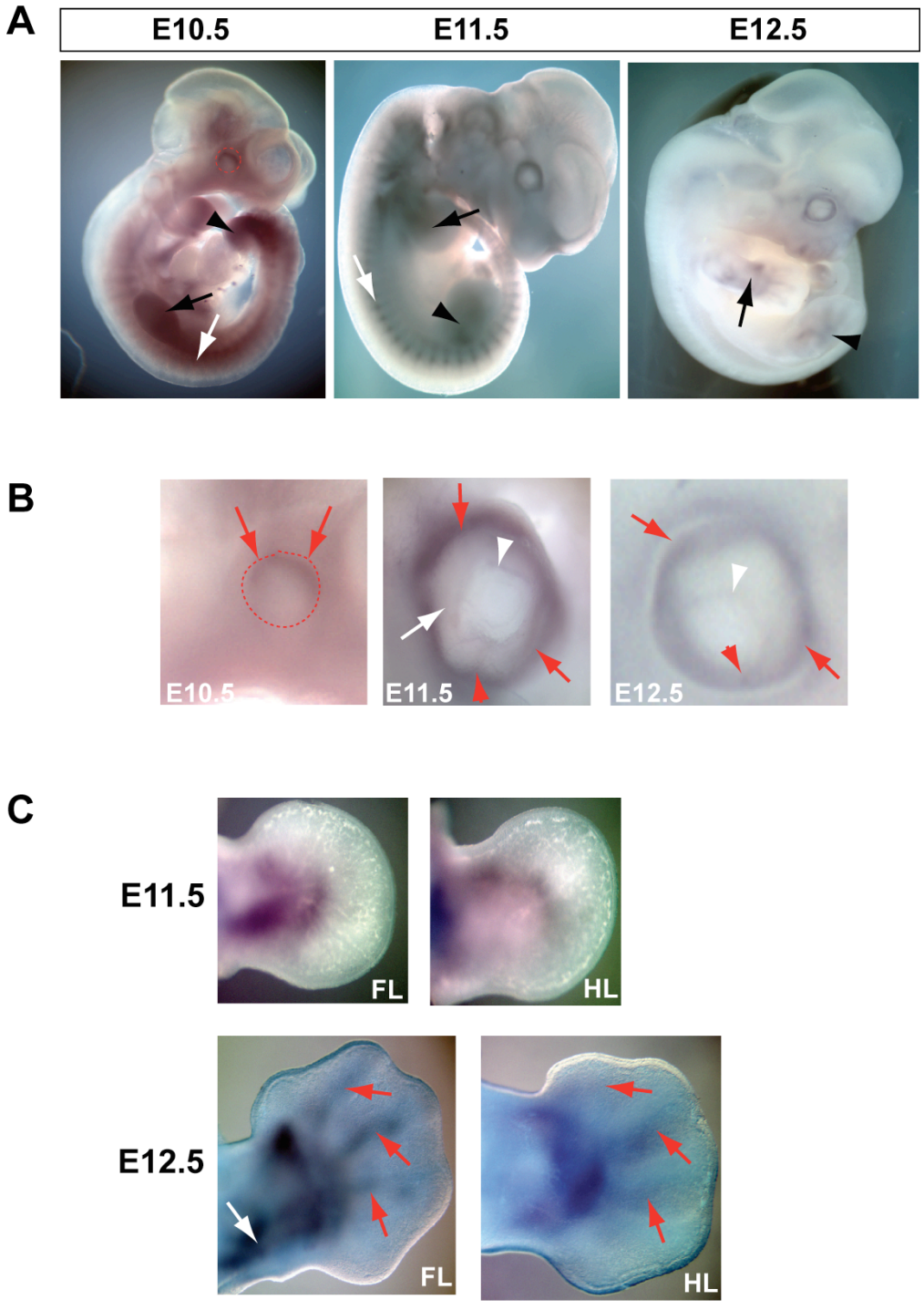

**Figure 4.4.1 WISH expression of *Fbn2* in wild type animals was consistent with the *Mp* phenotype.**

Whole mount *in situs* (WISH) were performed on wild-type embryos at stages E10.5; E11.5; and E12.5 (**A**). At E10.5, the *Fbn2* probe was positive for expression in tissue surrounding the dorsal eye (red arrows), and somites (white arrows), but appeared negative in both the fore and hind limb-buds at this stage. By E11.5, the ocular expression domain had spread laterally to surround the entire eye region, but maintained the strongest signal dorsally. There was also *Fbn2* expression in the proximal regions of the developing limb-buds (forelimbs - black arrows; hindlimbs -arrowheads), but not in the distal limb areas, i.e. the developing hand-plates, at this stage. At E12.5 the ocular expression appeared refined to the peripheral retina. At the same stage, the limb expression was more pronounced in both fore- and hind-limbs and it was possible to correspond *Fbn2* signal to the developing digit, wrist and proximal structures. Close-up views of eyes at stages E10.5; E11.5 and E12.5 (**B**) identified clear domains of *Fbn2* expression. Signal was seen in only the dorsal region of the E10.5 eye (red arrows, a dashed line outlines the ocular field), in peripheral retinal area likely to be periocular mesenchyme and not neural retina. However, in the E11.5 eye this domain had expanded laterally to surround the entire eye with strong signal. There is little or no expression seen in the central neural retina (white arrow), however a highly specific 'ringed' domain of expression was visible at the distal tip of the retina (white arrowhead) and also in the closing choroid fissure (red arrowhead) in the ventral retina. *Fbn2* expression at E12.5 was similar in distribution to E11.5 in the periocular mesenchyme (red arrows), and a reduced, but intense, signal was seen in the ventral retina in the region of the fissure (red arrowhead). The expression domain at the distal tip of the retina was maintained (white arrowhead). In the developing limbs (**C**), strong expression signal was visible in both forelimb (FL) and hindlimb (HL) at E11.5 within the central proximal regions, but not in the peripheral regions of the handplates. At E12.5 the strong signal was maintained in the proximal limb in both FL and HL, but in the FL there was extensive expression in the posterior region of this domain (arrowhead). In the FL there was signal in regions consistent with the condensations of digits 2; 3; and 4 (red arrows), but in contrast the corresponding regions in the HL did not show signal. Rather, there was signal in the inter-digital regions between the condensations (red arrows).

### 4.6.2. Expression of *Fbn2* was observed throughout the developing wild type eye

Section *in situ* of paraffin embedded eyes with the same *Fbn2* probe identified the specific domains of expression within the developing mouse eye (figure 4.4.2). At E12.5, expression was noted in the peri-ocular mesenchyme surrounding the eye (figure 4.4.2A & B) and in the lateral edges of the developing CB and adjacent RPE at the anterior region of the retina (figure 4.4.2C). Some signal was observed in mesenchymal cells of the developing cornea, but no signal was identified in the central retina. At E16.5, *Fbn2* expression was identified in the peri-ocular mesenchyme but not in the central retina (figure 4.4.2D). Expression in the CB was more intense than at E12.5 and covered the majority of the anterior tip of the retina (figure 4.4.2E & F). There was also expression in cells of the developing iris stroma (figure 4.4.2F). These domains of expression were entirely consistent with the expression patterns identified in whole embryos.

**Figure 4.4.2**

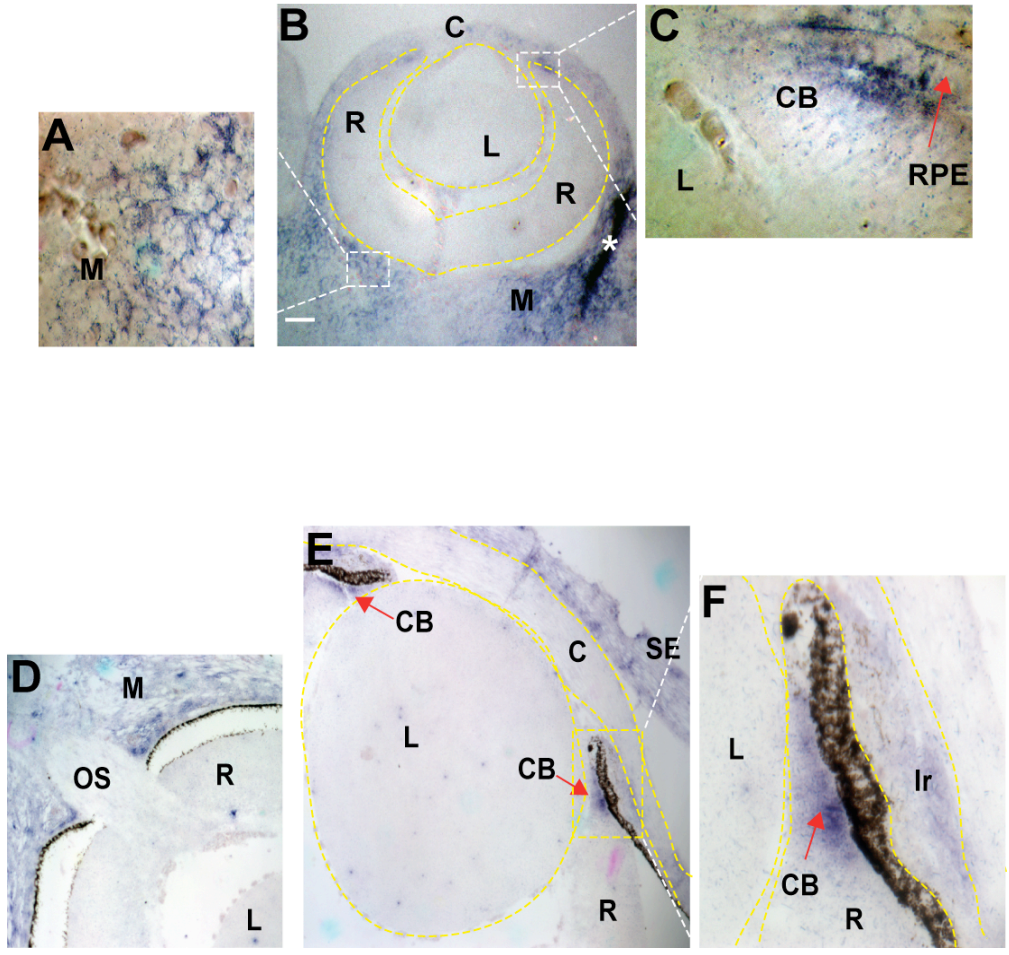

**Figure 4.4.2 *Fbn2* is expression was observed in various cell types during wild type eye development.**
Section *in situ* hybridisation on paraffin embedded wild-type eyes at E12.5 (A-C) and E16.5 (D-F) using probe for *Fbn2* 3'-UTR. At E12.5 cells positive for *Fbn2* transcripts were identified in large domains of expression within the periocular mesenchyme proximal to the retina (A & B), and in a small subset of cells of the developing ciliary body at the anterior tips of the retina (enlarged in C). This domain extended into some cells of the anterior region of the RPE. Low signal was also identified in some mesenchymal cells of the developing corneal stroma. However, cells of the retina, the vitreous body and the lens were not seen to express *Fbn2*. (Scale bar = 50 μm). At E16.5 positive cells were observed in the mesenchyme proximal to the retina (D), within cells of the ciliary body, the developing iris stroma, and in the surface ectoderm covering the cornea (E & F). As at E12.5, cells of the lens and retina were not seen as positive for *Fbn2* signal at this stage. C, cornea; CB, ciliary body; Ir, iris; L, lens; M, mesenchyme; OS, optic stalk; R, retina; SE, surface epithelium. Scale bar = 50 μm

### 4.6.3. *Isoc1* expression was unidentified in developing wild type embryos

Whole mount and section *in situ* hybridisation analysis of *Isoc1* expression was performed in embryos at developmental stages E10.5, E11.5 and E12.5 (figure 4.4.3). No evidence of expression was observed in any part of the embryos analysed in either whole mounts or sections. In whole mounts, particular attention was paid to those regions affected in the *Mp* phenotype, yet no expression was identified in eyes or limbs at either of the embryonic stages (figure 4.4.3). Additionally, analysis of developing eyes at higher resolution using section *in situ* also did not identify *Isoc1* expression.

## Figure 4.4.3

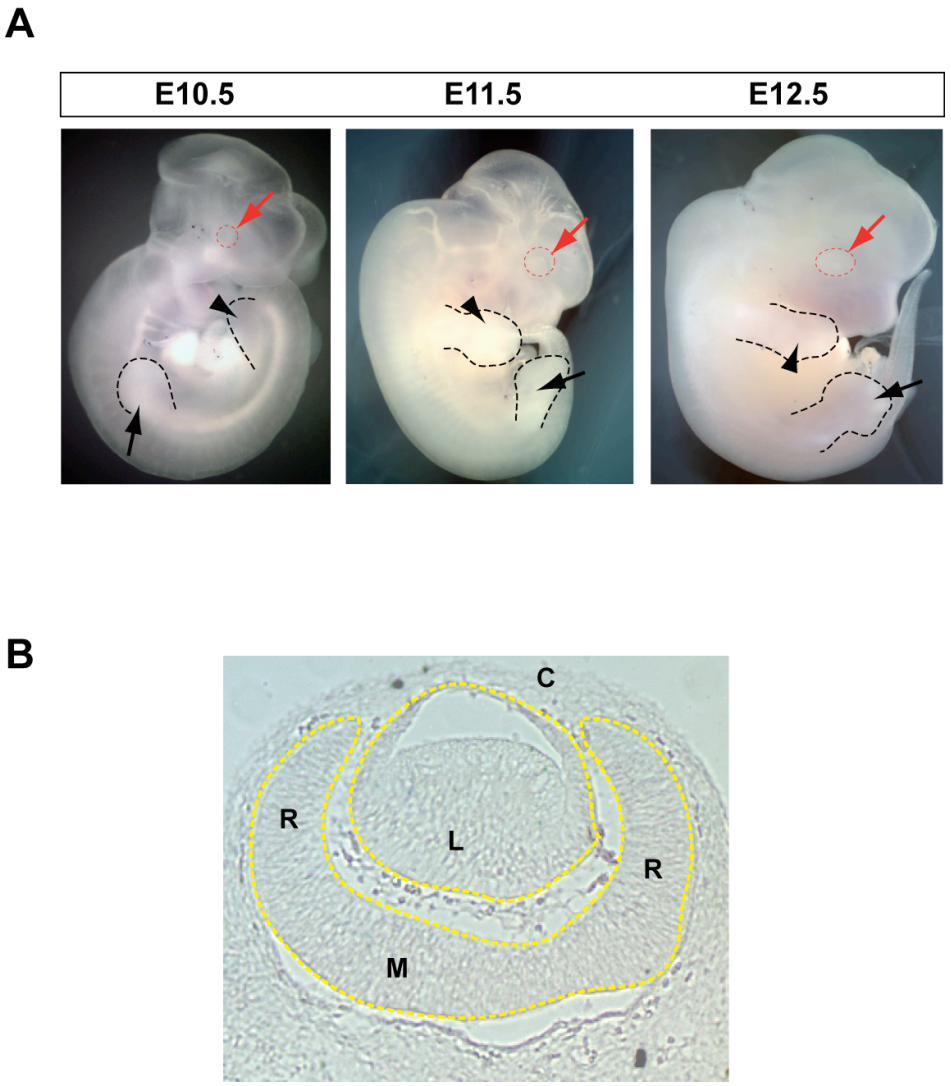


**Figure 4.4.3 Developmental expression of *Isoc1* was undetectable by RNA *in situ* hybridisation.**

Signal from the *Isoc1* probe (**A**) was undetectable at each stage of development analysed, with no expression apparent in any regions of the developing embryos including the developing limb (filled arrows and arrowheads) and eye structures (arrows) described as positive for *Fbn2* expression. Dashed lines indicate ocular (red) and limb (black) structures. Section in situs of paraffin embedded sections illustrated that at higher definition analysis there was no *Isoc1* expression identified within developing ocular structures at E12.5 (**B**).

### 4.6.4. Developmental *Fbn2*$^{Mp}$ expression in homozygotes is consistent with wild type Fbn2 expression in the eyes and limbs

As the *in situ* probe used above was complimentary to the 3'-untranslated region of the *Isoc1* gene, and the *Mp* genetic inversion resulted in this region fused to the *Fbn2* gene, and vice versa, the *Isoc1* probe was used to report *Fbn2* expression and the *Fbn2* probe was used to report *Isoc1* expression in mutant samples (figure 4.4.4A). In section *in situs*, *Fbn2*$^{Mp}$ expression in mutant eyes duplicated the wild type ocular *Fbn2* expression pattern (figure 4.4.4B & C), with *Fbn2*$^{Mp}$ transcripts identified in peri-ocular mesenchyme and distal retina (figure 4.4.4C). Additionally, expression analysis in mutant limbs (figure 4.4.4D) revealed similar results: mutant *Fbn2*$^{Mp}$ transcripts seen using the *Isoc1* probe in homozygote limbs reproduced the wild type *Fbn2* expression observed with the *Fbn2* probe. Expression of *Isoc1*$^{Mp}$ in the mutant was not identified with the *Fbn2* probe and there was no wild type expression observed with the *Isoc1*probe. Whole mount In Situs were done by Dr. Peter Branney (MRC Human Genetics Unit), Non-quantitative RT-PCR was used with RNA from whole embryos and revealed that Slc27a6 expression was maintained in mutants (figure 4.4.4E).

**Figure 4.4.4**

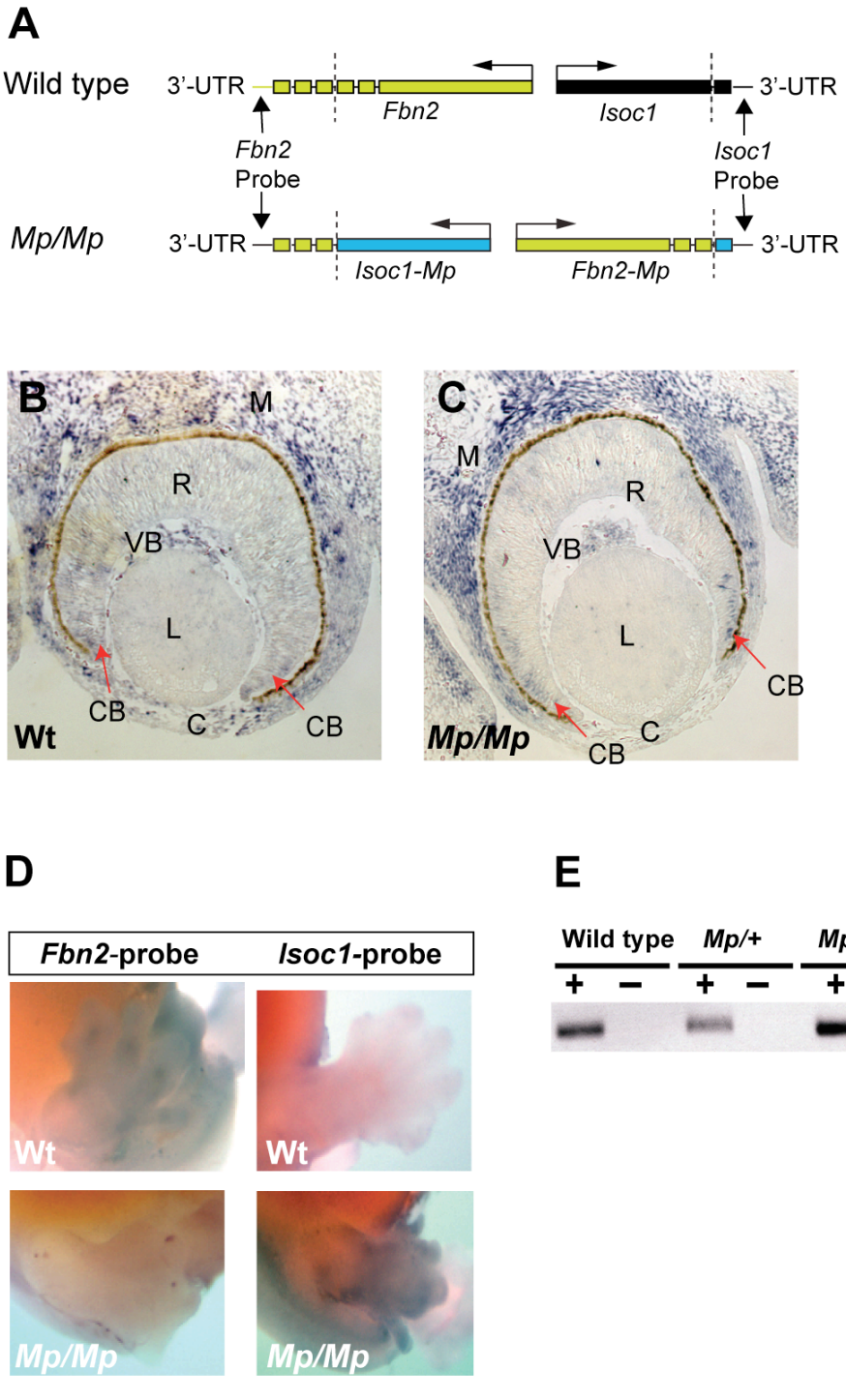
A
Wild type
3'-UTR
Fbn2
Isoc1
3'-UTR
Fbn2
Probe
Isoc1
Probe
Mp/Mp
3'-UTR
Isoc1-Mp
Fbn2-Mp
3'-UTR
B
M
R
VB
L
CB
C
CB
Wt
C
M
R
VB
L
CB
CB
C
Mp/Mp
D
Fbn2-probe
Isoc1-probe
Wt
Wt
Mp/Mp
Mp/Mp
E
Wild type
Mp/+
Mp/Mp
+
−
+
−
+
−

**Figure 4.4.4. The *Isoc1 In Situ* probe reported unchanged domains of *Fbn2*$^{Mp}$ expression in mutant eyes and limbs.**
The *In Situ* Probes used so far were designed for specificity to the 3'-UTRs of wild type *Isoc1* and *Fbn2*. However, due to the nature of the inversion at the *Mp* locus, these probes were suitable to report expression of the mutant transcripts, i.e. the *Isoc1* probe is predicted to report *Fbn2*$^{Mp}$ expression and, *vice versa,* the *Fbn2* probe should report *Isoc1*$^{Mp}$ expression (**A**). Section *In Situs* (**B** & **C**) at E13.5 using the *Isoc1* probe identified that expression of *Fbn2*$^{Mp}$ in the homozygote (**C**) was identical to *Fbn2* expression in the wild type (**B)**. Domains of overlapping *Fbn2*$^{Mp}$ and wild-type *Fbn2* expression were observed in cells of the peri-ocular mesenchyme (M), developing ciliary body (CB) and cells within the vitreous body (VB). There appeared to be possible loss of *Fbn2*$^{Mp}$ expression in the developing cornea (C) of *Mp* eyes, although surface ectoderm expression adjacent to the lateral retina was intact. In both cases, the lens (L) and central neural retina (R) did not display expression. These probes were also used for WISH analysis (**D**) on a litter of genotyped E13.5 embryos from an intercross between *Mp*-heterozygotes. Wild-type limbs displayed expression using the *Fbn2*-probe but homozygotes did not. In contrast, wild type limbs analysed with *Isoc1*-probe did not show expression, whereas homozygotes were positive. Expression of the gene lying between *Isoc1* and *Fbn2* on chromosome 18 was analysed qualitatively by RT-PCR on RNA collected from whole-embryos (**E**). Positive expression was identified in all three genotypes.

### 4.6.5. Ocular distribution of mutant Fbn2$^{Mp}$ protein was abnormal in developing *Mp* eyes

Using an anti-Fbn2 primary antibody, the localisation of wild type and mutant protein was investigated in developing eyes at E13.5 and E16.5 (figures 3.5A-D & E-F, respectively). Wild type protein was identified in the developing corneal mesenchyme, in the mesenchyme of the developing sclera, in the exterior surface membrane of the lens, in the inner limiting membrane between the retina and vitreous body, and distributed throughout the vitreous body, while there was no signal seen within either the anterior or central retina, or in RPE (figure 4.4.5 A &C). The strongest

signal was seen in regions where the lens and retina are adjacent, between the anterior internal retina and at the equator of the lens. At these foci, and amongst the cells of the corneal mesenchyme, wild type Fbn2 protein was clearly extracellular and appeared to be organised into matrix-like arrangements (figure 4.4.5C). In contrast, no Fbn2 was identified between lens and retina or in the vitreous body in mutant eyes (figure 4.4.5B). However, positive signal was observed in the CB, anterior retina, RPE, peri-ocular mesenchyme and in some regions of the central retina (figure 4.4.5B & D), with the strongest signal seen in anterior retina.

Localisation of the mutant protein appeared to be intracellular, as no Fbn2 was present in the extracellular regions identified in the wild type, and protein signals always appeared punctate and were associated with adjacent nuclei (figure 4.4.5D). The contrast between wild type and mutant protein distribution was most evident in the corneal mesenchyme, where Fbn2 was continuous and linear in wild type (figure 4.4.5C) but punctate and compact in the mutant (figure 4.4.5D). The same overall distribution patterns were also evident at E16.5, with wild type (figure 4.4.5E) signal present in the extracellular regions between lens and retina, inner limiting retinal membrane, and within the mesenchyme of developing cornea, sclera, and iris. While mutant Fbn2 was located intracellularly in CB, anterior retina, developing iris, cornea and scleral mesenchyme (figure 4.4.5F). No intracellular Fbn2 was identified in the wild type.

**Figure 4.4.5**

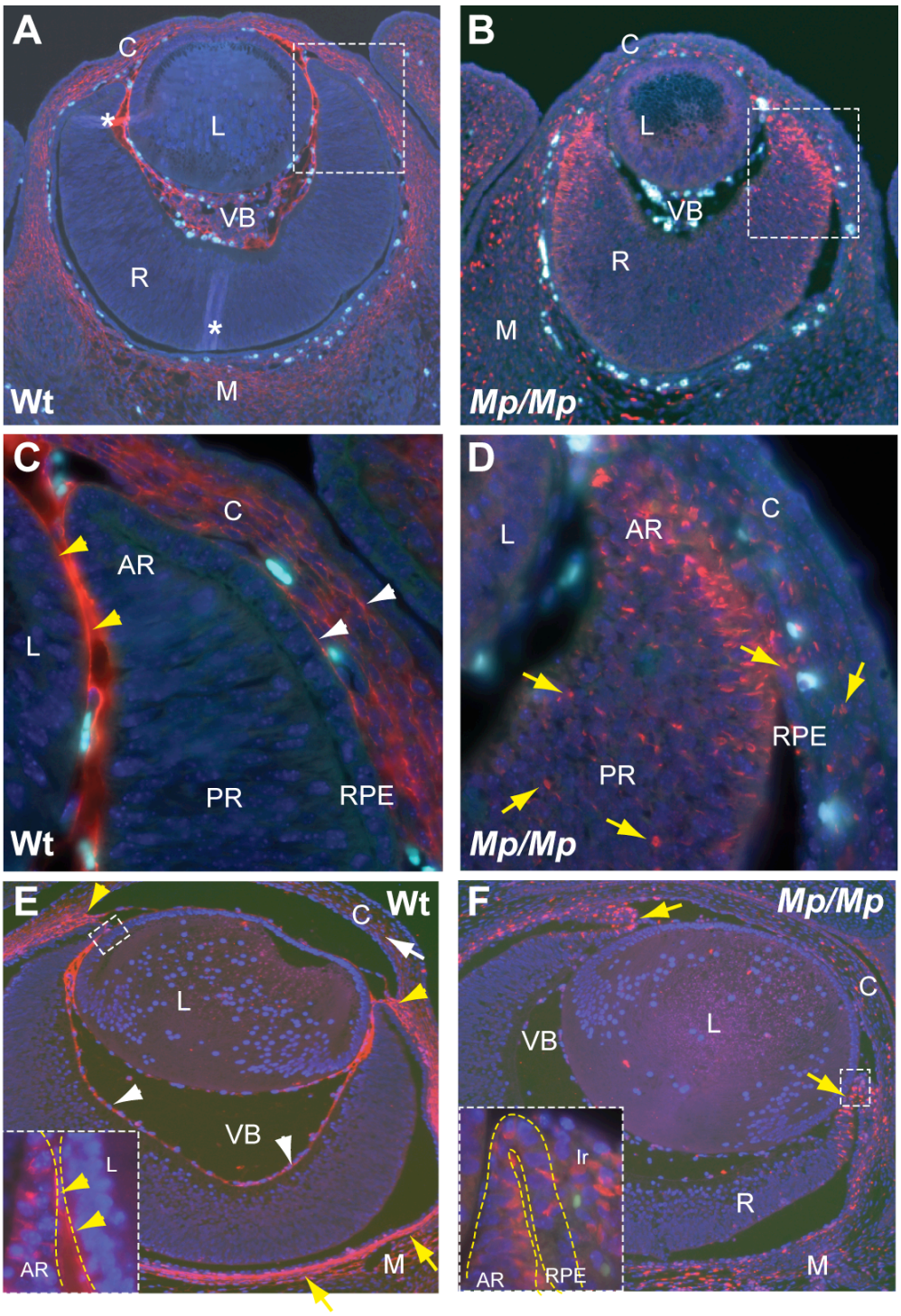
A
C
L
VB
R
M
Wt
B
C
L
VB
R
M
Mp/Mp
C
C
AR
L
PR
RPE
Wt
D
L
AR
C
RPE
PR
Mp/Mp
E
Wt
C
L
VB
L
AR
M
F
Mp/Mp
C
L
VB
Ir
R
AR
RPE
M

**Figure 4.4.5 Abnormal localisation of Fbn2 protein in *Mp/Mp* embryonic eyes.**

Using the anti-Fbn2 PAb 0868 on E13.5 embryonic sections (**A-D**), wild-type Fbn2 signal was identified in the developing cornea, in mesenchyme of the developing sclera, in the exterior surface of the lens, and in the inner limiting membrane between the retina and vitreous body, as well as in the vitreous body itself in wild-type eyes (**A** & **C**). In contrast, no extracellular signal from mutant protein was observed in the vitreous or external membranes of the lens or retina in mutant eyes (**B** & **D**). Some signal was observed dispersed with cells of the mesenchyme in both developing cornea and sclera, yet the strongest signal was seen within the anterior retina and CB. Enlarged views of both wild-type (**C**) and mutant (**D**) illustrated the difference in the distribution of Fbn2 protein, with the wild-type signal clearly localised to the extracellular space between the adjacent lens and retina (arrowheads), as well as forming matrix-like arrangements amongst cells of the developing cornea (white arrowheads). In contrast, mutant Fbn2 was not observed in extracellular regions and was localised adjacent to nuclei in punctate and non-continuous arrangements. There was no signal seen within either the anterior retina or peripheral retina, or in the RPE of the wild type. In the mutant however, $Fbn2^{Mp}$ signal was clearly observed within the retina, with the strongest signal seen in the anterior region, but also with cells distributed throughout the central retina. Additionally, many small regions of signal were observed throughout the RPE and developing cornea (arrows). At E16.5 (**E** & **F**), the distribution of wild-type protein (**E**) was similar to at E13.5. There was strong extracellular localisation in the region where the lens and anterior retina are directly apposed (highlighted & enlarged window), in and adjacent to the mesenchyme of the developing sclera (arrows) and cornea (white arrow), and in the forming iris (arrowheads). Signal was not present in the vitreous but was distributed throughout the inner limiting membrane of the retina (white arrowheads). Again, there was no Fbn2 observed within the retina of the wild type. An enlarged view of the distal retina indicated the extracellular localisation of Fbn2 protein in the wild type (**E**, inset). In the mutant (**F**), signal was observed in the anterior region of the retina (arrows). This was consistent with the $Fbn2^{Mp}$ localisation at E13.5 and was in contrast to the wild-type distribution. There was also signal present in developing iris, cornea, RPE and mesenchyme. An enlarged view of the anterior retina domain of expression indicated that the $Fbn2^{Mp}$ localisation might be intracellular, due to the intimate association of discrete signal foci with nuclei present in this region, and additionally the complete absence of extracellular signal. C, cornea; L, lens; VB, vitreous body; ILM, inner limiting membrane; R, retina; M, mesenchyme; AR, anterior retina; PR, peripheral retina; RPE, retinal pigmented epithelium; Ir, iris. (* in (**A**) indicates artefacts of processing).

### 4.6.6. $Fbn2^{Mp}$ protein formed intracellular inclusion bodies

Analysis of neonate skin cells using transmission Electron microscopy (TEM) revealed the presence of large organised inclusions within the mutant cells that were not present in wild type cells (figure 4.4.6). There were numerous foci of intracellular material throughout the cell body (figure 4.4.6B), which, when analysed at higher magnification, revealed that these inclusions were surrounded by membrane from the endoplasmic reticulum (ER). Further analysis by TEM with the anti-Fbn2 antibody identified the mutant intracellular inclusion bodies as positive for the presence of Fbn2 (figure 4.4.7A). The same analysis in the wild type revealed the presence of Fbn2-positive microfibrils of normal appearance. Prepared samples were shipped and all EM analysis was done by Doug Keene and Sara Tufa (Shriners Hospital for Children, Oregon Health Sciences University, Portland, Oregon).

Immunohistochemistry on MEFs (figure 4.4.7B) with the anti-Fbn2 antibody illustrated the intracellular nature of the inclusion bodies in the mutants and confirmed their close proximity to cell nuclei. In contrast, the Fbn2 signal in wild type MEFs was organised into extracellular matrix and no intracellular Fbn2 was observed. Higher magnification of a single Fbn2-positive MEF cell reveals the inclusion is organised into fibril-like structures within the cell and that these are closely bundled together adjacent to the nucleus.

**Figure 4.4.6**

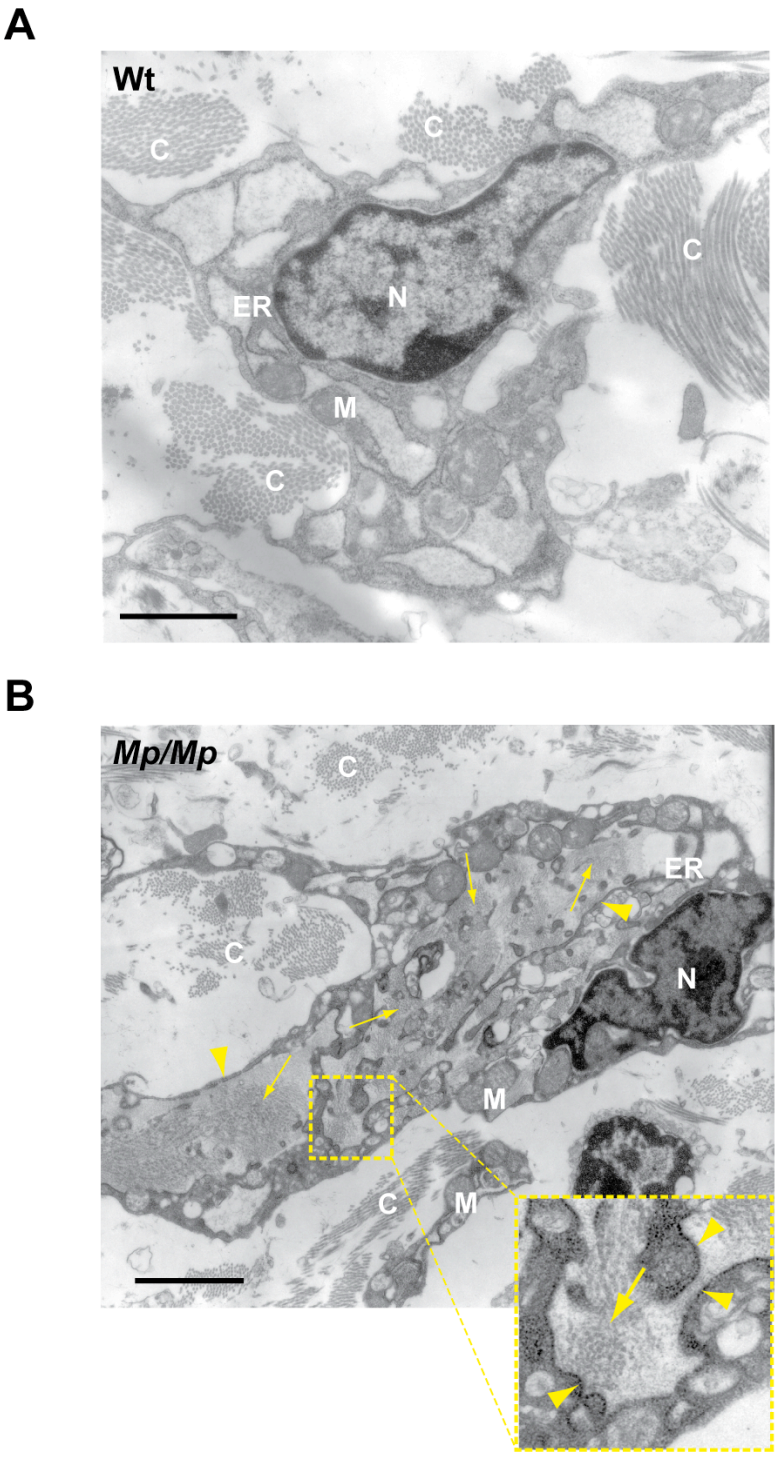

**Figure 4.4.6. Transmission EM revealed inclusion bodies in the ER of mutant cells.**

Transmission EM of a wild type cell processed from neonate skin (**A**) displayed regular cellular morphology and organelles and extracellular collagen fibres. In contrast, cells prepared from neonate *Mp/Mp* skin (**B**) revealed the presence of many large foci of intracellular material (arrows) throughout the cell body. Enlarged image (inset) indicated that the inclusions were surrounded by ER membranes, and suggested that their subcellular localisation was within the ER (arrowheads). Scale bars = 5 μm. Nucleus, N; endoplasmic reticulum, ER; mitochondrion, M; and extracellular collagen fibres, C.

**Figure 4.4.7**

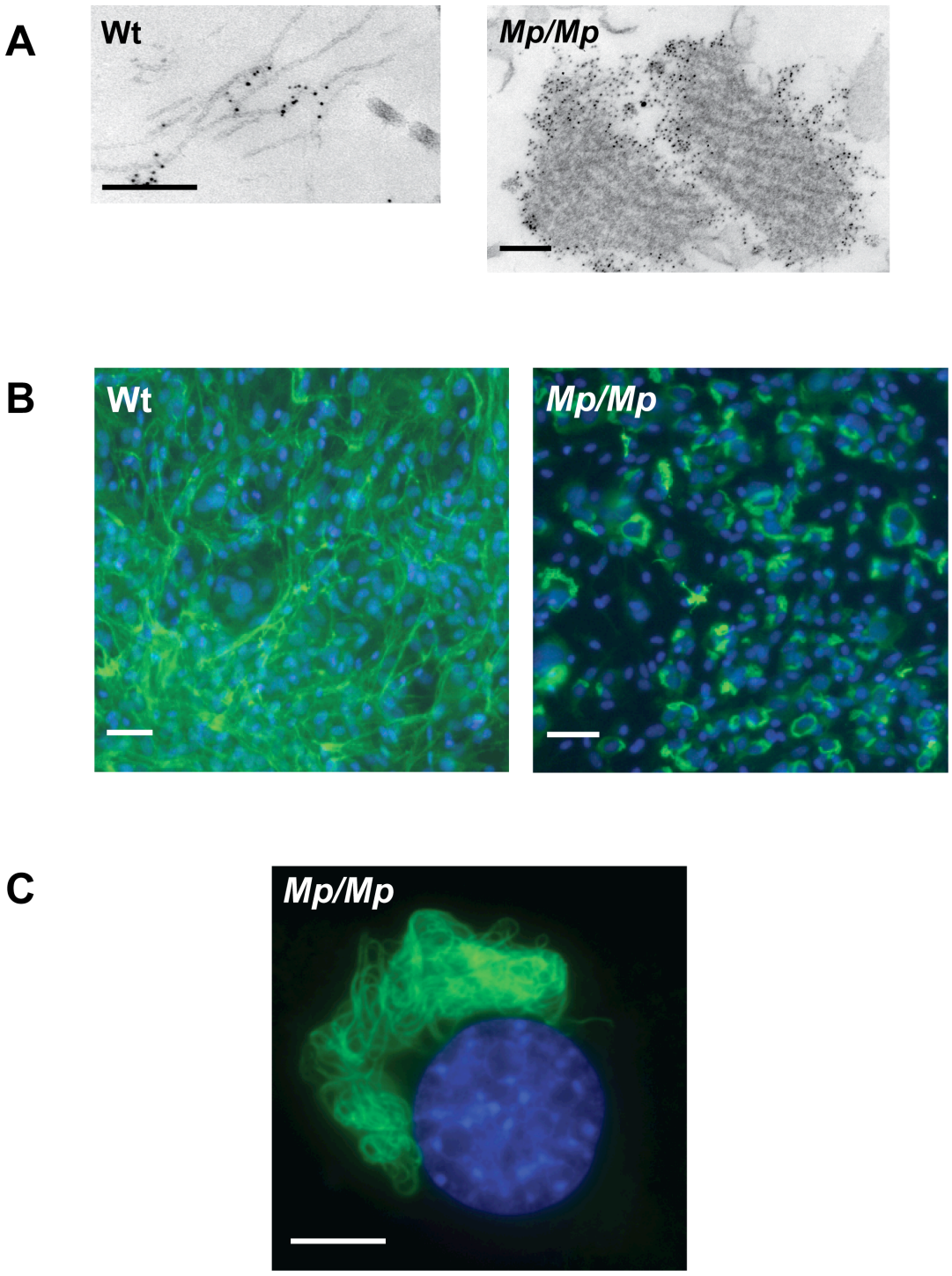

**Figure 4.4.7. Immunolocalisation and immunofluoresence revealed that intracellular inclusions were Fbn2-positive in *Mp/Mp* skin cells and embryonic fibroblasts.**
Using anti-Fbn2 PAb 0868 directed gold labelling, Fbn2 staining was only observed in extracellular microfibrils of the wild-type skin specimen. However, the intracellular inclusions of *Mp/Mp* skin were identified as positive for the presence of $Fbn2^{Mp}$ protein (**A**). Scale bars approx. 500 nm. Immunohistochemistry illustrated a normal Fbn2-positive extracellular matrix in 4 day-old wild-type MEF cultures and no intracellular signal (**B**). In contrast, equivalent *Mp/Mp* cultures were apparently absent for $Fbn2^{Mp}$ in the extracellular matrix but were positive for large aggregates of intracellular protein (scale bar = 50 μm). Enlarged view of single embryonic *Mp/Mp* fibroblast cell (**C**) illustrated the presence of large accumulations of protein adjacent to the nucleus displaying highly organised and bundled fibril-like structures (scale bar = 10 μm).

## 4.7. Towards a molecular mechanism for the *Mp* ocular phenotype

### 4.7.1. The UPR response is elicited in mutant MEF cultures.

Primary MEF cultures were established from E13.5 littermates. Two cell lines for each genotype were grown under normal conditions in 20% serum for 1 week and analysed for the presence of Fbn2 protein inclusions (figure 4.5.1A). Tunicamycin (Tn), a known inhibitor of glycoprotein synthesis and inducer of ER stress, was added to cultures for 30 min. Cells were cultured normally and then harvested after X hours. The unfolded protein response (UPR) was assayed for by RT-PCR of the *Xbp1* transcript. *Xbp1* is alternatively spliced under ER stress conditions to produce a transcript reduced by 26 bp and is thus a good marker for UPR. It was possible to assay for the ratio of unspliced (pU) to spliced (pS) *Xbp1* using ABI310 genetic analyser to measure for peak heights of the differently sized amplicons (figure 4.5.1B). The average ratios of unspliced to spliced *Xbp1* peak heights were plotted for triplicate reactions of 2x cell lines for each genotype (figure 4.5.1C). In cells cultured with the vehicle alone (DMSO), both heterozygote and homozygote ratios were significantly lower than in wild type cells, indicating enhanced levels of *Xbp1* splicing. The addition of 0.5 $\mu$g/ml Tn was sufficient to alter the wild type MEFs ratio to within comparable levels of the mutant vehicle alone samples and also reduced the homozygote ratios. The heterozygote ratio actually increased at this dose. An increased dose of 5.0 $\mu$g/ml Tn dramatically reduced the ratio in all samples tested, indicating that cells were exhibiting considerable UPR response.

The *Xbp1* splicing response to increased Tn dose in all of these cell groups indicates the validity of this assay and confirms the observation that in the vehicle-alone treatment group, the heterozygote and homozygote have elevated levels of spliced *Xbp1* and therefore are likely to already be under ER stress. This suggests that the accumulation of intracellular Fbn2 aggregates causes ER stress and elicits the UPR response in MEFs.

**Figure 4.5.1**

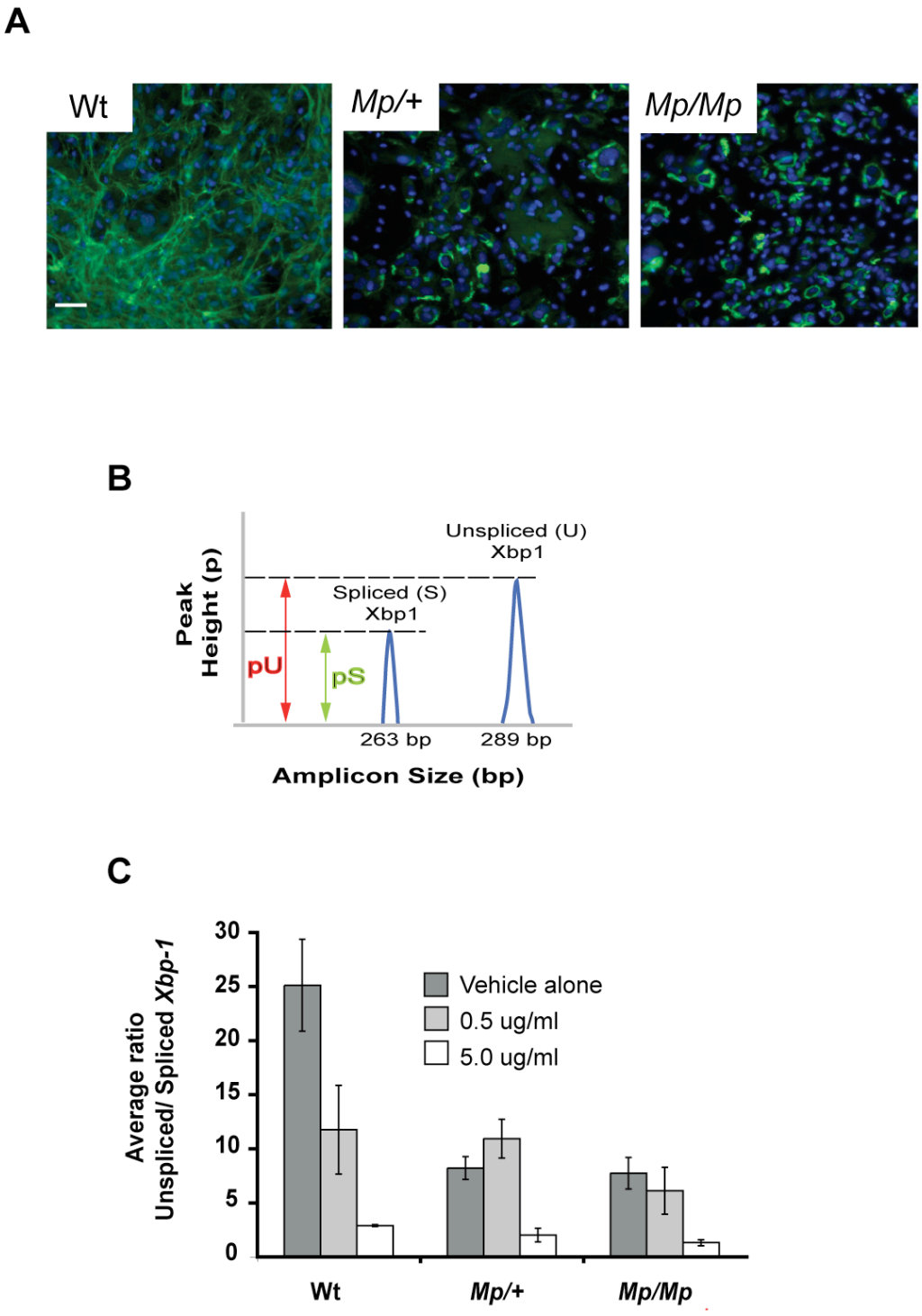
A
Wt
Mp/+
Mp/Mp
B
Unspliced (U)
Xbp1
Spliced (S)
Xbp1
Peak
Height (p)
pU
pS
263 bp
289 bp
Amplicon Size (bp)
C
Average ratio
Unspliced/ Spliced Xbp-1
30
25
20
15
10
5
0
Vehicle alone
0.5 ug/ml
5.0 ug/ml
Wt
Mp/+
Mp/Mp

**Figure 4.5.1 Fbn2 protein aggregates were associated with the UPR-response in mutant MEFs.**
Cultured MEFs derived from E13.5 embryos were cultured for X days and analysed for the presence of Fbn2 protein (**A**). Heterozygote and homozygote MEFs were positive for Fbn2 intracellular inclusions, in contrast to wild type MEFs, which displayed only extracellular Fbn2 (Scale bar = 50 μm). (**B**) Peak sizes of unspliced (pU) and spliced (pS) *Xbp1* amplicons were measured using an ABI310 Genetic Analyser. The pU:pS ratio was used as an indicator of *Xbp1* splicing levels in tested cell populations. MEFs expressing Fbn2 were assayed for the UPR response by the application of Tunicamycin (**C**). In cell populations treated with vehicle alone, both heterozygote and homozygote ratios were significantly lower than in wild type cells, indicating enhanced levels of *Xbp1* splicing. The addition of 0.5 μg/ml Tn reduced these ratios in wild type and homozygote populations, while the heterozygote ratio actually increased at this dose. However, all were lower than the wild type vehicle-alone group. Addition of 5.0 μg/ml Tn reduced ratios in all groups to comparable levels with high levels of spliced *Xbp1*. Two cell lines were tested per genotype; PCR reactions were performed in triplicate. Error bars indicate 95% confidence intervals.

### 4.7.2. The UPR response is elicited in mutant eyes at E16.5.

The heat shock protein Hspa5 (*Grp78* or *Bip*) is a member of the heat shock/stress response protein family and is a well-established marker for ER stress and the UPR response. We applied a BiP RNA *in situ* probe to ocular sections from mutant and wild type E16.5 embryos. *BiP* expression was observed in the iris, CB and anterior-lateral retina regions of mutant eyes (figure 4.5.2A & C). In contrast, these areas were either negative for *BiP* expression in wild types, or there was low-level expression that was more restricted to the ciliary body and iris (figure 4.5.2B; D & E). The regions of *BiP* expression in both mutant and wild type at E16.5 were consistent with *Fbn2* expression, and the domain of mutant *BiP* overlaps with the location of $Fbn2^{Mp}$ aggregates. Thus, mutant eyes exhibit enhanced expression of the UPR marker *BiP* in regions spatially and temporally consistent with $Fbn2^{Mp}$ aggregates.

The *Xbp1* splicing RT-PCR assay was applied to RNA collected from dissected eyes of E16.5 embryos (figure 4.5.2F). The ratio of unspliced to spliced *Xbp1* in the mutant eyes was significantly lower than in wild types, indicating enhanced splicing of *Xbp1* to the UPR isoform in mutant eyes. Agarose gels of *Xbp1* confirmed the specificity of the RT-PCR (figure 4.5.2G).

**Figure 4.5.2**

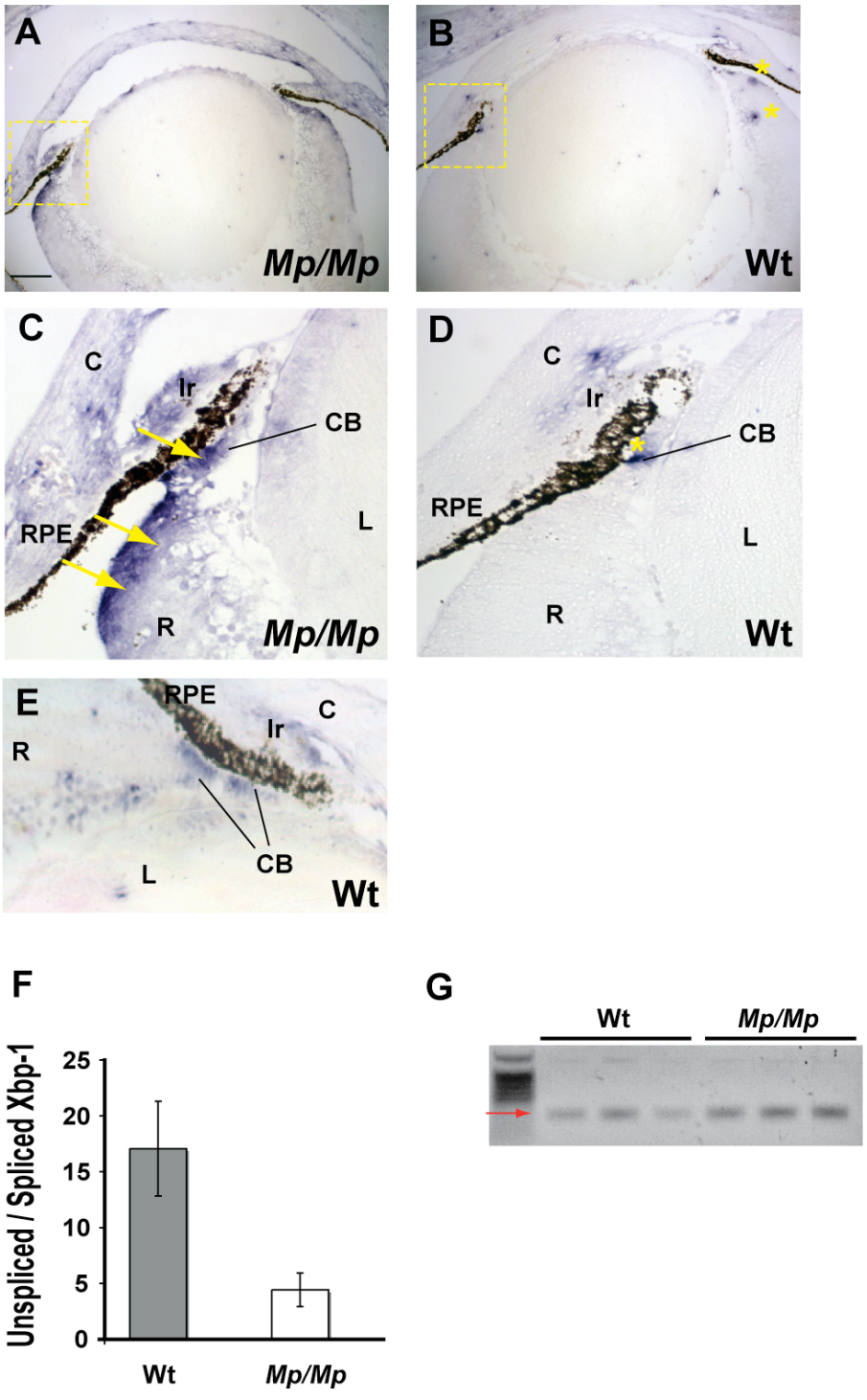
A
Mp/Mp
B
Wt
C
C
Ir
CB
RPE
L
R
Mp/Mp
D
C
Ir
CB
RPE
L
R
Wt
E
RPE
C
Ir
R
CB
L
Wt
F
Unspliced / Spliced Xbp-1
25
20
15
10
5
0
Wt
Mp/Mp
G
Wt
Mp/Mp

**Figure 4.5.2 The UPR-response was coincident with Fbn2 expression in mutant embryonic eyes.**
Expression of the UPR-response marker *Bip* was observed in regions of the mutant mouse eye overlapping with *Fbn2*$^{Mp}$ expression. Bip transcripts (arrows) were identified in the developing CB, the Iris stroma and in the lateral anterior retina of mutant eyes at E16.5 (**A** & **C**- enlarged). Cells in these foci were previously identified as positive for *Fbn2*$^{Mp}$ expression and Fbn2$^{Mp}$ aggregate build up. Some restricted foci of low positive signal were observed in developing wild type eyes (**B** & **D** – enlarged; & **E**). Weak expression was restricted solely to some cells of the CB and iris stroma, and was neither as strong, or diffuse, as in mutant samples, and did not extend into the lateral anterior retina (Scale bar = 100 μm). *Xbp1* spicing assay identified reduced ratios of pU:pS in RNA extracted from excised eyes of genotyped E16.5 littermates (**F**) and thus indicated increased levels of *Xbp1* spicing in mutant eyes. Agarose gel electrophoresis confirmed there to be no genomic contamination and PCR products were specific prior to ABI310 analysis (**G**).

### 4.7.3. Apoptotic cells were identified in mutant retinas at E13.5 and E16.5

Analysis of apoptotic cells in mutant and wild type eyes was performed at E13.5 (figure 4.5.3) and E16.5 (figure 4.5.4) using a primary antibody to activated caspase-3, an established marker for apoptotic cells. At E13.5 positive cells were identified throughout the central retina and in RPE of mutant eyes (figure 4.5.4A). In contrast, no positive cells were identified in wild type eyes at this stage (figure 4.5.4B & D). There were slightly more cells in the anterior region of the neural retina than in the central retina (figure 4.5.4C) and these positive cells displayed different morphologies, suggesting there was no one single cell type, but rather that there were various cell types undergoing apoptosis. Positive cells were dispersed throughout both inner and outer retinal layers. Co-immunostaining was attempted using antibodies to activated caspase-3 and Fbn2 in the mutant eyes (figure 4.5.4E), which showed that not all Fbn2 positive cells were apoptotic and that distribution of activated caspase-3 did not necessarily

associate with Fbn2 aggregates. The distribution of activated caspase-3 positive cells in E16.5 mutant eyes (figure 4.5.4 A & C) was consistent with E13.5. Cells were observed throughout the retina, and different cell types were seen to be positive, based on their morphology. However, there were no apoptotic cells observed in the inner neuroblastic layer. In contrast, there was only a single positive cell observed in the entire wild type retina at the same stage, and this was positioned in the inner neuroblastic layer. Together, these data suggest that mutant retinas are increased for apoptotic cells in comparison to wild types, and that various undifferentiated cell types are affected. Although the ocular locations of apoptotic cells are consistent with the distribution of $Fbn2^{Mp}$ inclusions, there was no direct association between $Fbn2^{Mp}$ inclusions and apoptosis.

**Figure 4.5.3**

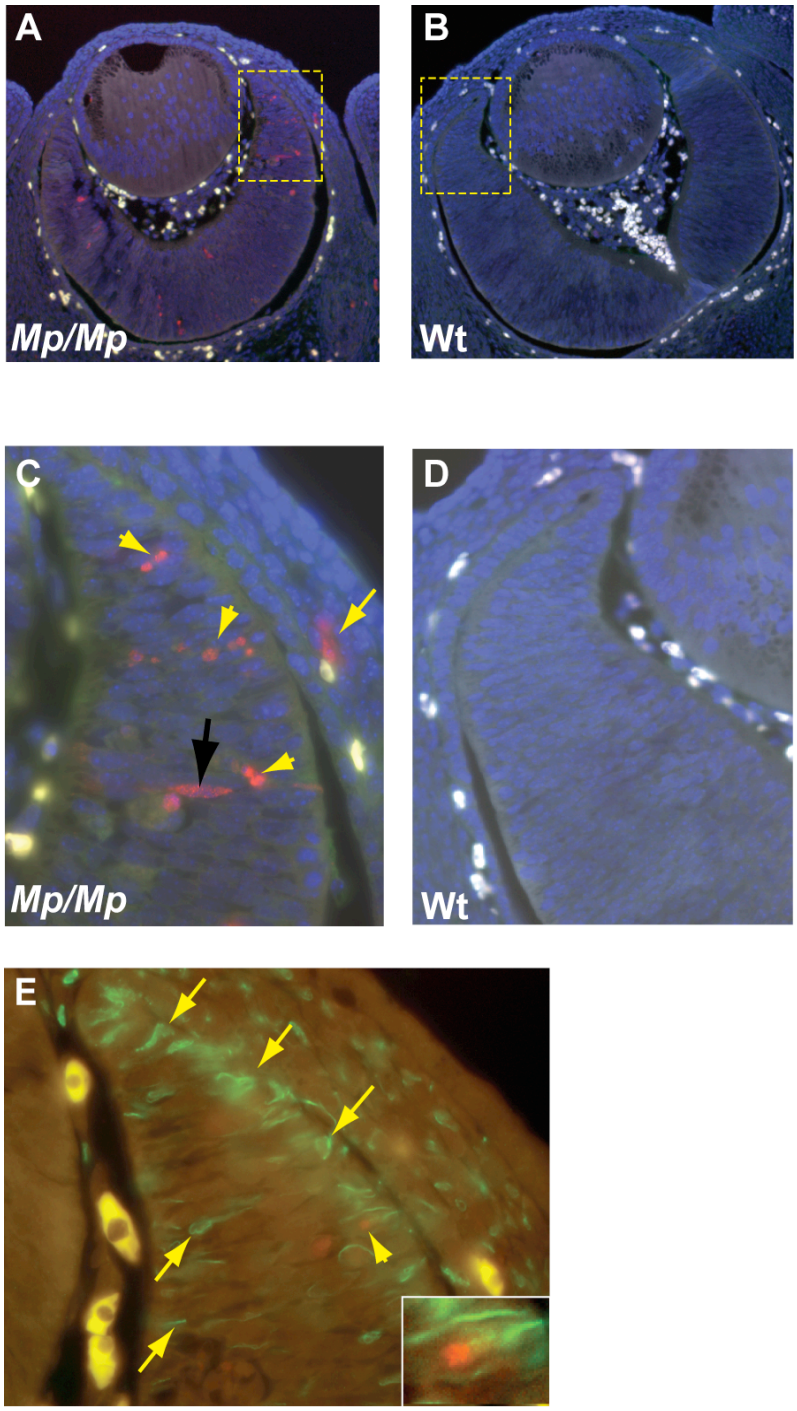

**Figure 4.5.3 Apoptotic retinal cells were identified in mutant eyes at E13.5.** Immunohistochemistry with an Activated Caspase-3 antibody identified positive cells (arrowheads) in the neuroblastic retina, and in RPE (arrows) of mutant eyes at E13.5 (**A** & **C** –enlarged). In contrast, no signal was observed in wild type littermate cells (**B** & **D** –enlarged). Positive cells in mutant retinas displayed different morphologies (black and yellow arrowheads), indicating them to be various cell types. Co-immunostaining with both Fbn2 (green) and Activated Caspase-3 (red) antibodies did not reveal extensive co-localisation of these proteins (**E**) and identified only one cell positive for both proteins (arrowhead and enlarged inset).

## Figure 4.5.4

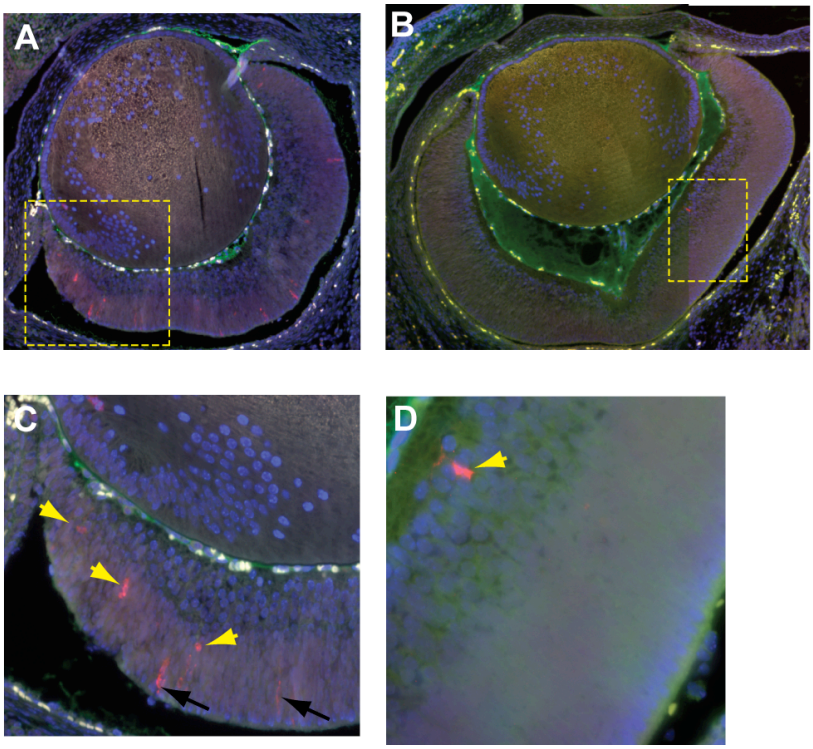


**Figure 4.5.4 Apoptotic retinal cells were identified in mutant eyes at E16.5.** Consistent with the E13.5 data, immunohistochemistry with an Activated Caspase-3 antibody identified positive cells (arrowheads) throughout the neuroblastic retina of mutant eyes at E16.5 (**A** & **C** –enlarged). In contrast, only a single positive cell was identified in the wild type (**B** & **D** –enlarged), with this cell positioned in the inner layer of the retina, not in the neuroblastic layer seen in mutants.

### 4.7.4. Retinal layer specification, as determined by Sox2 and Pax6 immunostaining, is normal in *Mp*

The inner neuroblastic layer of the neural retina was Pax6 positive and Sox2 negative in E13.5 developing eyes of both mutant and wild type (figure 4.5.5A & B). In contrast, the outer nuclear layer is Sox2 positive and Pax6 negative. These domains define retinal patterning throughout development and at E16.5 they remain intact (figure 4.5.5E & F). However, there were cells observed in the Pax6-positive inner layer that were expressing only Sox2, while there were also some Pax6-only expressing cells in the predominantly Sox2-positive outer layer. There was no difference observed between wild type and homozygote in these domains seen at either stage.

### 4.7.5. Anterior Sox2 and Pax6 positive domains define the developing ciliary body and are disrupted in *Mp.*

The developing CB at the anterior of the neural retina was Pax6-positive and Sox2-negative in both mutant and wild type eyes at E13.5 (figure 4.5.5C & D) and E16.5 (figure 4.5.5G & H). However, in wild types of both stages, there is a clear boundary between the anterior-most region of the outer nuclear layer of the retina and the distal portion of the developing CB, which was defined by a small and discrete band of Sox2 and Pax6 positive cells (figure 4.5.5C & G). In the mutants however, the Pax6-positive regions appeared truncated, while the Sox2/Pax6 positive cells were diffuse and spread into the outer nuclear layer of the neural retina (figure 4.5.5D & H). There was no

clear boundary of expression observed between the developing outer nuclear layer and CB in *Mp* mutant eyes at either embryonic stage.

**Figure 4.5.5.**

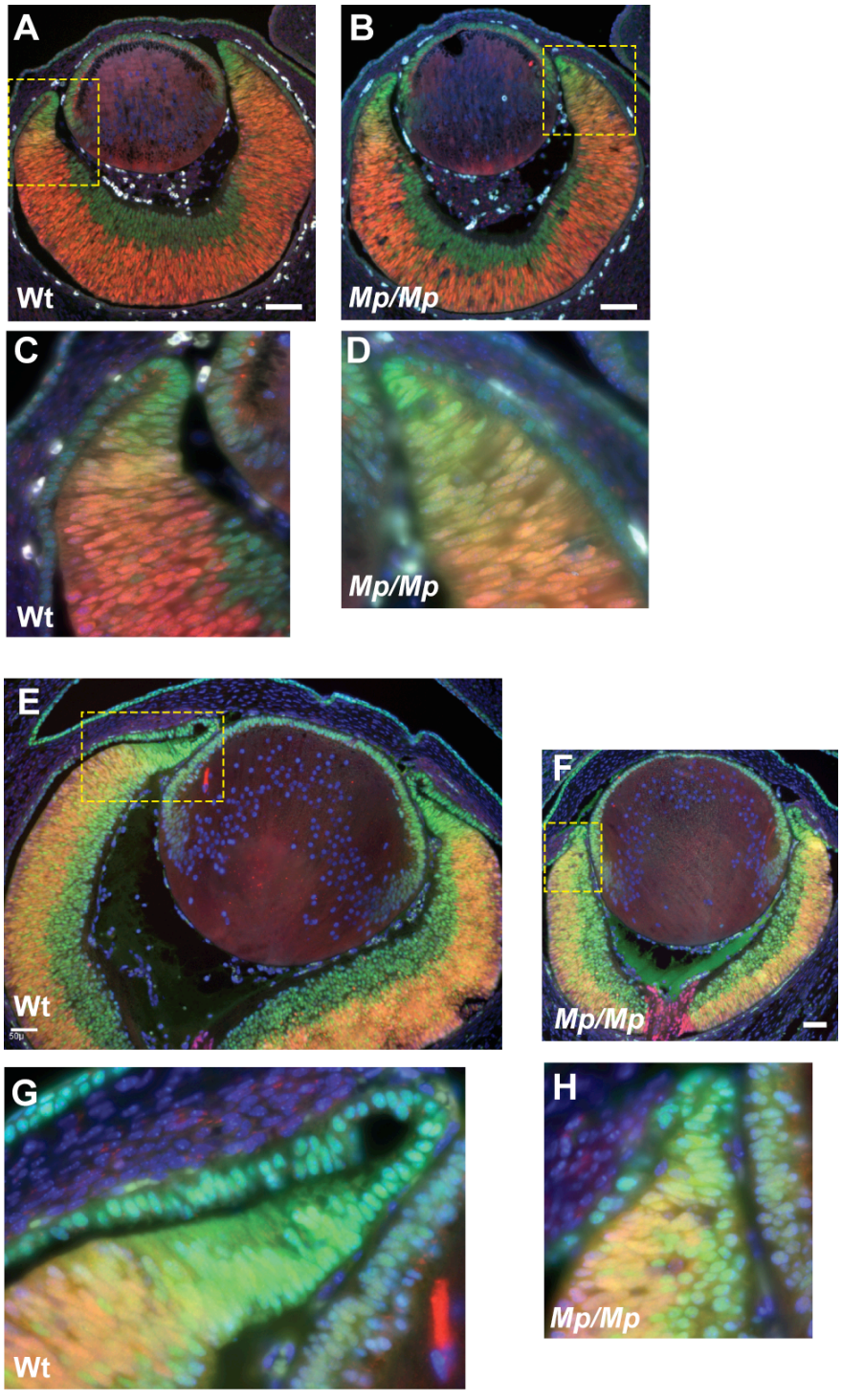

**Figure 4.5.5 Co-immunostaining with Sox2 and Pax6 revealed defects in the ciliary-retinal boundary.**
The developing retina at E13.5 (**A-D**) displayed clear domains of expression for Sox2 and Pax6. In the wild type (**A**) and mutant eye (**B**), the majority of nuclei in the outer neuroblastic layer of the central retina were Sox2 (red) positive, whereas nuclei in the inner neuroblastic region were pax6 positive (green). In both wild type and homozygote, these domains were clearly defined and non-overlapping. In the anterior retina, there were additional domains of Pax6 only expression at the distal-most tips. These were directly adjacent to a group of cells that were co-expressing *Sox2* and *Pax6* (arrows) in the wild type (**C**), which defined a clear boundary between central retina and the developing CB. In contrast, the mutant displayed subtle differences in this region. The co-expressing cells were more diffuse into the central retina and did not clearly define the retina-CB boundary (**D**). At E16.5 (**E-H**), the inner neuroblastic layers of both wild type (**E**) and homozygote (**F**) remained Pax6 positive and the outer neuroblastic layers were Sox2 positive. At this stage, there were also many nuclei within the outer layer that were positive for Pax6 only, and some that were expressing only Sox2. There were also some Sox2-only positive nuclei observed in the inner layer. This was consistent in both homozygote and wild type samples. Higher magnification of the anterior region of retinas revealed a large domain of Pax6-only nuclei in the developing CB in the wild type retina (**G**), while this domain is truncated in the mutant (**H**), with the domain of Pax6-Sox2 co-expressing nuclei shifted anteriorally within this region. Scale bars =50 μm.

### 4.7.6. Immunostaining of *Lef1* in *Mp* eyes revealed increased levels in ciliary body and ectopic retinal expression

Lef1 expression was analysed by immunostaining in developing wild type and mutant eyes at E13.5 and E15.5 (figure 4.5.6) and at E18.5 (figure 4.5.7). In wild type eyes at E13.5 (figure 4.5.6A-C), nuclear Lef1 was observed solely in the cells at the distal-most tip of CB and RPE and did not spread into the peripheral neural retina. In contrast, positive nuclei were observed in the CB domain and RPE of the mutant (figure 4.5.6D-F), with the CB domain extended into peripheral neural retina and displayed a more intense signal than in the wild type, indicating higher levels of Lef1 protein. In the wild type at E15.5, Lef1 signal in the anterior retina clearly defined the developing CB (figure 4.5.6D). This region contained only subsets of nuclei that were positive for Lef1

signal, and some that were positive for Lef1 in their cytoplasm (figure 4.5.6H & I). In the mutant, the CB was also positive for nuclear Lef1 signal, however in contrast to the wild type, the signal was increased in intensity and there were fewer non-expressing cells (figure 4.5.6J-K). RPE and iris stroma were also positive In addition, there were also nuclei, positively stained for Lef1 in the neural retina (figure 4.5.6L). These cells had circular nuclei and were situated in vacuoles, and were not intimately associated with the adjacent tightly packed retinal cells.

**Figure 4.5.6**

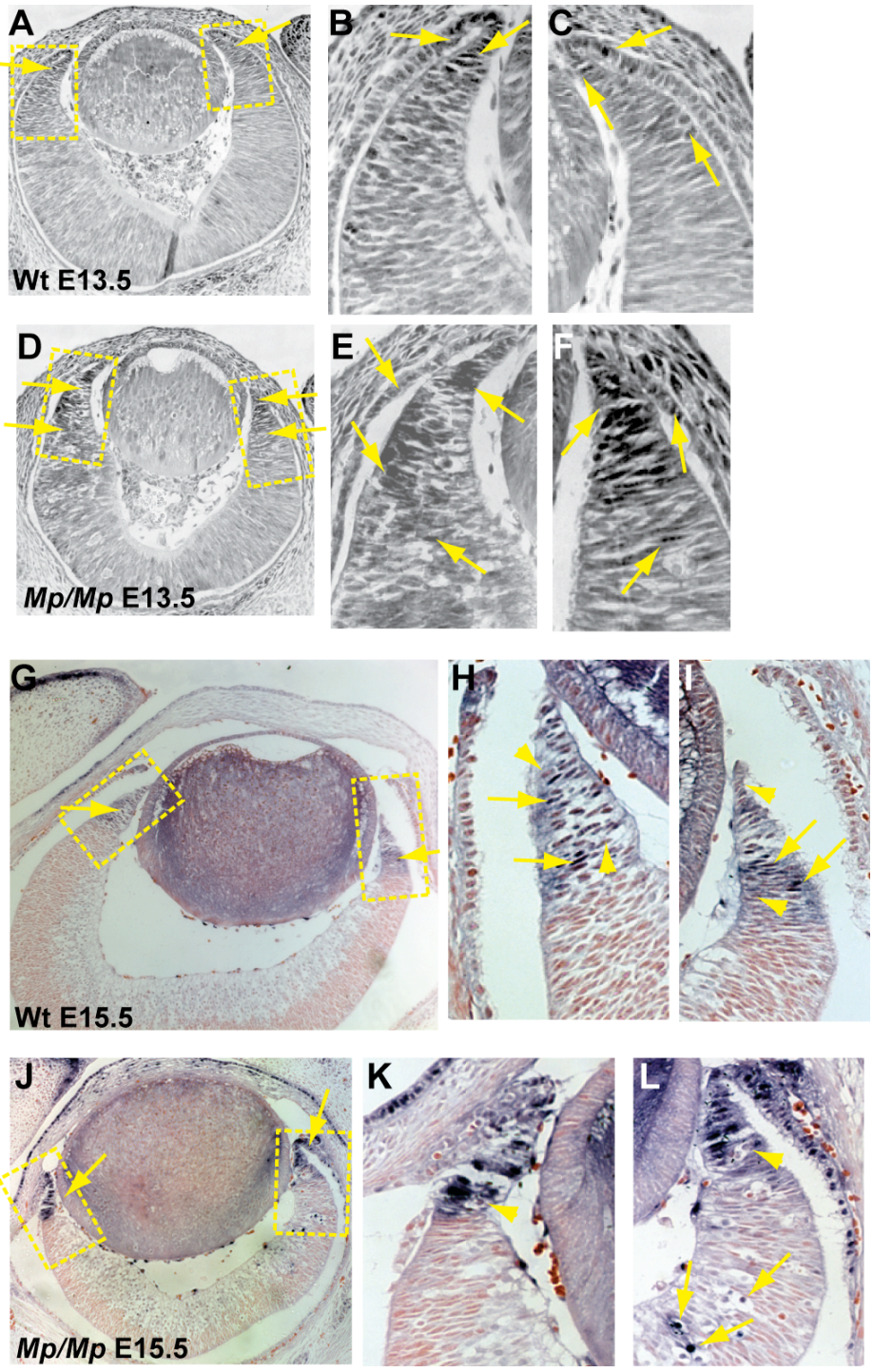

**Figure 4.5.6 Increased Lef1 immunostaining in the developing ciliary body and retinas of mutant eyes.**
Lef1 positive cells were identified in the anterior region of developing retinas at E13.5 (**A-F**). In the wild type (**A-C**), Lef1 signal was nuclear and positive cells were refined to the anterior-most group of cells of CB and RPE (arrows). In contrast, positive cell nuclei were identified in the anterior retina of both the RPE and CB but also the CB domain appeared to extend into the peripheral regions of the central retina in the mutant (**D-E**). Additionally, these cells appeared to be more intensely stained than in wild type, indicating higher levels of Lef1 expression. **B** & **C** and **E** and **F** are higher magnification images of **A** and **D**, respectively. At E15.5, the domains of Lef1 staining (arrows) clearly defined the developing CB of both wild type (**G**) and mutant (**J**). Higher magnification of the wild type domains (**H** & **I**) revealed that only subsets of the nuclei in this region were positively stained (arrows) and that there was also some cytoplasmic staining (arrowheads). In the mutant, although the region of Lef1 signal overlapped with the wild type, the signal was increased in the mutant (**K** & **L**). Also, there were fewer non-expressing cells in the mutant CB (arrowheads), while there were also cell nuclei identified within the central retina that were Lef1 positive (arrows). These circular nuclei were not intimately associated with the adjacent retinal cells and appeared to be positioned within vacuoles.

### 4.7.7. Immunostaining of *Mp* eyes at E18.5 revealed expansion of ectopic retinal Lef1

In wild type eyes, the only Lef1 positive domains were in cornea, iris stroma and CB (figure 4.5.7A). The cells of the CB displayed strongly nuclear staining (figure 4.5.7B) and clearly defined the ciliary from the neural retina. No staining was observed in the wild type neural retina at this stage. In the homozygote, iris and cornea were positive for Lef1 signal, in addition to the truncated CB (figure 4.5.7C & D). In contrast to the wild type, the mutant displayed numerous cells positive for Lef1within the inner nuclear layer of the neural retina (figure 4.5.7E). Although the mutant CB was small and thinner than the wild type, several nuclei were observed as positive for Lef1 expression (figure 4.5.7F).

**Figure 4.5.7**

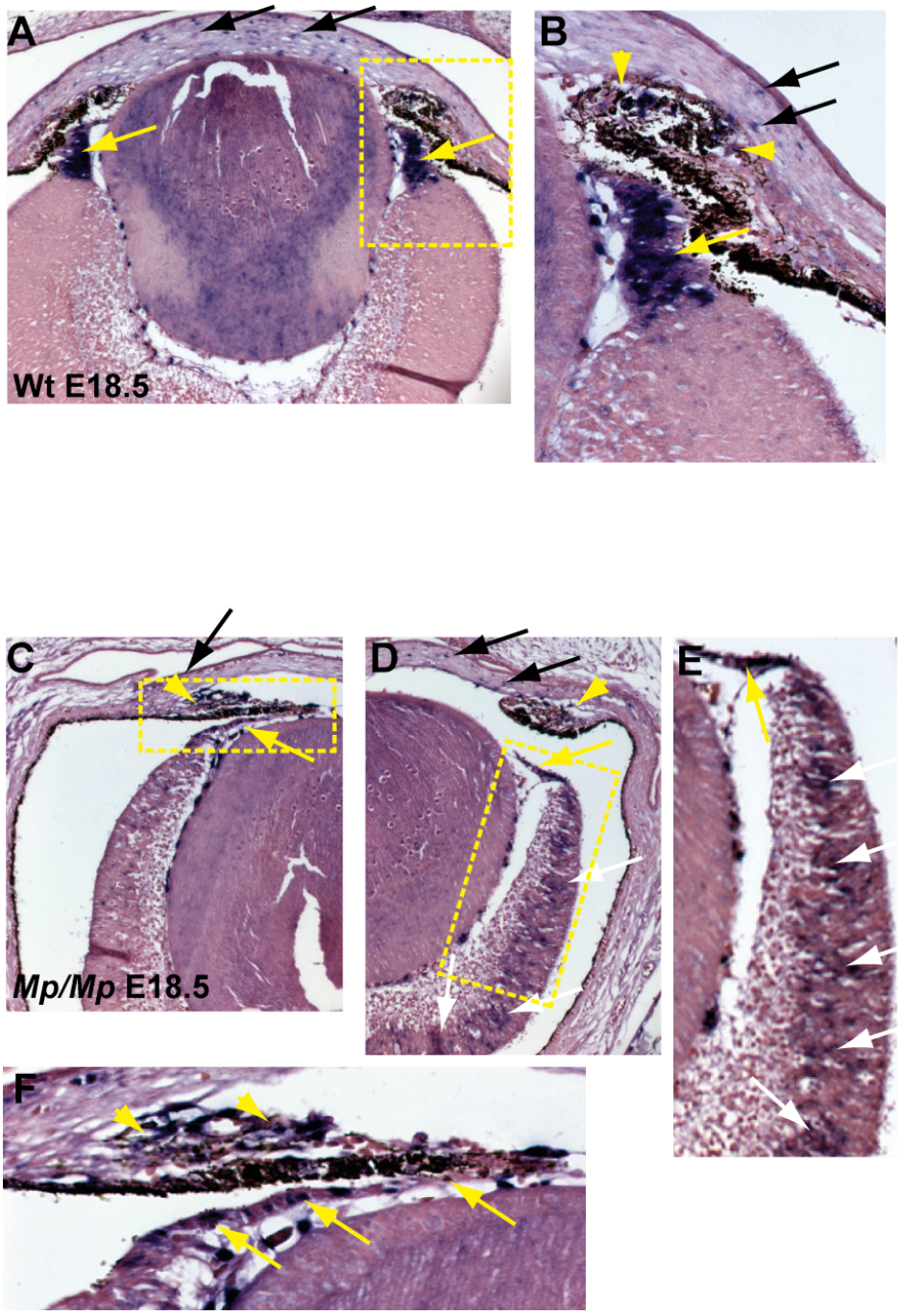

**Figure 4.5.7 Ectopic Lef1 immunostaining in the retinas of E18.5 mutant eyes.**
In wild type eyes at E18.5 (**A** & **B**), Lef1 signal was seen in the CB (arrows), cornea (filled arrows) and some cells of the iris stroma (**B**; arrowheads). The strongest signal intensity was seen in the nuclei of CB. In the mutant eye at E18.5 (**C-F**), consistent with wild type expression, Lef1 positive cells were seen in the CB (arrows), cornea (filled arrows) and iris stroma (arrowheads). However, strong signal was also observed within cells throughout the mutant retina (white arrows: **D** & **E**). Lef1 signal (arrows) was seen in some nuclei of the underdeveloped mutant CB (**F**), but was not as extensive as in the wild type.

### 4.7.8. Ectopic expression of *Chx10* in the outer nuclear layer of mutant retina

The homeodomain gene *Chx10* induces cells of the inner nuclear layer and thus was used as a marker for development of this region of the retina. The expression of *Chx10* was analysed by RNA *in situ* hybridisation on E15.5 eye sections. In the wild type (figure 4.5.8) expression was clearly restricted to the inner nuclear layer of the developing retina. In contrast, numerous *Chx10* expressing cells were observed in the outer nuclear layer in addition to those seen in the inner layer. Thus, the inner nuclear layer marker, *Chx10,* is ectopically expressed in the outer nuclear layer of the developing *Mp* retina.

## Figure 4.5.8

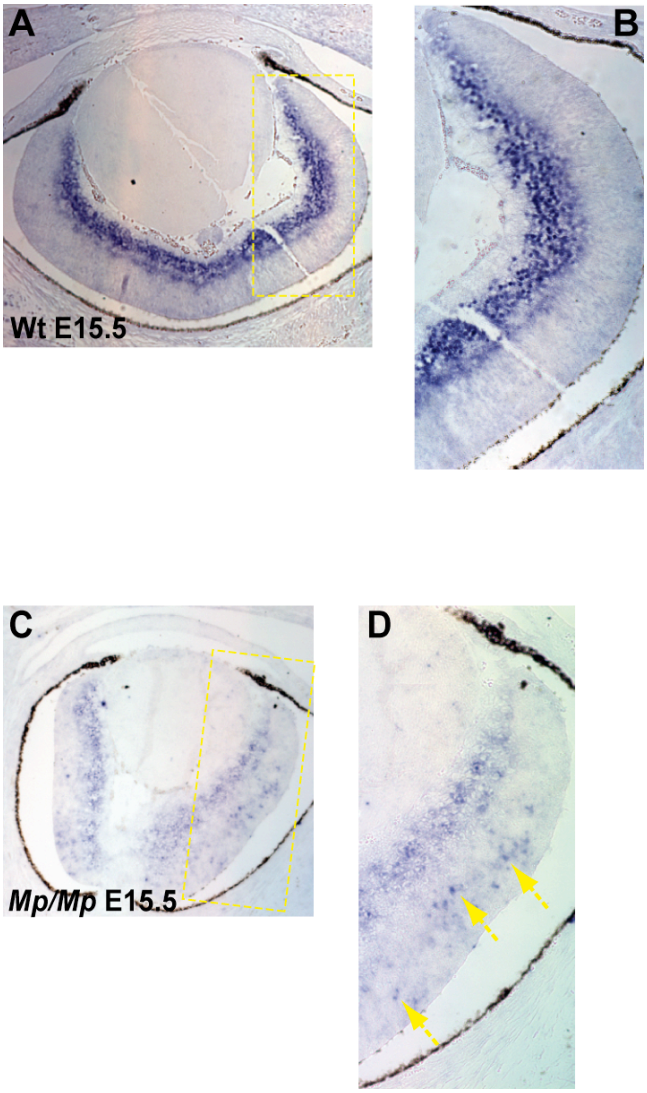


**Figure 4.5.8 Ectopic expression of *Chx10* in the retinas of E15.5 mutant eyes.**
RNA In Situ hybridisation using a probe specific to *Chx10* mRNA identified specific signal in cells of the inner neuroblastic layer of the developing wild type retina at E15.5 (**A** & **B**). There was no staining in the outer neuroblastic layer. In the mutant, although exact plane of section differed to the wild type sample, in addition to positive cells within the inner neuroblastic layer, *Chx10* expressing cells were also observed in the outer neuroblastic layer (arrows), indicating ectopic expression of *Chx10*.

# 5. Discussion

## 5.1. OAS project discussion

### 5.1.1. The OAS locus is a 3.4 Mb interval on central chromosome 14

A critical interval for OAS was identified by autozygosity mapping using 10k SNP arrays using meiotic recombination events in 4 affected individuals from 3 unrelated consanguineous families. The OAS interval mapped to between 69,425,921-73,059,612 Mb on chromosome 14 and this locus was confirmed by linkage analysis with a significant LOD score of 5.3 at *theta* = 0. By combining our data with that from other families typed by our Dutch collaborators we were able to refine the OAS interval slightly to 3.4 Mb between 69,652,605-73,059,612 Mb. The region contains 19 known protein-coding genes. The region contains 19 known protein-coding genes. Using bioinformatic resources, each gene was assessed for its candidacy as the likely OAS gene. Expression during embryonic development was analysed using the Visigene application available at UCSC (http://genome.ucsc.edu/index.html), together with the Gene Expression Database available at the Mouse Genome Informatics/JAX website (http://www.informatics.jax.org/expression.shtml), and information from the EMAGE Database of the Edinburgh Mouse Atlas Project (http://genex.hgu.mrc.ac.uk/). Known mutations in the mouse (spontaneous and generated knock-outs; http://www.informatics.jax.org/) were also analysed to look for comparable phenotypes. I also investigated published data of the currently known functions of these genes during development and disease, and whether there had been interactions identified with known genes important during ocular or limb development, or for any interactions with signaling

pathways that occur during these events. As none of these presented as obvious candidates, on the basis of these investigations, we decided to sequence all coding exons. For practical reasons these were prioritised for sequence analysis by their degree of sequence conservation through evolution.

### 5.1.2. No pathogenic mutations were identified in the OAS locus

So far, I have sequenced 61% of all the coding exons in the OAS interval in 8 unrelated affected individuals. 19 silent SNPs, 7 known missense polymorphisms and 5 missense changes not previously reported were identified. All of the known missense changes were considered to be non-pathogenic polymorphisms on the basis that either the allele frequencies were >1% in populations studied (rs2286838, ZFYVE1; rs2280792 & rs4903104, both in PAPLN) or they were in non-conserved amino acids within the encoded protein (ADAM21, rs8010994 & rs3829452). The only other SNP identified was rs3829456 (K247Q) also in ADAM21 and was in a conserved residue in the protein. However, it is highly unlikely that a SNP identified in the general population would be causative for OAS, based on the rarity of the disease; therefore all known SNPs were preliminarily discounted from further investigation.

Additionally, 4 of the 5 novel missense changes were identified in *ADAM21* (*a disintegrin and metalloprotease domain* family 21 gene), a 2.4 kb single exon gene encoding a single-pass membrane anchored protein implicated in cell-cell and cell-matrix adhesions that has no phenotype in a *Adam21* null mouse (MGI allele ID:

3663320). ADAM21 has not been associated with any human disease and its expression profile during vertebrate development remains unknown. All of the amino acid changes were predicted to be non-pathogenic. In three, the biochemical nature of the amino acid change was retained (V158L; I161V; V216M), with both alleles encoding non-polar sidechains. In one change (F159C), an aromatic non-polar side-chain was replaced by an uncharged polar side-chain. However, this missense change was also considered as non-pathogenic, as at the equivalent position in the homologous mouse protein, there is also an uncharged polar side-chain amino acid (N; asparagine). Overall, the ADAM21 gene has only 68% sequence similarity to the mouse homologue, suggesting it is not under strongly conserved functional selection.

The only other missense change identified so far was in the 36-exon gene, *Pecanex-like-1* (*PCNX*), a homologue of the Drosophila pecanex gene. *PCNX* function has been linked to spermatogenesis in mammals (Geisinger et al., 2005). The nucleotide identified change resulted in a T471S amino acid replacement. Both have uncharged polar side-chains and at the equivalent amino acid position in the mouse homologue is a glutamine residue, another uncharged amino acid with a polar side chain. Thus, these changes were not considered as pathogenic and were excluded as responsible for OAS.

### 5.1.3. *VSX2* and *Cis*-acting transcriptional regulation

In addition to minimal promoters, many genes additionally require multiple *cis*-acting genomic elements for correct spatiotemporal expression. These may be

enhancers or repressors and can be positioned within introns, or upstream and/or downstream of the gene over which they exert control, and may be positioned up to a distance of 1 Mb in either direction (Kleinjan and van Heyningen, 2005).

The homeodomain gene *VSX2* (formerly referred to as *CHX10*) is situated on chromosome 14 at 73,775,928- 73,799,194 Mb, and is therefore positioned 713 kb genomically distal to the critical interval identified for OAS. *VSX2* has been identified as defective in cases of recessive non-syndromic microphthalmia with cataracts and iris abnormalities (Percin et al., 2000). *VSX2* is embryologically expressed in mouse optic vesicle and the proliferative layers of the neural retina, while mice with a *Vsx2* null mutation present with microphthalmia (Burmeister et al., 1996). Our Dutch collaborators have sequenced the entire intragenic region of this gene in their OAS patient cohort and have not identified any mutations (Dr. Han Brunner, personal communication).

Although *VSX2* mutations in mouse or man have not been associated with any limb deformities, and its expression during limb development has not been reported, it may be possible that *cis*-regulatory elements that are important in the control of spatiotemporal expression of *VSX2*, or other genes in the candidate region, during development may have been perturbed in OAS. Therefore, future attention towards identifying conserved non-coding elements, particularly influencing transcriptional regulation of *VSX2*, and analysing them in the OAS patient cohorts is required.

The future of the OAS project will involve the use of microsatellite ($CA_n$) markers to further refine the candidate interval, analysis of a fourth "Edinburgh family" for autozygosity mapping and linkage. Additionally, amalgamation of sequencing data from the two collaborative groups will identify exons that still require sequencing. Analysis of the expression patterns of all the genes in the interval will be conducted to identify if any have specific, or overlapping expression with ocular and limb development at key embryonic stages. It may prove that sequencing of the entire candidate region may be necessary to identify the genetic lesion in OAS. For this, cell lines will need to be established to generate sufficient DNA quantities to enable next-generation sequence capture technologies

## 5.2. *Mp* project discussion

### 5.2.1. An expanded phenotypic description of *Mp*

The original description of the major external features of *Mp* associated with heterozygous and homozygous mice were confirmed in our reconstituted lines on two independent strain backgrounds. However, I did find some important differences in other aspects of the original phenotype report of the *Mp* line (Phipps, 1964). In particular we did not observe the reported neonatal mortality in homozygotes. In our facility these animals were viable and survived normally post weaning. This is likely to be due to differences in stain background and/or animal husbandry procedures. It was also clear that when the eyes were dissected the homozygotes were microphthalmic and not anophthalmic.

I was also able to expand the descriptive ocular pathology associated in adult *Mp* animals. This pathology was pan ocular and begins relatively early in development with an ocular growth phenotype identifiable by E15.5, with a graded reduction in eye size between *Mp*/+ and *Mp*/*Mp,* compared to wild type. The post natal phenotype was characterised by; lens cataracts, abnormal lamination and rosette structures in the neural retina, an absence of vitreous body and abnormally formed ciliary body. In *Mp*/*Mp* adults the ocular features were similar but were of substantially increased severity. Marked corneal thickening was only seen in homozygotes. The retinal rosettes were mainly composed of disorganised rod photoreceptors, and were associated with a reduced

number of cells within the inner nuclear layer. Abnormal development of the ciliary body was identified from E15.5 onwards in both homozygote and heterozygote.

### 5.2.2. *Fbn2* as a candidate gene for *Mp*

*Mp* was mapped to a region on chromosome 18, between 53-67 Mb. This interval contains 119 gene sequences according to the Ensembl database, however of these *Fibrillin2* (*Fbn2*) stood out as a very strong candidate gene.

There are currently four alleles of mouse *Fbn2* (Figure 5.2.1), which display hindlimb oligodactyly identical to *Mp*. In all, this phenotype occurs as a result of synostosis of phalanges between autopodia rays 2 to 4, (osseous syndactyly). Consistent with *Mp*, oligodactyly was never noted in digits 1 or 5 in these animals. The shaker-with-syndactylism (*Sy)* phenotype is caused by an irradiation-induced 0.7 cM deletion of the *Fbn2* locus (Chaudhry et al., 2001; Johnson et al., 1998) (Figure 5.1) and includes the two solute channel genes *Slc26a6* and *Slc12a2*. The auditory/vestibular defects have been attributed to the loss of *Slc12a2* and are genetically separate from loss of *Fbn2* (Chaudhry et al., 2001). The fused-phalanges allele ($Sy^{fp}$) resulted from a spontaneous single nucleotide deletion in exon 39, which resulted in frameshift of the transcript and introduced a premature termination codon after 44 amino acid residues (Chaudhry et al., 2001). No Fbn2 protein was detected in immunoblots with protein samples prepared from *Sy*/*Sy* and $Sy^{fp}/Sy^{fp}$ mice. In contrast, the $Sy^{fp\text{-}2j}$ mouse also has fused phalanges but Fbn2 protein can be detected by immunoblots. However, the spontaneous mutation results in a 21-nucleotide deletion including the last 7 nucleotides at the 3'-end of exon 38. This results in exon-skipping and is predicted to affect the structure and function of the mutant protein (Chaudhry et al., 2001). The $Fbn2^{ko}$ mouse line was created by gene-targeted

replacement of exon-1 of the *Fbn2* gene with a neomycin cassette (Artega-Solis et al., 2001), resulting in loss of detectable Fbn2 protein.

**Figure 5.1.1 Mouse Fbn2 allelic series.**


**Figure 5.1.1 Mouse *Fbn2* allelic series.** There are currently four published mouse mutations in the *Fbn2* gene that result in oligodactyly. Shaker-with-syndactylism (*Sy*) is a 0.7cM irradiation induced genomic deletion; fused phalanges ($Sy^{fp}$) is a spontaneous frame-shift allele with the introduction of a termination codon after 44 amino acids; a second spontaneous allele with fused phalanges ($Sy^{fp\text{-}2j}$) results from an exon-skipping mutation affecting exons 38-39; and the gene-targeted Fbn2-null mouse ($Fbn2^{ko}$). (Arteaga-Solis et al., 2001; Chaudhry et al., 2001; Johnson et al., 1998)

### 5.2.3. Fibrillin family proteins

Mouse *Fbn2* is a 65 exon, 315 kDa cysteine-rich extracellular matrix (ECM) glycoprotein belonging to the fibrillin family of proteins (Hubmacher et al., 2006). In humans, bovines and avians, there are three fibrillins, *FBN1*, *FBN2*, and *FBN3*. However, in the mouse, there is no *Fbn3* homologue, possibly due to a genomic rearrangement event during evolutionary divergence (Corson et al., 2004). The protein structure of the

fibrillins is closely related at the domain level (Hubmacher et al., 2006). Their prominent motif is the epidermal growth factor (EGF)-like domain, of which there are between 46-47, depending on the protein (human and mouse FBN2 have 47), and most of these EGF-domains are calcium-binding (cbEGF) common to many ECM domains. Human FBN2 has 43 cbEGF domains, while mouse has 42. The third characteristic motif of the FBNs is the transforming growth factor (TGF)-binding domain (TB domain). These domains are only present in the FBNs and in the latent transforming growth factor binding group of proteins (LTBPs), which have 7x and 3x motifs, respectively. The combined binding of FBNs and LTBPs to extracellular TGFβ ligands has recently been identified as a potent mechanism for the control of growth factor signaling in development and disease (Charbonneau et al., 2004; Habashi et al., 2006; Hubmacher et al., 2006; Kaartinen and Warburton, 2003). The human and mouse Fbn2 proteins share 96.3% sequence identity at the amino acid level (with 100% coverage).

### 5.2.4. Human fibrillinopathies

In humans, autosomal dominant mutations in *FBN1* result in the skeletal, cardiovascular and ocular features of Marfan syndrome (MIM #154700), whereas *FBN2* mutations appear to only affect the skeletal regions, and patients present with long digits (arachnodactyly), distal joint contractures and crumpled ears, in the syndrome Congenital Contractural Arachnodactyly (also referred to as Beals syndrome; MIM+0121050). A mutation in *FBN1* (a deletion of exon 41) has been identified in autosomal-dominant Weill Marchesani syndrome (MIM #277600) (Faivre et al., 2003b), a congenital disease

of connective tissue, brachydactyly, joint stiffness, thickened skin and ocular malformations, including ectopia lentis and microspherophakia (Faivre et al., 2003a). The *FBN3* is located close to the autosomal recessive Weill Marchesani locus on human chromosome 19p13. However, although *FBN3* mutations may yet be identified associated with this disease, only mutations in the extracellular metalloprotease *ADAMTS10* have so far been identified (Dragoneau et al., 2004). The two separately inherited forms of the disease have been extensively reviewed and display clinical homogeneity, despite genetic heterogeneity (Faivre et al., 2003a).

The fibrillinopathies have convincing phenotypic overlap with the features described for the *Mp* mouse and in combination to the features described for the allelic series of *Fbn2* described for the mouse, *Fbn2* was an excellent candidate for *Mp*. Thus, further mapping studies were focused on this gene.

### 5.2.5. *Mp* is due to a 660kb inversion

*Mp* is associated with an inversion of 660 kb. The inversion break points are situated within the 3'- exons of two genes: *Fbn2* and *Isochorismatase domain containing-1* (*Isoc1*). *Isoc1* is 5-exon gene encoding a novel 32 kDa protein with a possible peroxisomal cellular localisation but whose role remains undefined in mammalian organisms. The Isochorismatase domain, also known as 2, 3-dyhydroxybenzoate synthase, is predicted to belong to a family of hydrolase enzymes involved in catalysing the conversion of isochorismate to 2,3-dyhydroxybenzoate and pyruvate in bacteria (Rusnak et al., 1990) [http://supfam.cs.bris.ac.uk/SUPERFAMILY/cgi-

bin/scop.cgi?sunid=52499]. No mutations or developmental expression patterns of this gene have so far been described in mammals and there have been no knock-out studies completed in the mouse from which to infer a role in eye development.

### 5.2.6. Differing fates of the *Mp*-affected mRNAs

The *Mp* inversion results in two reciprocal fusion transcripts, identifiable by RT-PCR. The last (3'-) exon of *Isoc1* was replaced by the final three exons of 3'-*Fbn2* gene, and vice versa. This resulted in premature termination codons for both transcripts. However, the locations of the induced nonsense codons predicts two contrasting transcript fates: The *Isoc1* transcript was predicted to be degraded by nonsense mediated decay (NMD), a cellular surveillance mechanism that selectively degrades mRNA species harbouring a premature stop codon occurring 5' to the last intron (Chang et al., 2007; Nagy and Maquat, 1998). Conversely, the induced termination codon in *Fbn2* was within the 5'-most exon (i.e. the fused last *Isoc1* exon) with no 3'-introns and therefore was predicted to translate to a truncated but stable mRNA, resulting in a Fbn2 protein missing C-terminal amino acids. This included the loss of the last cbEGF domain, and the unique C-terminus sequence, including an N-glycosylation site and a proprotein processing site. The sequence encoded by the *Isoc1* fusion was out of frame and resulted in seven additional amino acids prior to a termination codon. The foreign amino acids did not display similarity to any known protein motifs.

### 5.2.7. Loss of Fbn2 causes hind limb oligodactyly in the mouse

WISH analysis of spatial gene expression revealed the presence of *Fbn2* transcripts in limbs at E10.5, E11.5 and E12.5. These are key developmental stages during limb development, when patterning of the autopod, growth and chondrogenesis occur, and therefore is temporally consistent with *Fbn2* loss-of-function in the developing limb causing an oligodactyly phenotype. In addition, this phenotype is consistent with the *Fbn2* allelic series in the mouse. This phenotype has been attributed to abnormal TGFβ signaling between digit primordial as a result of loss of functional Fbn2 in the extracellular matrix in the developing autopod (Arteaga-Solis et al., 2001). Indeed, the prodomain of Bmp7 has been shown to interact directly with the N-terminal region of Fbn1 (Gregory et al., 2005), and is suggested to similarly bind with Fbn2. Compound heterozygote mice for $Bmp7^{-/+}$ and $Fbn2^{-/+}$ exhibit phenotypic limb-pattering defects consistent with the combined null mutations of each gene. Therefore, the complete absence of Fbn2 in the mid-axial region of the developing limb autopod may abolish targeting or deposition of Bmp7 to the ECM (Hubmacher et al., 2006), and therefore affect the precise growth factor cues required for the correct decisions between PCD and chondrogenesis within the interdigital rays. Therefore, the functional and developmental consequences of Fbn2 loss-of-function in mouse hindlimbs was not perused further in this study.

### 5.2.8. Evidence for Fbn2$^{Mp}$ aetiology in the *Mp* ocular phenotype

No eye phenotype has yet been reported in Fbn2 null mice (Arteaga-Solis et al., 2001; Chaudhry et al., 2001) or associated with *FBN2* mutations in humans. Unsurprisingly therefore, the ocular developmental expression pattern of *Fbn2* has not been extensively examined in either. However, the specific temporal and spatial expression pattern of *Fbn2* I have identified in the mouse suggests a functional requirement for Fbn2 during ocular development. Specifically, transcripts of both species (wild type and mutant) were identified in the ciliary body and mesenchyme of the developing eye at E13.5-E16.5 by section *in situs*, in addition to the ocular *Fbn2* expression observed by whole-mount *in situs* at E10.5-E12.5.

At the protein level, wild type Fbn2 was located in the extracellular matrix of the corneal and pre-scleral mesenchyme, in the inner limiting membrane of the retina, in early vitreous body and high levels were observed in the vitreous space where lens and retina are opposed and in contact at the anterior of the eye. In *Mp* mutant animals, *Fbn2$^{Mp}$* expression was consistent with the wild type expression pattern in the eye. In contrast however, no mutant protein was identified in the extracellular spaces, vitreous, membranes or between cells in the eye. Instead, signal was identified *inside* cells in regions overlapping with wild type and mutant *Fbn2* expression; in the developing ciliary body and RPE in anterior retina and in the pre-scleral mesenchyme. Additionally, several positively stained cells were identified distributed throughout the central retina, which had different morphologies to adjacent cells and therefore were considered to be different cell types. This suggested that in *Mp* mice, consistent with *Fbn2*-null mice, there is no

Fbn2 incorporated into the ECM within ocular tissues, however in contrast to *Fbn2*-null mice, there is intracellular Fbn2 retained within *Fbn2*-expresing cells.

No antibody was available to identify the location of Isoc1 protein, however in both wild types and mutants, *Isoc1* and *Isoc1*$^{Mp}$ expression was undetectable by RNA *In Situ* studies in the eye. Expression of the *Slc27a6* gene, which encodes member of the fatty acid transport protein family involved in the transfer of long-chain fatty acids across membranes lies genomically between *Fbn2* and *Isoc1* within the inverted interval. Theoretically, *Slc27a6* gene expression could have been affected by the *Mp* mutation, however analysis by RT-PCR revealed expression in the eye appeared unaltered in *Mp*. Additionally, in the *shaker with syndactyly* spontaneous mutation *Fbn2*$^{sy}$, caused by a 7cM genomic deletion, this gene is completely removed and no ocular phenotype has been described.

Although loss of *Isoc1* function cannot be completely disregarded as the pathogenic cause of the ocular mutation seen in *Mp*, the distribution of *Fbn2* transcripts and protein in developing wild type and mutant eyes indicated strongly that mutant *Fbn2* was likely be the main aetiology towards the ocular pathology of *Mp*. Therefore, investigations into the *Mp* ocular pathology were focused on *Fbn2*.

### 5.2.9. Mutant Fbn2 was retained in the ER of expressing cells and caused ER stress

We investigated the subcellular localisation of Fbn2$^{Mp}$ protein in expressing cells. The ER is the first component of the secretory pathway for transmembrane or secreted

proteins and is their intracellular location for protein folding and post-translational modifications (e.g. N-glycosylation and sulphide-bond formation), before translocation to the golgi and secretion or membrane integration. Therefore, numerous secretory and membrane proteins are reliant on normal passage through the ER and golgi for function.

For Fbn2 protein to be transported to extracellular matrix, it must be processed via the secretory pathway and thus travel through the ER. As the N-terminal of Fbn2 was unaffected in *Mp*, the nascent peptide was presumed to engage and direct conventional secretory pathway protein synthesis into the ER (Nothwehr and Gordon, 1990). However, the loss of the C-terminal region of $Fbn2^{Mp}$, including removal of a furin cleavage site, predicted an arrest of its transport through the ER/trans-golgi network (Lonnqvist et al., 1998). The intracellular localisation of mutant protein aggregates and the lack of extracellular Fbn2 in mutants were consistent with this hypothesis, in that mutant $Fbn2^{Mp}$ was retained and accumulated in the ER. Using skin cells from mutant animals for transmission EM analyses, large intracellular inclusions were identified that immunostained positively for Fbn2 and appeared to be associated with the ER membrane. In fibroblasts, immunocytochemistry identified large Fbn2 protein aggregates directly adjacent to the nucleus, again consistent with ER localisation. It was therefore accepted that intracellular $Fbn2^{Mp}$ aggregates were localised to within the ER of expressing cells.

### 5.2.10. The ER stress response

Cell autonomous quality control mechanisms exist to ensure that only correctly folded and modified proteins exit the ER (Malhotra and Kaufman, 2007; Schroder, 2008).

Slowly folding or permanently unfolded proteins are either retained within the ER lumen in complexes with chaperones or are targeted for degradation via the ER-associated proteasomal degradation mechanism (ERAD), or removed and degraded by autophagy. However, the accumulation of misfolded proteins, immune to ERAD and autophagy may perturb ER homeostasis and cause ER stress, and this stress triggers the evolutionarily conserved unfolded protein response (UPR).

To maintain homeostasis of the ER, several ER-transmembrane proteins monitor the folding status of proteins within the ER lumen and can initiate adaptive responses to ER stress. PERK (eukaryotic translation initiation factor2-alpha kinase) is a transmembrane kinase; IRE1 (endonuclease inositol-requiring enzyme-1) is a transmembrane protein kinase endoribonuclease; and ATF6 (activating transcription factor 6) is a transmembrane bZIP transcription factor. Each has domains extending into the ER lumen. The heat-shock protein family member HSP70 protein and *ER stress* sensor BiP (GRP78 or Kar2p) is thought to relate the status of the ER lumen to the luminal domains of these proteins. Normally bound to these sensors in non-stress situations, it is released and binds to hydrophobic patches exposed on protein folding intermediates. Upon increased accumulation of unfolded proteins, BiP protein is released from the ER-lumen domains of PERK, IRE1 and possibly ATF6, and induces their UPR specific responses.

Activated PERK and IRE1 are *trans*-autophosphorylated and cooperate to coordinate protective responses to *ER stress* (Schroder, 2008). These include the

inhibition of global mRNA translation by the phosphorylation of eIF2α by PERK. Additionally, PERK also induces the selective transcription of the majority of UPR-dependent chaperone genes, required to increase protein-folding activity within the stressed ER.

IRE1 initiates the non-conventional splicing of the *X-box binding protein-1* transcription factor ( *Xbp1*) by ATF6 (Yoshida et al., 2001) to introduce a potent transcriptional activation domain that binds and activates transcription from the UPR-element, a minimal motif found upstream of many UPR-target genes necessary and sufficient for UPR gene activation (Malhotra and Kaufman, 2007). This leads to an increase in the expression of *BiP* and other chaperone proteins for enhanced ER protein-folding activity. The IRE1 ribonuclease activity removes a 26-nucleotide region from the *Xbp1* transcript to create a larger form of *Xbp1* protein. This differential in *Xbp1* transcript size has been effectively and routinely used as a marker for *ER stress* at the RNA level by RT-PCR (Lin et al., 2007; Ulianich et al., 2008) and has be supported by the analysis of *BiP* expression by RNA *in situ* hybridisation (Tsang et al., 2007).

Although the primary function of the UPR is to be protective, chronic ER stress can lead to apoptosis in cells as a tissue-protective mechanism, and its activation is triggered by persistent PERK activity after initial IRE1 responses have abated (Lin et al., 2007). Indeed, one mRNA that escapes translational inhibition during UPR and whose translation is actually activated in response to PERK-dependent P-eIF2α, is the bZIP transcription factor *ATF4*. This protein has a major role in the activation of the pro-

apoptotic bZIP transcription factor CHOP (DDIT3, or GADD153) after prolonged or severe ER stress (Malhotra and Kaufman, 2007; Schroder, 2008).

### 5.2.11. $Fbn2^{Mp}$ accumulation caused ER stress in *Mp* eyes

Increased *BiP* expression was identified in the developing ciliary body in E16.5 mutant but not normal eyes, overlapping with the expression of *Fbn2* and the spatial distribution of mutant protein aggregates. Furthermore, we designed a novel RT-PCR based assay to identify the ratio of spliced to unspliced *Xbp1* transcripts and revealed that *Fbn2* expressing MEFs from heterozygotes and homozygotes had increased levels of spliced *Xbp1* compared to wild types, consistent with the UPR response. The specificity of the assay was confirmed using chemical induction of ER stress with tunicamycin, and this assay was then performed with RNA isolated from dissected eyes and showed that homozygotes had an increased level of spliced *Xbp1,* compared to wild types. Together; these results indicated that $Fbn2^{Mp}$ aggregates triggered the ER stress response in mutant eyes, specifically in the developing CB.

### 5.2.12. ER stress in *Mp* eyes did not necessarily associate with apoptosis

Prolonged ER stress can trigger activation of cell death pathways (Schroder, 2008). We investigated the abundance of Activated-Caspase-3 (A-Casp3) protein as a specific marker for cell death in mutant eyes. Caspase-3 is a cysteine aspartic acid protease and is one of the *effector caspases*, which are cleaved from their inactive pro-enzyme forms into an active multimeric enzymes, either by self-proteolysis or by other

active (*initiator*-) capases, in cells undergoing apoptosis (Thornberry and Lazebnik, 1998). We observed numerous positively stained cells within the retinas of mutant eyes, but not in wild types. Although these apoptotic cells were observed throughout the retinas, there was no specific enrichment for co-localisation with the highly positive $Fbn2^{Mp}$ cells identified in the developing ciliary body that had been shown to be positive for elevated *BiP* expression. Furthermore, although suggestive data was found, co-immunofluorescence could not fully confirm co-localisation of $Fbn2^{Mp}$ aggregates with A-Casp3 in all cases. This indicated that although apoptosis was possibly linked to the accumulation of intracellular $Fbn2^{Mp}$, and therefore ER stress, the presence of aggregates did not necessarily result in programmed cell death. Additionally, the apoptotic cells dispersed throughout the retina, as determined by positive A-Casp3 staining, may be the same cells identified with abnormal morphology observed within the outer layer of the neural retina at E16.5 and E18.5 by H&E staining. The rosetting seen in the cells of adult retinas may be a direct consequence of regionalised apoptosis in cells with $Fbn2^{Mp}$ aggregates, by disrupting intercellular signaling and causing disorientation of the projections and polarity of local photoreceptor cells required for normal cell-specific lamination.

### 5.2.13. Fbn2$^{Mp}$ aggregates in the peripheral *Mp* retina may affect production of a retinal lamination and ciliary body determining factor

Cells in the developing anterior retinal have recently been identified in both mouse and chick as producers of a factor required for correct retinal lamination and vital for ciliary development: Wnt2b (formerly Wnt13)(Cho and Cepko, 2006; Kubo et al., 2003; Nakagawa et al., 2003). Wnts are secreted morphogenetic ligands vital for many aspects of development (Logan and Nusse, 2004). They are lipid-modified glycoproteins that undergo post-translational modifications that are vital to their secretion and function; glycosylation and the addition of the lipid moieties palmitate and palmitoleic acid by palmitoylation within the ER (Hausmann et al., 2007). Loss of *Wnt2b* results in complete failure of ciliary development, while its ectopic expression in the central neural retina induces ciliary marker expression and retinal folding reminiscent of mature ciliary processes (Cho and Cepko, 2006). In addition, Wnt2b signal emanating from CB cells has been identified as an important factor determining correct lamination of retinal cells by maintenance of the early neuroepithelial layer, while Wnt2b added to disorganised neural retina cells in culture can restore correct lamination (Nakagawa et al., 2003). Blocking of Wnt downstream signaling by a dominant-negative Lef1 resulted in premature neuronal differentiation in the developing ciliary body and inhibited proliferation (Kubo et al., 2003). Thus Wnt2b may diffuse from the peripheral retina into the central retina and confer early patterning of the neural retina and provide competence for later lamination-specific events.

The requirement of Wnt2b for both ciliary body formation and correct retinal lamination was therefore intriguing in the context of the *Mp* ocular pathology, where there is a failure both. In mouse and chick, *In Situ* studies have identified *Wnt2b* transcripts in the developing ciliary body and distal RPE (Cho and Cepko, 2006; Liu et al., 2003). This overlaps both temporally and spatially with the location of *Fbn2* expression and protein aggregate build up in *Mp*. Thus, loss of ciliary-specific Wnt2b signal predicts a loss of correct CB development, and vice versa, and abnormal retinal lamination as a consequence. Therefore misregulation of canonical Wnt signaling, specifically through the Wnt2b ligand, represents a plausible candidate mechanism for the ocular pathogenesis in *Mp*, distinct from a loss of function of *Fbn2*.

### 5.2.14. Aberrant *Lef1* expression indicates Wnt responses were abnormal in the developing *Mp* ciliary body

The transcription factor Lef1 (Lymphoid enhancer factor, a HMG group protein) is a positive activator of canonical Wnt signaling that initiates the expression of Wnt target genes in cooperation with nuclear β-catenin, T-cell transcription factor (Tcf) family proteins and various other cooperative transcription factors. As we were unable to directly assess the Wnt2b expression pattern and distribution in *Mp* eyes, either by *In Situ* hybridisation or immunostaining, a Lef1 antibody was used as a marker for canonical Wnt signaling. In Wild types, a positive domain of Lef1 localisation was clearly identified in the ciliary body and distal tip RPE at E13.5, becoming a clearly defined boundary of non-expressing cells at the peripheral limit of the ciliary at E15.5. This is

consistent with the known *Wnt2b* expression domain. The domains of Lef1 expression in *Mp* were consistent with wild type, but the signal was increased at E13.5 and E15.5, and the boundary at the peripheral margin of the ciliary was poorly defined at E15.5 and spread slightly into the peripheral retina.

The differential Lef1 staining in the ciliary between wild type and mutants indicated that mis-regulation of Wnt signaling was likely, either by an increase in localised Wnt signaling or inappropriate activation of the canonical Wnt pathway. Equally however, there could be disruption to feedback mechanisms controlling *Lef1* expression, possibly independent of the presence of Wnt ligand, resulting in increased and ectopic expression. Without *In Situ* or immunostaining data for Wnt2b and co-expression data for $Fbn2^{Mp}$ in these cells, it is difficult to evaluate misregulation of Wnt2b as a mechanism for *Mp* ciliary pathology. Work is on going to identify the relationship between *Lef1* up-regulation and Wnt2b status.

### 5.2.15. A Pax6/Lef1-Sox2 boundary defines the developing ciliary body and was abnormal in *Mp*

*SOX2* is an SRY-related HMG-box (SOX) transcription factor involved in stem-cell maintenance in the developing central nervous system. Heterozygous loss of function mutations in *SOX2* results in severe ocular malformations (Fantes et al., 2003). However, nuclear Lef1 has been identified as a positive activator of *Sox2* expression through direct binding to the *Sox2* (N-1) promoter in chick (Takemoto et al., 2006). Nuclear Sox2 protein was identified in the neuroblastic region of the neural retina at E13.5 and E16.5,

but was excluded from the Lef1-positive developing ciliary body. In contrast, the paired-box transcription factor, *Pax6*, was excluded form these regions and was specifically localised to the inner layer of differentiating cell nuclei within the retina and extended into the ciliary body to the anterior tip.

*PAX6* mutations have also been implicated in ocular malformations, such as aniridia and Peter's anomaly, and result in the *small eye* phenotype in the mouse. Sox2 protein overlapped with Pax6 in the ciliary-retinal boundary at E13.5 and E16.5 but showed mutually exclusive distribution in the developing central retina; with nuclear Sox2 protein localised to the neuroblastic outer regions, and Pax6 within the nuclei of cells in the inner layer of differentiating neurons. These domains of expression were defined by clear boundaries in wild type eyes. In the mutant ciliary, these margins were blurred and the coexpressing domains seemed to extend into the central retina at E13.5, suggesting a possible reduction in *Sox2* expression and/or increased activation of *Pax6*. In contrast, at E16.5 the clearly visible Pax6-only domain in the wild type ciliary was reduced in the mutant and the coexpressing cells of the CB-retinal boundary were shifted anteriorally. Together these data suggest Sox2 is excluded from the developing ciliary body, but that Pax6 is be required for its development. The presence of Sox2/Pax6 positive cells in the CB-retinal boundary may specifically identify the ciliary marginal zone, a previously described population of multipotent stem cells at the retina-ciliary margin (Kubo and Nakagawa, 2008). In the mutants, the Pax6-only zone is truncated and probably reflects the loss of developing ciliary cells. Additionally, the Pax6/Sox2 domain had extended toward the central retina, reflecting a possible increase in Pax6, or a

decrease in Sox2 expression. Otherwise, the retinal patterning of Sox2 and Pax6 was unaffected in *Mp*. From this data, coexpression of *Pax6* and *Lef1* in the absence of *Sox2* expression defines the developing ciliary body in normal eyes.

Although co-expression studies were not carried out, the distribution of Sox2 and Lef1 suggests cells that were Lef1-positive were Sox2-negative in wild type and mutant retinas. As the upregulation of Lef1 is considered as a marker for the active state of the canonical Wnt pathway, our data is in direct contrast to the current model where Lef1 acts as an activator for *Sox2* expression (Takemoto et al., 2006). Lef proteins can assume diverse regulatory functions on gene targets by their association with different nuclear proteins. Lef1 transcription factors mediate transcriptional response to Wnt signals by interacting with stabilised beta-catenin. In the absence of Wnt ligand-receptor binding, and thus an unstable beta-catenin, Lef proteins can associate with Tle homologues of the Drosophila Groucho co-repressor family of proteins to repress target gene activation (Levanon et al., 1998).

Whether Lef1 can also act as a transcriptional repressor in the presence of activated Wnt signaling is obscure, and additionally the specific Tle interactors for Lef1 in the developing ciliary body are currently unknown. It is clear from our data here involving Sox2 in the developing ciliary that more research on the Wnt/Lef/Sox2 pathway is required within this context.

### 5.2.16. Rosetting was a non-specific response to general retinal stress

*Mp* retinas are dysplastic with lamination defects and rosetting. The *Mp* rosettes were comprised of disorganised photoreceptor cells, shown by morphology and immunohistochemical staining for Rhodopsin. The rosettes were not identified during embryogenic retinal development and were only seen in eyes studied at P21 and onwards, after retinal differentiation has occurred. Similar developmental defects are seen with mutations in various genes involved in diverse processes during retinal development: *Notch1* conditional knock-outs leading to the precocious differentiation of neural progenitors (Jadhav et al., 2006), toxigenic ablation by expression of the *Diptheria toxin-A* gene from the RPE affecting signaling interactions between RPE and retina (Raymond and Jackson, 1995), Selective removal of the miRNA activating enzyme *Dicer* from developing retinal cells and therefore affecting microRNA function (Damiani et al., 2008), loss of combined retinoic acid receptors reducing retinal progenitor proliferation (Grondona et al., 1996), loss of photoreceptor determining specific nuclear receptor (*NR2E3*) (Akhmedov et al., 2000); and, *in vitro*, the loss of ciliary-derived *Wnt2b* as previously explained (Nakagawa et al., 2003). This type of retinal dysplasia is thus generally considered to be a non-specific response to diverse stimuli that aberrantly affect retinal differentiation during development, and the general morphology is similar regardless of the molecular mechanism.

### 5.2.17. Fbn2$^{Mp}$ aggregates may promote dedifferentiation of retinal cells through ER stress response mechanisms

Chx10, Calbindin, PKCα and DAPI immunostaining revealed an overall reduction in the cell numbers of the inner nuclear layer in adults, but no gross structural malformations. Why cells of this particular region of the retina are reduced is unclear, as both Fbn2$^{Mp}$-positive and A-Casp3-positive cells were not enriched within any specific retinal layer. Although the reduction in cells of the adult inner nuclear layer reflects the overall increased apoptosis observed in *Mp*, it may be more indicative of reduced proliferation of neuroblastic progenitor cells, or of precocious, or deviant, differentiation programmes. Ectopic *Chx10* expressing and Lef1-positive cells were identified by histological analysis in the outer (neuroblastic) layer of the embryonic retina. Although it was not specifically identified in these cells, it seems reasonable to infer that these are Fbn2$^{Mp}$-positive cells and therefore eliciting the UPR.

The initial response of the UPR in response to ER stress is protective. Therefore not all cells that elicit the UPR will undergo apoptosis. Surviving ER stress by the UPR, however, can affect the transcription and translation of genes required for particular cell differentiation programmes, resulting in altered differentiation and even dedifferentiation. For example, in the differentiating chondrocytes of transgenic mice expressing a mutant form of *Col10a1,* the mutant protein was retained in the ER and UPR markers were preferentially identified. Consequently, although these expressing cells survived, their differentiation programme was severely interrupted and they re-entered the cell-cycle, resulting in disruption to the highly coordinated events of endochondral ossification and

consequently a chondroplasia phenotype (Tsang et al., 2007). Similarly, chemically induced ER stress in PC Cl3 thyroid cells resulted in inhibition of differentiation in the absence of apoptosis, together with an epithelial to mesenchymal transition (Ulianich et al., 2008).

*Lef1* and *Vsx2* expression are markers for undifferentiated cells under the influence of Wnt2b signaling in the ciliary body and are mediators of gene transcription in undifferentiated, proliferating cells (Burmeister et al., 1996; Kubo et al., 2005). It is therefore possible in these cells that the intrinsic gene expression profile required for an inner nuclear layer cell fate has been perturbed, and has been replaced by the expression of genes required for proliferation. As a consequence, it is likely that they would also affect adjacent cells, probably through the creation of foci of aberrant cell extrinsic signaling. The absence of specific differentiation could then paradoxically lead to an overall decrease in cell numbers of the inner nuclear layer, due to the inability to respond to spatially-specific cues for correct cell-type specification. It may also lead to the localised increase in rod photoreceptor cells, which are organised into rosettes. Indeed, in *Notch1* conditional mutants, the retinal phenotype of rosetting in the outer nuclear layer and a decrease in retinal cell types and size was attributed to the early differentiation of photoreceptors and an associated reduction in progenitors (Jadhav et al., 2006). Quantitative analysis of inner nuclear layer and photoreceptor cell numbers was not done in this study, however careful examination of the ratios between these cell-types may reveal clues into the formation of rosettes.

### 5.2.18. Vitreous pathology as an indirect consequence of Fbn2$^{Mp}$ aggregates

Cells of the ciliary body, as with chondrocytes and P13 Cl3 thyroid cells (collagens and thyroglobulin, respectively), synthesise and excrete large quantities of proteins through their ER, many of which require various post-translational modifications. Ciliary cells have been identified as the main expressing cells of those collagens that are vital for vitreous body development and function (*Col2a1, Col9a1* and *Col11a1*) (Bishop et al., 2002). During protein synthesis events, pro-collagens pass through the ER where they are extensively processed and post-translationally modified by glycosylation, hydroxylation and disulfide-bond formation (Lodish, 1999). They are then secreted extracellularly into the vitreous where they fulfil vital structural and possibly signaling-regulation functions.

Arrest in global transcription and translation within *ER stress*ed cells of the ciliary due to Fbn2$^{Mp}$ aggregates and the eventual loss of a functional CB would presumably prevent such major constituents of the VB from being synthesised and thus would be predicted have severe implications to the development of the VB. We were unable to identify *Collagen2A1* or *Collagen11A1* expression overlapping with wild type ciliary *Fbn2* expressing cells or ciliary cells positive for Fbn2$^{Mp}$ inclusions by *In Situ* hybridisation, or by using an anti- Collagen2A1 monoclonal antibody in developing eyes in this study. Nevertheless, the ciliary body has been implicated as the major source of collagen production in mouse and chick (Bishop et al., 2002; Ihanamaki et al., 2004), and overlaps both temporally and spatially with the localisation of Fbn2$^{Mp}$ aggregates and *ER stress* in *Mp*. Additionally, the disruption of healthy VB has been implicated in various

ocular phenotypes including dominant disorders associated with collagen mutations, such as Sticklers syndrome, Marshall syndrome, and Kniest dysplasia (Ihanamaki et al., 2004), and in the regulation of eye size in mice (Halfter et al., 2006). It is possible therefore that the absence of VB in *Mp* mice was due to a combination of (i) a reduced number of ciliary body cells capable of producing vitreous components and (ii) the arrest of normal post-translational modification and transport through the ER/trans-golgi protein secretory pathway of collagens due to ER stress in those developing CB cells remaining in the *Mp* eye. It is worth pointing out that these are not mutually exclusive and are also transposable to Wnt2b signaling and synthesis.

### 5.2.19. A Synodiporic effect of the ER stress response may underlie 'worse than null' pathologies

Although currently unproven in this model, the potential loss of collagens or Wnt2b synthesis due to the UPR caused by the *Mp* mutation raises an intriguing and novel paradigm for disease pathology. Any developmentally critical membrane or secretory protein that requires passage through, and post-translational modification within, the ER for its correct synthesis and function (perhaps a morphogen or membrane-integrated ligand-receptor), has a dependency on undisturbed ER function. Somatic loss-of-function mutations in such genes may have specific pathologies associated with their global loss. However, tissue and time specific co-expression of a second secretory or membrane protein that is abnormal (either chronically misfolded or over-expressed) and that subsequently triggers the ER stress response has the potential to prevent the normal

function of the first protein, thus resulting in tissue-specific phenotypic consequences indirect from the pathology associated with loss of the mutant protein. We have termed this a “synodiporic effect”, from the Greek, *synodiporia* meaning fellow travellers or those walking the street together. Such effects may have significant implications for human disease and may provide explanation for other “worse than null” mutations.

## 5.3. Perspectives and further work

### 5.3.1. Retrospective lessons from the two projects

The finding that a truncated from of *Fbn2* resulting from a balanced rearrangement has implications for the OAS project. The *Mp* mutation was not picked up by direct sequencing of coding exons, and would be unlikely to have been identified by SNP array analysis. However, we have used both of these strategies to investigate the genetic aetiology of OAS. It is possible that a small genetic rearrangement may be present in the candidate interval but is unidentifiable by direct exon sequencing.

Of interest in the OAS candidate region are two *ADAM* genes. These share homology with the *ADAMTS* genes, which also contain thrombospondin motifs. Thrombospondins are secreted proteins that associate with the extracellular matrix and *ADAMTS10* has been identified as a matrix-localised protein (Dagoneau et al., 2004). Recessive mutations in *ADAMTS10* cause Weil-Marchesani syndrome (Dagoneau et al., 2004) closely associated with fibrillinopathies, but with ocular features such as ectopia of the lens, microspherophakia, myopia and glaucoma. The complete sequencing of the two *ADAM* genes may yet yield pathogenic mutations, but additionally there may be other genes within the interval that have as yet unknown associations with the extracellular matrix and may also have important roles in the development of eyes and limbs. The extracellular matrix as an important, higher level component of signalling cascades, through the sequestration and controlled release of growth factors, is becoming

increasingly appreciated within the field of developmental biology and must be considered as a potential involvement in the pathogenicity of OAS.

### 5.3.2. OAS project further work

In order to maximise the chances of identifying the causative mutation of OAS, I plan to initially narrow the critical region already mapped and looked for shared haplotypes in the OAS families within the current Edinburgh cohort. This will be done using highly informative microsatellite PCR markers. Additionally, we have recently recruited a fourth OAS family to the current Edinburgh cohort. This family contains a female proband with classical OAS features. There are two unaffected sisters and the parents are reported as non-consanguineous, however they originate from the same village in Northern Portugal. DNA from this family will be assessed using SNP arrays and autozygosity mapping to potentially reduce the critical interval for OAS.

Concurrently, efforts will be made to finish sequencing of all of the exons in the Edinburgh cohort and to perform a fully combined analysis of the sequence datasets from both collaborative groups, as it is possible that the mutation has not been identified because the exon(s) containing causative mutation(s) have simply not been sequenced yet, or that there is a genomic deletion that encompasses several exons but that has been unnoticed due to these exons failing PCR reactions and shared between the two groups.

We will also look for non-genic deletions, duplications and insertions using both custom and whole genome array comparative genome hybridisation (aCGH). Additionally, it may be appropriate to tailor next-generation sequence capture technologies to obtain patient sequence data targeted for the entire critical interval.

### 5.3.3. *Mp* mouse project further work

For the *Mp* mouse, confirmation of $Fbn2^{Mp}$ as the sole aetiological agent in the ocular phenotype is currently being assessed using global RNAi knockdown of endogenous *Fbn2* expression. This antisense transcript has been designed in a vector to be ubiquitously expressed and therefore should prevent global translation of *Fbn2* transcripts. RNAi-Fbn2 knockdowns in *Mp*/+ and *Mp*/*Mp* animals should therefore rescue the ocular phenotype, as there will be no mutant protein aggregates to accumulate in the ER of expressing cells. Loss of Fbn2 should therefore recapitulate the hind-limb oligodactyly in both mutants and in wild types, consistent will loss of Fbn2 protein seen in the *Fbn2*-allelic series. Thus, if proven experimentally, this will confirm mutant *Fbn2* as the sole aetiological agent responsible for the ocular phenotype in *Mp*.

Co-immunohistochemistry analyses are ongoing to identify whether intracellular $Fbn2^{Mp}$ containing cells are also positive for Wnt2b, Lef1, or Sox2, and markers of apoptosis, and additionally to confirm that all Lef1-positive cells were negative for Sox2 in both wild type and mutant eyes. It will be interesting to identify the consequence of *ER stress* on Wnt2b expression in the early CB and therefore immunostaining and *in situs* are currently being repeated, and will be complimented by quantitative RT-PCR analysis on

dissected eyes. It will also be interesting to identify what the binding partners of Lef1 are in the context of *Sox2* repression and what are the chromatin regions involved in such *Sox2* repression. This work would benefit from the establishment of primary cultures of embryonic ciliary cells for applications such as immunoprecipitation and chromatin immunoprecipitation, and this resource would also be useful to generate information of the transcriptional consequence of ER stress invoked by $Fbn2^{Mp}$ aggregates.

A conditional Wnt2b KO mouse, specifically within the developing ciliary body, may provide valuable data on the relationship between Wnt signaling and ciliary development, and also demonstrate the effect of loss of Wnt2b on retinal lamination. It may also be useful to cross the *Mp* mouse with the BAT-gal mouse; a model to report cells responding to canonical Wnt signaling through a *ß*-catenin activated LacZ reporter transgene (Maretto et al., 2003). Furthermore, inducing chronic ER stress specifically in the ciliary body by the forced expression of mutant secretory proteins, or by gross overexpression of normal ER-processed proteins could recapitulate the primary ciliary pathology seen in *Mp* and could reinforce the concept of the synodiporic effect.

# 6. Appendix

## 6.1. Sequence conservation of OAS Critical Interval exons

| Gene name | Exon ID | Exon Physical Position | Exon size (bp) | Conservation score |
|---|---|---|---|---|
| NUMB | ENSE00001023973 | 72852851 | 33 | 1.000 |
| RBM25 | ENSE00000807985 | 72650747 | 48 | 1.000 |
| RBM25 | ENSE00001097359 | 72636128 | 84 | 1.000 |
| RBM25 | ENSE00001228548 | 72635841 | 54 | 1.000 |
| DPF3 | ENSE00001487855 | 72430518 | 32 | 1.000 |
| RGS6 | ENSE00001487858 | 72076502 | 54 | 1.000 |
| SIPA1L1 | ENSE00000911799 | 71241191 | 63 | 1.000 |
| PCNX | ENSE00001344332 | 70547962 | 58 | 1.000 |
| MED6 | ENSE00001013677 | 70122226 | 28 | 1.000 |
| SYNJ2BP | ENSE00000658851 | 69924940 | 137 | 1.000 |
| PCNX | ENSE00001136831 | 70532211 | 185 | 1.000 |
| RBM25 | ENSE00001228606 | 72656174 | 93 | 1.000 |
| RGS6 | ENSE00001320224 | 72009333 | 82 | 1.000 |
| RBM25 | ENSE00001228669 | 72608103 | 106 | 1.000 |
| RBM25 | ENSE00001424956 | 72612780 | 50 | 1.000 |
| PCNX | ENSE00001136843 | 70505491 | 90 | 1.000 |
| MED6 | ENSE00000911704 | 70129766 | 83 | 1.000 |
| PCNX | ENSE00001136850 | 70498696 | 106 | 1.000 |
| SIPA1L1 | ENSE00001097265 | 71194803 | 104 | 1.000 |
| NUMB | ENSE00000911849 | 72859591 | 75 | 1.000 |
| RGS6 | ENSE00001306101 | 71888556 | 100 | 1.000 |
| RBM25 | ENSE00001228492 | 72648613 | 99 | 1.000 |
| PCNX | ENSE00000658877 | 70504668 | 46 | 1.000 |

| | | | | |
|---|---|---|---|---|
| MED6 | ENSE00001094579 | 70137086 | 22 | 1.000 |
| RGS6 | ENSE00001327135 | 72002219 | 65 | 1.000 |
| ZFYVE1 | ENSE00001239379 | 72514598 | 98 | 1.000 |
| RBM25 | ENSE00001228568 | 72619955 | 58 | 1.000 |
| RBM25 | ENSE00001228514 | 72644287 | 74 | 1.000 |
| PCNX | ENSE00001376246 | 70646265 | 141 | 0.999 |
| RBM25 | ENSE00001291453 | 72633376 | 186 | 0.999 |
| MAP3K9 | ENSE00001137119 | 70272431 | 69 | 0.999 |
| PCNX | ENSE00001136916 | 70593979 | 216 | 0.999 |
| SIPA1L1 | ENSE00000911800 | 71241692 | 119 | 0.999 |
| PSEN1 | ENSE00000808001 | 72734492 | 99 | 0.999 |
| RGS6 | ENSE00001310174 | 72098878 | 41 | 0.999 |

| Gene name | Exon ID | Exon Physical Position | Exon size (bp) | Conservation score |
|---|---|---|---|---|
| SIPA1L1 | ENSE00001097258 | 71274711 | 85 | 0.999 |
| PCNX | ENSE00000658912 | 70563242 | 111 | 0.999 |
| SIPA1L1 | ENSE00001487894 | 71274714 | 82 | 0.999 |
| PCNX | ENSE00001136837 | 70525037 | 133 | 0.999 |
| PSEN1 | ENSE00001153963 | 72753587 | 119 | 0.999 |
| MED6 | ENSE00000911710 | 70133081 | 92 | 0.999 |
| RGS6 | ENSE00001316047 | 72011086 | 75 | 0.999 |
| PCNX | ENSE00001324795 | 70546104 | 91 | 0.999 |
| RGS6 | ENSE00001318934 | 71994732 | 107 | 0.999 |
| PSEN1 | ENSE00000808004 | 72742847 | 87 | 0.999 |
| RGS6 | ENSE00001301612 | 72006468 | 77 | 0.999 |
| RBM25 | ENSE00001097369 | 72639653 | 287 | 0.999 |
| PCNX | ENSE00000911750 | 70610015 | 254 | 0.999 |
| DPF3 | ENSE00001487849 | 72260094 | 96 | 0.999 |
| MED6 | ENSE00000911712 | 70134088 | 160 | 0.999 |
| RBM25 | ENSE00001426056 | 72613830 | 168 | 0.999 |
| PSEN1 | ENSE00001383186 | 72755595 | 156 | 0.999 |
| MED6 | ENSE00000940919 | 70129350 | 109 | 0.999 |
| PCNX | ENSE00000658918 | 70570401 | 106 | 0.999 |
| RBM25 | ENSE00001310903 | 72624462 | 161 | 0.999 |
| ZFYVE1 | ENSE00001097340 | 72512012 | 171 | 0.999 |
| RGS6 | ENSE00001322773 | 71990989 | 51 | 0.998 |
| RBM25 | ENSE00000807981 | 72645803 | 151 | 0.998 |
| PCNX | ENSE00000911764 | 70625662 | 151 | 0.998 |
| ZFYVE1 | ENSE00001097332 | 72514388 | 118 | 0.998 |
| NUMB | ENSE00001130483 | 72892087 | 126 | 0.998 |
| NUMB | ENSE00001428128 | 72892087 | 126 | 0.998 |
| RGS6 | ENSE00001313498 | 72014729 | 62 | 0.998 |
| PCNX | ENSE00000658913 | 70565170 | 92 | 0.998 |
| NUMB | ENSE00001343504 | 72815742 | 144 | 0.998 |
| SIPA1L1 | ENSE00000911788 | 71197780 | 158 | 0.998 |
| NUMB | ENSE00000911845 | 72833672 | 75 | 0.998 |
| PCNX | ENSE00000911762 | 70624800 | 101 | 0.998 |
| NUMB | ENSE00001343493 | 72823571 | 205 | 0.998 |

| Gene name | Exon ID | Exon Physical Position | Exon size (bp) | Conservation score |
|---|---|---|---|---|
| RGS6 | ENSE00001370140 | 72072694 | 43 | 0.998 |
| PCNX | ENSE00001013713 | 70559670 | 33 | 0.998 |
| NUMB | ENSE00000911841 | 72829195 | 141 | 0.998 |
| SIPA1L1 | ENSE00000911792 | 71208818 | 275 | 0.998 |
| ZFYVE1 | ENSE00001341037 | 72507343 | 233 | 0.997 |
| MAP3K9 | ENSE00000658869 | 70286403 | 149 | 0.997 |
| PCNX | ENSE00000807893 | 70591974 | 59 | 0.997 |
| SYNJ2BP | ENSE00000658850 | 69912146 | 96 | 0.997 |
| WDR21A | ENSE00001097316 | 72483603 | 50 | 0.997 |
| ZFYVE1 | ENSE00001097334 | 72518250 | 107 | 0.997 |
| RGS6 | ENSE00001297037 | 72076502 | 67 | 0.997 |
| RGS6 | ENSE00001296991 | 72072647 | 90 | 0.997 |
| RGS6 | ENSE00001365869 | 72098878 | 51 | 0.997 |
| PSEN1 | ENSE00001023918 | 72723314 | 68 | 0.997 |
| RGS6 | ENSE00001487857 | 72076711 | 21 | 0.997 |
| SIPA1L1 | ENSE00001097255 | 71260117 | 240 | 0.996 |
| PCNX | ENSE00000911774 | 70639865 | 275 | 0.996 |
| PCNX | ENSE00001097234 | 70555479 | 154 | 0.996 |
| RGS6 | ENSE00001315171 | 72072647 | 45 | 0.996 |
| NUMB | ENSE00001343510 | 72818820 | 147 | 0.996 |
| PCNX | ENSE00000911740 | 70587122 | 109 | 0.996 |
| PCNX | ENSE00001218898 | 70483385 | 209 | 0.996 |
| PCNX | ENSE00000807888 | 70572535 | 93 | 0.996 |
| RGS6 | ENSE00001379107 | 71501262 | 84 | 0.996 |
| ZFYVE1 | ENSE00001097329 | 72515322 | 109 | 0.995 |
| TTC9 | ENSE00001332325 | 70207546 | 80 | 0.995 |
| RGS6 | ENSE00001294400 | 72031613 | 111 | 0.995 |
| RBM25 | ENSE00001228524 | 72642657 | 90 | 0.995 |
| SIPA1L1 | ENSE00000911784 | 71186805 | 175 | 0.994 |
| RGS6 | ENSE00001300134 | 72046615 | 126 | 0.994 |
| RGS6 | ENSE00001307727 | 71996093 | 52 | 0.994 |
| PCNX | ENSE00000911736 | 70584277 | 178 | 0.993 |
| ZFYVE1 | ENSE00001097346 | 72529604 | 215 | 0.993 |
| PSEN1 | ENSE00001343119 | 72684481 | 87 | 0.992 |
| PSEN1 | ENSE00000807988 | 72684481 | 75 | 0.991 |

| Gene name | Exon ID | Exon Physical Position | Exon size (bp) | Conservation score |
|---|---|---|---|---|
| PCNX | ENSE00000658919 | 70583434 | 142 | 0.990 |
| PSEN1 | ENSE00001130583 | 72710027 | 142 | 0.990 |
| ZFYVE1 | ENSE00001097338 | 72511240 | 181 | 0.990 |
| ZFYVE1 | ENSE00001097333 | 72534272 | 505 | 0.989 |
| RBM25 | ENSE00001228635 | 72647989 | 275 | 0.988 |
| PSEN1 | ENSE00000807997 | 72729105 | 221 | 0.987 |
| SIPA1L1 | ENSE00000911782 | 71160518 | 189 | 0.986 |
| DPF3 | ENSE00001487851 | 72268268 | 128 | 0.984 |
| SIPA1L1 | ENSE00001097260 | 71270136 | 147 | 0.983 |
| RBM25 | ENSE00001331913 | 72647292 | 325 | 0.983 |
| MAP3K9 | ENSE00001229326 | 70278821 | 241 | 0.983 |
| SIPA1L1 | ENSE00000911796 | 71235451 | 147 | 0.982 |
| C14orf112 | ENSE00000658846 | 69865644 | 63 | 0.981 |
| RBM25 | ENSE00001023894 | 72642320 | 223 | 0.981 |
| PAPLN | ENSE00000659138 | 72782097 | 61 | 0.980 |
| HEATR4 | ENSE00001331701 | 73035528 | 70 | 0.980 |
| PCNX | ENSE00000807890 | 70588353 | 130 | 0.980 |
| SIPA1L1 | ENSE00001385874 | 71275488 | 144 | 0.980 |
| MED6 | ENSE00000940920 | 70127736 | 116 | 0.975 |
| PCNX | ENSE00000658943 | 70645922 | 141 | 0.972 |
| PCNX | ENSE00000911728 | 70581603 | 151 | 0.969 |
| MAP3K9 | ENSE00001137138 | 70276512 | 123 | 0.967 |
| SIPA1L1 | ENSE00000911790 | 71207589 | 574 | 0.967 |
| RGS6 | ENSE00001323708 | 72013203 | 99 | 0.967 |
| MAP3K9 | ENSE00001137145 | 70337137 | 414 | 0.966 |
| C14orf112 | ENSE00000996466 | 69862803 | 117 | 0.963 |
| PCNX | ENSE00000911755 | 70612659 | 231 | 0.959 |
| MAP3K9 | ENSE00000658868 | 70285299 | 176 | 0.956 |
| WDR21A | ENSE00000807942 | 72476681 | 158 | 0.955 |
| WDR21A | ENSE00001154214 | 72490625 | 99 | 0.955 |
| DPF3 | ENSE00001487854 | 72308194 | 161 | 0.952 |
| C14orf112 | ENSE00000658847 | 69879128 | 72 | 0.949 |
| MAP3K9 | ENSE00001229351 | 70297472 | 181 | 0.947 |
| SIPA1L1 | ENSE00000911798 | 71238851 | 125 | 0.944 |

| Gene name | Exon ID | Exon Physical Position | Exon size (bp) | Conservation score |
|---|---|---|---|---|
| SIPA1L1 | ENSE00001097256 | 71271747 | 115 | 0.943 |
| PCNX | ENSE00000658917 | 70569899 | 110 | 0.938 |
| SIPA1L1 | ENSE00000911794 | 71221832 | 270 | 0.934 |
| WDR21A | ENSE00001097312 | 72492847 | 115 | 0.934 |
| PAPLN | ENSE00000659144 | 72787368 | 124 | 0.928 |
| PCNX | ENSE00000807899 | 70645074 | 443 | 0.925 |
| PAPLN | ENSE00000493787 | 72788125 | 173 | 0.925 |
| PCNX | ENSE00000911770 | 70638460 | 231 | 0.924 |
| PCNX | ENSE00001294182 | 70549455 | 218 | 0.924 |
| TTC9 | ENSE00000940946 | 70204034 | 183 | 0.915 |
| HEATR4 | ENSE00001331697 | 73034612 | 190 | 0.912 |
| RGS6 | ENSE00001299646 | 72054812 | 187 | 0.909 |
| HEATR4 | ENSE00001331713 | 73042924 | 105 | 0.908 |
| SIPA1L1 | ENSE00001097259 | 71261140 | 166 | 0.907 |
| WDR21A | ENSE00001097307 | 72488259 | 80 | 0.907 |
| SIPA1L1 | ENSE00001369903 | 71124343 | 1498 | 0.905 |
| SIPA1L1 | ENSE00001097254 | 71266525 | 247 | 0.899 |
| SIPA1L1 | ENSE00000911801 | 71245692 | 443 | 0.897 |
| NUMB | ENSE00001412617 | 72820542 | 294 | 0.895 |
| SIPA1L1 | ENSE00000911780 | 71155227 | 131 | 0.891 |
| WDR21A | ENSE00001097314 | 72490847 | 98 | 0.888 |
| SYNJ2BP | ENSE00000807864 | 69909461 | 141 | 0.886 |
| WDR21A | ENSE00001390019 | 72476788 | 51 | 0.884 |
| MAP3K9 | ENSE00001401213 | 70266850 | 485 | 0.882 |
| PAPLN | ENSE00000659146 | 72787947 | 81 | 0.874 |
| HEATR4 | ENSE00001331694 | 73033058 | 79 | 0.872 |
| PCNX | ENSE00000658910 | 70562587 | 172 | 0.864 |
| MAP3K9 | ENSE00001137128 | 70274715 | 154 | 0.863 |
| WDR21A | ENSE00001097303 | 72491984 | 174 | 0.856 |
| ZFYVE1 | ENSE00001097326 | 72560487 | 483 | 0.844 |
| HEATR4 | ENSE00001331709 | 73039352 | 119 | 0.843 |
| WDR21A | ENSE00001097298 | 72482345 | 144 | 0.842 |
| SYNJ2BP | ENSE00000807865 | 69953370 | 64 | 0.841 |
| PAPLN | ENSE00000659147 | 72788479 | 124 | 0.838 |

| Gene name | Exon ID | Exon Physical Position | Exon size (bp) | Conservation score |
|---|---|---|---|---|
| MAP3K9 | ENSE00001013682 | 70270856 | 113 | 0.832 |
| PAPLN | ENSE00000659136 | 72781105 | 116 | 0.830 |
| ZFYVE1 | ENSE00001097327 | 72510541 | 114 | 0.823 |
| WDR21A | ENSE00001097293 | 72479455 | 103 | 0.817 |
| NUMB | ENSE00001426692 | 72813039 | 716 | 0.817 |
| NUMB | ENSE00001431562 | 72813039 | 716 | 0.817 |
| MED6 | ENSE00001094575 | 70121283 | 131 | 0.815 |
| NUMB | ENSE00001332295 | 72820684 | 152 | 0.811 |
| WDR21A | ENSE00001130632 | 72495073 | 194 | 0.800 |
| WDR21A | ENSE00000807943 | 72478206 | 80 | 0.800 |
| PCNX | ENSE00001136840 | 70513412 | 1707 | 0.788 |
| PAPLN | ENSE00000659142 | 72786445 | 131 | 0.784 |
| PAPLN | ENSE00000808009 | 72802962 | 128 | 0.776 |
| PCNX | ENSE00001218491 | 70444321 | 153 | 0.743 |
| PSEN1 | ENSE00000807990 | 72707258 | 251 | 0.730 |
| MAP3K9 | ENSE00000807873 | 70269009 | 804 | 0.723 |
| PAPLN | ENSE00000659148 | 72789110 | 127 | 0.697 |
| PAPLN | ENSE00000494198 | 72805018 | 164 | 0.688 |
| PAPLN | ENSE00000659140 | 72782534 | 103 | 0.661 |
| HEATR4 | ENSE00001331705 | 73037007 | 181 | 0.644 |
| PAPLN | ENSE00000659152 | 72791338 | 142 | 0.642 |
| PAPLN | ENSE00000808010 | 72803184 | 109 | 0.627 |
| HEATR4 | ENSE00001331730 | 73055480 | 141 | 0.601 |
| PAPLN | ENSE00001413827 | 72808956 | 170 | 0.594 |
| DPF3 | ENSE00001487853 | 72289725 | 108 | 0.581 |
| HEATR4 | ENSE00001331717 | 73044591 | 161 | 0.558 |
| PAPLN | ENSE00000493778 | 72790215 | 208 | 0.553 |
| PCNX | ENSE00000807898 | 70641705 | 206 | 0.544 |
| PSEN1 | ENSE00001153970 | 72748230 | 174 | 0.540 |
| C14orf112 | ENSE00000996467 | 69895989 | 69 | 0.537 |
| PAPLN | ENSE00000659159 | 72801831 | 138 | 0.534 |
| PAPLN | ENSE00000659154 | 72795861 | 146 | 0.524 |
| PAPLN | ENSE00000659155 | 72797617 | 139 | 0.491 |
| PSEN1 | ENSE00001130552 | 72748230 | 90 | 0.467 |
| HEATR4 | ENSE00001331720 | 73045769 | 162 | 0.445 |

| Gene name | Exon ID | Exon Physical Position | Exon size (bp) | Conservation score |
|---|---|---|---|---|
| PAPLN | ENSE00000659157 | 72800672 | 125 | 0.441 |
| PAPLN | ENSE00001391023 | 72808956 | 67 | 0.410 |
| MAP3K9 | ENSE00000807879 | 70345236 | 406 | 0.407 |
| PAPLN | ENSE00001371832 | 72800672 | 150 | 0.381 |
| PAPLN | ENSE00001385454 | 72797170 | 121 | 0.375 |
| TTC9 | ENSE00001167125 | 70178258 | 745 | 0.354 |
| HEATR4 | ENSE00001331733 | 73057309 | 188 | 0.354 |
| HEATR4 | ENSE00001331723 | 73048463 | 144 | 0.330 |
| PAPLN | ENSE00000519940 | 72798811 | 478 | 0.309 |
| PAPLN | ENSE00000659134 | 72776240 | 54 | 0.305 |
| PAPLN | ENSE00000659156 | 72800106 | 138 | 0.296 |
| PAPLN | ENSE00001372628 | 72795730 | 277 | 0.281 |
| HEATR4 | ENSE00001331724 | 73050488 | 204 | 0.257 |
| PAPLN | ENSE00000659153 | 72795440 | 81 | 0.237 |
| ADAM21 | ENSE00000940930 | 69993970 | 2169 | 0.217 |
| RGS6 | ENSE00001422262 | 72098921 | 291 | 0.216 |
| HEATR4 | ENSE00001331690 | 73031685 | 160 | 0.213 |
| PAPLN | ENSE00000659151 | 72790974 | 183 | 0.189 |
| HEATR4 | ENSE00001331685 | 73029523 | 59 | 0.156 |
| HEATR4 | ENSE00001331736 | 73015064 | 237 | 0.126 |
| ADAM20 | ENSE00000911696 | 70059047 | 2331 | 0.124 |
| WDR21A | ENSE00001377695 | 72474440 | 98 | 0.095 |
| WDR21A | ENSE00000807940 | 72474440 | 92 | 0.093 |
| WDR21A | ENSE00001374971 | 72476263 | 101 | 0.075 |
| DPF3 | ENSE00001487847 | 72148929 | 147 | 0.051 |
| PAPLN | ENSE00000659149 | 72789622 | 66 | 0.030 |
| PAPLN | ENSE00001487683 | 72798966 | 323 | 0.029 |
| PAPLN | ENSE00000519943 | 72801017 | 171 | 0.023 |
| PAPLN | ENSE00001387318 | 72801049 | 139 | 0.015 |
| MAP3K9 | ENSE00000807874 | 70270227 | 42 | 0.005 |
| RGS6 | ENSE00001402687 | 72077558 | 35 | 0.000 |

## 6.2. Oligonucleotide primer sequences and predicted product size

| Exon ID | Fwd oligo sequence | Rev oligo sequence | Product size (bp) |
|---|---|---|---|
| ENSE00000996466 | AGACATAGTCTCGCTCTGTTCG | ATTTGTGAGGCCGAGGTG | 243 |
| ENSE00000658846 | TGGCTATAGTATTTCAGCCATCTC | CTTTTAAGGCAGATAAAACCAGTAAC | 228 |
| ENSE00000658847 | GAATTCTGGTCTTCTGTTTTGC | ACAATTCTCCTAAACCAGAACATAC | 186 |
| ENSE00000996467 | CCGAGCACCAAATAACCAAG | ACATGGGGACTCCATAGCC | 199 |
| ENSE00000807864 | CATGGTGAAACCCCATGTC | TCTTTTCCTCCCTCTTGCTG | 288 |
| ENSE00000658850 | TTTGGCCATTTGAAAATAAATTG | ACAGTGCAAAAGCCTGGTG | 219 |
| ENSE00000658851 | CTTTCTTCTTCACCCCCATC | GGCTTAGGGAGCAAAGGAC | 230 |
| ENSE00000807865 | AGGCTGCTGAAACCGAAAC | GACCCTTTCCGCACATACC | 194 |
| ENSE00000940930 | TGCCTCACACCTTGTCCTC | TGTGCTCAGTTTCAGGGATG | 2317 |
| ENSE00000911696 | CAGCTTCATAATGGCAGTGG | TGAGGGACAACAGCTTGAAAC | 2473 |
| ENSE00001094575 | TGCATGTAGATGCTTTTAAAACTG | GATTCCACTTCTGGAACTCTATCC | 284 |
| ENSE00001013677 | TTGCCAAGTTGACCTGTTTTC | CCACAGCTCATTTCACATGC | 186 |
| ENSE00000940920 | GACACCAAACTAAGTAGGCAATG | ATGCCATAAAGAAGTGTCAAATC | 217 |
| ENSE00000940919 | TGAGTATTTACTTTGGAAAGTTTGGTC | GAAAACAGCTTCATTCTCAGAGG | 239 |
| ENSE00000911704 | TTAGCAGTTTGTGTCCATAGCTG | GCAACTTACACAAGGCAGAGG | 236 |
| ENSE00000911712 | TGTTTGTTGGATTGGATTCTTTC | GCACTTCATGATCCACAGTTTG | 308 |
| ENSE00001094579 | CCCTCTTCCGCTCTACGTC | AACATCCCAAACTGGTCCAC | 199 |
| ENSE00001167125 | TTAATCCTCCCCTCCTTCG | CACAGCAGGAGAATCTGCAC | 914 |
| ENSE00000940946 | AGAGCTGGCCACTGTTGTG | CACCAGAGCAGGGAGGAAG | 278 |
| ENSE00001332325 | CTGCAGACACAGCCTTTGC | AGGGGATGCCTGGAAGTC | 224 |
| ENSE00001401213 | CATTTGCTGCCTGGATGTG | AGCGATTCTCCTGCCTCAG | 587 |
| ENSE00000807873 | TTCCTGCCACCTCATTTCC | TGAGGAGGCACAAAGAAAGG | 906 |
| ENSE00000807874 | AGGGCAAGAGGAGAAAAAGTG | GCTGGGTGTGTCTGTGAGG | 216 |
| ENSE00001013682 | CATGGAGCTGAGGGTCAAG | CAGGGAGCAGGGAGACAG | 227 |
| ENSE00001137119 | CTTGGGTGTTTTGGTGTGG | AAGGAAATGGAAGGGAGATTG | 209 |
| ENSE00001137128 | AGCCCTGTCTGTCCATTTTC | TCCTATGTTTAAATGGTACATCCATC | 268 |
| ENSE00001137138 | CTGTCCCTCAAGGATGCTG | AGGTGCCCCTGTGTGTTC | 268 |
| ENSE00001229326 | GCACTGAGCACCCCAGTC | CGAGTTCTTTGCCCTGCTC | 338 |
| ENSE00000658868 | TTGCTTCTGTCCATTCATGC | CCAGAGGTCCCTGTGAGTG | 314 |
| ENSE00000658869 | GGGAGAATGTGGGATGCTC | CAAGAGGCAAAGTGTCTCCAG | 291 |
| ENSE00001229351 | TGTTCTGTGGTTTCCCTGTG | TGTGTGTGCCACCAAGATG | 303 |

| Exon ID | Fwd oligo sequence | Rev oligo sequence | Product size (bp) |
|---|---|---|---|
| ENSE00001137145 | GCCGTGTTTACCCACTCAG | TCGTGGGATACAACTGCAAC | 562 |
| ENSE00000807879 | - | - | - |
| ENSE00001218491 | - | - | - |
| ENSE00001218898 | - | - | - |
| ENSE00001136850 | CAAAGGAAAAGCATTGGAGTC | TCAGGAGGAGGGAAAAAGG | 215 |
| ENSE00000658877 | TTTTGTTTGATAATCTTGCTAGTGTG | AACCAAAATGAAAGGGAAAGG | 186 |
| ENSE00001136843 | TGCCACCCTACAGCCTTAC | AAACTTCTGCCAAATTGTATGC | 240 |
| ENSE00001136840 | - | - | 1500bp |
| ENSE00001136837 | TGGGAAGTCAAGGGAAAGC | TGGCGGAACAGATTAGAAGG | 283 |
| ENSE00001136831 | TTTTCTCTTTTCTTCCCTGTAATG | CAATTGTTACCCATCATCTGC | 302 |
| ENSE00001324795 | AAGGAAAAATTCTGAGTATTCTAATGG | TGGCAAACATATGAAAGTACACAC | 195 |
| ENSE00001344332 | TGAATCTCATCTGAATGTTAAAGG | TTCATCAATTTTTATGGCTTTTATAG | 234 |
| ENSE00001294182 | - | - | - |
| ENSE00001097234 | AACTTCATATTTATGTCTTCCCTTCC | CAAAATCCTCTGCCTTTTAACAC | 309 |
| ENSE00001013713 | TTTCAGGCATTTTGAAAGTTG | TGATGCATTCCAAACAAAAC | 210 |
| ENSE00000658910 | - | - | - |
| ENSE00000658912 | CTCTCAGTGGACACAAGAATGG | TGGAAAAGCATTTTAATGGTCAG | 264 |
| ENSE00000658913 | AATATTTTAAATGCTTTTCAGTGACC | CGATACCAGGGGAAGAAATC | 276 |
| ENSE00000658917 | TTTTTCCAAAATACGTACATAAAAGG | AAAGGCATTGGGAAAAAGAG | 290 |
| ENSE00000658918 | TGCCCGTTTGAATTACTGG | TTCCTCATATAACATGATCAACTGTC | 241 |
| ENSE00000807888 | TGCCAATTGGGAATAAAGG | GCCTGGGTGACAGAGTGAG | 237 |
| ENSE00000911728 | ACAATGAGTCTCAAAATCACTCC | TCAATATAGCAAAGGGAAAAACTC | 266 |
| ENSE00000658919 | TTCTTTCTCATCACATTGACAAAC | AACAGCCCCCAGTAGTCAG | 257 |
| ENSE00000911736 | - | - | - |
| ENSE00000911740 | AGAACTTCTCCTAATACATTTTACAGG | AAGGTCATGCCTATAAACCAAC | 286 |
| ENSE00000807890 | TTTTGCGAGGGTTTGTTTG | TTCCCAGTAGGAAAGATAAAAATTG | 249 |
| ENSE00000807893 | CATTTCCTATAGTTTCTTCCTCAGTC | TTCATAGAGGATTCCCAACAAG | 243 |
| ENSE00001136916 | AACAATCTTGTTTGTCAAGAGGAC | AGGTGCCACAGGAGTATGC | 331 |
| ENSE00000911750 | TTCCCACTTTCTGGTTTTCC | TCATTCCCAAGAAGAAACTCTG | 362 |
| ENSE00000911755 | TTGGAATTTATTTCATTGAGTAATCTG | TGCATCTTTGGAAAAACCTG | 369 |
| ENSE00000911762 | CGCTATATTATTTCGATTTATGATTTG | GCTATACAGCTTCCCATGCTC | 230 |
| ENSE00000911764 | AGGTGATTCTGATGCACACG | CAGCAGCGTGAGAATGGAC | 330 |
| ENSE00000911770 | - | - | - |

| Exon ID | Fwd oligo sequence | Rev oligo sequence | Product size (bp) |
|---|---|---|---|
| ENSE00000911774 | TTATTCTTGGCCCCTTAACC | GGTCAGGAATACACCAGCAC | 366 |
| ENSE00000807898 | CCCATTTTGAAGTGATCTTGG | AGCCTCTATGGCTAAGAAGCTAAC | 313 |
| ENSE00000807899 | GGGGAAAAAGTCTTAGAAACTGC | TTCACAACAGTCCTTCATTCAAC | 615 |
| ENSE00000658943 | CTGTGAAAAGCATTTTGTTTGAG | ACCATGCATCCAAGTGAGG | 297 |
| ENSE00001376246 | GTATATTCCAGGTCTCCAGTGC | CAATGCCTTGGAATTGAGAG | 245 |
| ENSE00001369903 | TGGAAGCCATTCTCCAAAAG | TTCAGAAAGTACTGCAAAAGAAAATG | 1640 |
| ENSE00000911780 | CTGAGTGACAACCTTAAATACTGAGC | TGCTTTCTTCCCCATTTCAG | 275 |
| ENSE00000911782 | TGTTCAGGCATCTCACATCC | CGGAAGCCTAGCAATAAACC | 300 |
| ENSE00000911784 | TGGGACAAAGTGGATCTGC | TGCACAACAGCACAACAGG | 289 |
| ENSE00001097265 | - | - | - |
| ENSE00000911788 | GGGGGAAGCAAATGATTG | AACCAGCCAACATCCACAG | 255 |
| ENSE00000911790 | TTGTGAGACTGAGAAATACTGACG | TGAAAACTTTATGAAAGAGAAACTGC | 679 |
| ENSE00000911792 | CCAGTTCCATGTCCACCAC | GTACACAAACCCTGCACTCG | 397 |
| ENSE00000911794 | ATGTGGTTCCACCAGCAAG | TTACATTTGGGGCAGAGAGAG | 386 |
| ENSE00000911796 | CCTTGGGATTTTCCCTTTG | TGAAAGAAATGATGCCAACAG | 256 |
| ENSE00000911798 | TCCCCTCATGGGTAAGGTC | ACCTAAGTCACCTTGTAAAAGCAAC | 234 |
| ENSE00000911799 | TGGAACCCCATCTTGAACG | CAGGCATGGATGCAATCAC | 209 |
| ENSE00000911800 | CACCATGTGCTTGTTTCTGC | GGCCATGCAGAGGAAAGAG | 270 |
| ENSE00000911801 | TCTGTTATTCTCTTGTTCAGGAAGC | GGAACTGGGCTTAGGTCTGG | 559 |
| ENSE00001097255 | TGTTCAACCCAGCCATCAC | CCGGCCTCTTTTGTTGTAAG | 430 |
| ENSE00001097259 | AGCCAGCCTTGTTGAGTTG | CCCATCATGTCTGGCTTG | 271 |
| ENSE00001097254 | ACCTTGGTCTCAGGGATCTG | CATCATCAACAGGGCCATC | 355 |
| ENSE00001097260 | TTCCACAGGCACAAGAAGC | GAGTGGATGGAGACTGCTCAC | 260 |
| ENSE00001097256 | AGATAGGGCCAGGGATGTG | TGGCAGATGTGACACAAGG | 222 |
| ENSE00001097258 | AACAAACCCAGCCATGGAG | GGGCTCTCATGGTTCAAGG | 206 |
| ENSE00001487894 | AACAAACCCAGCCATGGAG | GGGCTCTCATGGTTCAAGG | 206 |
| ENSE00001385874 | TGGGGCCAACACCTCTTAG | GCTGCAGGACACTCACTGG | 249 |
| ENSE00001379107 | TCCTTCGTGACTTAATGGTTTATTC | AACAGTCCACACGGACAGC | 190 |
| ENSE00001306101 | - | - | - |
| ENSE00001322773 | AACATGTTTCTTCTGCCACAG | GCAGGGGAATCTAGTTTGG | 202 |
| ENSE00001318934 | CTGGGGGTGATGACAGTTG | TCAGATGATGTTGTGAAGAAAAGG | 259 |
| ENSE00001307727 | CTGGGTGTGGGAGGGAAG | CTGCACCCCCAGAAGTGAC | 181 |
| ENSE00001327135 | TGGACAGATGGATGGATGG | CGGAGCTGCAGATATGATTTTAC | 206 |
| ENSE00001301612 | AAGCATAGGTGTCGATGTGC | TTCACACCATTTCCAAATTCC | 210 |

| Exon ID | Fwd oligo sequence | Rev oligo sequence | Product size (bp) |
|---|---|---|---|
| ENSE00001320224 | ACGCTGGAGCAAGTGTCAG | CACCTGGTGGCTAAAGACG | 247 |
| ENSE00001316047 | TGTGACATGGGCTAAATTGG | TGGAAGGGCTATTCACATCAG | 195 |
| ENSE00001323708 | AAGCCACCCTCCAATTCTG | AAACTGGCCACGTCTCCTC | 203 |
| ENSE00001313498 | TGCAGGATTTGGGTTTGTG | CTTGGCATTGAACACATTCG | 236 |
| ENSE00001294400 | GGGTTTTCTAAGGAAATCAGTGG | CTCATGATCTCATGGATTTTTGTC | 225 |
| ENSE00001300134 | TGACACGAGCTTTTCTCTGG | GAGATGGAGAGACCGATTATGC | 256 |
| ENSE00001299646 | CATGGGACATCAGCTCTGG | GAAGGGGACAAATGAACACC | 324 |
| ENSE00001296991 | ACTGGTTGACAGCCCTTCC | CAAGCAGCAGGCAAGAGTC | 195 |
| ENSE00001315171 | ACTGGTTGACAGCCCTTCC | GCAGCAGGCAAGAGTCAAC | 192 |
| ENSE00001370140 | ACTGGTTGACAGCCCTTCC | CAAGCAGCAGGCAAGAGTC | 195 |
| ENSE00001487858 | TGCTGCTGTTTGGGAACC | AAAACCAAAACCAAAAGAAAAGC | 187 |
| ENSE00001297037 | TGCTGCTGTTTGGGAACC | CCACCCCAAAGGAAACAAC | 243 |
| ENSE00001487857 | - | - | - |
| ENSE00001402687 | GTCGGCCCAAGATTTGAAC | TCAACAGAGGTGGAACAAAGG | 198 |
| ENSE00001310174 | TCACCTGTCTGGCTCTCTGTC | GGAAACTCTGTCCGCAGATG | 210 |
| ENSE00001365869 | CTCTGTCCCTCTGTGTGTGC | TCCTCGTAAGGAAACTCTGTCC | 199 |
| ENSE00001422262 | GTGCCTCTCTGTCGCTGTC | TGACAGGAACCCCACGAC | 405 |
| ENSE00001487847 | GGATCGAGCAGCCTTCTTC | GCACACCCCAACATGAAAG | 299 |
| ENSE00001487849 | TTCCCTTTGCATTTCGTTTC | CCCAGCCTCCCTCATCTC | 194 |
| ENSE00001487851 | CCCTGCCTGCTTCTAGTGG | TTCTGGAAGCGCTATGGTG | 238 |
| ENSE00001487853 | GAATGACGGGGTTAGTCAGG | CTCCCACCTTTCCCATCAC | 238 |
| ENSE00001487854 | CCCTCTGGGTGTGTTTCAG | TGGTTTCCCAGACAAGCTG | 303 |
| ENSE00001487855 | - | - | - |
| ENSE00001377695 | CCATGCCCACACACAGAG | AATGCCAGAAGCACACTGG | 200 |
| ENSE00000807940 | CCATGCCCACACACAGAG | AATGCCAGAAGCACACTGG | 200 |
| ENSE00001374971 | CGTCAGAATGGCTGGAACTC | TCTCAGCCTTCCCTGTGTG | 216 |
| ENSE00000807942 | GTGGTCAGTTCACAGTGGTTG | AGTGGATGGACAGGTGCTG | 272 |
| ENSE00001390019 | AAACGCTACTTCCGCTTGC | AGTGGATGGACAGGTGCTG | 188 |
| ENSE00000807943 | ACATTCTCCATCATCCCCTAAC | CCATGAAAATAAGAAACAGGAAAAG | 213 |
| ENSE00001097293 | CCCCGAATCTTCTTCATGG | GGTTTGATGACTGGCAACG | 248 |
| ENSE00001097298 | CCTCTTAGGCAGTCCACCAG | CTACCCCCAGGGTCAAGTG | 257 |
| ENSE00001097316 | TGTGTCCCCACATGTTATTCC | GCCCACAGATACCCAGGTC | 200 |
| ENSE00001097307 | CTGAAGGGTAAATGTCCATGC | AGCTCTCGGGAGACAGAGG | 204 |
| ENSE00001154214 | TTTCCGAACCCAGTGGTC | GGCCTGTTAAGGCCTCTTC | 216 |

| Exon ID | Fwd oligo sequence | Rev oligo sequence | Product size (bp) |
|---|---|---|---|
| ENSE00001097314 | GTTGTCCCTCTCCCCAGAC | TCTGGCCAAATTTCTACATGG | 220 |
| ENSE00001097303 | CCAGCCTCAGAGGGATGTC | TTCAGCAGAACCCTTTCACC | 306 |
| ENSE00001097312 | CTTCCTGGCTTTGCACTTG | CCTCTGCTGCTGAAGTTGC | 273 |
| ENSE00001130632 | ATCTTGGGAAGCCATGTCC | TTACTCCCGTAAGTCAAATCCAC | 327 |
| ENSE00001341037 | TTCTCCTCAAGAGCCTGGAC | GGAAGGCACTGATGGAATG | 364 |
| ENSE00001097327 | TTTTCCATTTGGGAGAGGAC | CTCAACCCGCATCCACTAC | 217 |
| ENSE00001097338 | TCAGCTGAGCAGACATGTACC | GGAGGTTCTCCCCTCCAC | 288 |
| ENSE00001097340 | TCACCAAACATCCCTCTTCC | GCAAAGCGGCATTAAGTAGG | 309 |
| ENSE00001097332 | TTCTGGTGCGTTTGTCTCC | CATGAAAAACTGAACGACACAAG | 239 |
| ENSE00001239379 | GCTGGTAAAACCCCGTGTC | GGGAGACAAACGCACCAG | 222 |
| ENSE00001097329 | TGGCTCCTTTAGCCGTCTC | TGCCAAAGAGAGAGTGGTCAG | 216 |
| ENSE00001097334 | GCCTGTGTTGCTTGTACGG | AGGGGATCTGCATCCACAC | 294 |
| ENSE00001097346 | TGCTAGGGTTACAGGTGTGG | GCTGGCGAACTGAGTGTTC | 386 |
| ENSE00001097333 | TTCCTTGTCCTTGGGAAGC | ACCAAATAGCTGCCTCCTTG | 659 |
| ENSE00001097326 | - | - | - |
| ENSE00001228669 | TCAAATAAAATGATTTGTCATGTCC | CACAAAGACAAAAGTACAAGTTTAACG | 211 |
| ENSE00001424956 | TTAATTGTGTGGCATGTTGTTG | TGTTCAGCTTAAAAGCACTAGCAC | 181 |
| ENSE00001426056 | TGTGGTAGGAAATTTAATTGCTG | AAAAAGCAATCACTGAAAGTCTTC | 314 |
| ENSE00001228568 | - | - | - |
| ENSE00001310903 | TGGACTCTAGTGATTCTACTTTTCC | ACACTGAAATAGCACAGTCTGG | 300 |
| ENSE00001291453 | GAGTGATTTTGATTTTCTTGCTTG | AAAAAGAAAACTGACATGTAATCAAAG | 335 |
| ENSE00001228548 | ATAGGGCATTGCTTTGCAG | CAACAATCAGCAGTAAACACAGG | 183 |
| ENSE00001097359 | AACTGTTTATATTGAAGTAGGGTGTTC | TTTGTCTCTTTGCTTTGGATTC | 214 |
| ENSE00001097369 | GCCGGGAAAAATCTGAATAC | TGAATGCAAATGGTACTCTGG | 433 |
| ENSE00001023894 | TGTTGTCCTCCTTTACTTTGGTC | TTGATTAACCTATTAAGGGATACCAAG | 356 |
| ENSE00001228524 | GCCTTTATTCTTAAATCTTGGTATCC | GCTTGTGCATTTCAATTATTAAGTTAC | 287 |
| ENSE00001228514 | GTCTGGGTCAGAAAAATCTGTTTAC | TGCAGATGGAAAAACACAGC | 232 |
| ENSE00000807981 | TTGAAAAGAGGTGCTGTTGG | CTGGGATTACAGGCGTGAG | 290 |
| ENSE00001331913 | AAAACAAAAATCAAGTTGAATGG | GTATTTGCAGGGGTGAAGG | 442 |
| ENSE00001228635 | GCATTGCTTTTGAGGGATG | TGGCATATTCCAACTGTTCC | 411 |
| ENSE00001228492 | TCTCAGGAAAAATCATGAAGC | GGAACTTGACTCTGTAAAATTTCTG | 277 |
| ENSE00000807985 | AAGTTCCTGTATGAATTTGAGGATTC | AACGTGGTGAGACCCCATC | 241 |
| ENSE00001228606 | TGGCAGATGTTGATGATTGC | GTCCTTAAAAGGGTGGCAAAG | 207 |
| ENSE00001343119 | TCAAGAGGCTTTGTTTTCTGTG | CTAGCCCCCTCAGCATTTC | 223 |

| Exon ID | Fwd oligo sequence | Rev oligo sequence | Product size (bp) |
|---|---|---|---|
| ENSE00000807988 | TTTCCCTTTTCAGAACCTCAAG | CTGGCAAAGGCAGTTTCAG | 187 |
| ENSE00000807990 | CCGTTACCTTGATTCTGCTG | GGCCTTCAAGGTGATGATG | 390 |
| ENSE00001130583 | GGAGGTGGTAATGTGGTTGG | ACCCAACCATAAGAAGAACAGG | 265 |
| ENSE00001023918 | TTTAAGGGTTGTGGGACCTG | AATGATAGCTACACAGCACAAAGG | 183 |
| ENSE00000807997 | TTGGGAGCCATCACATTATTC | GTGGGGCATTCCTGTGAC | 348 |
| ENSE00000808001 | TCCTCCCTACCACCCATTTAC | TGTGCTTCAGTTCCGATAAATTC | 235 |
| ENSE00000808004 | ACTGGCGATTTGTGTGGAG | AACAGTGACCCTGAAAAATCAAG | 228 |
| ENSE00001153970 | TGTTTCCATGTAATTTTCTTAAAGG | AGCTACCTAAAGGAATCCATGAC | 298 |
| ENSE00001130552 | TGTTTCCATGTAATTTTCTTAAAGG | TGCTGGAAAGTTCCTGGAC | 219 |
| ENSE00001153963 | GGGGTTGAGTAGGGCAGTG | GAACTGCCTTAAAGGGACTGTG | 285 |
| ENSE00001383186 | TTGAGTTTTGCCTGAAAATGC | TTTGTCCTCCCCAGATTTTG | 289 |
| ENSE00000659134 | GGGCCATAGGGAGAGACG | GACTCCCCTGCAGGTTCC | 201 |
| ENSE00000659136 | GGCTCAGGCTGTGAGTGG | CCCCTGCTCCTGCTTTAAC | 212 |
| ENSE00000659138 | TGCAGAGAGCCCCAGAAC | ATCCCAATGGGGAAATCG | 204 |
| ENSE00000659140 | - | - | - |
| ENSE00000659142 | GGTAAGCCTTGGGTCTTGG | GGGTGATGGACAGGGAAAC | 279 |
| ENSE00000659144 | CTGATGTGGCCATGATGC | GAAGGGACAGGCAAGGAAG | 231 |
| ENSE00000659146 | GAGAGGGATAGCCCAGCAC | AGTCAGCCAGAGGGAGCAG | 203 |
| ENSE00000493787 | AGGTCCTAGGCAGGTCTGG | GAGCTTGGCAGCCTCTTG | 320 |
| ENSE00000659147 | GAGTGGCTCTGGGCTTGAG | GGAGAGGGCTGTGACTTGC | 309 |
| ENSE00000659148 | CGCTTGGTGAATGTTGACTG | CCCTTCCCACCCAAGTTC | 238 |
| ENSE00000659149 | CAGCAGAGGGTTTGGCTTG | GTGACAGGGTGGCACCAG | 211 |
| ENSE00000493778 | CTCAGGGCTGGGTTTCTG | GCTACCCAGGTCCAGCAC | 315 |
| ENSE00000659151 | CGCTAGCTGTCCGAACTGG | TGCCAGAGACCAGGGTCAG | 303 |
| ENSE00000659152 | ACCTTCCCCTGCCTCTCTC | TGCTTGCTGGGTTTGTAGC | 295 |
| ENSE00000659153 | TCCTCTCTTCCTCCCTCTCC | ACCCCCATGTACCATCCAC | 202 |
| ENSE00001372628 | GAAGGTGGGTCCAACGTG | CCACCTTCCCTCTTTGACG | 408 |
| ENSE00000659154 | CAGGGGAGAACGAGGTGAC | CCACCTTCCCTCTTTGACG | 273 |
| ENSE00001385454 | CATGGGGAGCCTCAGAGC | CAAAGCGGCAAAGATCCTG | 294 |
| ENSE00000659155 | CAACAATGGCCAGATCCAC | TGGTGGGAGCAGAGTCTACC | 244 |
| ENSE00000519940 | GGAGGCTGAGAGGATGGAG | CTGGCATGCTCCTTGTCTG | 611 |
| ENSE00001487683 | GCCAATGTAACCGCTTCTG | TGTCTGGGCGTCCTAACC | 439 |
| ENSE00000659156 | TTAGGGTGGTTCTGGTCCTG | GGGGCTGTCACACCTGTC | 245 |
| ENSE00000659157 | GACTCACTGTTGCCCTTGG | ATCCTGGCCTTCCCACTC | 244 |

| Exon ID | Fwd oligo sequence | Rev oligo sequence | Product size (bp) |
|---|---|---|---|
| ENSE00001371832 | AAGACTCACTGTTGCCCTTG | GGAATTGACTCAGAGAGACACC | 310 |
| ENSE00000519943 | CGTAAGTCCCTGCTGGTCTC | CGTTCCCCTCCTTATCCAC | 308 |
| ENSE00001387318 | CCCTTTTCCTCACAGCTCAC | CGTTCCCCTCCTTATCCAC | 266 |
| ENSE00000659159 | AGGTGCCCATGGGAGTAGG | GGGCTGGAGGCAGAATAGG | 251 |
| ENSE00000808009 | GAGAGGGGAGGCTCCTTG | TACCCATGCCACCTGACC | 226 |
| ENSE00000808010 | TGGGTAGGGCAGGATCTTC | TGTGAAGGTCTGGGGACAG | 206 |
| ENSE00000494198 | TCCCTCTGTCTCCCAGACC | AGAGCCAGCCCTTGAGAAC | 303 |
| ENSE00001413827 | AGGAAATGAAATGGCAGGTG | CCAGCCAGAGAGAGGAAGC | 340 |
| ENSE00001391023 | AGGAAATGAAATGGCAGGTG | ACAGCTGGCACAGCAGAAG | 211 |
| ENSE00001426692 | AAAAGCCAAAATCTTTATTTTTATGC | TGGAGAGTAAGACCAAAAGAACG | 868 |
| ENSE00001431562 | AAAAGCCAAAATCTTTATTTTTATGC | TGGAGAGTAAGACCAAAAGAACG | 868 |
| ENSE00001343504 | TGACTGACACAGCTCCAAGG | TCACTTATCTGATCCCAGAATCC | 270 |
| ENSE00001343510 | AAGTGCCAGCTTGCATCATAC | GGAAGCTCAGGATGCCAAC | 320 |
| ENSE00001412617 | AAGGACCTAGAGGGCTTTCG | CATGGGAAGTGATGAGAATGC | 451 |
| ENSE00001332295 | TCTGATGCCACGACCTCTC | CATGGGAAGTGATGAGAATGC | 276 |
| ENSE00001343493 | TCTCAAAAACAAAACAAAACAAAAG | TTGGGAAAAACTGCATTCC | 341 |
| ENSE00000911841 | TGCATCATGAAATGAACATCC | CCAGAAAGAGCCCAGCTAAC | 286 |
| ENSE00000911845 | TTTGGAAGGCAGAGTCAGTG | AGCCTGGGTGACAAGAGTG | 245 |
| ENSE00001023973 | - | - | - |
| ENSE00000911849 | TCAACCTGTATTCAATTTTCACC | AAACACAGTTTTTACTGGGTCAC | 266 |
| ENSE00001130483 | TTTTGGACATCAGATTTTTGG | TTGTCAGTTCTTTTCCACATACAG | 286 |
| ENSE00001428128 | TTTTGGACATCAGATTTTTGG | TTGTCAGTTCTTTTCCACATACAG | 286 |
| ENSE00001331736 | CAGGCCTAACCACACGAAG | GGGCGTGGAAAAATATGC | 401 |
| ENSE00001331685 | TGAAATGATCACGGATCAAGG | GATTCTCCGCTGCCACTG | 213 |
| ENSE00001331690 | GCTGCCTAGTACAGGTGTTTTG | CATCCAGATCCTGGAAGAGG | 282 |
| ENSE00001331694 | GGGATTCTTACCTGATTCCAAG | AGGAGGACAGGGTCTGAGG | 247 |
| ENSE00001331697 | CAAAAGGGAAGGTATTGTTTGC | GCAGGGACATATTCAATGAGC | 368 |
| ENSE00001331701 | GCACCCAGCTGTTTCTGG | CCTGCACTTCACCCCATTAG | 238 |
| ENSE00001331705 | GGGTTGGGGGTTAGGTACTG | GCCCTCTTCAGGTCAATCAG | 293 |
| ENSE00001331709 | AAAACAGCACAACGCCAAG | GCCTGCCTCCTAAACACTTC | 255 |
| ENSE00001331713 | ATGCAGGATGCCATTTCAG | TCAGCCTCTCTTAGGCTTTCTG | 243 |
| ENSE00001331717 | AGGGGGAAAACACATCACC | GACCTAATTGCTCCCCAAAAC | 261 |
| ENSE00001331720 | CATGGCTGTAGGAAGGAAGC | GAGGAAAGGACTGGGAAAGC | 316 |
| ENSE00001331723 | AACCCTAACCAGGTGGTTCTC | CCTGGGTCCCTACCAGTTC | 270 |
| ENSE00001331724 | TGTGTGGCAGGGCCTAAG | GCCTAGTCCCAGATGAGAACC | 327 |
| ENSE00001331730 | AGGAACCCAGGGAGAAAGG | GGGTAATGATGGGAAGTAGCC | 275 |
| ENSE00001331733 | GAGGAAAGGGAACGAGCTG | ACCTTCCTGGCCCATGTC | 333 |

Dashes indicate oligonucleotides that were designed individually using Primer3 due to a failure to generate primers with the original program.

## 6.3. Chi-Square goodness of fit test for *Mp* penetrance analysis

Data of affected and non-affected animals from the crosses were analysed using chi-square goodness of fit tests to investigate the penetrance of the *Mp* phenotype. The null hypothesis in this case is that the distribution of the data is not related and that penetrance is thus not full. The alternative hypothesis is that the data fits the accepted distribution for full penetrance of the phenotype, i.e. in heterozygote Vs wild-type crosses, the probability of an individual progeny being heterozygote is $p = 0.5$.

**Parameters for test:**

$\chi^2$= [(observed-expected)$^2$/expected]+ [(observed-expected)$^2$/expected]

Degrees of freedom ($v$) =total parameters-1

Confidence limit is $p$>0.05

### 6.3.1. 3rd Outcross to C56Bl6/j

| *n*=131 | Wild Type | Heterozygote |
|---|---|---|
| Observed | 56 | 75 |
| Expected | 65.5 | 65.5 |

$v$=1, $\chi^2$=2.756; $p$=0.097

Thus we can reject the null hypothesis that the penetrance is not full, or more accurately, we cannot reject the alternative hypothesis. I.e. the probability that a value of 2.756 or larger would come from the $\chi^2_1$distribution is <10%, or put another way if this was repeated numerous times then these values would occur <10% of the time. Although this value is small, it is greater than the standard 5% ($p<0.05$) used as a cut-off to determine whether values should be accepted from within the $\chi^2_1$distribution)

### 6.3.2. 4th Outcross to C56Bl6/j

| *n*=95 | Wild Type | Heterozygote |
|---|---|---|
| Observed | 52 | 43 |
| Expected | 47.5 | 47.5 |

$v$=1; $\chi^2$=0.853; $p$=0.356

Verdict: we reject the null hypothesis for this outcross.

### 6.3.3. 5th Outcross to C56Bl6/j

| *n*=18 | Wild Type | Heterozygote |
|---|---|---|
| Observed | 7 | 11 |
| Expected | 9 | 9 |

$v$=1; $\chi^2$=0.889; $p$=0.346

Verdict: we reject the null hypothesis for this outcross.

### 6.3.4. 1st Outcross to CD1

| *n*=39 | Wild Type | Heterozygote |
|---|---|---|
| Observed | 20 | 19 |
| Expected | 19.5 | 19.5 |

$v$=1; $\chi^2$=0.026; $p$=0.873

Verdict: we reject the null hypothesis for this outcross.

### 6.3.5. Intercrosses on C56Bl6/j strain background

| *n*=87 | Wild Type | Heterozygote | Homozygote |
|---|---|---|---|
| Observed | 19 | 51 | 19 |
| Expected | 21.75 | 43.5 | 21.75 |

$v$= 2; $\chi^2$= 2.678; $p$= 0.262

Verdict: we reject the null hypothesis for this outcross.

### 6.3.6. Intercrosses on CD1 strain background

| *n*=22 | Wild Type | Heterozygote | Homozygote |
|---|---|---|---|
| Observed | 5 | 11 | 6 |
| Expected | 5.5 | 11 | 5.5 |

$v$= 2; $\chi^2$= 0.091; $p$= 0.956

Verdict: we reject the null hypothesis for this outcross.

## 6.4. Oligonucleotide primers used for PCR reactions in the *Mp* project

### 6.4.1. Microsatellite mapping

| Name | 5'-3' sequence | Size | Fluorescent Tag |
|---|---|---|---|
| D11Mit35_Forw | AGTAACATGGAACATCGACGG | 21 | |
| D11Mit35_Rev | TGCTCAGCTCTGGAGTGCTA | 20 | |
| D11Mit286_Forw | AAGGCATATTAAATCTAAGGCTGTG | 25 | |
| D11Mit286_Rev | CTAATCTCCTTGGCAGCAGG | 20 | |
| D11Mit132_Fwd | GGTCAGAGGACAATCTTACATGC | 23 | |
| D11Mit132_Rev | GTTCCAAGACAATGAGAGACCC | 22 | |
| D11Mit360_Fwd | CTCTCTCACTGGAACCGTCC | 20 | |
| D11Mit360_Rev | AGAGAAAGGCTCTGTGAGAAACA | 23 | |
| D11Mit333_Forw | CATGTGGTTATTTTCTAGCCCC | 22 | |
| D11Mit333_Rev | AGGCATCAATAACTATTTTTCAGTG | 25 | |
| D11Mit181_Fwd | TCATCTGTCCCTGCCTCC | 18 | |
| D11Mit181_Rev | TACTGTATTTGATACATATACGTGCCC | 27 | |
| D11Mit61_Forw | ACCCTTTCTCAGCTTACAAGTCC | 23 | |
| D11Mit61_Rev | GTATCAGAATCTGGTGCTTCTGG | 23 | |
| D11Mit119Fwd | AAGCTTTTTCTATTTCAACCCTAA | 24 | |
| D11Mit119Rev | GTCTTTTACAGCCCTTTTTGTAGC | 24 | |
| D11Mit39Fwd | TTTCATGACCCCTAATTTCCC | 21 | |
| D11Mit39Rev | GTGGGTGTGCCTGTCAATC | 19 | |
| D11MIT320_Fwd | CCCATATAGTGAAGCAAGAAACG | 23 | |
| D11MIT320_Rev | TTATAGTGTATGCATCCAGGTGTG | 24 | |
| D11Mit288_Fwd | AGCATGAATTTAAAAGGCCTG | 21 | |
| D11Mit288_Rev | GGCTGCTAGTTTTCCTGATG | 20 | |
| D18MIT94_Fwd | TCACCTAGGACCCCCCTC | 18 | |
| D18MIT94_Rev | AAGTAGTGAGAGGCCACCACA | 21 | |
| D18MIT64_Fwd | 6TCAGATTCACTGCTAAGTCTTTTC | 24 | 5'-6-FAM |
| D18MIT64_Rev | AGCAAGAAAAGCAGGTGAGG | 20 | |
| D18MIT116_Fwd | 8CCTTAAAGGAGTGTGTATATTTTTGTG | 27 | 5'-HEX |
| D18MIT116_Rev | TTGATGTTATCCTCTGGGCC | 20 | |
| D18MIT226_Fwd | 8CAGGCAGGGTGCATATATTATAA | 23 | 5'-HEX |
| D18MIT226_Rev | TATCTGTTTATGTGTGTACATTGTGTG | 27 | |
| D18MIT74_Fwd | AGCCAGAGCTACAAAGTTTCAA | 22 | |
| D18MIT74_Rev | GCTCTTGTAGAGCCATCATTCC | 22 | |
| D18MIT184_Fwd | 9CACACATGTGTAGGTAGGTAGGTAGG | 26 | 5'-TET |
| D18MIT184_Rev | CGCACAAGGACTACTGAAACA | 21 | |

### 6.4.2. Oligonucleotides for *Fbn2* transcript analysis

| Name | 5'-3' sequence | Size |
|---|---|---|
| FBN2cDNA1_Fwd | TCTCCAGCCCTACTTCGTGT | 20 |
| FBN2cDNA1_Rev | GCTGGACACATCTCACAAGG | 20 |
| FBN2cDNA2_Fwd | GCCCGTGTTTCACTCAAGTC | 20 |
| FBN2cDNA2_Rev | CCATTACTGCAGGGATTGGA | 20 |
| FBN2cDNA3_Fwd | GATCCTTCCGCTGTGACTGT | 20 |
| FBN2cDNA3_Fwd | AGGAAGCAGTGCTCCATACG | 20 |
| FBN2cDNA3_Rev | AGGAAGCAGTGCTCCATACG | 20 |
| FBN2cDNA4_Fwd | AATGAATGCGAGGTGTTTCC | 20 |
| FBN2cDNA4_Rev | CGTAGCTTCCTTCGGAGTTG | 20 |
| FBN2cDNA5_Fwd | TGATCGGAACTTACCAGTGCT | 21 |
| FBN2cDNA5_Rev | GTTTCCTCCTGTCCTGTCCA | 20 |
| FBN2cDNA6_Fwd | AGTGTGAGATGGGCTTCACC | 20 |
| FBN2cDNA6_Rev | TGTCAAAGGTGAATCCAGGAA | 21 |
| FBN2cDNA7_Fwd | ACAAAGAGGATGTGCTGCTG | 20 |
| FBN2cDNA7_Rev | GAGCCCTCCAAATTCTGACA | 20 |
| FBN2cDNA8_Fwd | GCAACGAGGGTTACGAACTG | 20 |
| FBN2cDNA8_Rev | CCAGGCTTAGTCCTGCATTC | 20 |
| FBN2cDNA9_Fwd | CTGGACGAGTGTGCTGAGG | 19 |
| FBN2cDNA9_Rev | TCTTCACAGTTCAGCCCAGA | 20 |
| FBN2cDNA10_Fwd | GTCTCAGCCTTCCCTCTGTG | 20 |
| FBN2cDNA10_Rev | GTCGTCCTCATTGTGCTCCT | 20 |

### 6.4.3. Oligonucleotide primers for Fbn2 3'-exon and intron analysis

| Name | 5'-3' sequence | Size |
|---|---|---|
| Fbn2_Ex62_Fwd | TTTGTTCCCATTAAAGGTTGTG | 22 |
| Fbn2_Ex62_Rev | GCTTATCCAGACACTGAGGTTG | 22 |
| Fbn2_Ex63_Fwd | TTCATCCCCTCTGCCCC | 17 |
| Fbn2_Ex63_Rev | GCTGCCTGACCCTGACC | 17 |
| Fbn2_Ex64_Fwd | TGCGTCCATGTTTCCTAAAG | 20 |
| Fbn2_Ex64_Fwd | CAGGGCCAAGGAACACG | 17 |
| Fbn2_Ex64_Rev | CAGGGCCAAGGAACACG | 17 |
| Fbn2_Ex65_Fwd | TATCAGTCAATCGCAGGTGG | 20 |
| Fbn2_Ex65_Rev | CTTCTGAAGGCCGGCTG | 17 |

### 6.4.4. Oligonucleotide primers for *Fbn2* intron 62 analysis

| Name | 5'-3' sequence | Size |
|---|---|---|

| | | |
|---|---|---|
| Fbn2Int_1Fwd | AACACGGCTGCCAGAATATC | 20 |
| Fbn2Int_1Rev | CCAGGCACGGTAATGTATGTC | 21 |
| Fbn2Int_2Fwd | AGGGCTAGGGTTAGCTCAGG | 20 |
| Fbn2Int_2Rev | GGGTTTCTTATGGGGAGCAC | 20 |
| Fbn2Int_3Fwd | TCGGAATAAATGCTGCTGAC | 20 |
| Fbn2Int_3Rev | TGATTGGCTGTTTAACTCAACG | 22 |
| Fbn2Int_4Fwd | GACTGCAGGCTTCATGGTTAG | 21 |
| Fbn2Int_4Rev | TCCATTTGTCATGGGATGTG | 20 |
| Fbn2Int_5Fwd | CTGTGTGCAGCTTGAAGAGG | 20 |
| Fbn2Int_5Rev | TCTGCTGTTCTGACGGACAC | 20 |
| Fbn2Int_6Fwd | ATCCCTCAGGGTTTCTGCTC | 20 |
| Fbn2Int_6Rev | TGCCTTGTTTGGCTATGTTG | 20 |
| Fbn2Int_7Fwd | AACGGGCAGCAGATATGAAC | 20 |
| Fbn2Int_7Rev | ACCGAAGCGCAGGTATTAG | 19 |
| Fbn2Int_8Fwd | TTCGCATATTAAGCAAATGACC | 22 |
| Fbn2Int_8Rev | CTTAGCACTTCCCCCAGCTC | 20 |
| Fbn2Int_9Fwd | GGGTCCTTTCCTGAATTTCTC | 21 |
| Fbn2Int_9Rev | CCACTCTGAAGTACCCTGGTG | 21 |

### 6.4.5. *Fbn2* 3'-RACE oligonucleotide primers

| Name | 5'-3' sequence | Size |
|---|---|---|
| 3'-RACE_d(T) | GACTCGAGTCGACATCGATTTTTTTTTTTTTTTT | 35 |
| 3'-RACE_adaptor | GACTCGAGTCGACATCG | 17 |

### 6.4.6. Oligonucleotide primers for *Isoc1* transcript analysis

| Name | 5'-3' sequence | Size |
|---|---|---|
| Isoc1_cDNA_Rev | TGCACAATTTAAGAATACTTCACCA | 25 |
| Isoc1_cDNA_Fwd | CATTAGTGTGGGACAGAGACTGTTGC | 26 |

### 6.4.7. Oligonucleotide primers for *Isoc1* intron 5

| Name | 5'-3' sequence | Size |
|---|---|---|
| Isoc1_Ex5_ampli | TCGAGAAGCATGATGGACAG | 20 |
| Isoc1_Ex5_2_Fwd | TCCACTCTCTGTGCTTGCAT | 20 |
| Isoc1_Ex5_2_Rev | GGGCCCACAGAATCAACTAA | 20 |
| Isoc1_Ex5_3_Fwd | GCAGTCCAGTAGGGGGAAG | 19 |
| Isoc1_Ex5_3_Rev | ACCTGACCTCACCTGCAGAC | 20 |
| Isoc1_Ex5_4_Fwd | GTGCAGTGTCTGCAGGTGAG | 20 |
| Isoc1_Ex5_4_Rev | GAGCAGACAAAGTCAGGCAAT | 21 |
| Isoc1_Ex5_5_Fwd | GCCAGCTCCCTTTCTTCTTT | 20 |
| Isoc1_Ex5_5_Rev | GGGCCTCAGCCATAGACATA | 20 |
| Isoc1Real_6_Fwd | GGAACCAGCCTTCCTTTTTC | 20 |
| Isoc1Real_6_Rev | TTGAACTTCGGGTGGTCTTT | 20 |

### 6.4.8. Oligonucleotide primers for genotyping PCR

| Name | 5'-3' sequence | Size |
|---|---|---|
| Fbn2_FineMap_F | AGAAGCACCTTGAGCAGAGC | 20 |
| Fbn2_FineMap_R | GCCTTGTTTGGCTATGTTGG | 20 |
| Isoc1Ex5_4_Fwd2 | AGGTGATGGTGTGCAGTGTC | 20 |

### 6.4.9. Oligonucleotide primers for RT-PCR

| Name | 5'-3' sequence | Size | Fluorescent Tag |
|---|---|---|---|
| 18sRNA_Fwd | AGATCAAAACCAACCCGGTGA | 21 | |
| 18sRNA_Rev | GGTAAGAGCATCGAGGGGGC | 20 | |
| HPRT_QRTPCR_Fwd | CTGGTGAAAAGGACCTCTCG | 20 | |
| HPRT_QRTPCR_Rev | CAAGGGCATATCCAACAACA | 20 | |
| SLC27a6_cDNAFwd | TGGAATTGGTGGATGTGTTG | 20 | |
| SLC27a6_cDNARev | CGAAGTTCTCCTGGTCTTGG | 20 | |
| *Xbp1*_SYBR_Fwd | CTGAGTCCGCAGCAGGTG | 19 | |
| *Xbp1*_SYBR_Rev1 | CCAGAATGCCCAAAAGGATA | 20 | |
| Xbp-1_Fwd_FAM | TTACGGGAGAAAACTCACGGCC | 22 | 5'-6-FAM |
| *Xbp1*_Rev | GGGTCCAACTTGTCCAGAAT | 20 | |

### 6.4.10. Oligonucleotide primers for Riboprobe synthesis

| Name | 5'-3' sequence | Size |
|---|---|---|
| CHX10_T7_Fwd | TAATACGACTCACTATAGGGGCAGAGCTGTGATTGGATT | 39 |
| CHX10_T3_Rev | AATTAACCCTCACTAAAGGGACAGGTTTGGGGAAGGACT | 39 |
| Isoc1_Fwd_T3 | AATTAACCCTCACTAAAGGAACAGATGGGAGTGGTTTGC | 39 |
| Isoc1_Rev_T7 | TAATACGACTCACTATAGGAGAGGATTCCCCTCCTTTGA | 39 |
| Fbn2_Fwd_T3 | AATTAACCCTCACTAAAGGCAAAAAGGGAAACTCGCTTG | 39 |
| Fbn2_Rev_T7 | TAATACGACTCACTATAGGAGGTGTTCCTGCTCAAAGGA | 39 |
| Bip_Riboprobe_Rev_T7 | TAATACGACTCACTATAGGTTTCTTCTGGGGCAAATGTC | 39 |
| Bip_Riboprobe_Fwd_T3 | AATTAACCCTCACTAAAGGGCTTCGTGTCTCCTCCTGAC | 39 |

# 7. Acknowledgement

There are many people who deserve my gratitude and without whom I simply would not have completed this study or put this thesis together. They are too numerous to list, but too valuable to forget. Thank you all.

I would, however, like to give special mention to a few people. Firstly, to David, who has always been there for me with encouragement, insight, enthusiasm and understanding, and of course for his unparalleled omniscience. Also to Margaret, who expedited the mouse project through her meticulous record keeping, judicious crosses and excellent sample taking. Without her the mouse project would have been a chaotic mess. Thirdly, to Ian for being there at all times to guide me through the basics of mouse genetics and for fully supporting the *Mp* work and for his faith in just letting me get on with it.

I would also like to thank my friends and family who have all been there for me over the last three years, and especially for their support throughout my recent problems outside work. I also have a deep gratitude to Kim and her family for their help in getting me out of the kitchen and believing in me. I also wish to thank my grandparents for not judging, and for their unwavering support, and Mum who will always listen.

Lastly, there are three people who require an extra special mention. Jacqueline, you are the loveliest. Thank you for everything you did to help me during the final months of this thesis, and for the fun you have put back into my life. Polly, you nurtured it all don't you know? You are an inspiration. Finally, I want Dad to know just how grateful I am for bringing me up in such a wonderfully happy environment and for educating me about the world. You taught me to ask *Why*?

# 8. References


Acampora, D., Mazan, S., Avantaggiato, V., Barone, P., Tuorto, F., Lallemand, Y., Brulet, P., and Simeone, A. (1996). Epilepsy and brain abnormalities in mice lacking the Otx1 gene. Nat Genet *14*, 218-222.

Akhmedov, N.B., Piriev, N.I., Chang, B., Rapoport, A.L., Hawes, N.L., Nishina, P.M., Nusinowitz, S., Heckenlively, J.R., Roderick, T.H., Kozak, C.A., *et al.* (2000). A deletion in a photoreceptor-specific nuclear receptor mRNA causes retinal degeneration in the rd7 mouse. Proc Natl Acad Sci U S A *97*, 5551-5556.

al Gazali, L.I., Sabarinathan, D.K., and Khidir, A. (1994). Microphthalmia and distal limb abnormalities in a child of consanguineous parents. Clin Dysmorphol *3*, 258-262.

Arteaga-Solis, E., Gayraud, B., Lee, S.Y., Shum, L., Sakai, L., and Ramirez, F. (2001). Regulation of limb patterning by extracellular microfibrils. J Cell Biol *154*, 275-281.

Badano, J.L., Mitsuma, N., Beales, P.L., and Katsanis, N. (2006). The ciliopathies: an emerging class of human genetic disorders. Annu Rev Genomics Hum Genet *7*, 125-148.

Bamshad, M., Lin, R.C., Law, D.J., Watkins, W.C., Krakowiak, P.A., Moore, M.E., Franceschini, P., Lala, R., Holmes, L.B., Gebuhr, T.C., *et al.* (1997). Mutations in human TBX3 alter limb, apocrine and genital development in ulnar-mammary syndrome. Nat Genet *16*, 311-315.

Bandyopadhyay, A., Tsuji, K., Cox, K., Harfe, B.D., Rosen, V., and Tabin, C.J. (2006). Genetic analysis of the roles of BMP2, BMP4, and BMP7 in limb patterning and skeletogenesis. PLoS Genet *2*, e216.

Barbieri, A.M., Lupo, G., Bulfone, A., Andreazzoli, M., Mariani, M., Fougerousse, F., Consalez, G.G., Borsani, G., Beckmann, J.S., Barsacchi, G., *et al.* (1999). A homeobox gene, vax2, controls the patterning of the eye dorsoventral axis. Proc Natl Acad Sci U S A *96*, 10729-10734.

Bardakjian, T. (2007). Anophthalmia/ Microphthalmia Overview. GeneReviews: wwwncbinlmnihgov/bookshelf.

Beebe, D.C. (1986). Development of the ciliary body: a brief review. Trans Ophthalmol Soc U K *105 ( Pt 2)*, 123-130.

Bishop, P.N., Takanosu, M., Le Goff, M., and Mayne, R. (2002). The role of the posterior ciliary body in the biosynthesis of vitreous humour. Eye *16*, 454-460.

Burmeister, M., Novak, J., Liang, M.Y., Basu, S., Ploder, L., Hawes, N.L., Vidgen, D., Hoover, F., Goldman, D., Kalnins, V.I., *et al.* (1996). Ocular retardation mouse caused by Chx10 homeobox null allele: impaired retinal progenitor proliferation and bipolar cell differentiation. Nat Genet *12*, 376-384.

Bylund, M., Andersson, E., Novitch, B.G., and Muhr, J. (2003). Vertebrate neurogenesis is counteracted by Sox1-3 activity. Nat Neurosci *6*, 1162-1168.

Caksen, H., Odabas, D., Oner, A.F., Abuhandan, M., and Calebi, V. (2002). Ophthalmo-acromelic syndrome in a Turkish infant: case report. East Afr Med J *79*, 339-340.

Capdevila, J., and Izpisua Belmonte, J.C. (2001). Patterning mechanisms controlling vertebrate limb development. Annu Rev Cell Dev Biol *17*, 87-132.

Chang, Y.F., Imam, J.S., and Wilkinson, M.F. (2007). The nonsense-mediated decay RNA surveillance pathway. Annu Rev Biochem *76*, 51-74.

Charbonneau, N.L., Ono, R.N., Corson, G.M., Keene, D.R., and Sakai, L.Y. (2004). Fine tuning of growth factor signals depends on fibrillin microfibril networks. Birth Defects Res C Embryo Today *72*, 37-50.

Chaudhry, S.S., Gazzard, J., Baldock, C., Dixon, J., Rock, M.J., Skinner, G.C., Steel, K.P., Kielty, C.M., and Dixon, M.J. (2001). Mutation of the gene encoding fibrillin-2 results in syndactyly in mice. Hum Mol Genet *10*, 835-843.

Cho, S.H., and Cepko, C.L. (2006). Wnt2b/beta-catenin-mediated canonical Wnt signaling determines the peripheral fates of the chick eye. Development *133*, 3167-3177.

Chow, R.L., and Lang, R.A. (2001). Early eye development in vertebrates. Annu Rev Cell Dev Biol *17*, 255-296.

Corson, G.M., Charbonneau, N.L., Keene, D.R., and Sakai, L.Y. (2004). Differential expression of fibrillin-3 adds to microfibril variety in human and avian, but not rodent, connective tissues. Genomics *83*, 461-472.

Dahn, R.D., and Fallon, J.F. (2000). Interdigital regulation of digit identity and homeotic transformation by modulated BMP signaling. Science *289*, 438-441.

Damiani, D., Alexander, J.J., O'Rourke, J.R., McManus, M., Jadhav, A.P., Cepko, C.L., Hauswirth, W.W., Harfe, B.D., and Strettoi, E. (2008). Dicer inactivation leads to progressive functional and structural degeneration of the mouse retina. J Neurosci *28*, 4878-4887.

Danno, H., Michiue, T., Hitachi, K., Yukita, A., Ishiura, S., and Asashima, M. (2008). Molecular links among the causative genes for ocular malformation: Otx2 and Sox2 coregulate Rax expression. Proc Natl Acad Sci U S A *105*, 5408-5413.

de Iongh, R.U., Abud, H.E., and Hime, G.R. (2006). WNT/Frizzled signaling in eye development and disease. Front Biosci *11*, 2442-2464.

Dias da Silva, M.R., Tiffin, N., Mima, T., Mikawa, T., and Hyer, J. (2007). FGF-mediated induction of ciliary body tissue in the chick eye. Dev Biol *304*, 272-285.

Drossopoulou, G., Lewis, K.E., Sanz-Ezquerro, J.J., Nikbakht, N., McMahon, A.P., Hofmann, C., and Tickle, C. (2000). A model for anteroposterior patterning of the vertebrate limb based on sequential long- and short-range Shh signalling and Bmp signalling. Development *127*, 1337-1348.

Faivre, L., Dollfus, H., Lyonnet, S., Alembik, Y., Megarbane, A., Samples, J., Gorlin, R.J., Alswaid, A., Feingold, J., Le Merrer, M.*, et al.* (2003a). Clinical homogeneity and genetic heterogeneity in Weill-Marchesani syndrome. Am J Med Genet A *123A*, 204-207.

Faivre, L., Gorlin, R.J., Wirtz, M.K., Godfrey, M., Dagoneau, N., Samples, J.R., Le Merrer, M., Collod-Beroud, G., Boileau, C., Munnich, A.*, et al.* (2003b). In frame fibrillin-1 gene deletion in autosomal dominant Weill-Marchesani syndrome. J Med Genet *40*, 34-36.

Fantes, J., Ragge, N.K., Lynch, S.A., McGill, N.I., Collin, J.R., Howard-Peebles, P.N., Hayward, C., Vivian, A.J., Williamson, K., van Heyningen, V.*, et al.* (2003). Mutations in SOX2 cause anophthalmia. Nat Genet *33*, 461-463.

Favor, J., Sandulache, R., Neuhauser-Klaus, A., Pretsch, W., Chatterjee, B., Senft, E., Wurst, W., Blanquet, V., Grimes, P., Sporle, R., *et al.* (1996). The mouse Pax2(1Neu) mutation is identical to a human PAX2 mutation in a family with renal-coloboma syndrome and results in developmental defects of the brain, ear, eye, and kidney. Proc Natl Acad Sci U S A *93*, 13870-13875.

Ferda Percin, E., Ploder, L.A., Yu, J.J., Arici, K., Horsford, D.J., Rutherford, A., Bapat, B., Cox, D.W., Duncan, A.M., Kalnins, V.I., *et al.* (2000). Human microphthalmia associated with mutations in the retinal homeobox gene CHX10. Nat Genet *25*, 397-401.

Fitzpatrick, D.R., and van Heyningen, V. (2005). Developmental eye disorders. Curr Opin Genet Dev *15*, 348-353.

Furuta, Y., and Hogan, B.L. (1998). BMP4 is essential for lens induction in the mouse embryo. Genes Dev *12*, 3764-3775.

Galasso, C., Bombardieri, R., Cerminara, C., Stranci, G., and Curatolo, P. (2007). Anophthalmia-Waardenburg syndrome with expanding phenotype: does neural crest play a role? J Child Neurol *22*, 1252-1255.

Garavelli, L., Pedori, S., Dal Zotto, R., Franchi, F., Marinelli, M., Croci, G.F., Bellato, S., Ammenti, A., Virdis, R., Banchini, G., *et al.* (2006). Anophthalmos with limb anomalies (Waardenburg opththalmo-acromelic syndrome): report of a new Italian case with renal anomaly and review. Genet Couns *17*, 449-455.

Geisinger, A., Alsheimer, M., Baier, A., Benavente, R., and Wettstein, R. (2005). The mammalian gene pecanex 1 is differentially expressed during spermatogenesis. Biochim Biophys Acta *1728*, 34-43.

Glaser, T., Jepeal, L., Edwards, J.G., Young, S.R., Favor, J., and Maas, R.L. (1994). PAX6 gene dosage effect in a family with congenital cataracts, aniridia, anophthalmia and central nervous system defects. Nat Genet *7*, 463-471.

Graham, V., Khudyakov, J., Ellis, P., and Pevny, L. (2003). SOX2 functions to maintain neural progenitor identity. Neuron *39*, 749-765.

Graw, J. (2003). The genetic and molecular basis of congenital eye defects. Nat Rev Genet *4*, 876-888.

Gregory, K.E., Ono, R.N., Charbonneau, N.L., Kuo, C.L., Keene, D.R., Bachinger, H.P., and Sakai, L.Y. (2005). The prodomain of BMP-7 targets the BMP-7 complex to the extracellular matrix. J Biol Chem *280*, 27970-27980.

Grindley, J.C., Davidson, D.R., and Hill, R.E. (1995). The role of Pax-6 in eye and nasal development. Development *121*, 1433-1442.

Grondona, J.M., Kastner, P., Gansmuller, A., Decimo, D., Chambon, P., and Mark, M. (1996). Retinal dysplasia and degeneration in RARbeta2/RARgamma2 compound mutant mice. Development *122*, 2173-2188.

Habashi, J.P., Judge, D.P., Holm, T.M., Cohn, R.D., Loeys, B.L., Cooper, T.K., Myers, L., Klein, E.C., Liu, G., Calvi, C.*, et al.* (2006). Losartan, an AT1 antagonist, prevents aortic aneurysm in a mouse model of Marfan syndrome. Science *312*, 117-121.

Halfter, W., Winzen, U., Bishop, P.N., and Eller, A. (2006). Regulation of eye size by the retinal basement membrane and vitreous body. Invest Ophthalmol Vis Sci *47*, 3586-3594.

Hatakeyama, J., and Kageyama, R. (2004). Retinal cell fate determination and bHLH factors. Semin Cell Dev Biol *15*, 83-89.

Hausmann, G., Banziger, C., and Basler, K. (2007). Helping Wingless take flight: how WNT proteins are secreted. Nat Rev Mol Cell Biol *8*, 331-336.

Hill, R.E., Favor, J., Hogan, B.L., Ton, C.C., Saunders, G.F., Hanson, I.M., Prosser, J., Jordan, T., Hastie, N.D., and van Heyningen, V. (1991). Mouse small eye results from mutations in a paired-like homeobox-containing gene. Nature *354*, 522-525.

Hubmacher, D., Tiedemann, K., and Reinhardt, D.P. (2006). Fibrillins: from biogenesis of microfibrils to signaling functions. Curr Top Dev Biol *75*, 93-123.

Ihanamaki, T., Pelliniemi, L.J., and Vuorio, E. (2004). Collagens and collagen-related matrix components in the human and mouse eye. Prog Retin Eye Res *23*, 403-434.

Inoue, T., Hojo, M., Bessho, Y., Tano, Y., Lee, J.E., and Kageyama, R. (2002). Math3 and NeuroD regulate amacrine cell fate specification in the retina. Development *129*, 831-842.

Jackson, I.J., and Bennett, D.C. (1990). Identification of the albino mutation of mouse tyrosinase by analysis of an in vitro revertant. Proc Natl Acad Sci U S A *87*, 7010-7014.

Jadhav, A.P., Mason, H.A., and Cepko, C.L. (2006). Notch 1 inhibits photoreceptor production in the developing mammalian retina. Development *133*, 913-923.

Jamieson, R.V., Perveen, R., Kerr, B., Carette, M., Yardley, J., Heon, E., Wirth, M.G., van Heyningen, V., Donnai, D., Munier, F.*, et al.* (2002). Domain disruption and mutation of the bZIP transcription factor, MAF, associated with cataract, ocular anterior segment dysgenesis and coloboma. Hum Mol Genet *11*, 33-42.

Johnson, K.R., Cook, S.A., and Zheng, Q.Y. (1998). The original shaker-with-syndactylism mutation (sy) is a contiguous gene deletion syndrome. Mamm Genome *9*, 889-892.

Kaartinen, V., and Warburton, D. (2003). Fibrillin controls TGF-beta activation. Nat Genet *33*, 331-332.

Kamachi, Y., Uchikawa, M., Tanouchi, A., Sekido, R., and Kondoh, H. (2001). Pax6 and SOX2 form a co-DNA-binding partner complex that regulates initiation of lens development. Genes Dev *15*, 1272-1286.

Kang, S., Graham, J.M., Jr., Olney, A.H., and Biesecker, L.G. (1997). GLI3 frameshift mutations cause autosomal dominant Pallister-Hall syndrome. Nat Genet *15*, 266-268.

Kara, F., Yesildaglar, N., Tuncer, R.A., Semerci, N., Onat, N., Yilmazer, Y.C., Sipahi, T., and Erkaya, S. (2002). A case report of prenatally diagnosed ophthalmo-acromelic syndrome type Waardenburg. Prenat Diagn *22*, 395-397.

Kim, J.W., and Lemke, G. (2006). Hedgehog-regulated localization of Vax2 controls eye development. Genes Dev *20*, 2833-2847.

Kleinjan, D.A., and van Heyningen, V. (2005). Long-range control of gene expression: emerging mechanisms and disruption in disease. Am J Hum Genet *76*, 8-32.

Kondoh, H., Uchikawa, M., and Kamachi, Y. (2004). Interplay of Pax6 and SOX2 in lens development as a paradigm of genetic switch mechanisms for cell differentiation. Int J Dev Biol *48*, 819-827.

Kubo, F., and Nakagawa, S. (2008). Wnt signaling in retinal stem cells and regeneration. Dev Growth Differ *50*, 245-251.

Kubo, F., Takeichi, M., and Nakagawa, S. (2003). Wnt2b controls retinal cell differentiation at the ciliary marginal zone. Development *130*, 587-598.

Kubo, F., Takeichi, M., and Nakagawa, S. (2005). Wnt2b inhibits differentiation of retinal progenitor cells in the absence of Notch activity by downregulating the expression of proneural genes. Development *132*, 2759-2770.

Lander, E., and Kruglyak, L. (1995). Genetic dissection of complex traits: guidelines for interpreting and reporting linkage results. Nat Genet *11*, 241-247.

Lander, E.S., and Botstein, D. (1987). Homozygosity mapping: a way to map human recessive traits with the DNA of inbred children. Science *236*, 1567-1570.

Lang, R.A. (2004). Pathways regulating lens induction in the mouse. Int J Dev Biol *48*, 783-791.

Le Merrer, M., Nessmann, C., Briard, M.L., and Maroteaux, P. (1988). Ophthalmo-acromelic syndrome. Ann Genet *31*, 226-229.

Levanon, D., Goldstein, R.E., Bernstein, Y., Tang, H., Goldenberg, D., Stifani, S., Paroush, Z., and Groner, Y. (1998). Transcriptional repression by AML1 and LEF-1 is mediated by the TLE/Groucho corepressors. Proc Natl Acad Sci U S A *95*, 11590-11595.

Li, S., Mo, Z., Yang, X., Price, S.M., Shen, M.M., and Xiang, M. (2004). Foxn4 controls the genesis of amacrine and horizontal cells by retinal progenitors. Neuron *43*, 795-807.

Lin, J.H., Li, H., Yasumura, D., Cohen, H.R., Zhang, C., Panning, B., Shokat, K.M., Lavail, M.M., and Walter, P. (2007). IRE1 signaling affects cell fate during the unfolded protein response. Science *318*, 944-949.

Liu, H., Mohamed, O., Dufort, D., and Wallace, V.A. (2003). Characterization of Wnt signaling components and activation of the Wnt canonical pathway in the murine retina. Dev Dyn *227*, 323-334.

Lodish, H.F. (1999). Molecular cell biology, 4th ed. edn (New York ; Basingstoke, W.H. Freeman).

Logan, C.Y., and Nusse, R. (2004). The Wnt signaling pathway in development and disease. Annu Rev Cell Dev Biol *20*, 781-810.

Lonnqvist, L., Reinhardt, D., Sakai, L., and Peltonen, L. (1998). Evidence for furin-type activity-mediated C-terminal processing of profibrillin-1 and interference in the processing by certain mutations. Hum Mol Genet *7*, 2039-2044.

Lyon, M.F., Jamieson, R.V., Perveen, R., Glenister, P.H., Griffiths, R., Boyd, Y., Glimcher, L.H., Favor, J., Munier, F.L., and Black, G.C. (2003). A dominant mutation within the DNA-binding domain of the bZIP transcription factor Maf causes murine cataract and results in selective alteration in DNA binding. Hum Mol Genet *12*, 585-594.

Malhotra, J.D., and Kaufman, R.J. (2007). The endoplasmic reticulum and the unfolded protein response. Semin Cell Dev Biol *18*, 716-731.

Maretto, S., Cordenonsi, M., Dupont, S., Braghetta, P., Broccoli, V., Hassan, A.B., Volpin, D., Bressan, G.M., and Piccolo, S. (2003). Mapping Wnt/beta-catenin signaling during mouse development and in colorectal tumors. Proc Natl Acad Sci U S A *100*, 3299-3304.

Martinez-Morales, J.R., Rodrigo, I., and Bovolenta, P. (2004). Eye development: a view from the retina pigmented epithelium. Bioessays *26*, 766-777.

Mathers, P.H., Grinberg, A., Mahon, K.A., and Jamrich, M. (1997). The Rx homeobox gene is essential for vertebrate eye development. Nature *387*, 603-607.

Megarbane, A., Souraty, N., and Tamraz, J. (1998). Ophthalmo-acromelic syndrome (Waardenburg) with split hand and polydactyly. Genet Couns *9*, 195-199.

Moran, J.L., Bolton, A.D., Tran, P.V., Brown, A., Dwyer, N.D., Manning, D.K., Bjork, B.C., Li, C., Montgomery, K., Siepka, S.M., *et al.* (2006). Utilization of a whole genome SNP panel for efficient genetic mapping in the mouse. Genome Res *16*, 436-440.

Morrow, E.M., Furukawa, T., Raviola, E., and Cepko, C.L. (2005). Synaptogenesis and outer segment formation are perturbed in the neural retina of Crx mutant mice. BMC Neurosci *6*, 5.

Morton, N.E. (1955). Sequential tests for the detection of linkage. Am J Hum Genet *7*, 277-318.

Mui, S.H., Kim, J.W., Lemke, G., and Bertuzzi, S. (2005). Vax genes ventralize the embryonic eye. Genes Dev *19*, 1249-1259.

Muragaki, Y., Mundlos, S., Upton, J., and Olsen, B.R. (1996). Altered growth and branching patterns in synpolydactyly caused by mutations in HOXD13. Science *272*, 548-551.

Nagy, E., and Maquat, L.E. (1998). A rule for termination-codon position within intron-containing genes: when nonsense affects RNA abundance. Trends Biochem Sci *23*, 198-199.

Nakagawa, S., Takada, S., Takada, R., and Takeichi, M. (2003). Identification of the laminar-inducing factor: Wnt-signal from the anterior rim induces correct laminar formation of the neural retina in vitro. Dev Biol *260*, 414-425.

Ng, D., Thakker, N., Corcoran, C.M., Donnai, D., Perveen, R., Schneider, A., Hadley, D.W., Tifft, C., Zhang, L., Wilkie, A.O., *et al.* (2004). Oculofaciocardiodental and Lenz microphthalmia syndromes result from distinct classes of mutations in BCOR. Nat Genet *36*, 411-416.

Nishida, A., Furukawa, A., Koike, C., Tano, Y., Aizawa, S., Matsuo, I., and Furukawa, T. (2003). Otx2 homeobox gene controls retinal photoreceptor cell fate and pineal gland development. Nat Neurosci *6*, 1255-1263.

Nishiguchi, S., Wood, H., Kondoh, H., Lovell-Badge, R., and Episkopou, V. (1998). Sox1 directly regulates the gamma-crystallin genes and is essential for lens development in mice. Genes Dev *12*, 776-781.

Nothwehr, S.F., and Gordon, J.I. (1990). Targeting of proteins into the eukaryotic secretory pathway: signal peptide structure/function relationships. Bioessays *12*, 479-484.

Pallotta, R., and Dallapiccola, B. (1984). A syndrome with true anophthalmia, hand-foot defects and mental retardation. Ophthalmic Paediatr Genet *4*, 19-23.

Phipps, E.L. (1964). Mouse News Lett *31*

Quarrell, O.W. (1997). Anophthalmia-Waardenburg syndrome or ophthalmo-acromelic syndrome: what is in a name? Am J Med Genet *69*, 432.

Ragge, N.K., Brown, A.G., Poloschek, C.M., Lorenz, B., Henderson, R.A., Clarke, M.P., Russell-Eggitt, I., Fielder, A., Gerrelli, D., Martinez-Barbera, J.P., *et al.* (2005). Heterozygous mutations of OTX2 cause severe ocular malformations. Am J Hum Genet *76*, 1008-1022.

Raymond, S.M., and Jackson, I.J. (1995). The retinal pigmented epithelium is required for development and maintenance of the mouse neural retina. Curr Biol *5*, 1286-1295.

Richieri-Costa, A., Gollop, T.R., and Otto, P.G. (1983). Brief clinical report: autosomal recessive anophthalmia with multiple congenital abnormalities--type Waardenburg. Am J Med Genet *14*, 607-615.

Riddle, R.D., Johnson, R.L., Laufer, E., and Tabin, C. (1993). Sonic hedgehog mediates the polarizing activity of the ZPA. Cell *75*, 1401-1416.

Rusnak, F., Liu, J., Quinn, N., Berchtold, G.A., and Walsh, C.T. (1990). Subcloning of the enterobactin biosynthetic gene entB: expression, purification, characterization, and substrate specificity of isochorismatase. Biochemistry *29*, 1425-1435.

Sasagawa, S., Takabatake, T., Takabatake, Y., Muramatsu, T., and Takeshima, K. (2002). Axes establishment during eye morphogenesis in Xenopus by coordinate and antagonistic actions of BMP4, Shh, and RA. Genesis *33*, 86-96.

Sayli, B.S., Akarsu, A.N., and Altan, S. (1995). Anophthalmos-syndactyly (Waardenburg) syndrome without oligodactyly of toes. Am J Med Genet *58*, 18-20.

Scherz, P.J., McGlinn, E., Nissim, S., and Tabin, C.J. (2007). Extended exposure to Sonic hedgehog is required for patterning the posterior digits of the vertebrate limb. Dev Biol *308*, 343-354.

Schimmenti, L.A., de la Cruz, J., Lewis, R.A., Karkera, J.D., Manligas, G.S., Roessler, E., and Muenke, M. (2003). Novel mutation in sonic hedgehog in non-syndromic colobomatous microphthalmia. Am J Med Genet A *116A*, 215-221.

Schroder, M. (2008). Endoplasmic reticulum stress responses. Cell Mol Life Sci *65*, 862-894.

Sharpe, J., Ahlgren, U., Perry, P., Hill, B., Ross, A., Hecksher-Sorensen, J., Baldock, R., and Davidson, D. (2002). Optical projection tomography as a tool for 3D microscopy and gene expression studies. Science *296*, 541-545.

Siepel, A., Bejerano, G., Pedersen, J.S., Hinrichs, A.S., Hou, M., Rosenbloom, K., Clawson, H., Spieth, J., Hillier, L.W., Richards, S.*, et al*. (2005). Evolutionarily conserved elements in vertebrate, insect, worm, and yeast genomes. Genome Res *15*, 1034-1050.

Stallings RL, Ford AF, Nelson D, Torney DC, Hildebrand CE, Moyzis RK. *Genomics*. 1991 Jul;10(3):807-15

Stoll, C., Alembik, Y., Dott, B., and Roth, M.P. (1997). Congenital eye malformations in 212,479 consecutive births. Ann Genet *40*, 122-128.

Suyugul, Z., Seven, M., Hacihanefioglu, S., Kartal, A., Suyugul, N., and Cenani, A. (1996). Anophthalmia-Waardenburg syndrome: a report of three cases. Am J Med Genet *62*, 391-397.

Takemoto, T., Uchikawa, M., Kamachi, Y., and Kondoh, H. (2006). Convergence of Wnt and FGF signals in the genesis of posterior neural plate through activation of the Sox2 enhancer N-1. Development *133*, 297-306.

Taranova, O.V., Magness, S.T., Fagan, B.M., Wu, Y., Surzenko, N., Hutton, S.R., and Pevny, L.H. (2006). SOX2 is a dose-dependent regulator of retinal neural progenitor competence. Genes Dev *20*, 1187-1202.

Teiber, M.L., Garrido, J.A., and Barreiro, C.Z. (2007). Ophthalmo-acromelic syndrome: report of a case with vertebral anomalies. Am J Med Genet A *143A*, 2460-2462.

Tekin, M., Tutar, E., Arsan, S., Atay, G., and Bodurtha, J. (2000). Ophthalmo-acromelic syndrome: report and review. Am J Med Genet *90*, 150-154.

Thornberry, N.A., and Lazebnik, Y. (1998). Caspases: enemies within. Science *281*, 1312-1316.

Thut, C.J., Rountree, R.B., Hwa, M., and Kingsley, D.M. (2001). A large-scale in situ screen provides molecular evidence for the induction of eye anterior segment structures by the developing lens. Dev Biol *231*, 63-76.

Tickle, C. (2006). Making digit patterns in the vertebrate limb. Nat Rev Mol Cell Biol *7*, 45-53.

Torres, M., Gomez-Pardo, E., and Gruss, P. (1996). Pax2 contributes to inner ear patterning and optic nerve trajectory. Development *122*, 3381-3391.

Traboulsi, E.I., Nasr, A.M., Fahd, S.D., Jabbour, N.M., and Der Kaloustian, V.M. (1984). Waardenburg's recessive anophthalmia syndrome. Ophthalmic Paediatr Genet *4*, 13-18.

Tsang, K.Y., Chan, D., Cheslett, D., Chan, W.C., So, C.L., Melhado, I.G., Chan, T.W., Kwan, K.M., Hunziker, E.B., Yamada, Y.*, et al.* (2007). Surviving endoplasmic reticulum stress is coupled to altered chondrocyte differentiation and function. PLoS Biol *5*, e44.

Ulianich, L., Garbi, C., Treglia, A.S., Punzi, D., Miele, C., Raciti, G.A., Beguinot, F., Consiglio, E., and Di Jeso, B. (2008). ER stress is associated with dedifferentiation and an epithelial-to-mesenchymal transition-like phenotype in PC Cl3 thyroid cells. J Cell Sci *121*, 477-486.

*van Allen M. I.*: Urinary Tract. *In: Human Malformations and Related Anomalies*. R. E. Stevenson, J. Hall, R.M. Goodman (eds). New York, Oxford, Oxford University Press, 1993, 501-562.

van Heyningen, V., and Williamson, K.A. (2002). PAX6 in sensory development. Hum Mol Genet *11*, 1161-1167.

Voronina, V.A., Kozhemyakina, E.A., O'Kernick, C.M., Kahn, N.D., Wenger, S.L., Linberg, J.V., Schneider, A.S., and Mathers, P.H. (2004). Mutations in the human RAX homeobox gene in a patient with anophthalmia and sclerocornea. Hum Mol Genet *13*, 315-322.

Waardenburg, P.J. (1961). Genetics and Ophthalmology. By P. J. Waardenburg, etc (Blackwell Scientific Publications: Oxford; Assen printed).

Wamstad, J.A., and Bardwell, V.J. (2007). Characterization of Bcor expression in mouse development. Gene Expr Patterns *7*, 550-557.

Wright, E., Hargrave, M.R., Christiansen, J., Cooper, L., Kun, J., Evans, T., Gangadharan, U., Greenfield, A., and Koopman, P. (1995). The Sry-related gene Sox9 is expressed during chondrogenesis in mouse embryos. Nat Genet *9*, 15-20.

Yang, Y., and Cvekl, A. (2005). Tissue-specific regulation of the mouse alphaA-crystallin gene in lens via recruitment of Pax6 and c-Maf to its promoter. J Mol Biol *351*, 453-469.

Yoshida, H., Matsui, T., Yamamoto, A., Okada, T., and Mori, K. (2001). *XBP1* mRNA is induced by ATF6 and spliced by IRE1 in response to ER stress to produce a highly active transcription factor. Cell *107*, 881-891.

Zhao, S., Chen, Q., Hung, F.C., and Overbeek, P.A. (2002). BMP signaling is required for development of the ciliary body. Development *129*, 4435-4442.